

*Research Project Number TPF-5(193) Suppl. #14
WisDOT Sponsoring Agency Code RFPF-WISC-3*

**DEVELOPMENT OF A DESIGN PROCEDURE FOR
CONCRETE TRAFFIC BARRIER ATTACHMENTS TO BRIDGE
DECKS UTILIZING EPOXY CONCRETE ANCHORS**

Submitted by

Benjamin J. Dickey, M.S.C.E., E.I.T.
Former Graduate Research Assistant

Ronald K. Faller, Ph.D., P.E.
Research Assistant Professor
Interim MwRSF Director

Scott K. Rosenbaugh, M.S.C.E., E.I.T.
Research Associate Engineer

Robert W. Bielenberg, M.S.M.E., E.I.T
Research Associate Engineer

Karla A. Lechtenberg, M.S.C.E., E.I.T
Research Associate Engineer

Dean L. Sicking, Ph.D., P.E.,
Emeritus Professor
Former MwRSF Director

MIDWEST ROADSIDE SAFETY FACILITY

Nebraska Transportation Center
University of Nebraska-Lincoln
130 Whittier Research Center
2200 Vine Street
Lincoln, Nebraska 68583-0853
(402) 472-0965

Submitted to

WISCONSIN DEPARTMENT OF TRANSPORTATION

4802 Sheboygan Avenue
Madison, Wisconsin 53707

MwRSF Research Report No. TRP-03-264-12

November 26, 2012

TECHNICAL REPORT DOCUMENTATION PAGE

1. Report No. TRP-03-264-12	2.	3. Recipient's Accession No.	
4. Title and Subtitle Development of a Design Procedure for Concrete Traffic Barrier Attachments to Bridge Decks Utilizing Epoxy Concrete Anchors		5. Report Date November 26, 2012	
		6.	
7. Author(s) Dickey, B.J., Faller, R.K., Rosenbaugh, S.K., Bielenberg, R.W., Lechtenberg, K.A., Sicking, D.L.		8. Performing Organization Report No. TRP-03-264-12	
9. Performing Organization Name and Address Midwest Roadside Safety Facility (MwRSF) Nebraska Transportation Center University of Nebraska-Lincoln 130 Whittier Research Center 2200 Vine Street Lincoln, Nebraska 68583-0853		10. Project/Task/Work Unit No.	
		11. Contract © or Grant (G) No. TPF-5(193) Suppl. #14	
12. Sponsoring Organization Name and Address Wisconsin Department of Transportation 4802 Sheboygan Avenue Madison, Wisconsin 53707		13. Type of Report and Period Covered Final Report: 2009-2012	
		14. Sponsoring Agency Code RPFPP –WISC-3	
15. Supplementary Notes Prepared in cooperation with U.S. Department of Transportation, Federal Highway Administration.			
16. Abstract (Limit: 200 words) <p>The objective of this project was to determine if epoxy adhesive anchors could be utilized to anchor concrete barriers to bridge decks and to develop design procedures for implementing epoxy adhesive anchorages into concrete bridge railings. A series of 16 dynamic bogie tests and one static test was conducted to investigate the behavior of epoxy adhesive anchors under dynamic load. Additional dynamic tests were conducted on 1 1/8 in. (29 mm) diameter A307 threaded rods, which was the anchorage required for the F-shape temporary concrete barrier developed by MwRSF. Results from the testing of the on 1 1/8 in. (29 mm) diameter A307 threaded rods suggested that they can be safely used with epoxy adhesive to anchor the F-shape PCB and reduce deflections, but some increase in deflection and significant damage to the bridge deck was expected in severe impacts.</p> <p>Comparisons were made between the component tests and analytical models for epoxy adhesive anchors. The cone and full uniform bond model and ACI 318-11 procedures were both compared with the component tests in order to verify their effectiveness. Review of the comparisons between the analytical models and the tensile component tests found that both the cone and full uniform bond model and ACI 318-11 provided reasonable predictions for the failure mode of the epoxy adhesive anchors, but both were conservative in prediction of design loads. It was recommended that the ACI 318-11 procedures be combined with the proposed dynamic increase factors for design of epoxy adhesive anchors based on the performance in these comparisons and its wide accessibility and ease of implementation. Following the selection of the ACI 318-11 procedures, a design methodology for the use of epoxy adhesive anchors for cast-in-place concrete bridge rails was presented. This method combines yield line analysis and ACI 318-11 to develop acceptable anchor and barrier designs. Recommendations for future research were made to fill gaps in the existing research effort and to evaluate the conservative nature of the proposed design methodology.</p>			
17. Document Analysis/Descriptors Highway Safety, Epoxy Adhesive Anchors, Dynamic Loads, Concrete Bridge Railing, Bond Stress, Barrier Loads		18. Availability Statement No restrictions. Document available from: National Technical Information Services, Springfield, Virginia 22161	
19. Security Class (this report) Unclassified	20. Security Class (this page) Unclassified	21. No. of Pages 313	22. Price

DISCLAIMER STATEMENT

This report was completed with funding from the Federal Highway Administration, U.S. Department of Transportation. The contents of this report reflect the views and opinions of the authors who are responsible for the facts and the accuracy of the data presented herein. The contents do not necessarily reflect the official views or policies of the Wisconsin Department of Transportation nor the Federal Highway Administration, U.S. Department of Transportation. This report does not constitute a standard, specification, regulation, product endorsement, or an endorsement of manufacturers.

UNCERTAINTY OF MEASUREMENT STATEMENT

The Midwest Roadside Safety Facility (MwRSF) has determined the uncertainty of measurements for several parameters involved in standard full-scale crash testing and non-standard testing of roadside safety features. Information regarding the uncertainty of measurements for critical parameters is available upon request by the sponsor and the Federal Highway Administration. Test nos. WEAB-1 through WEAB-17 were component tests conducted for research and development purposes only.

INDEPENDENT APPROVING AUTHORITY

The Independent Approving Authority (IAA) for the data contained herein was Dr. John Reid, Professor.

ACKNOWLEDGEMENTS

The authors wish to acknowledge several sources that made a contribution to this project:

(1) the Wisconsin Department of Transportation for sponsoring this project, (2) the Hilti Corporation for donating materials and time, and (3) MwRSF personnel for constructing and conducting the component tests.

Acknowledgement is also given to the following individuals who made a contribution to the completion of this research project.

Midwest Roadside Safety Facility

J.D. Reid, Ph.D., Professor
J.C. Holloway, M.S.C.E., E.I.T., Test Site Manager
C.L. Meyer, B.S.M.E., E.I.T., Former Research Associate Engineer
M. Mongiardini, Ph.D., Former Post-Doctoral Research Assistant
A.T. Russell, B.S.B.A., Shop Manager
K.L. Krenk, B.S.M.A., Maintenance Mechanic
S.M. Tighe, Laboratory Mechanic
D.S. Charroin, Laboratory Mechanic
Undergraduate and Graduate Research Assistants

Wisconsin Department of Transportation

Jerry Zogg, P.E., Chief Roadway Standards Engineer
John Bridwell, P.E., Standards Development Engineer
Erik Emerson, P.E., Standards Development Engineer

TABLE OF CONTENTS

TECHNICAL REPORT DOCUMENTATION PAGE	i
DISCLAIMER STATEMENT	ii
UNCERTAINTY OF MEASUREMENT STATEMENT	ii
INDEPENDENT APPROVING AUTHORITY	ii
ACKNOWLEDGEMENTS	iii
TABLE OF CONTENTS	iv
LIST OF FIGURES	viii
LIST OF TABLES	xii
1 INTRODUCTION	1
1.1 Background	1
1.2 Research Objectives	2
1.3 Research Approach	2
2 LITERATURE REVIEW	4
2.1 Overview	4
2.2 Design Standards	4
2.3 Previous Research for Static Tensile Loads	6
2.4 Previous Research for Static Shear Loads	19
2.5 Previous Research for Dynamic Tensile Loads	20
2.6 Material Properties of Structural Epoxy Adhesives	22
2.7 Effects of Protective Coatings on Steel Anchors	24
2.8 Creep Effects of Epoxy Adhesive Anchors	27
2.9 Anchorage Used for Temporary Concrete Barriers	28
2.9.1 F-Shape Steel-Strap Tie-Down with Drop-In Anchors	28
2.9.2 F-Shape Steel-Strap Tie-Down with Mechanical Screw-In Anchors	30
2.9.3 F-Shape Tie-Down with Three A307 Steel Anchors	30
2.9.4 Steel H-Section Temporary Barrier	32
2.10 Anchors Used in Bridge Rail Retrofit Applications	33
2.10.1 California Type 25 Concrete Barrier with Adhesive Anchors	33
2.10.2 UT-Austin Impact Tests on New Jersey Bridge Rails	34
2.10.3 MwRSF Crash Tests with Adhesive Anchors	35
2.10.4 MDOT Analysis of Railings with Adhesive Anchors	36
2.10.5 SUT (10000S) Vehicle Crash Test with New Jersey Barrier	36
2.10.6 Texas T501 and T203 Railings Modified for use with Epoxy Anchors	37
2.11 Load Distributions for Vehicular Bridge Rails	39
2.12 Bridge Railing Design Load Background	41
2.12.1 AASHTO Standard Specifications for Highway Bridges	41

2.12.2 AASHTO LRFD Bridge Design Specifications	42
2.13 State Standard Bridge Rail Designs	45
3 INITIAL MODEL DEVELOPMENT	49
3.1 Overview	49
3.2 Conventional Anchorage Design Strength	49
3.3 Tensile Failure Modes	51
3.4 Tensile Design Models	52
3.4.1 Steel Rupture Model	52
3.4.2 Concrete Cone Model	53
3.4.3 Full Uniform Bond Stress Model	54
3.4.4 Cone or Full Uniform Bond Model	55
3.4.5 Cone or Partial Uniform Bond with Calculated Cone Height	55
3.4.6 Cone or Partial Uniform Bond with Assumed Cone Height	56
3.4.7 Cone or Cone Plus Partial Uniform Bond Model with Calculated Cone Height	56
3.4.8 Cone or Cone Plus Partial Uniform Bond Model with Assumed Cone Height	56
3.4.9 Modified Cone or Cone Plus Partial Uniform Bond Model with Assumed Cone Height	57
3.4.10 Elastic Bond Stress Model	57
3.5 Shear Design Models	64
3.6 Pullout Model Comparisons to Manufacturer Test Data	64
3.6.1 Comparison of Proposed Models with Test Data	66
3.7 Creep Consideration	69
3.8 Discussion	69
4 EPOXY ANCHOR DYNAMIC TESTING	70
4.1 Purpose	70
4.2 Scope	70
4.3 Test Facility	73
4.4 Equipment and Instrumentation	74
4.4.1 Accelerometers	74
4.4.2 Test Jigs	75
4.4.3 Bogie	76
4.4.4 Pressure Tape Switches	78
4.4.5 Digital Cameras	78
4.4.6 Data Processing	79
5 DYNAMIC TESTING RESULTS AND DISCUSSION	81
5.1 Dynamic Testing Results	81
5.1.1 Test No. WEAB-1	82
5.1.2 Test No. WEAB-2	84
5.1.3 Test No. WEAB-3	86
5.1.4 Test No. WEAB-4	88
5.1.5 Test No. WEAB-5	90
5.1.6 Test No. WEAB-6	92

5.1.7 Test No. WEAB-7.....	94
5.1.8 Test No. WEAB-8.....	97
5.1.9 Test No. WEAB-9.....	100
5.1.10 Test No. WEAB-10.....	103
5.1.11 Test No. WEAB-11.....	106
5.1.12 Test No. WEAB-12.....	109
5.1.13 Test No. WEAB-13.....	112
5.1.14 Test No. WEAB-14.....	114
5.1.15 Test No. WEAB-15.....	117
5.1.16 Test No. WEAB-16.....	119
5.2 Discussion of Results.....	122
6 EPOXY ANCHOR STATIC TESTING.....	128
6.1 Purpose.....	128
6.2 Scope.....	128
6.3 Test Setup.....	128
6.4 Test Facility	129
6.5 Equipment and Instrumentation.....	129
6.5.1 Load Cells.....	129
6.5.2 Hydraulic Ram.....	129
6.5.3 Test Jig.....	131
6.5.4 Digital Cameras	131
6.5.5 Data Processing.....	132
7 STATIC TESTING RESULTS AND DISCUSSION	133
7.1 Results.....	133
7.1.1 Test No. WEAB-17.....	133
7.2 Discussion.....	136
8 EVALUATION OF ADHESIVE ANCHOR MODELS	138
8.1 Adhesive Anchor Models	138
8.2 Comparison of Tension Calculation Procedures for Post-Installed Adhesive Anchors.....	141
8.2.1 Non-Factored, As-Tested Materials Comparison	142
8.2.2 Factored, As-Tested Comparison.....	147
8.2.3 Design Comparison.....	156
8.3 Shear Model.....	163
8.3.1 Non-Factored, As-Tested Materials Comparison	163
8.3.2 Factored, As-Tested Comparison.....	168
8.3.3 Design Comparison.....	172
8.4 Discussion of Post-Installed Adhesive Anchor Models.....	176
9 BRIDGE RAIL ANCHORAGE DESIGN METHODOLOGY	179
10 SUMMARY, CONCLUSIONS, AND RECOMMENDATIONS.....	184
10.1 Summary and Conclusions	184
10.2 Recommendations.....	186
10.3 Future Work.....	187

11 REFERENCES 189

12 APPENDICES 197

- Appendix A. Comparison of Epoxy Manufacturers’ Test Data198
- Appendix B. Conventional Anchorage Design Calculations.....203
- Appendix C. Conversion of Cook’s Equations from Metric to English Units212
- Appendix D. Static Model Comparison to Hilti HIT-RE 500 Test Data.....214
- Appendix E. Test Jig Design Calculations and Drawings219
- Appendix F. Test Setup Drawings246
- Appendix G. Material Specifications.....265
- Appendix H. Bogie Test Results.....273

LIST OF FIGURES

Figure 1. Single versus Double Concrete Cone Failures	7
Figure 2. Comparison of Uniform and Elastic Bond Stress Models versus Embedment Depth [10].....	10
Figure 3. Shear Stress Distribution with Increasing Applied Load [13].....	15
Figure 4. Projected Concrete Failure Areas for Adhesive Anchors [15].....	18
Figure 5. Temporary Concrete Barrier Steel Strap Tie-Down.....	29
Figure 6. F-Shape Tie-Downs with 1 1/8 in. (29 mm) A307 Steel Anchors	31
Figure 7. Steel H-Section Temporary Barrier Anchors	32
Figure 8. New Jersey Barrier Used in Crash Test with 10000S Single Unit Truck [48].....	37
Figure 9. Epoxy Anchor Retrofit for the Texas T501 Barrier [49].....	39
Figure 10. Yield Line Patterns for Continuous Bridge Railing [54].....	44
Figure 12. Failure Modes for Epoxy Anchors Loaded in Tension	52
Figure 13. Adhesive Anchor Used to Develop the Elastic Model.....	58
Figure 14. Tension Test Setup, Test Nos. WEAB-1 Through WEAB-4, WEAB-7 and WEAB-8	71
Figure 15. Shear Test Setup, Test Nos. WEAB-5 and WEAB-6.....	72
Figure 16. Tensile Jig.....	75
Figure 17. Shear Jig	76
Figure 18. Tensile Test Setup	77
Figure 19. Shear Test Setup	78
Figure 20. Free Body Diagram of the Tension Test Jig.....	80
Figure 21. Pre- and Post-Test Photographs, Test No. WEAB-1.....	82
Figure 22. Force vs. Time, Test No. WEAB-1	83
Figure 23. Sequential Photographs, Test No. WEAB-1	83
Figure 24. Pre- and Post-Test Photographs, Test No. WEAB-2.....	84
Figure 25. Force vs. Time, Test No. WEAB-2	85
Figure 26. Sequential Photographs, Test No. WEAB-2	85
Figure 27. Pre- and Post-Test Photographs, Test No. WEAB-3.....	86
Figure 28. Force vs. Time, Test No. WEAB-3	87
Figure 29. Sequential Photographs, Test No. WEAB-3	87
Figure 30. Pre- and Post-Test Photographs, Test No. WEAB-4.....	88
Figure 31. Force vs. Time, Test No. WEAB-4	89
Figure 32. Sequential Photographs, Test No. WEAB-4	89
Figure 33. Pre- and Post-Test Photographs, Test No. WEAB-5.....	90
Figure 34. Force vs. Time, Test No. WEAB-5	91
Figure 35. Sequential Photographs, Test No. WEAB-5	91
Figure 36. Pre- and Post-Test Photographs, Test No. WEAB-6.....	92
Figure 37. Force vs. Time, Test No. WEAB-6	93
Figure 38. Sequential Photographs, Test No. WEAB-6	93
Figure 39. Pre- and Post-Test Photographs, Test No. WEAB-7.....	95
Figure 40. Post-Test Anchor Photographs, Test No. WEAB-7	95
Figure 41. Force vs. Time, Test No. WEAB-7	96
Figure 42. Sequential Photographs, Test No. WEAB-7	96
Figure 43. Pre- and Post-Test Photographs, Test No. WEAB-8.....	97
Figure 44. Post-Test Anchor Photographs, Test No. WEAB-8	98

Figure 45. Force vs. Time, Test No. WEAB-8	99
Figure 46. Sequential Photographs, Test No. WEAB-8	99
Figure 47. Pre- and Post-Test Photographs, Test No. WEAB-9.....	100
Figure 48. Post-Test Anchor Photograph, Test No. WEAB-9.....	101
Figure 49. Force vs. Time, Test No. WEAB-9	102
Figure 50. Sequential Photographs, Test No. WEAB-9	102
Figure 51. Pre- and Post-Test Photographs, Test No. WEAB-10.....	103
Figure 52. Post-Test Anchor Photograph, Test No. WEAB-10.....	104
Figure 53. Force vs. Time, Test No. WEAB-10	105
Figure 54. Sequential Photographs, Test No. WEAB-10	105
Figure 55. Pre- and Post-Test Photographs, Test No. WEAB-11.....	106
Figure 56. Post-Test Anchor Photograph, Test No. WEAB-11.....	107
Figure 57. Force vs. Time, Test No. WEAB-11	108
Figure 58. Sequential Photographs, Test No. WEAB-11	108
Figure 59. Pre- and Post-Test Photographs, Test No. WEAB-12.....	109
Figure 60. Post-Test Anchor Photograph, Test No. WEAB-12.....	110
Figure 61. Force vs. Time, Test No. WEAB-12	111
Figure 62. Sequential Photographs, Test No. WEAB-12	111
Figure 63. Pre- and Post-Test Photographs, Test No. WEAB-13.....	112
Figure 64. Force vs. Time, Test No. WEAB-13	113
Figure 65. Sequential Photographs, Test No. WEAB-13	113
Figure 66. Pre- and Post-Test Photographs, Test No. WEAB-14.....	114
Figure 67. Post-Test Anchor Photograph, Test No. WEAB-14.....	115
Figure 68. Force vs. Time, Test No. WEAB-14	116
Figure 69. Sequential Photographs, Test No. WEAB-14	116
Figure 70. Pre- and Post-Test Photographs, Test No. WEAB-15.....	117
Figure 71. Force vs. Time, Test No. WEAB-15	118
Figure 72. Sequential Photographs, Test No. WEAB-15	118
Figure 73. Pre- and Post-Test Photographs, Test No. WEAB-16.....	119
Figure 74. Post-Test Anchor Photograph, Test No. WEAB-16.....	120
Figure 75. Force vs. Time, Test No. WEAB-16	121
Figure 76. Sequential Photographs, Test No. WEAB-16	121
Figure 77. Tension Test Setup, Test No. WEAB-17	130
Figure 78. Static Test Setup.....	131
Figure 79. Pre- and Post-Test Photographs, Test No. WEAB-17.....	133
Figure 80. Force vs. Time, Test No. WEAB-17	134
Figure 81. Sequential Photographs, Test No. WEAB-17	134
Figure 82. Post-Test Anchor Photograph, Test No. WEAB-17.....	135
Figure 83. Schematic of Assumed Epoxy Adhesive Anchor Layout	180
Figure B-1. Wisconsin Sloped Face Parapet ‘LF’ Detailed Drawing [70].....	204
Figure E-1. Tensile Test Jig.....	225
Figure E-2. Tensile Test Jig Weld Details	226
Figure E-3. Tensile Test Jig Base Plate Detail	227
Figure E-4. Tensile Test Jig Kick Plate Detail	228
Figure E-5. Tensile Test Jig W6x25 Beam Detail	229
Figure E-6. Tensile Test Jig Plate Gusset Detail	230
Figure E-7. Tensile Test Jig Post Gusset Detail	231

Figure E-8. Tensile Test Jig Post Stiffener Detail	232
Figure E-9. Tensile Test Jig Wedge Bolt Detail	233
Figure E-10. Tensile Test Jig Bill of Materials.....	234
Figure E-11. Shear Test Jig.....	235
Figure E-12. Shear Test Jig Weld Details.....	236
Figure E-13. Shear Test Jig Base Plate Detail	237
Figure E-14. Shear Test Jig Front Gusset Detail	238
Figure E-15. Shear Test Jig Skid Plate Detail.....	239
Figure E-16. Shear Test Jig Skid Tube Channel Detail	240
Figure E-17. Shear Test Jig Top Gusset Detail.....	241
Figure E-18. Shear Test Jig Coupler Strap Detail.....	242
Figure E-19. Shear Test Jig End Plate Detail	243
Figure E-20. Shear Test Jig Fixture Guide Detail.....	244
Figure E-21. Shear Test Jig Bill of Materials	245
Figure F-1. Tension Test Setup, Test Nos. WEAB-1 Through WEAB-4 and WEAB-7 Through WEAB-8.....	247
Figure F-2. Shear Test Setup, Test Nos. WEAB-5 Through WEAB-6	248
Figure F-3. Anchor Attachment Details, Test Nos. WEAB-1 Through WEAB-8	249
Figure F-4. Test Matrix, Test Nos. WEAB-1 Through WEAB-8	250
Figure F-5. Tension Test Setup, Test Nos. WEAB-9 Through WEAB-12	251
Figure F-6. Shear Test Setup, Test No. WEAB-13.....	252
Figure F-7. Anchor Attachment Details, Test Nos. WEAB-9 Through WEAB-13	253
Figure F-8. Test Matrix, Test Nos. WEAB-9 Through WEAB-13	254
Figure F-9. Tension Test Setup, Test No. WEAB-14.....	255
Figure F-10. Shear Test Setup, Test No. WEAB-15.....	256
Figure F-11. Anchor Attachment Details, Test Nos. WEAB-14 and WEAB-15	257
Figure F-12. Test Matrix, Test Nos. WEAB-14 and WEAB-15	258
Figure F-13. Tension Test Setup, Test No. WEAB-16.....	259
Figure F-14. Anchor Attachment Details, Test No. WEAB-16.....	260
Figure F-15. Test Matrix, Test No. WEAB-16.....	261
Figure F-16. Tension Test Setup, Test No. WEAB-17.....	262
Figure F-17. Anchor Attachment Details, Test No. WEAB-17.....	263
Figure F-18. Test Matrix, Test No. WEAB-17.....	264
Figure G-1. Concrete Cylinder Test Results.....	266
Figure G-2. Concrete Cylinder Test Results.....	267
Figure G-3. Reinforcing Steel Specifications, Test Nos. WEAB-1 Through WEAB-8.....	268
Figure G-4. Reinforcing Steel Specifications, Test Nos. WEAB-9 Through WEAB-13.....	269
Figure G-5. Reinforcing Steel Specifications, Test Nos. WEAB-9 Through WEAB-13.....	270
Figure G-6. Reinforcing Steel Specifications, Test Nos. WEAB-9 Through WEAB-13.....	271
Figure G-7. Reinforcing Steel Specifications, Test Nos. WEAB-9 Through WEAB-13.....	272
Figure H-1. Results of Test No. WEAB-1 (EDR-3).....	274
Figure H-2. Results of Test No. WEAB-1 (DTS).....	275
Figure H-3. Results of Test No. WEAB-2 (EDR-3).....	276
Figure H-4. Results of Test No. WEAB-2 (DTS).....	277
Figure H-5. Results of Test No. WEAB-3 (EDR-3).....	278
Figure H-6. Results of Test No. WEAB-3 (DTS).....	279
Figure H-7. Results of Test No. WEAB-4 (EDR-3).....	280

Figure H-8. Results of Test No. WEAB-4 (DTS).....	281
Figure H-9. Results of Test No. WEAB-5 (EDR-3).....	282
Figure H-10. Results of Test No. WEAB-5 (DTS).....	283
Figure H-11. Results of Test No. WEAB-6 (EDR-3).....	284
Figure H-12. Results of Test No. WEAB-6 (DTS).....	285
Figure H-13. Results of Test No. WEAB-7 (EDR-3).....	286
Figure H-14. Results of Test No. WEAB-7 (DTS).....	287
Figure H-15. Results of Test No. WEAB-8 (EDR-3).....	288
Figure H-16. Results of Test No. WEAB-8 (DTS).....	289
Figure H-17. Results of Test No. WEAB-9 (EDR-3).....	290
Figure H-18. Results of Test No. WEAB-9 (DTS).....	291
Figure H-19. Results of Test No. WEAB-10 (EDR-3).....	292
Figure H-20. Results of Test No. WEAB-10 (DTS Set 1)	293
Figure H-21. Results of Test No. WEAB-10 (DTS Set 2)	294
Figure H-22. Results of Test No. WEAB-11 (EDR-3).....	295
Figure H-23. Results of Test No. WEAB-11 (DTS Set 1)	296
Figure H-24. Results of Test No. WEAB-11 (DTS Set 2)	297
Figure H-25. Results of Test No. WEAB-12 (EDR-3).....	298
Figure H-26. Results of Test No. WEAB-12 (DTS Set 1)	299
Figure H-27. Results of Test No. WEAB-12 (DTS Set 2)	300
Figure H-28. Results of Test No. WEAB-13 (EDR-3).....	301
Figure H-29. Results of Test No. WEAB-13 (DTS Set 1)	302
Figure H-30. Results of Test No. WEAB-13 (DTS Set 2)	303
Figure H-31. Results of Test No. WEAB-14 (EDR-3).....	304
Figure H-32. Results of Test No. WEAB-14 (DTS Set 1)	305
Figure H-33. Results of Test No. WEAB-14 (DTS Set 2)	306
Figure H-34. Results of Test No. WEAB-15 (EDR-3).....	307
Figure H-35. Results of Test No. WEAB-15 (DTS Set 1)	308
Figure H-36. Results of Test No. WEAB-15 (DTS Set 2)	309
Figure H-37. Results of Test No. WEAB-16 (EDR-3).....	310
Figure H-38. Results of Test No. WEAB-16 (DTS Set 1)	311
Figure H-39. Results of Test No. WEAB-16 (DTS Set 2)	312

LIST OF TABLES

Table 1. Material Properties of Hardened Epoxies	23
Table 2. Material Properties Obtained from Epoxy Manufacturers	24
Table 3. Load Distributions for the Texas T203 and T501 Concrete Railings.....	40
Table 4. AASHTO Design Forces and Geometric Properties [54].....	45
Table 5. State Standard Bridge Rail Summary (English Units).....	47
Table 6. State Standard Bridge Rail Summary (Metric Units).....	48
Table 7. Summary of Model Comparison with Hilti Test Data.....	67
Table 8. Dynamic Bogie Test Matrix	73
Table 9. Dynamic Bogie Testing Summary.....	123
Table 10. Comparison of Tensile Capacity Calculations for ACI 318-11 and the Cone or Full Uniform Bond Model.....	140
Table 11. Comparison of ACI 318-11, Cone or Full Uniform Bond Model, and WEAB Testing - Non-Factored and As-Tested Materials.....	146
Table 14. Comparison of ACI 318-11, Cone or Full Uniform Bond Model, and WEAB Testing - Factored and As-Tested Materials.....	155
Table 15. Comparison of ACI 318-11, Cone or Full Uniform Bond Model, and WEAB Testing – Design Data.....	162
Table 16. Comparison of ACI 318-11 Shear Procedures and WEAB Testing - Non-Factored and As-Tested Materials	167
Table 17. Comparison of ACI 318-11 Shear Procedures and WEAB Testing - Factored and As-Tested Materials.....	171
Table 18. Comparison of ACI 318-11 Shear Procedures and WEAB Testing – Design Data...	175
Table A-1. Epoxy Manufacturers’ Test Data with Threaded Rod.....	199
Table A-2. Epoxy Manufacturers’ Test Data with Deformed Reinforcing Bars.....	202
Table D-1. Model Comparison Using the Bond Stress Specified in the Hilti Documentation ..	215
Table D-2. Model Comparison Using the Bond Stress Specified in ICC-ES ESR-2322.....	217

1 INTRODUCTION

1.1 Background

The traditional method for attaching concrete traffic barriers to concrete bridge decks has utilized cast-in-place concrete around vertical reinforcing bars protruding out of the top of the deck slab. However, this technique presents two major shortcomings: (1) it includes the need for extension hand finishing of large portions of the deck; and (2) it lacks the flexibility to be utilized for a variety of different traffic barriers once the deck is formed because vertical cast-in-place anchor bars can only be installed before concrete placement. Alternative anchoring options include post-installed mechanical anchors, chemical or epoxy adhesive, and bolt-through anchors. In particular, previous full-scale crash testing has been successfully conducted on bolt-through designs, however, epoxy adhesive anchorages have had limited testing for bridge rail applications.

Chemical or epoxy adhesive anchors are capable of developing the full strength of the surrounding concrete and can provide tensile and shear strengths comparable to any straight bar anchors in cast-in-place concrete with similar embedment. Further, epoxy adhesive is typically stronger than the surrounding concrete and provides distribution of the anchor loads over a larger area of the concrete. This can result in higher capacities for epoxy adhesive anchors than straight cast-in-place bars with similar embedment depths. However, cast-in-place anchor bars typically contain bent hooks at the end of the embedment depth to increase their strength. This enables the cast-in-place anchor bar to obtain capacities that typically cannot be matched by epoxy adhesive anchors with limited embedment.

Rated shear and tensile capacities published by epoxy adhesive anchor manufactures are largely based on static tests and contain large factors of safety. When used in conjunction with traffic barriers and under impact loading conditions, epoxy adhesive anchors can potentially

resist much higher capacities based on consideration of actual ultimate strengths and dynamic load factors. As such, it may be overly conservative to design epoxy adhesive traffic barrier anchors based solely on their published load ratings.

Additionally, all anchor components used in concrete bridge rail applications are required to have some sort of corrosion protection in order to ensure long term durability. However, published ratings for epoxy adhesive anchor bars are based on testing without any corrosion protection. Corrosion protection could affect anchor capacities as compared to black steel due to the varying frictional resistance of the corrosion protection surfaces. As such, dynamic tests would be required to determine the dynamic capacity of epoxy adhesive anchors when corrosion protection was incorporated in design.

1.2 Research Objectives

The purpose of this research study was to determine if epoxy adhesive masonry anchors can be utilized to attach crash barriers to bridge decks and create a design methodology that can be used to configure epoxy adhesive anchorages for a variety of concrete bridge railings. This would allow for the installation of precast aesthetic concrete traffic barriers or in-board cast-in-place concrete traffic barriers without the need to cast barrier anchorage into the deck surface. Also, the epoxy adhesive anchors could potentially be used to anchor temporary concrete barriers or retrofit permanent concrete or steel bridge railings.

1.3 Research Approach

The research project began with a literature review of previously developed design procedures for estimating the capacity of epoxy adhesive anchors for both static and dynamic loading conditions. A dynamic uniform bond stress model was then developed based on the findings of the literature review and the fundamental mechanics involved with epoxy adhesive anchors. A series of 16 dynamic bogie tests were conducted to refine and verify the accuracy of

the model. A static test was also conducted to investigate the strain rate effects of epoxy adhesive anchorages. Following completion of the component testing, the data was analyzed and compared with the previous developed methodologies for estimation of adhesive anchor capacities. Following that analysis, conclusions and recommendations were prepared regarding procedures for estimating the capacity of epoxy adhesive anchors for use in the attachment of concrete traffic barriers.

It should be noted that the large portion of this research effort was completed and documented as part of the requirements for a master's thesis for Ben Dickey [1].

2 LITERATURE REVIEW

2.1 Overview

For the initial part of the research effort, publications pertaining to the analysis, design, and behavior of epoxy adhesive anchors under static and dynamic loading conditions were examined. Additionally, manufacturers' specifications and Pooled Fund State standards for bridge railings were also investigated to identify the anticipated anchor sizes and requirements.

2.2 Design Standards

A Load and Resistance Factor Design (LRFD) specification for the design of cast-in-place and post-installed mechanical concrete anchors is included in Appendix D of the American Concrete Institute (ACI) publication ACI 318-08, *Building Code Requirements for Structural Concrete and Commentary* [2]. This procedure details the design of single concrete anchors as a function of both material and geometric properties. It also includes procedures to adjust the strength of anchor groups based on the spacing and edge distances from other anchors and concrete edges, respectively. An interaction equation is included that allows for the design of an anchor loaded under simultaneous shear and tension. Strength and reduction factors are provided for the various failure mechanisms to ensure a statistically acceptable measure of reliability.

Several of the design procedures for estimating the capacity of concrete anchors presented in ACI 318-08 come from the Concrete Capacity Design (CCD) method [3]. The CCD method is a simpler design procedure than the one contained in ACI 349-85, *Code Requirements for Nuclear Safety-Related Concrete Structures and Commentary* [4]. For calculation of the concrete breakout strength of anchors in tension, ACI 349-85 assumes a concrete cone shape with the fracture line angled at 45 degrees from the concrete surface. Alternatively, the CCD method assumes a pyramidal concrete shape with the fracture line angled at 35 degrees from the concrete surface to approximate an idealized cone. This allows for easier calculations of the

projected failure surface, especially for a group of closely spaced anchors or anchors located near a concrete edge.

A study conducted in 1995 by Breen, Eligehausen, Fuchs, and Werner evaluated the accuracy of the CCD method and the method presented in ACI 349-85 against a database of reinforcing bar tests [3]. The CCD method correlated rather well with the mean test results for both shear and tensile loads. The procedure presented in ACI 349-85 was found to be conservative for shallow embedment depths and un-conservative for deep embedment depths. However, the CCD method requires greater spacing and edge distances to develop the full capacity strength for both shear and tensile forces. Based on the simpler design procedure and accuracy obtained by the CCD method, the CCD method was recommended over the procedure presented in ACI 349-85.

It should be noted that the method presented in ACI 318-08 does not include provisions to design adhesive anchors embedded in concrete. ACI is currently working on developing a specification that incorporates a design procedure to account for the mechanics of adhesive bonded anchors. Until this study is complete, The International Code Council Evaluation Services Inc. (ICC-ES) publication AC308, *Acceptance Criteria for Post-Installed Adhesive Anchors in Concrete Elements* [5], is being used as an interim design and product approval standard [6]. The design procedure presented in ICC-ES AC308 provides additional and substitutive sections that allow the anchorage procedure in ACI 318-08 to be used in accordance with ICC-ES AC308 to meet the design requirements of adhesive anchors.

In particular, ICC-ES AC308 utilizes a uniform bond stress theory to calculate the pullout strength of anchors in tension. The equation used in the uniform bond stress model to calculate the mean nominal tensile strength (N_n) is shown in Equation (1) and is a function of the uniform bond stress (τ_0), anchor diameter (d), and anchor embedment depth (h_{ef}). Due to the similar

behavior and capacity observed when comparing the shear loading of adhesive and cast-in-place or mechanical anchors, the shear design procedure in AC308 is nearly identical to the procedure in ACI 318-08.

$$N_n = \tau_0 \pi d h_{ef} \quad (1)$$

Difficulty exists in developing a standard for estimating the capacities of adhesive anchors due to the wide variation of many different manufacturers. This is a result of varying material properties (i.e., bond stress) from product to product. For this reason, many designers have utilized manufacturers' specifications based on proprietary shear and tensile test data to design adhesive anchors. Essentially, ICC-ES AC308 provides a more generalized procedure for designing adhesive anchors based on parameters obtained from test data. However, many of the design parameters require extensive testing for each particular product.

2.3 Previous Research for Static Tensile Loads

Previous research has been conducted on adhesive anchors embedded in concrete and subjected to static tensile loading conditions. Many of these research projects focused on developing a theoretical model for predicting the ultimate tensile strength of the adhesive anchor. Then, tests were conducted using a hydraulic ram test machine to validate the proposed theories. Still, much debate exists over how the loads are transferred across the adhesive interface. Two main theories have been proposed: (1) a uniform bond stress distribution over the entire embedment depth and (2) an elastic bond stress distribution.

In 1984, Luke published a thesis that summarized the findings of 69 reinforcing bar pullout tests that utilized an epoxy adhesive as the bonding agent [7]. Four different failure mechanisms were identified and observed: (1) fracturing/yielding of the dowel bar; (2) pullout/excessive slip of the dowel bar; (3) cone failure of the concrete; and (4) splitting of the

concrete. In most cases, a combination of a concrete cone failure and dowel bar pullout slip was present. Both single and double concrete cone failures were observed as shown in Figure 1. The single concrete cone failures had uniform sloped edges at the concrete failure surface. Double concrete cone failures were similar to the single concrete cone failures except that a flexural concrete cone surface of lesser slope was located near the concrete surface. Although there was not a noticeable difference in the pullout strengths observed between the two concrete cone types, the double concrete cone failure generally occurred on bars with deeper embedment depths.

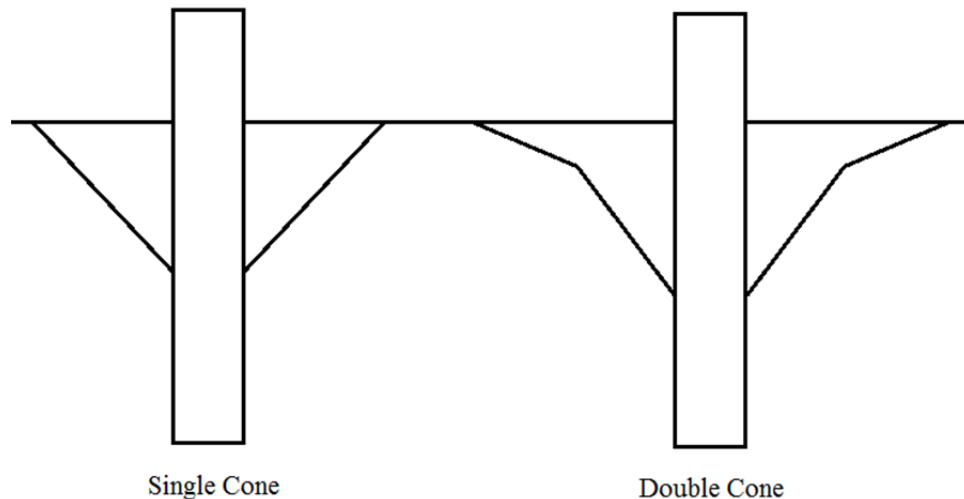


Figure 1. Single versus Double Concrete Cone Failures

Additionally, several methods for cleaning the anchor holes were investigated during the study. It was concluded that drilled holes should be thoroughly cleaned by repeated vacuuming and brushing with a stiff bottle brush or a wire brush. Failure typically occurred along the epoxy-concrete interface for unclean holes and in some cases the concrete cone did not form. For very clean holes, the failure occurred along either the epoxy-steel or epoxy-concrete interfaces. The cleaner holes generally lead to a high pullout strength which suggested that adhesion played an important role in the load transfer at the adhesive interface.

In 1989, Doerr and Klingner suggested that an adhesive anchor loaded in tension has three failure modes: (i) fracture of the anchor steel, (ii) pullout of the adhesive core, and (iii) cone failure of the concrete (with some core pullout) [8]. A test procedure was conducted that consisted of 105 threaded rod specimens adhesively bonded to concrete with embedment depths between 4 and 8 in. (102 and 203 mm). A bond stress distribution model using an elastic solution accurately predicted the test results. The elastic model is based on Equation (2), which is a function of the maximum bond stress (τ_{max}), hole diameter (d_0), anchor embedment depth (h_{ef}), and the adhesive stiffness parameter (λ').

$$N_n = \left(\frac{\pi \tau_{max} d_0^{1.5}}{\lambda'} \right) \tanh \left(\frac{\lambda' (h_{ef} - 2)}{\sqrt{d_0}} \right) \quad (2)$$

A uniform stress distribution model was found to be reasonably consistent with the test results for short embedment depths (less than 8 in. (203 mm)), but grossly overestimated the capacity of longer embedment depths.

The most common failure mode observed was the formation of a shallow concrete cone accompanied by the pullout of the adhesive core. However, concrete cone formation was not found to correlate to a significant increase in the anchor strength. It was concluded that for short embedment depths the capacity of a fully bonded anchor could be closely approximated by the capacity of a partially bonded anchor with the adhesive length equal to the embedment depth less the height of the concrete cone. The typical concrete cone documented in that study had an average height of 1 to 2 in. (25 to 51 mm).

Also in 1989, Collins, Klingner, and Polyzois published a report on the study of several different types of cast-in-place concrete and post-installed adhesive concrete anchors [9]. The load transfer for post-installed adhesive anchors was found to be dependent on the mechanical interlock and chemical bond between both the adhesive and the concrete and the adhesive and

the anchor steel. The failure modes of tensile pullout tests included fracture of the anchor shank, cone failure of the concrete, pullout of the anchor, and pullout of the anchor accompanied by a concrete cone. The anchor pullout behavior occurred with the failure of the bond surfaces between both the adhesive-concrete and adhesive-steel interfaces. However, only a limited number of these failures occurred at the bond surface between the adhesive and the steel.

Two different bond stress models were developed in this study to predict the pullout capacity of adhesive anchors and the concrete cone depth. The first assumed a uniform bond stress over the entire embedment depth while the second assumed a linear stress distribution. For the linear distribution, the bond stress was distributed such that if the stress equaled zero at the bottom of the embedded end of the anchor and had maximum stress at the concrete surface. The majority of the test specimens displayed a failure mode with the formation of a concrete cone that radiated outward from the anchor head and had a depth between 1 and 2 in. (25 and 51 mm). Based on the test data, the height of the concrete cone tended to decrease with increased embedment depth. This behavior would tend to indicate that a non-uniform stress distribution was present. Therefore, a non-uniform bond stress model was suggested. Analysis using finite element methods suggested that the bond stress distribution of adhesive anchors was not only non-uniform, but also non-linear.

In 1993, Cook reviewed several models for predicting the strength of adhesive anchors and developed a new model based on three modes of failure which varied with anchor embedment depth [10]. The three modes were found to be: concrete cone failure, bond failure, and cone-bond failure. Two models of bond failure, a uniform and an elastic bond stress distribution, were analyzed with a database of test data to determine the proper use of each model. The elastic bond stress model matched well with the uniform bond stress model up to bonded lengths of 40 times the square root of the hole diameter in millimeters. A graph of

predicted capacity of the two stress distribution models versus embedment depth is shown in Figure 2.

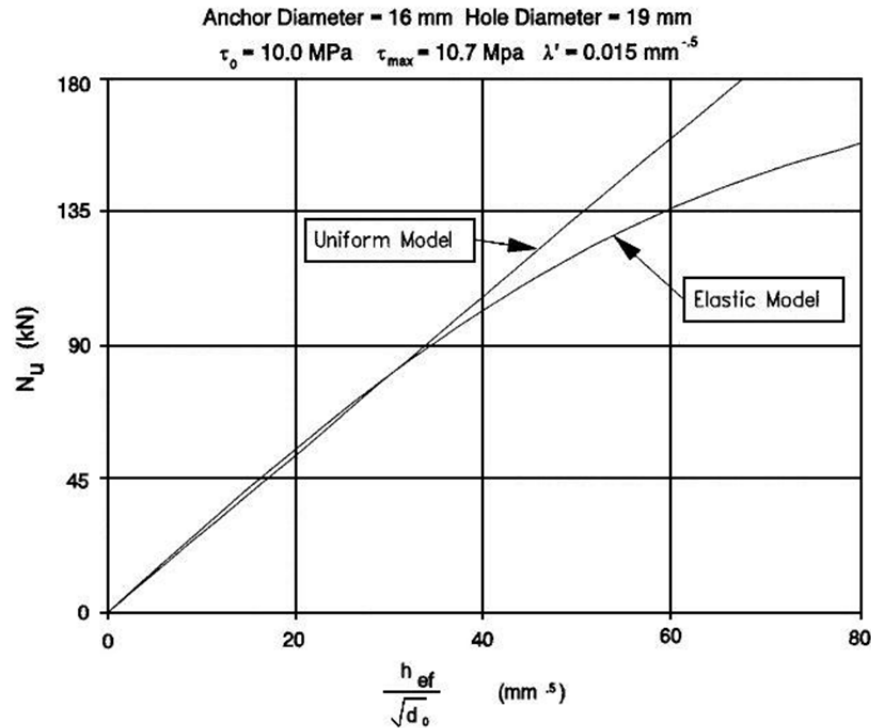


Figure 2. Comparison of Uniform and Elastic Bond Stress Models versus Embedment Depth [10]

Cook developed an equation that estimated the height of the concrete cone (h_{cone}) that was a function of the uniform bond stress (τ_0), the diameter of the hole (d_0), and the compressive strength of the concrete (f_c') as shown by Equation (3). It should be noted that this equation did not agree with the observations by Collins, Klingner, and Polyzois that the height of the concrete cone varied with the anchor embedment depth [9]. Cook suggested that for embedment depths less than the calculated cone height, the concrete cone model should be utilized. The primary variable in the equation to calculate the mean nominal tensile strength (N_n) for the concrete cone model of adhesive anchors was the embedment depth (h_{ef}), as can be seen in Equation (4).

$$h_{cone} = \frac{\tau_0 \pi d_0}{1.84 \sqrt{f'_c}} \quad (3)$$

$$N_n = 0.92 h_{ef}^2 \sqrt{f'_c} \quad (4)$$

For embedment depths greater than the height of the concrete cone but less than 40 times the square root of the hole diameter plus the height of the concrete cone (in millimeters), a uniform stress distribution model with the concrete cone was suggested, as shown by Equation (5).

$$N_n = \tau_0 \pi d_0 (h_{ef} - h_{cone}) + 0.92 h_{cone}^2 \sqrt{f'_c} \left[\frac{40 \sqrt{d_0} - (h_{ef} - h_{cone})}{40 \sqrt{d_0}} \right] \quad (5)$$

For embedment depths over 40 times the square root of the hole diameter plus the height of the concrete cone (in millimeters), the elastic bond stress model with the concrete cone was recommended. Equation (6) was suggested to calculate the mean nominal tensile strength for the elastic model and utilizes the following additional adhesive properties: the maximum bond stress (τ_{max}) and the adhesive stiffness parameter (λ'). The cone breakout strength is not included in this equation because it has a negligible effect on the capacity of anchors with deep embedment depths.

$$N_n = \tau_{max} \pi d_0 \left[\frac{\sqrt{d_0}}{\lambda'} \tanh \frac{\lambda' (h_{ef} - h_{cone})}{\sqrt{d_0}} \right] \quad (6)$$

This method correlated well with the results from the test database and agreed with the conclusion made by Doerr and Klinger that the uniform bond stress model fit the test data for short embedment depths [8]. Both Equation (5) and Equation (6) are based on the geometric variables of the anchor and three basic bond properties: (1) the uniform bond stress (τ_0), (2) the maximum bond stress (τ_{max}), and (3) the adhesive stiffness parameter (λ').

A report by Biller, Cook, Fagundo, and Richardson in 1991 detailed test procedures for determining the three adhesive bond properties [11]. The uniform bond stress was calculated as the failure load divided by the bonded area. The failure load was determined by a confined tensile test using a hydraulic ram. The confined tensile test consisted of placing a bearing surface closely around the anchor to prevent concrete cone breakout and isolate failure of the cohesive bond. During the test, applied loads and the displacements were measured in order to obtain a load-displacement graph. The failure load was determined as the max load prior to slip (nonlinear) was determined as a function of the λ' , d , l , and failure load P . It was determined that d_o was between approximately 0.80 to 0.99 of τ_{\max} . The stiffness parameter of the adhesive was a function of the slope of the linear portion of the load-displacement graph, hole diameter, and embedment length of a given adhesive anchor size.

In 1993, Cook, Doerr, and Klinger published a journal article that verified the accuracy of the elastic model with experimental data [12]. A procedure for calculating the maximum bond stress was proposed that consisted of conducting a pullout test of a partially bonded anchor with the top two inches not bonded to the concrete. This lowered the point of load transfer so that a concrete cone did not form, and the capacities of the partially bonded anchors were only dependent on the adhesive bond. The maximum bond stress was calculated as the ultimate load divided by the bonded area. An alternate method for calculating the stiffness parameter of the adhesive was determined by a least-squares fit between the test data and Equation (6).

A combined cone and bond failure model was derived based on the elastic model, as shown in Equation (7). This equation included the approximate angle of the concrete cone fracture line relative to the concrete surface (α) and the effective concrete tensile stress over the projected area of the cone (f_t).

$$N_n = f_t \pi \left(\frac{h_{cone}}{\tanh(\alpha)} \right)^2 \frac{\sinh\left(\frac{\lambda' h_{ef}}{\sqrt{d_0}}\right)}{\sinh\left(\frac{\lambda' h_{ef}}{\sqrt{d_0}}\right) - \sinh\left(\frac{\lambda' (h_{ef} - h_{cone})}{\sqrt{d_0}}\right)} \quad (7)$$

This model shown in Equation (7) overestimated the tensile capacities observed in the experimental data. Some possible reasons for the inaccuracy of this model were that the bond strength did not appear in the equation, and that the equation included the tensile strength of the concrete, which was highly variable. The elastic bond failure model, shown by Equation (6) proved to be more accurate based on the experimental data. That model assumed that the bond failure occurred after the concrete cone failure. Therefore, the capacity of the anchor was only dependent on the bond stress below the concrete cone.

Further, strength reduction factors were suggested in this study based on the calculated capacity in relation to the horizontal asymptote of the elastic model, calculated by Equation (8). A higher strength reduction factor of 0.80 was utilized when the calculated capacity was greater than or equal to 95 percent of the horizontal asymptote, while a smaller reduction factor of 0.65 was utilized when the calculated capacity was below 95 percent of the horizontal asymptote. The more conservative reduction factor was suggested to be used with shorter embedment depths because a greater drop in the capacity was observed on the elastic bond stress model with decreasing embedment depth.

$$\text{Elastic Model Horizontal Asymptote} = \frac{\pi \tau_{max} d^{1.5}}{\lambda'} \quad (8)$$

Finally, the effect of anchor spacing was also investigated in the study. It was observed that closely spaced, fully bonded anchors had only small concrete cone overlaps that contributed to only a small reduction in the capacity of the adhesive anchors. Therefore, it was suggested that anchor spacing had a negligible effect on the capacity of a group of anchors. However, for

anchor groups with hole diameters between 0.5 and 1.0 in. (13 and 25 mm) and spacings less than 8 in. (203 mm), a capacity reduction of 15 percent was suggested to account for the uncertainty associated with the effects of the overlapping cones until more extensive testing confirmed the effects were negligible. No reduction in capacity was recommended for anchors with spacings greater than 8 in. (203 mm) hole diameters between 0.5 and 1.0 in. (13 and 25 mm).

In 1996, Cook, Krishnamurthy, and McVay reviewed previous empirical and theoretical methods for predicting the failure of chemically bonded anchors loaded in tension, developed an elasto-plastic finite element model of an adhesive anchor, and compared the numerical results to experimental data [13]. The results of the numerical analysis indicated bond stress distribution for relatively low loads corresponded closely with the elastic bond stress model to adhesive anchors. While at higher loads the bond stress distribution displayed a generally uniform bond stress. The uniform bond stress was observed at high loads because the epoxy adhesive and the concrete began to yield, which redistributed the stress toward the bottom of the adhesive layer.

A plot from this study representing the finite element model shear stress distribution along the epoxy-concrete interface of an adhesive anchor with an embedment depth of 5 in. (127 mm) is shown in Figure 3. Five different solutions are shown with increasing applied loads. The left-most line illustrates the elastic bond stress solution that corresponds to a relatively low applied load while the right-most line illustrates the uniform bond stress solution that corresponds to a high applied load. A transition from an elastic bond stress distribution to a relatively uniform bond stress distribution is illustrated by the middle lines. This occurs as the materials begin to yield when the load is increased. Based on this research, a uniform average bond stress applied over the entire embedded anchor area did an excellent job of predicting the tensile failure capacity of the chemically bonded anchors investigated.

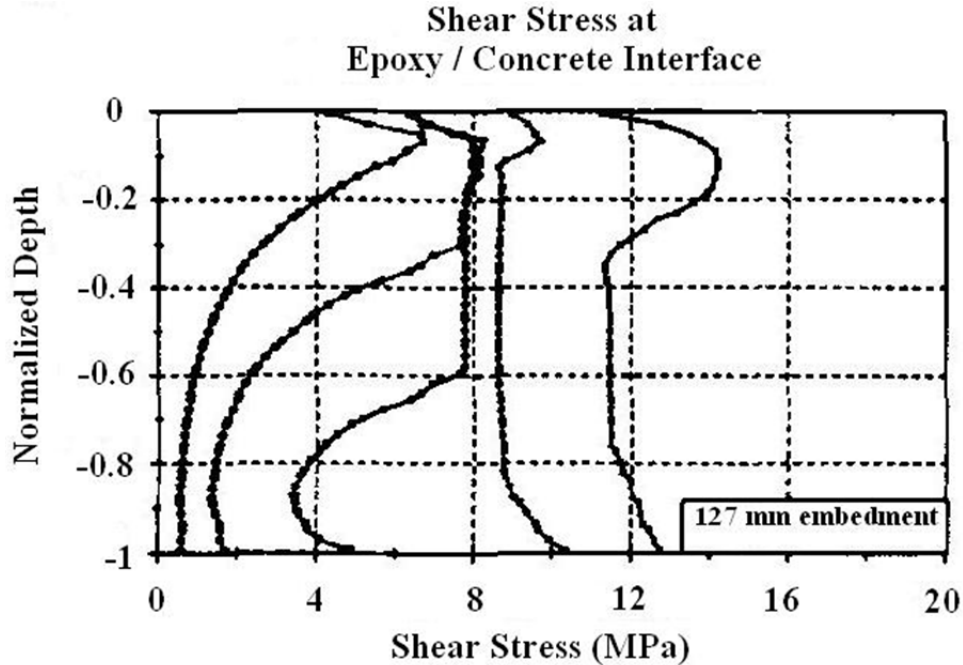


Figure 3. Shear Stress Distribution with Increasing Applied Load [13]

In 1998, Cook, Fuchs, Konz, and Kunz published an article that reviewed several previously developed models for predicting the tensile capacities of adhesive anchors [14]. The models were statistically compared to a worldwide database of test data to determine the accuracy and precision of each method based on varying concrete strength. A new model was then developed that statistically fit the database of pullout tests that were analyzed. This model was based on the uniform bond stress model with an added coefficient to account for the effect of the concrete strength. Equation (9) shows the modified equation as a function of the uniform bond stress (τ_0), anchor diameter (d), embedment depth (h_{ef}), and the modification factor for concrete strength (ψ_c). The modification factor for concrete strength was based on a function of variables determined by tests of individual adhesive products in various concrete strengths.

$$N_n = \tau_0 \pi d h_{ef} \psi_c \quad (9)$$

The concrete cone model, shown in Equation (4), provided the worst fit to the database of adhesive anchor test because of the inherent differences between the behavior of adhesive and mechanical anchors. A uniform bond stress model for use with or without the shallow concrete cone, as shown in Equation (10), provided a good fit to the test data. However, a bond stress model that neglected the stress at the top of the anchor was not considered viable as the stress distribution was not accurate when compared to finite element studies.

$$N_n = \tau_0 \pi d (h_{ef} - 3d) \quad (10)$$

A concrete cone with an adhesive bond model was also investigated that consisted of using either Equation (1) or Equation (4) based on the expected failure mode of either concrete cone or adhesive bond failure. This methodology was ruled out as the uniform bond stress method in Equation (10) fit the data better than the cone failure method in Equation (4) even in the event that a cone failure occurred. A combined concrete cone and bond failure model, shown in Equation (11), was originally thought to provide the best theoretical analysis of adhesive anchors since it accounted for both failure modes present (e.g., partial concrete breakout and partial bond failure). However, in this study, this method did not provide as good of a fit to the database as the uniform bond stress model in Equation (9), which was also easier to implement. As such, the modified uniform bond stress model in Equation (9) was determined to be the best method for approximation of adhesive anchor tensile load.

$$N_n = 0.92h^2\sqrt{f'_c} + \tau_0\pi d(h_{ef} - h_{cone}) \quad (11)$$

Implementation of the coefficient for the concrete strength in the uniform bond stress model reduced the overall coefficient of variation from 0.218 to 0.203. This modified uniform bond stress model exhibited the best fit to the database of all the previously reviewed methods

and was suggested for implementation in future specifications. It also agreed with nonlinear analytical studies of the adhesive concrete anchors.

In 2006, Appl, Cook, and Eligehausen published an article that proposed a behavioral model for predicting the average failure load of adhesive bonded single anchors and groups of anchors embedded in concrete when loaded in tension [15]. The method developed was similar to the method presented in Appendix D of ACI 318-08 and the CCD method based on the square concrete cone assumption. In order to evaluate the new method, several numerical analyses were conducted using a three-dimensional, nonlinear finite element code and was compared to the predicted loads of the model as well as a database of test results.

The new method for predicting any failure load considered the design provisions in ACI 318-08 for steel strength in tension to be applicable to adhesive anchors. A new equation was developed for the tensile pullout capacity of adhesive anchors based on a uniform bond stress model, as shown in Equation (12). This equation utilized the uniform bond stress at the adhesive-steel interface (τ) instead of previous studies where the uniform bond stress was based on the adhesive-concrete interface. The ratio of the projected concrete failure area of a single or group of anchors (A_{Nc}) to the area of the projected concrete failure area of a single anchor (A_{Nco}) was used to account for the overlapping of the concrete cones. These projected areas are shown in Figure 4.

$$N_n = \frac{A_{Nc}}{A_{Nco}} \psi_{ed,N} \psi_{g,N} \tau \pi d h_{ef} \quad (12)$$

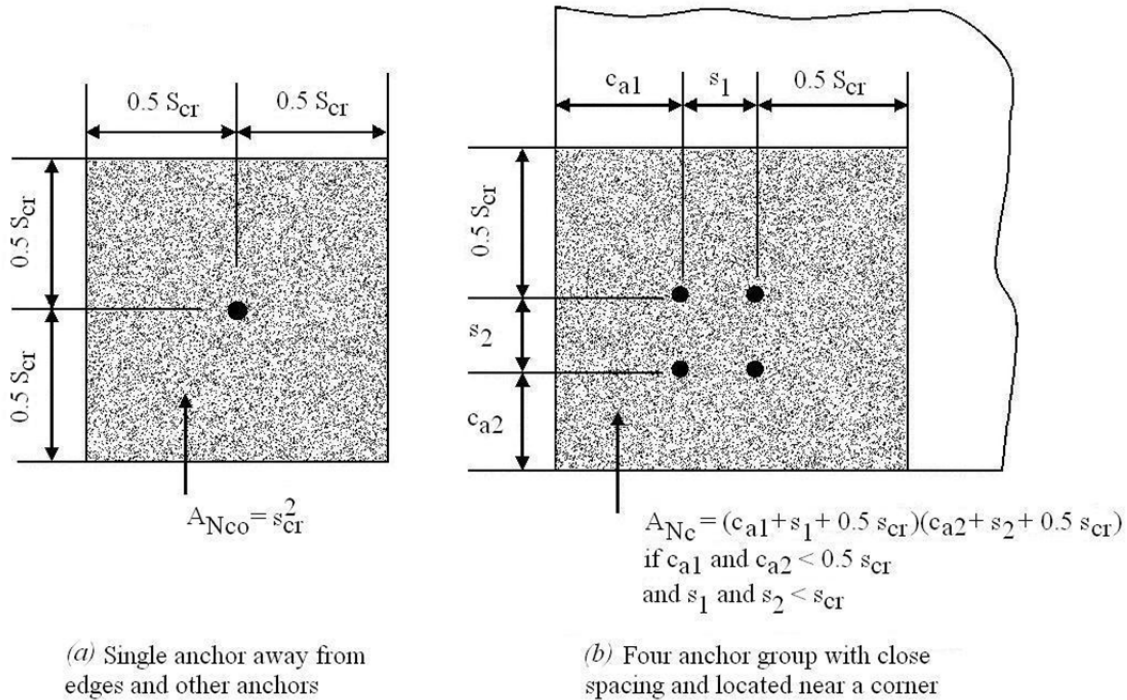


Figure 4. Projected Concrete Failure Areas for Adhesive Anchors [15]

A factor used to modify the tensile strength of anchors based on the proximity to the edges of the concrete member ($\psi_{ed,N}$) and a factor used to modify the tensile strength of adhesive anchors based on the number and spacing of anchors in a group and the mean bond strength ($\psi_{g,N}$) were utilized in the developed model as well. This model agreed with the results obtained from the test database and closely resembles the design procedure that was adopted in ICC-ES AC308 and ACI 318.

The critical anchor spacing (s_{cr}) was defined as the minimum spacing between anchors where the strength of the anchor group was not influenced by the close proximity of the anchors. Equations that calculated the critical anchor spacing were derived by a regression analysis of several anchor tests where the spacing varied. They are shown in Equation (13)(a) for English units and Equation (13)(b) for Metric units.

$$s_{cr,in.} = 20d \left(\frac{\tau}{1450} \right)^{0.5} \quad (13)(a)$$

$$s_{cr,mm} = 20d \left(\frac{\tau}{10} \right)^{0.5} \quad (13)(b)$$

According to the results obtained from the test program in this study, it was observed that the failure load of adhesive anchors was limited to the concrete breakout failure load of post-installed mechanical anchors. Thus, an equation for the maximum bond strength was derived by setting the equation for the capacity of post-installed mechanical anchors equal to the uniform bond stress equation and solving for the bond stress. The resulting equation for the maximum bond stress is shown in English units in Equation (14)(a) and shown in Metric units in Equation (14)(b).

$$\tau_{max,psi} = \frac{11.1\sqrt{f'_c}\sqrt{h_{ef}}}{d} \quad (14)(a)$$

$$\tau_{max,MPa} = \frac{4.7\sqrt{f'_c}\sqrt{h_{ef}}}{d} \quad (14)(b)$$

2.4 Previous Research for Static Shear Loads

In 2002, Bickel and Shaikh conducted a study to determine the differences in capacities of concrete headed stud anchors and adhesive concrete anchors loaded in shear [16]. Design methods based on the shear strength of headed studs were statistically analyzed to determine if the models could be used to predict the shear strength of adhesive anchors. One method was based on the Precast/Prestressed Concrete Institute (PCI) Handbook [17] and the other method was based on the CCD method discussed perviously. The CCD method consisted of calculating a failure surface area to determine the concrete shear strength while the PCI method was a function of the distance from a free concrete edge.

The failure behaviors of adhesive and headed stud anchors loaded in shear are similar because the capacity of both anchors is more dependent by the anchor bearing on the concrete than the adhesive anchors bear on the concrete. However, adhesive anchors investigated in the study of mechanical interlock generally had higher shear capacities compared to headed studs because the adhesive allowed for the stresses to distribute more uniformly over a larger portion of the embedment depth. Based on statistical analysis, the PCI and the CCD methods tended to be more accurate and more conservative in predicting the adhesive anchor capacities than the headed stud capacities.

A regression analysis of the test data for adhesive concrete anchors was performed for both the PCI and CCD methods. The results from this analysis suggested a change to the calibration coefficient in the PCI method from 12.5 to 15 to better predict the capacity of adhesive anchors. The resulting shear strength is shown in Equation (15) where (d_e) is the distance from the anchor to a free concrete edge.

$$V_n = 15\sqrt{f'_c}d_e^{1.5} \quad (15)$$

The CCD equation was also modified based on the regression analysis by changing the calibration coefficient and the exponents of the variables. It was suggested that the modified equation in the CCD method would more accurately and conservatively predict the strength of adhesive anchors loaded in shear. This study was limited to single anchors only, and it did not include an investigation of whether the modification factors which accounted for anchor locations near free edges could be used.

2.5 Previous Research for Dynamic Tensile Loads

Most manufacturers of adhesive anchors publish their rated capacities based on static testing or specifications developed to estimate the static load capacities. Further, the methods for

estimating the capacities presented by ICC-ES AC308 and ACI 318 were developed based on static loading. However, the load rate has an influence on the behavior of adhesive anchors bonded to concrete. Dynamic load capacities of adhesive anchors are generally higher than the rated static capacities. In previous research, many have attempted to correlate the static load capacities with dynamic capacities.

In 2003, Fujikak, Ishibashi, Mindess, Nakayama, and Sato conducted a series of tests on chemically bonded anchors embedded in concrete and subjected to various dynamic, tensile loading rates [18]. A dynamic increase factor (DIF) was defined as the ratio of the average dynamic ultimate bond strength to the average static ultimate bond strength. It was observed that the dynamic increase factor increased as the loading rate increased. An empirical equation based on an exponential regression analysis of the test data was developed to estimate the dynamic increase factor as a function of loading rate. The dynamic increase factor was multiplied by Equation (1) for mean nominal tensile strength to calculate the mean dynamic nominal pullout capacity ($N_{n,d}$) as seen in Equation (16). The last factor in this equation is the dynamic increase factor which is the ratio of the dynamic loading rate (\dot{p}) to the static reference loading rate (\dot{p}_s) raised to the 0.013 power.

$$N_{n,d} = \tau_0 \pi d_0 h_{ef} \left(\frac{\dot{p}}{\dot{p}_s} \right)^{0.013} \quad (16)$$

The most common failure mode observed during testing was adhesive bond stress failure combined with the formation of a concrete cone. The test results indicated that the dynamic pullout strengths were closely related to the calculated values based on the ultimate uniform bond strength. It was observed that the cone failure was fully developed before the bond failure occurred; therefore, the capacity of the adhesive anchor was most commonly controlled by the bond strength of the adhesive anchor below the cone failure. This agrees with the theory

proposed by Cook, Doerr, and Klingner [12], but under dynamic conditions rather than static conditions. It was noted that the behavior of chemically bonded anchors under dynamic loading was strongly dependent on the particular bonding agent.

In 2005, Solomos and Berra utilized a Hopkinson bar technique to determine the effect of dynamic loading rates on post-installed anchors [19]. The static and dynamic test results were compared to the values predicted by the design codes of ACI 349-97 and the CCD method. For static loading conditions, the experimental capacities were always higher than the predicted ones, especially compared to ACI 349-97. The capacities under dynamic loading conditions were substantially higher than the predicted values as the experimental capacities were between 1.59 and 2.39 times as high as the predicted values for static conditions. A dynamic increase factor of 1.25 is permitted to increase the axial concrete strength for impact loads according to ACI 349-97. The study concluded that this dynamic increase factor was reasonable for chemical adhesive anchors. However, the dynamic increase factor of concrete in tension could be as high as 3 or 4 for very high strain rates.

In 2009, Braimah, Constestabile, and Guilbeault conducted several “mass drop” tests on epoxy adhesive anchors. The experiment consisted of a mass falling down a steel guide rod while a PCB Piezotronics preloaded force ring (compression load cell) with a neoprene pad formed an anvil assembly for the falling mass. The dynamic capacities were compared to results obtained from a static test program [20]. It was concluded that the dynamic capacity of adhesive concrete anchors could be increased by minimum factors of 1.2 and 3.2 for normal loads and loads applied at a 45 degree angle, respectively, compared to static capacities.

2.6 Material Properties of Structural Epoxy Adhesives

In 1996, Kruger and Lin conducted several tests to determine the material properties of two different types of epoxy adhesives [21]. Both epoxy adhesive products used in the tests were

two-part cold cure epoxy adhesives. One epoxy adhesive consisted of an unfilled resin and the other epoxy adhesive was a heavily filled resin with a highly dispersed, amorphous, pure silicon filler.

For each material, the tensile strength, compressive strength, Young’s Modulus, shear strength, shear modulus, Poisson’s ratio, and percent elongation at break were determined. The material properties of the two adhesives are shown in Table 1. Several tests were conducted to determine the effects of curing time and temperature on the ultimate bond strength. It was observed that the bond strength of the adhesive was significantly reduced when subjected to moisture. For a hardened concrete to hardened concrete bond, the strength could be reduced by as much as 20 to 50 percent from the effects of moisture. From creep tests, it was concluded that cured epoxy adhesives have low creep strain values compared to other structural adhesives. However, the creep resistance is greatly reduced as the material approaches the heat deflection temperature.

Table 1. Material Properties of Hardened Epoxies

Material Property	Unfilled Epoxy Resin	Heavily Filled Resin with Reinforcing Filler
Tensile Strength	4,950 psi (34.1 MPa)	3,090 psi (21.3 MPa)
Percent Elongation at Break	4.82 %	4.69 %
Compressive Strength	11,200 psi (77.3 MPa)	10,100 psi (69.8 MPa)
Young’s Modulus	464 ksi (3.2 GPa)	609 ksi (4.2 GPa)
Shear Strength	> 5,800 psi (> 40 MPa)	5,800 psi (40 MPa)
Shear Modulus	174 ksi (1.2 GPa)	218 ksi (1.5 GPa)
Poisson’s Ratio	0.39	0.37
Heat Deflection Temperature	124 °F (51.0 °C)	127 °F (52.5 °C)

The material properties for three different manufacturers, Hilti, Adhesives Technologies, and Simpson epoxy adhesive systems were obtained from a review of the manufacturers’ specifications [22-26]. The material properties for several epoxy adhesive products are shown in

Table 2. Summary tables of static tensile and shear capacities for various epoxy adhesive anchor products are shown in Appendix A [22-29].

Table 2. Material Properties Obtained from Epoxy Manufacturers

Material Property	Hilti HIT-RE 500	Adhesives Technology HS2000	Adhesives Technology Ultrabond 1	Adhesives Technology Ultrabond 3	Simpson ET
Bond Strength	1,800 psi (12.4 MPa)	2,400 psi (16.5 MPa)	1,640 psi (11.3 MPa)	1,960 psi (13.5 MPa)	2,030 psi (14.0 MPa)
Compressive Strength	12,000 psi (82.7 MPa)	15,260 psi (105 MPa)	10,990 psi (75.8 MPa)	10,110 psi (69.7 MPa)	13,390 psi (92.3 MPa)
Compressive Modulus	220 ksi (1.52 GPa)	322 ksi (2.22 GPa)	214 ksi (1.48 GPa)	201 ksi (1.39 GPa)	658 ksi (4.54 GPa)
Tensile Strength	6,310 psi (43.5 MPa)	7,080 psi (48.8 MPa)	6,790 psi (46.8 MPa)	7,840 psi (54.1 MPa)	-
Elongation at Break	2.00%	1.50%	1.90%	1.60%	-
Heat Deflection Temperature	146 °F (63.3 °C)	152 °F (66.7 °C)	134 °F (56.7 °C)	138 °F (58.9 °C)	168 °F (75.6 °C)

2.7 Effects of Protective Coatings on Steel Anchors

Galvanized or epoxy-coated steel reinforcement is commonly used on bridge projects to deter the effects of corrosion. In fact, many Midwest Pooled Fund States require bridge rail reinforcement to be epoxy-coated to prevent corrosion due to the use of salt and other chemicals to combat snow and ice. Unfortunately, very little information on the bond strength of epoxy-coated anchors bonded to concrete by the use of an epoxy adhesive was available. However, several sources of epoxy-coated bars bonded to concrete were used to investigate the effects that epoxy coatings have on bond strength.

In 1976, Clifton and Mathey conducted several pullout tests of coated deformed reinforcing bars embedded in concrete [31]. A universal electromechanical testing machine was used to apply a tensile load to the bars with a bearing surface closely surrounding the bars which

prevented a concrete cone failure. Failure was determined by one of the following: (1) a slip of 0.01 in. (0.25 mm) at the loaded end, (2) a slip of 0.002 in. (0.05 mm) at the embedded end, or (3) yielding of the steel bar. The study involved testing several different types of epoxy and polyvinylchloride coatings.

The polyvinylchloride coating bond strengths were considerably less than uncoated bars and were not recommended for structural use. However, epoxy-coated bars with the coating thickness less than 10 mils (0.25 mm) provided bond strengths of only six percent less than the bond strength for uncoated bars and were considered suitable to develop the yield strength of the reinforcement.

In 1989, Jirsa and Treece conducted several tests to compare the development of epoxy-coated reinforcing bars as compared to uncoated bars [32]. The tests consisted of using a four-point beam bending setup with steel reinforcement placed in the tensile region of the beam and reinforcement splices in the middle of the beam. Load was applied to the beam until tensile cracks formed in the constant moment section of the beam. The bond strength was then calculated based on the stress developed in the steel at the time of failure.

After each test, the concrete cover surrounding the reinforcing steel was removed to observe the bond at failure. The uncoated bars showed evidence of good adhesion as concrete particles were firmly attached to the bars. Concrete in contact with the bars had a dull, rough surface, and there was crushing of the concrete due to bearing against the bar lugs. Conversely, the epoxy-coated bars had a smooth glassy surface, and there were no signs that the concrete was crushed against the bar deformations.

The bond strength between the reinforcing bars and the concrete was reduced by 35 percent when the reinforcing bars were coated with epoxy. This reduction in bond strength did not vary with the concrete strength. Design recommendations were proposed which stated that

the required development length should be multiplied by 1.5 for epoxy-coated bars with concrete cover less than three times the bar diameter or clear spacing less than six times the bar diameter. For all other cases of epoxy-coated bars, the required development length should be multiplied by 1.15. However the product of the combining factor for top reinforcement and the epoxy-coated reinforcement factor should never exceed 1.7. These coating factors were later adopted by ACI committee 318 in the *Building Code Requirements for Structural Concrete*. In the literature review, it was noted that the six percent decrease in bond strength from the testing program by Clifton and Mathey [31] did not represent the ultimate bond strength because of the criteria used to categorize failure.

A failure hypothesis in the study explained that two forces, bearing and friction, act on the ribs of the bar. For epoxy-coated bars, the friction component was nearly lost resulting in a reduced bond strength. It was suggested that if the face of the rib formed a 90 degree angle with the axis of the bar, all the bond strength would be produced by direct bearing, and friction would be unnecessary.

In 1991, Yeomans investigated the performance of galvanized and epoxy-coated reinforcing bars embedded in concrete cylinders and exposed to an accelerated corrosion test program [30]. This consisted of two different methods: (i) repetitive wetting and drying of the specimens in a salt bath, and (ii) exposing the specimens in a salt fog chamber. The results of the corrosion tests indicated that the galvanized finish significantly delayed the onset of corrosion as compared to uncoated black steel, and the epoxy coating effectively eliminated corrosion. However, for both the galvanized and epoxy-coated finishes, the coatings needed to be repaired at points where damage to the coatings occurred or else premature corrosion would occur.

The results of the pullout tests conducted in this study indicated that there was not a significant difference in the bond strength between black, galvanized, and epoxy-coated

deformed reinforcing bars. However, for straight, non-deformed segments, there was a 17 percent decrease in the bond strength of epoxy-coated reinforcement and a 31 percent increase in the bond strength of galvanized reinforcement compared to plain black steel reinforcement.

Also in 1991, Cleary and Ramirez conducted 4-point bending slab tests (similar to Jirsa and Treece) to study the effects epoxy coating had on the bond strength to concrete [33]. Independent tests were performed for 4 different splice lengths for both coated and uncoated reinforcement. The epoxy coating contributed to reductions of 15 and 5 percent for specimens where the steel did not yield. For the other two coated test pairs, the steel in the uncoated specimens yielded. The test data was considered not as useful as the other tests, but indicated a strength reduction of at least 15 percent.

In 1992, Cusens and Yu published an article that summarized the findings of pullout tests for three different types of deformed steel reinforcing bars and studied how epoxy coatings affected the bond strength to concrete [34]. The critical bond stress was determined for each test, which corresponded to the lower bond stress value obtained from either the free or the loaded end of the reinforcing bar. The epoxy coating contributed to reductions of 56, 22, and 14 percent for the three different types and sizes of reinforcement. The 56 percent reduction corresponded to a reinforcing bar with significantly smaller deformation rib height and spacing compared to the other two samples. Therefore, a conclusion was made that larger and more closely spaced deformation patterns are required to provide satisfactory bond strengths with epoxy-coated reinforcing bars.

2.8 Creep Effects of Epoxy Adhesive Anchors

Tests to examine the effect of sustained long-term loads are contained in several documents. The ICC-ES report AC58 was published in 1995 and was superseded by AC308 in 2007. These documents are used by manufacturers to qualify their adhesive anchor products. In

AC58, creep testing of adhesive anchors was optional while in AC308, creep testing is mandatory [6]. Creep tests are conducted in uncracked concrete at standard and maximum temperature conditions. The anchor is loaded to 55 percent of its mean ultimate load multiplied by a factor based on concrete strength and the load is sustained for 42 days. Then a confined tension test to failure is conducted on the anchor following the sustained load test. The anchor must achieve at least 90 percent of its tension capacity after the sustained load test to pass creep test criteria.

The ACI 355.4-11 report [35] will replace the AC308 report and contains only minor changes to the creep testing criteria. However, all anchors must be approved for creep in ACI 355.4-11. Therefore, all qualified products are required to pass creep test criteria. The strength of sustained tensile loaded adhesive anchors is also addressed in ACI 318-11 [36]. The nominal capacity of an adhesive anchor subject to sustained tensile loads can only be taken as 55 percent the nominal strength of the anchor.

It is possible that long term tensile loads applied to adhesive anchors that exceed the creep load limit may reduce the capacity of the anchor. As such, it is critical for designers to keep long term loads on adhesive anchors at or below the allowable loads. In addition, users should closely follow manufacturer recommendations for torque requirements when installing threaded rod adhesive anchors such that the anchor preload does not cause anchor creep and a potential reduction in anchor capacity.

2.9 Anchorage Used for Temporary Concrete Barriers

2.9.1 F-Shape Steel-Strap Tie-Down with Drop-In Anchors

MwRSF developed a steel strap tie-down system for the Iowa F-shape temporary concrete barrier in 2002 [37, 38]. The goal of the project was to develop a tie-down system that would constrain and limit barrier deflection and rotation during an impact event and did not

utilize epoxied anchor studs or anchor bolts that passed through the bridge deck. The design consisted of a steel strap that attached to the connecting pin of adjacent barriers and utilized two 3/4 in. (19 mm) diameter by 3 3/8 in. (81 mm) long Red Head drop-in anchors [39]. The actual outside diameter of the sleeve of the drop in anchor was slightly larger than the nominal diameter of the 3/4 in. (19 mm) diameter by 1 3/4 in. (44 mm) long Grade 5 bolts. The results of the crash test demonstrated that a total of 4 anchor bolts (located near the impact location) were pulled completely out of the concrete or sheared off. However, all the remaining bolts were effectively anchored to the concrete decking and retained to PCB system on the simulated bridge deck. The addition of the tie-down strap limited the dynamic deflection to 37.80 in. (0.96 m) as compared to 45.28 in. (1.15 m) in previous testing of the F-shape portable concrete barrier in a free-standing configuration [37, 38]. A picture of the steel strap tie-down design is shown in Figure 5.

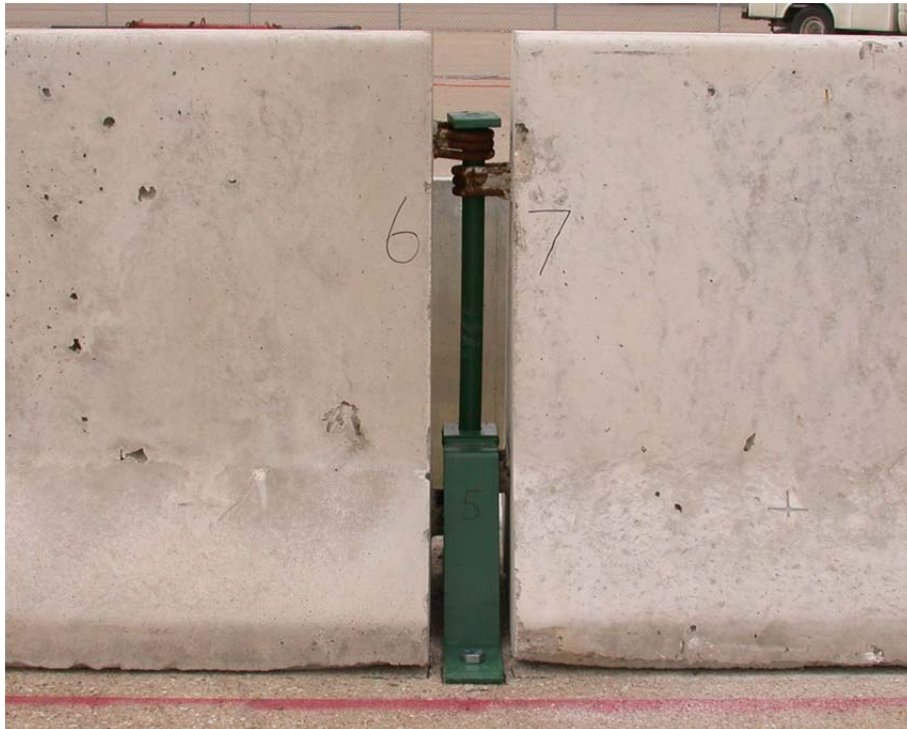


Figure 5. Temporary Concrete Barrier Steel Strap Tie-Down

2.9.2 F-Shape Steel-Strap Tie-Down with Mechanical Screw-In Anchors

An alternative design for anchorage of the steel strap tie-down design was developed by MwRSF in 2007 [40]. Dynamic shear and tensile tests were conducted on the 3/4 in. (19 mm) diameter Red Head drop-in anchor with 3/4 in. Grade 5 bolts used for the original steel strap development in 2002. The average peak tensile load for this anchor was found to be 18.7 kips (83.2 kN) and the average peak shear load was found to be 25.6 kips (113.9 kN). It was desired to replace the drop-in anchor with a screw-in anchor that would be easier to install and remove. Several screw-in anchors were tested and two observations were made: (1) the screw-in anchors generally had higher tensile strengths due to their slightly longer embedment depth and (2) the screw-in anchors did not perform as well with regards to their shear capacity because the smaller diameter anchors produced less earing area on the concrete and the steel used in the mechanical anchors was of lower grade than the Grade 5 bolts used in the drops. It was suggested that any alternative anchors needed to meet a peak tensile load of 18.7 kips (83.2 kN) and a peak shear load of 25.6 kips (113.9 kN) in order to be considered an acceptable retrofit for the 3/4 in. (19 mm) Red Head drop-in anchor. Two alternatives were identified: (1) the Red Head Large Diameter Tapcon (LDT) 3/4 in. (19 mm) diameter by 4 1/2 in. (114 mm) long anchor which had ultimate tensile and shear capacity of 19.5 kips (86.7 kN) and 26.0 kips (115.7 kN), respectively, and (2) the Simpson Titen HD 3/4 in. (19 mm) diameter by 5 in. (127 mm) long anchor which had tensile and shear capacities of 19.0 kips (84.5 kN) and 34.3 kips (152.6 kN), respectively.

2.9.3 F-Shape Tie-Down with Three A307 Steel Anchors

In 2003, MwRSF developed a tie-down system for use on reinforced concrete bridge decks with a redesigned F-shape temporary concrete barrier [41]. This design consisted of bolting through the F-shape barrier at 3 locations along the impact side of the barrier. The threaded rods were made from ASTM A307 steel and had an anchor diameter of 1 1/8 in. (29

mm). The design was successfully crash tested with the anchors attached to a concrete slab by Power Fasteners Power-Fast Epoxy with an embedment depth of 12 in. (305 mm). An alternate anchorage procedure that was considered acceptable was to run the bolt entirely through a bridge deck and use a nut and washer (bearing plate) on the bottom of the bridge deck. The anchorage was intended to develop the ultimate capacity of the A307 threaded rod. A picture of the barrier and bolting pattern is shown in Figure 6. The Wisconsin Department of Transportation adopted this temporary concrete barrier anchorage design and required that epoxy adhesive could be used as long as the adhesure and embankment could develop the ultimate tensile and shear capacity of the A307 threaded rod [42].



Figure 6. F-Shape Tie-Downs with 1 1/8 in. (29 mm) A307 Steel Anchors

2.9.4 Steel H-Section Temporary Barrier

In 2003, MwRSF developed tie down system for a steel H-section temporary barrier to limit the dynamic deflection. The H-section temporary barrier was originally developed in 1989 by MwRSF [37, 43]. The original H-section barrier tie-down design consisted of anchoring the traffic side face of the H-section barrier with two 3/4 in. (19 mm) Red Head drop-in anchors with 3/4 in. (19 mm) ASTM A325 bolts that were 1 3/4 in. (44 mm) long. Four anchors were used with two anchors at each end of the 20-ft (6.10-m) long barrier segments. The initial crash test conducted with a 4,478-lb (2,031 kg) pickup truck failed due to vehicle rollover. Thus, anchor bolts were changed from ASTM A325 to ASTM A307 grade bolts to reduce the load capacity of the tie-down attachments and allow a slight increase in the deflection of the system. Modifications were also implemented to reduce vehicle snag on the face of the barrier. The modified system was successfully crash tested. Four of the anchor bolts failed by shear fracture while one anchor bolt failed by tensile pullout. A picture of the anchorage of the H-section temporary barrier is shown in Figure 7.



Figure 7. Steel H-Section Temporary Barrier Anchors

2.10 Anchors Used in Bridge Rail Retrofit Applications

2.10.1 California Type 25 Concrete Barrier with Adhesive Anchors

In 1979, the California Department of Transportation (CALTRANS) conducted research on utilizing grouted deformed reinforcing bars to attach a new California Type 25 Concrete Barrier to an existing bridge deck [44]. A series of dynamic pullout tests and static barrier tests were performed to evaluate different types of cement and epoxy-mortar grouts. The preferred adhesive material was the Type II Portland Cement Grout because of its superior strength and low cost. However, the average dynamic pullout strength of specimens with an epoxy-mortar was found to be equivalent to the Type II Portland Cement Grout. The anchors were tested with no. 5 and 6 reinforcing bars with embedment depths of 5 and 6 in. (127 and 152 mm).

The dynamic pullout test results of specimens with 5 in. (127 mm) embedment were inconsistent while specimens with 6 in. (152 mm) embedment produced results that were more consistent. The capacity of specimens with 6 in. (152 mm) embedment depths had capacities approximately 40 percent higher than specimens with 5 in. (127 mm) embedment depths.

The conventional anchorage design for the California Type 25 concrete barrier examined utilized cast-in-place no. 5 reinforcing bars with hooks on the embedded ends. The bars were spaced 15 in. (381 mm) apart on the traffic side of the barrier. A no. 5 cast-in-place dowel bar spaced 30 in. (762 mm) apart was utilized on the back side of the railing. A 3-ft (0.91-m) section of the conventional design was constructed and tested by applying a static load to the top of the barrier. This section of the barrier was found capable of sustaining a load of 28.7 kips (128 kN) before failure.

Two retrofit designs were tested using Type II Portland Cement grouted anchors with embedment depths of 5 and 6 in. (127 and 152 mm). The 5-in. (127-mm) embedment design utilized no. 6 (metric no. 19) dowels spaced at 11 in. (279 mm) on the traffic side and 30 in. (762

mm) on the back side of the bridge rail. The 6-in. (152-mm) embedment design utilized no. 6 (metric no. 19) dowels spaced at 15 in. (381 mm) on the traffic side of the bridge rail and 30 in. (762 mm) on the back side of the railing. A 3-ft (0.91-m) section of each design was tested in a similar manner as the conventional design and the ultimate horizontal loads applied at the top of the barriers were 34.3 kips (153 kN) and 41.2 kips (183 kN) for the 5-in. (127-mm) and 6-in. (152-mm) embedment designs, respectively. Both of the retrofit designs demonstrated higher load capacity than the conventional design.

The final retrofit design consisted of using no. 6 (metric no. 19) grouted dowels with embedment depths of 6 in. (152 mm) spaced at 15 in. (381 mm) on the traffic side. The back side of the railing called for no. 6 (metric no. 19) grouted dowels with embedment depths of 5 in. (127 mm) spaced at 30 in. (762 mm). It was suggested that whenever possible, the anchors along the traffic side of the barrier should always have a 6 in. (152 mm) embedment depth. However, in special cases where embedment depths of 6 in. (152 mm) is not possible, slightly less embedment depths should be allowed. Embedment depths less than 5 in. (127 mm) were not recommended or allowed.

2.10.2 UT-Austin Impact Tests on New Jersey Bridge Rails

In 1985, the Center for Transportation Research at the University of Texas at Austin conducted static and dynamic tests that used ASTM A36 anchor bolts to attach cast-in-place and precast New Jersey bridge rails to a standard Texas bridge deck [45]. The goal of the research was to develop an anchorage design that exhibited a ductile failure mode. The original anchorage design utilized 1-in. (25-mm) diameter, ASTM A193 Grade B7 anchor bolts spaced at 50 in. (1,270 mm). Each bolt was attached with washers and nuts on the underside of the slab. It was believed that a more ductile failure mode could be achieved by using 1-in. (25-mm) diameter, ASTM A36 anchor bolts spaced at 25 in. (635 mm) that were attached with nuts on the underside

of the slab. The lower strength ASTM A36 steel was chosen to lower the ultimate strength of the anchors and allow a much longer yield plateau to increase the amount of energy absorbed. Anchor spacings of 50 and 75 in. (1,270 and 1,905 mm) were also tested.

The testing program consisted three static tests and one impact test. A hydraulic ram was used to apply a static force to the top of the 12-ft 6-in. (3.81-m) long barriers. The impact testing consisted of applying a set of three impulse loads which started at low magnitudes and gradually increased until failure.

The barrier was heavily reinforced beyond the normal design to prevent a concrete failure and force anchor failure. However, failure of the concrete still occurred before rupture of the steel anchors. It was noted that the anchors resisted a portion of the shear force at the barrier/deck interface, but for design purposes most of the shear was assumed to be resisted by the frictional force between the barrier and the slab. This assumption was confirmed from the tests as there was no evidence of shear distress in any of the anchor bolts.

For the impact tests, a series of three repeated loads were applied at each load magnitude. Damage and failure of the concrete barrier was observed prior to anchor failure. Thus, anchorage design was considered to lack the required ductility because the anchorage was too strong, which lead to brittle failures of the railing.

2.10.3 MwRSF Crash Tests with Adhesive Anchors

In 1991, MwRSF conducted three crash tests on a modified New Jersey bridge railing with a small car, a pickup truck, and a single unit truck [46]. The bridge railing was attached to a concrete slab-on-ground by two no. 5 reinforcing bars spaced at 12 in. (305 mm) that were embedded 8 in. (203 mm) into the concrete slab. An epoxy grout was used as the bonding agent. Reinforcing bars were placed near the traffic side and the back side of the barrier. The distance between the bars was approximately 10 1/2 in. (267 mm). Although the primary purpose of the

study was not to design the anchorage for the bridge rail, it was observed that the anchorage design was adequate to sustain the loads applied by a 1,759 lb (798 kg) car travelling at a speed of 62.5 mph (100.6 km/h) and at an impact angle of 20 degrees, a 5,460 lb (2,477 kg) pickup truck travelling at a speed of 63.5 mph (102.2 km/h) and at an impact angle of 20 degrees, and an 18,111 lb (8,215 kg) single unit truck travelling at a speed of 52.5 mph (84.5 km/h) and at an impact angle of 16.1 degrees. No visible lateral movement of the bridge rail occurred in any of the crash three tests.

2.10.4 MDOT Analysis of Railings with Adhesive Anchors

In 2001, the Michigan Department of Transportation investigated the effectiveness of using adhesive anchors to retrofit concrete bridge railing attachments to bridge decks [47]. The overall barrier redirective strength was calculated using the AASHTO LRFD Bridge Design Specifications, and the maximum tensile strength of the anchorage was also calculated. The original anchorage design consisted of no. 5 grade 60 steel reinforcement spaced at 12 in. (305 mm) with an embedment depth equal to 7 1/2 in. (191 mm). It was suggested to revise the design to no. 4 grade 60 steel reinforcing bars spaced at 8 in. (203 mm) with a shorter embedment depth of 6 in. (152 mm) to decrease the chance of cracking concrete on the bottom of the bridge deck when drilling holes for the adhesive anchors. The literature review noted that the bond stress at the concrete-epoxy interface for impact loading was found to be 150 percent greater than that of static loading and that cold winter temperatures had no effect on the dynamic bond strength of the anchors tested.

2.10.5 SUT (10000S) Vehicle Crash Test with New Jersey Barrier

In 2006, MwRSF conducted a crash test with a 10000S Single Unit Truck (SUT) vehicle in order to assess the effects of the proposed update the NCHRP Report No. 350 [48]. The permanent reinforced concrete New Jersey safety shape barrier was 32 in. (813 mm) tall and was

attached to a concrete slab-on-ground by two no. 5 reinforcing bars spaced at 8 in. (203 mm) that were embedded 10 in. (254 mm) into the concrete slab. Fast Set Formula Power-Fast High Strength Adhesive Epoxy was used as the bonding agent. The reinforcing bars were placed near the traffic side and back side of the barrier, and the distance between the bars was approximately 11 3/8 in. (289 mm). The 22,045 lb (9,999 kg) SUT impacted the barrier travelling at a speed of 56.5 mph (90.9 km/h) and at an angle of 16.2 degrees. There was no visible lateral movement of the bridge or the bridge rail anchorage due to the impact. Therefore, the anchorage size and spacing was adequate to withstand the impact. However, the crash test was deemed a failure due to the vehicle rolling over the top of the barrier. A cross section of the barrier and reinforcement is shown in Figure 8.

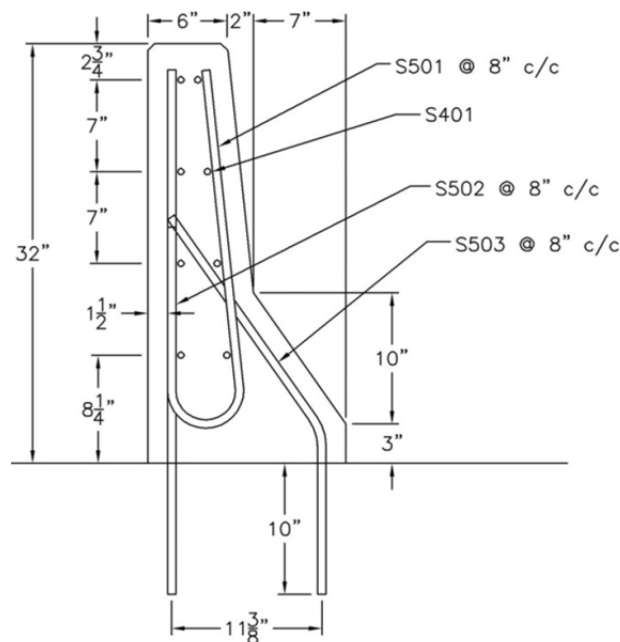


Figure 8. New Jersey Barrier Used in Crash Test with 10000S Single Unit Truck [48]

2.10.6 Texas T501 and T203 Railings Modified for use with Epoxy Anchors

The Texas Transportation Institute (TTI) conducted research on using epoxy adhesive anchors to attach two different types of bridge rails to a standard bridge deck in 2007 [49]. TTI

evaluated the Texas T501 New Jersey-shaped barrier and the Texas T203 open concrete railing with conventional cast-in-place anchoring. The New Jersey-shaped bridge rail design consisted of a 32-in. (813-mm) tall barrier that was continuously attached to the bridge deck with no. 5 U-shaped reinforcing bars spaced at 8 in. (203 mm). The open concrete bridge rail was a 27-in. (686-mm) tall railing that was attached to the bridge deck by 5-ft (1.5 m) wide posts that were spaced between 5-ft (1.5 m) long openings. The conventional anchoring for the open concrete bridge rail consisted of no. 4 U-shaped reinforcing bars spaced at 5 in. (127 mm).

Both static and dynamic tests were conducted for each bridge rail with strain gauges mounted on the reinforcing bars that experienced tensile forces. The static test utilized a hydraulic ram to apply a load to the top of the barriers over a bearing length of 3 ft – 6 in. (1.1 m). A rigid frame bogie with a 3-ft 6-in. (1.1-m) wide crushable nose was used for the dynamic testing.

After observing the tensile forces in the reinforcing bars with conventional cast-in-place anchoring, TTI developed a retrofit design for anchoring the bridge rails to the bridge deck using epoxy adhesive anchors. The bonding agent used for all designs in that report was the Hilti HIT-RE 500 epoxy adhesive. For the continuous New Jersey bridge rail, a single no. 6 reinforcing bars with an embedment depth of 5 1/4 in. (133 mm) spaced at 16 in. (406 mm) in the mid-section of the bridge rail and 8 in. (203 mm) near the ends of the bridge rail were used to develop anchorage to the bridge deck. The middle posts of the open concrete bridge rail utilized two rows of no. 5 reinforcing bars with embedment depths of 5 1/4 in. (133 mm) spaced at 8 in. (203 mm) on the traffic side of the bridge rail and 14 in. (356 mm) on the back side of the bridge rail. The end post section utilized two rows of no. 5 reinforcing bars with embedment depths of 5 1/4 in. (133 mm) spaced at 6 1/2 in. (165 mm) on the traffic side of the bridge rail and 13 in. (330 mm) on the back side of the bridge rail. Both the New Jersey and open concrete rail epoxy adhesive

anchorages were evaluated with bogie crash tests. The results from these tests showed both retrofit anchorage designs to be adequate. A detail of the modified Texas T501 bridge railing with epoxy adhesive anchors is shown in Figure 9.

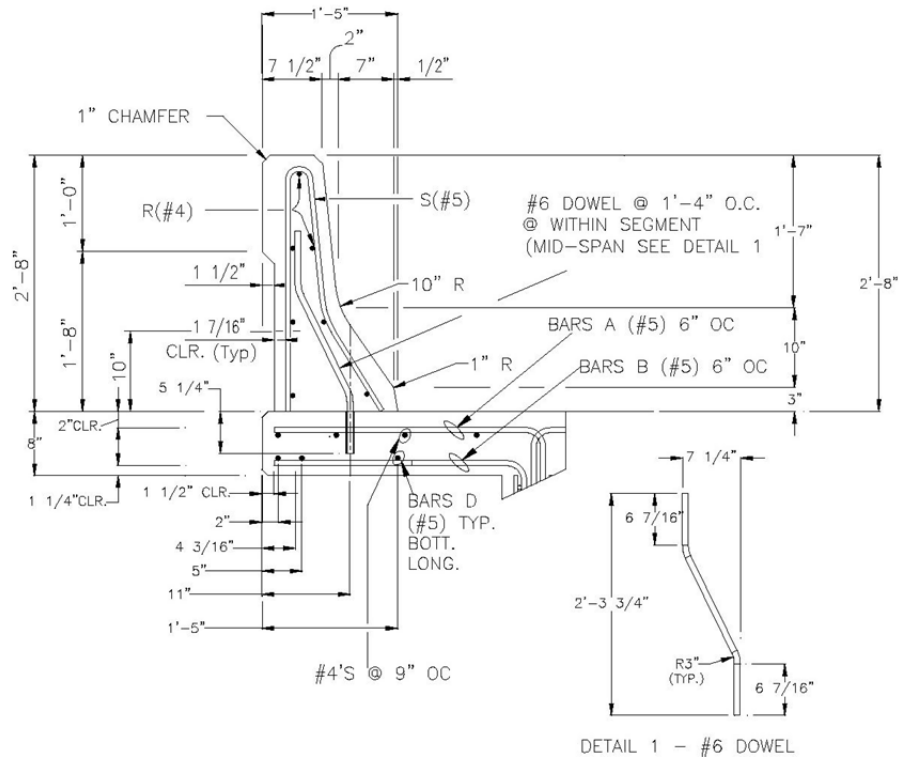


Figure 9. Epoxy Anchor Retrofit for the Texas T501 Barrier [49]

2.11 Load Distributions for Vehicular Bridge Rails

In 2006, the Center for Transportation Research at the University of Texas at Austin analyzed the static and dynamic load distributions that occurred when a lateral load was applied to an open concrete bridge railing and a continuous bridge railing with conventional cast-in-place anchoring [50]. The open concrete rail analyzed was the Texas T203 concrete barrier that consisted of a 14-in. by 13 1/2 -in. (356-mm by 343-mm) concrete railing that was supported by 5-ft (1.52-m) wide by 7 1/2-in. (191-mm) thick posts spaced 10 ft (3.1 m) apart. The continuous railing analyzed was the Texas T501 concrete barrier, which was a 32-in. (813-mm) tall New

Jersey bridge rail. These railings have been crash tested to both TL-3 and TL-4 standards as defined by the National Highway Cooperative Research Program (NCHRP) Report No. 350 [51].

The peak dynamic, 50-ms average dynamic, and static capacities were obtained from testing done by TTI in 2002 [50]. The static and dynamic structural analysis program SAP was used to determine the amount of the barrier capacity that was carried by the overturning capacity of the barrier (e.g., loads that were transferred vertically to the bridge deck beneath the location of the applied load) and the continuity of the barrier (e.g., loads that were transferred longitudinally along the length of the barrier). The findings of the barrier capacities and the proportion of the capacities carried by the stand alone strength of the barrier and anchorage versus the continuity of the barrier are summarized in Table 3.

Table 3. Load Distributions for the Texas T203 and T501 Concrete Railings

			Capacity Carried by the Overturning Resistance of the Anchorage	Capacity Carried by the Continuity of the Barrier
Open Concrete Railing (Texas T203)	Peak Dynamic Capacity	160 kips (712 kN)	30% 50 kips (222 kN)	70% 110 kips (489 kN)
	50-ms Average Dynamic Capacity	68 kips (302 kN)	40% 27 kips (120 kN)	60% 40 kips (178 kN)
	Static Capacity	72 kips (320 kN)	50% 36 kips (160 kN)	50% 36 kips (160 kN)
New Jersey Barrier (Texas T501)	Peak Dynamic Capacity	155 kips (689 kN)	40% 60 kips (267 kN)	60% 95 kips (423 kN)
	50-ms Average Dynamic Capacity	68 kips (302 kN)	54% 37 kips (165 kN)	46% 31 kips (138 kN)
	Static Capacity	70 kips (311 kN)	57% 40 kips (178 kN)	43% 30 kips (133 kN)

For the open concrete rail design under static loading, approximately half the capacity was carried by both the overturning capacity of the posts, while the continuity of the barrier accounted for the other half of the capacity. As the loading rate increased, approximately 10 percent more of the capacity was carried by the continuity of the barrier rather than the overturning capacity and the anchorage beneath the applied load. It was suggested that this barrier needed to withstand a 50-ms average lateral dynamic load of 60 kips (267 kN) and a lateral static load of 54 kips (240 kN) to meet the design requirements of the crash tested barrier. Further, the anchorage capacity of the barrier needed to resist the overturning force.

For the continuous New Jersey barrier, approximately 3 percent more of the capacity was carried by the overturning capacity than the continuity of the barrier under static loads relative to the 50-ms average dynamic load. Results from the dynamic analysis were conflicting as the stand alone capacity carried slightly more of the load when considering the 50-ms average, but slightly less of the capacity when considering the peak dynamic capacity as compared to the capacity of the barrier carried by the continuity of the barrier.

Based on findings from the Center for Transportation Research, approximately 50 percent of the applied lateral loads to bridge barriers are transferred to the anchorage beneath the applied load while the other 50 percent is distributed throughout the longitudinal length of the barrier. Also based on the testing and analysis of the barrier sections, it was observed that the barriers and slab remained essentially elastic throughout the impact. The dynamic increase factor for bridge barriers was proposed to be between 1.2 and 1.6.

2.12 Bridge Railing Design Load Background

2.12.1 AASHTO Standard Specifications for Highway Bridges

The AASHTO Standard Specifications for Highway Bridges [52] has provided guidance for the design loads that bridge railings need to resist. Before 1965, bridge railings were required

to resist a lateral horizontal force of 0.150 kips/ft (2.19 kN/m) and a vertical force of 0.100 kips/ft (1.46 kN/m) applied to the top of the railing [82]. The railing was required to have a minimum height of 27 in. (686 mm) and a maximum height of 42 in. (1,067 mm).

In 1962, because of poor accident history, the U.S. Department of Commerce, Bureau of Public Roads (BPR), which is now the Federal Highway Administration, proposed that bridge railings needed to resist a transverse load of 30 kips (133.4 kN) using plastic design procedures [82].

Later and in 1965, AASHTO adopted the requirement that bridge railings needed to resist a transverse load of 10 kips (44.5 kN) using elastic, allowable stress design procedures. This load was to be applied as a concentrated load at the mid-span of railing panels and distributed over a longitudinal length of 5 ft (1.52 m) for parapet walls. The minimum height of the railing was required to be 27 in. (686 mm). It can be shown that the 10 kip (44.5 kN) load as determined by elastic analysis is approximately equal to a 30 kip (133.4 kN) load calculated by plastic analysis [82]. It is possible that the elastic design procedure was ultimately adopted because many of the AASHTO members were unfamiliar with plastic design procedures. This 10 kip (44.5 kN) load requirement essentially remained the same for the remaining releases of the AASHTO Standard Specifications for Highway Bridges.

2.12.2 AASHTO LRFD Bridge Design Specifications

In recent years, the AASHTO Load and Resistance Factor Design (LRFD) Bridge Design Specifications [54] has replaced the AASHTO Standard Specifications for Highway Bridges [52], and as of 2007, only the LRFD code has been allowed for new designs. Included in the AASHTO LRFD Bridge Design Specifications is an ultimate bridge rail design method based on yield line theory. Yield line design is an ultimate strength, plastic design procedure that is based on the principle that the internal energy absorbed by deformation equals the external work from

the applied forces and deflections [53]. The ultimate capacity calculated from the yield line analysis must be greater than the load imparted to the railing from the vehicle to ensure the adequacy of the bridge railing.

One of the key steps in determining the ultimate capacity using yield line theory is correctly predicting the yield line pattern. Yield line patterns are estimated configurations of the plastic hinges that form in two dimensional members such as panels, walls, floors, and slabs. Often times in loaded concrete walls and slabs, yield lines are visible as crack patterns. Theoretically, several yield line patterns could occur in a structure. However, one configuration will provide the lowest failure load. This configuration is known as the yield line solution. An investigation of only a few simple and obvious patterns is needed because the solutions of these patterns are usually within a few percent of the correct solution [53].

In the AASHTO LRFD Bridge Design Specifications [54], the yield line patterns have already been derived as well as simple, user-friendly equations that coincide with the yield line pattern. The bridge railing needs to be analyzed at both the middle of the railing and at the ends to account for interior and end vehicular impacts, respectively. The yield line patterns for an interior and end region of a continuous parapet are shown in Figure 10. As can be seen, the interior regions consist of three cracks, or yield lines, while the end region only contains only one yield line.

Based on the yield line patterns shown in Figure 10, the AASHTO LRFD Bridge Design Manual provides equations for the nominal railing resistance to transverse load applied at the top of the wall (R_w). This is a function of the critical length of the yield line pattern failure (L_c), the longitudinal length of distribution of impact forces (L_t), the flexural resistance of the cantilevered walls about an axis parallel to the longitudinal axis of the bridge (M_c), the flexural resistance of the wall about its vertical axis (M_w), the additional flexural resistance of a beam in

addition to M_w (M_b), and the height of the wall (H). The equations for the nominal railing resistance to transverse load for the interior and end regions of a railing are shown in Equations (17) and (19), respectively.

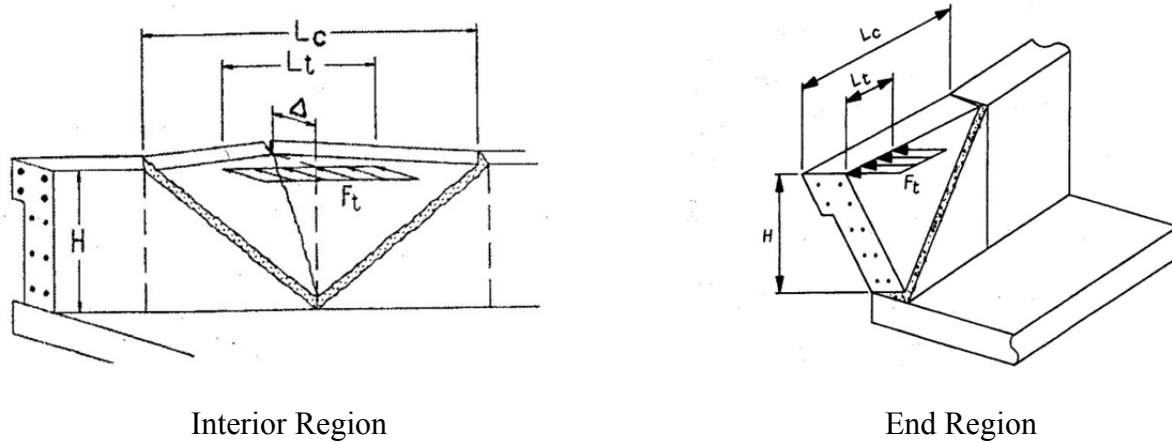


Figure 10. Yield Line Patterns for Continuous Bridge Railing [54]

For Interior Regions:

$$R_w = \left(\frac{2}{2L_c - L_t} \right) \left(8M_b + 8M_w + \frac{M_c L_c^2}{H} \right) \quad (17)$$

$$L_c = \frac{L_t}{2} + \sqrt{\left(\frac{L_t}{2} \right)^2 + \frac{8H(M_b + M_w)}{M_c}} \quad (18)$$

For End Regions:

$$R_w = \left(\frac{2}{2L_c - L_t} \right) \left(M_b + M_w + \frac{M_c L_c^2}{H} \right) \quad (19)$$

$$L_c = \frac{L_t}{2} + \sqrt{\left(\frac{L_t}{2} \right)^2 + H \left(\frac{M_b + M_w}{M_c} \right)} \quad (20)$$

Table A13.2-1 in the 2007 AASHTO LRFD Bridge Design Manual also provides required design forces and geometric parameters for the yield line analysis procedure. These values are shown in Table 4. The parameters correspond to test level conditions consistent with

NCHRP Report No. 350 [51]. The load levels were determined from full-scale instrumented wall crash tests to measure the forces imparted to “rigid” barriers. These instrumented wall tests consisted of four relatively rigid concrete wall panels that were supported laterally by load cells to measure the impact force magnitude and location. The panels were instrumented with accelerometers to account for inertial effects. The force data was processed by averaging the data over 50 millisecond intervals [55]. Therefore, the transverse force (F_t) is the ultimate lateral 50 ms average dynamic load required to resist the impact.

Table 4. AASHTO Design Forces and Geometric Properties [54]

Design Forces and Designations	Railing Test Levels					
	TL-1	TL-2	TL-3	TL-4	TL-5	TL-6
F_t Transverse, kips (kN)	13.5 (60)	27 (120)	54 (240)	54 (240)	124 (552)	175 (778)
F_L Longitudinal, kips (kN)	4.5 (20)	9 (40)	18 (80)	18 (80)	41 (182)	58 (258)
F_v Vertical Down, kips (kN)	4.5 (20)	4.5 (20)	4.5 (20)	18 (80)	80 (356)	80 (356)
L_t and L_L , ft (m)	4 (1.22)	4 (1.22)	4 (1.22)	3.5 (1.07)	8 (2.44)	8 (2.44)
L_v , ft (m)	18 (5.49)	18 (5.49)	18 (5.49)	18 (5.49)	40 (12.19)	40 (12.19)
Min H_e , in. (mm)	18 (457)	20 (508)	24 (610)	32 (813)	42 (1,067)	56 (1,422)
Min H , in. (mm)	27 (686)	27 (686)	27 (686)	32 (813)	42 (1,067)	90 (2,286)

2.13 State Standard Bridge Rail Designs

In order to develop an anchorage design procedure that would enable the new and retrofit barriers to behave similarly to the barriers with conventional cast-in reinforcing bars, the standard bridge rail plans for several Midwest Pooled Fund States were reviewed. Tables 5 and 6 summarize the sizes, shapes, and anchor spacings for several state standard bridge railings [56-76]. The anchorage designs were similar for all continuously attached barriers. Vertical, New

Jersey, and F-shaped barriers utilized stirrups that consisted of either no. 4, 5, or 6 reinforcing bars spaced between 8 and 12 in. (203 and 305 mm) for barriers of heights between 20 and 51 in. (0.51 and 1.30 m). No. 5 bars were the most commonly used bar size, and the equivalent steel area for the barrier anchorages ranged from 0.62 to 0.93 square inches per foot of barrier (1,312 to 1,969 square millimeters per meter of barrier). The open concrete rail designs consisted of posts with no. 7 bars on the traffic side face and no. 4 bars on the outside face of the barrier. There was no uniform spacing design for the open concrete rail due to the differing widths of the posts, but most posts had an equivalent steel area of approximately 2 square inches per foot of post (4,233 square millimeters per meter of post). Most reinforcing bars required some type of protective coating that consisted of either a galvanized finish or, most commonly, an epoxy coating. Bent hooks at the ends of the embedded bars were commonly used for anchorage.

Table 5. State Standard Bridge Rail Summary (English Units)

State	Bridge Rail Type	Anchor Rebar Size/Spacing	Steel Area Per Foot (in. ²)	Barrier Height	Other Notes
FL	Traffic Railing 'F' Shape - 32"	2-#5 @ 8" O.C.	0.93	2'-8"	See details for bar shapes, 6" min embedment depth
	Traffic Railing 'F' Shape - 42"	2-#5 @ 8" O.C.	0.93	3'-6"	See details for bar shapes, 8" min embedment depth
	Traffic Railing 'F' Shape Median	2-#5 @ 12" O.C.	0.62	2'-8"	See details for bar shapes, 6" min embedment depth
	Traffic Railing Vertical Shape - 32"	2-#5 @ 12" O.C.	0.62	2'-8"	Upside down U-stirrups with tail, 6" min embedment depth
	Traffic Railing Vertical Shape - 42"	2-#5 @ 12" O.C.	0.62	3'-6"	Upside down U-stirrups with tail, 6" min embedment depth
	Traffic Railing - Corral Shape	12-#4 @ Post, 12-#7 @ Post, Posts @ 10' O.C.	0.96	2'-8"	#7 bar= upside down U-stirrups with hook, #4 bar= L-shaped, 5' wide posts, 6" min embedment depth, 1.92 in. ² per foot of steel at the post
IA	Barrier Rail 2'-10"	2-#5 @ 12" O.C.	0.62	2'-10"	Epoxy-coated rebars, U-stirrups with hooks, 2" min clear cover, F-shaped
	Barrier Rail 3'-8"	2-#5 @ 12" O.C.	0.62	3'-8"	Epoxy-coated rebars, U-stirrups with hooks, for the first 4' from abutments of bridge: 2-#5 @6" O.C., required steel=1.24 in ² /ft, 2" min clear cover, F-shaped
IL	F Shaped Parapet	2-#5 @ 11" O.C.	0.68	2'-10" or 3'-6"	Epoxy-coated rebars, upside down V-stirrups with hooks
KS	F4 Barrier Curb	2-#5 @12" O.C.	0.62	2'-8"	Epoxy-coated rebars, upside down V-stirrups with hooks, F-shaped
	Corral Rail	8-#7 @ Post, 8-#4 @ Post, Posts @10' O.C.	0.64	2'-3" or 2'-8"	Epoxy-coated rebars, L-shaped bars @ slab/rail interface, 3' wide posts, 2.13 in. ² per foot of steel at the post
MO	CIP Barrier Curb	2-#5 @ 12" O.C.	0.62	2'-8"	Galvanized rebars, see details for bar shapes, NJ-shaped
	CIP Barrier Curb (Type D)	2-#5 @ 12" O.C.	0.62	3'-6"	Galvanized rebars, see details for bar shapes
OH	Bridge Railing Deflector Parapet	2-#6 @ 12" O.C.	0.88	3'-0" or 3'-6"	See details for bar shapes, NJ-shaped
WI	Sloped Face Parapet 'LF'	2-#5 @ 8" O.C.	0.93	2'-7 7/8"	Epoxy-coated rebars, upside down V-stirrups with hook, preferred on state and interstate highway bridges, 2" min clear cover, F-shaped
	Sloped Face Parapet 'HF'	2-#5 @ 8" O.C.	0.93	3'-6 1/8"	Epoxy-coated rebars, upside down V-stirrups with hook, used where there is a high truck traffic and curved horizontal alignment, 2" min clear cover, F-shaped
	Sloped Face Parapet '51F'	2-#5 @ 8" O.C.	0.93	4'-3"	Epoxy-coated rebars, upside down V-stirrups with hook, used in median area of adjacent structures, 2" min clear cover, F-shaped
	Sloped Face Parapet 'B'	2-#4 @ 9" O.C.	0.53	2'-8"	Epoxy-coated rebars, upside down V-stirrups with hook, 2" min clear cover, NJ-shaped
	Vertical Face Parapet 'TX'	2-#5 @ 9" O.C.	0.83	3'-6"	Epoxy-coated rebars, upside down U-stirrups with hook, decorative railing with windows, 2" min clear cover
	Vertical Face Parapet 'A'	2-#5 @ 12" O.C.	0.62	1'-8" or 2'-8"	Epoxy-coated rebars, upside down U-stirrups with hook, railing to be used alongside pedestrian walkway, 2" min clear cover

Table 6. State Standard Bridge Rail Summary (Metric Units)

State	Bridge Rail Type	Anchor Rebar Size/Spacing	Steel Area Per Meter (mm ²)	Barrier Height	Other Notes
FL	Traffic Railing 'F' Shape - 32"	2-#16 @ 203 mm O.C.	1,969	0.81 m	See details for bar shapes, 152 mm min embedment depth
	Traffic Railing 'F' Shape - 42"	2-#16 @ 203 mm O.C.	1,969	1.07 m	See details for bar shapes, 203 mm min embedment depth
	Traffic Railing 'F' Shape Median	2-#16 @ 305 mm O.C.	1,312	0.81 m	See details for bar shapes, 152 mm min embedment depth
	Traffic Railing Vertical Shape - 32"	2-#16 @ 305 mm O.C.	1,312	0.81 m	Upside down U-stirrups with tail, 152 mm min embedment depth
	Traffic Railing Vertical Shape - 42"	2-#16 @ 305 mm O.C.	1,312	1.07 m	Upside down U-stirrups with tail, 152 mm min embedment depth
	Traffic Railing - Open Concrete Rail	12-#13 @ Post, 12-#22 @ Post, Posts @3 m O.C.	2,032	0.81 m	#22 bar= upside down U-stirrups with hook, #13 bar= L-shaped, 1.52 m wide posts, 152 mm min embedment depth, 4,065 mm ² per foot of steel at the post
IA	Barrier Rail 2'-10"	2-#16 @ 305 mm O.C.	1,312	0.86 m	Epoxy-coated rebars, U-stirrups with hooks, 51 mm min clear cover, F-shaped
	Barrier Rail 3'-8"	2-#16 @ 305 mm O.C.	1,312	1.12 m	Epoxy-coated rebars, U-stirrups with hooks, for the first 1.22 m from abutments of bridge: 2-#16 @152 mm O.C., required steel=2,265 mm ² /m, 51 mm min clear cover, F-shaped
IL	F Shaped Parapet	2-#16 @ 279 mm O.C.	1,440	0.86 or 1.07 m	Epoxy-coated rebars, upside down V-stirrups with hooks
KS	F4 Barrier Curb	2-#16 @305 mm O.C.	1,312	0.81 m	Epoxy-coated rebars, upside down V-stirrups with hooks, F-shaped
	Corral Rail	8-#22 @ Post, 8-#13 @ Post, Posts @3 m O.C.	1,355	0.69 or 0.81 m	Epoxy-coated rebars, L-shaped bars @ slab/rail interface, 0.91 m wide posts, 4,508 mm ² per foot of steel at the post
MO	CIP Barrier Curb	2-#16 @ 305 mm O.C.	1,312	0.81 m	Galvanized rebars, see details for bar shapes, NJ-shaped
	CIP Barrier Curb (Type D)	2-#16 @ 305 mm O.C.	1,312	1.07 m	Galvanized rebars, see details for bar shapes
OH	Bridge Railing Deflector Parapet	2-#19 @ 305 mm O.C.	1,863	0.91 or 1.07 m	See details for bar shapes, NJ-shaped
WI	Sloped Face Parapet 'LF'	2-#16 @ 203 mm O.C.	1,969	0.81 m	Epoxy-coated rebars, upside down V-stirrups with hook, preferred on state and interstate highway bridges, 51 mm min clear cover, F-shaped
	Sloped Face Parapet 'HF'	2-#16 @ 203 mm O.C.	1,969	1.07 m	Epoxy-coated rebars, upside down V-stirrups with hook, used where there is a high truck traffic and curved horizontal alignment, 51 mm min clear cover, F-shaped
	Sloped Face Parapet '51F'	2-#16 @ 203 mm O.C.	1,969	1.30 m	Epoxy-coated rebars, upside down V-stirrups with hook, used in median area of adjacent structures, 51 mm min clear cover, F-shaped
	Sloped Face Parapet 'B'	2-#13 @ 229 mm O.C.	1,122	0.81 m	Epoxy-coated rebars, upside down V-stirrups with hook, 51 mm min clear cover, NJ-shaped
	Vertical Face Parapet 'TX'	2-#16 @ 229 mm O.C.	1,756	1.07 m	Epoxy-coated rebars, upside down U-stirrups with hook, decorative railing with windows, 51 mm min clear cover
	Vertical Face Parapet 'A'	2-#16 @305 mm O.C.	1,312	0.51 or 0.81 m	Epoxy-coated rebars, upside down U-stirrups with hook, railing to be used alongside pedestrian walkway, 51 mm min clear cover

3 INITIAL MODEL DEVELOPMENT

3.1 Overview

Design procedures for cast-in-place and post-installed mechanical anchors have been established and accepted by various organizations. The mechanics involved with these types of anchors can be explained with relatively simple equations. However, the strength and mechanics involved with adhesive anchors is highly dependent on the particular adhesive product. This makes it difficult to develop a general design procedure that is applicable for all adhesive anchors. As a result, the design of adhesive anchors is highly dependent on test data obtained from the manufacturer or an independent testing organization. This test data is usually very discrete and does not provide for much flexibility for scenarios not explicitly tested.

Several manufacturers have adopted the design procedure contained in ICC-ES AC308 which allows for much more flexibility of the physical aspects of the anchorage design (i.e. anchor size, embedment depth, spacing, etc). However, due to the complicated mechanics involved with adhesive anchors, extensive testing is required to determine the large amount of input parameters necessary for the design equations. In addition, the parameters developed for this procedure are based on static load conditions and does not take into consideration the dynamic effects of impact loading conditions.

3.2 Conventional Anchorage Design Strength

Concrete barriers that utilize epoxy adhesive anchorages need to develop either the strength of the conventional cast-in-place anchorage design or that required by the American Association of State Highway and Transportation Officials (AASHTO) LRFD Bridge Design Specification [77]. Section 13 of the AASHTO LRFD Bridge Design Specification states that minor details in approved crash tested designs for bridge rails can be changed provided that the proposed installation does not detract from the performance of the crash tested rail system [77].

Therefore, in order to retrofit epoxy adhesive anchors into an existing cast-in-place barrier, analytical calculations are needed first to determine the strength of the conventional design.

As illustrated in Chapter 2, the standard anchorage design with the most strength for the State of Wisconsin and the other Pooled Fund States utilized two no. 5 epoxy-coated reinforcing bars spaced 8 in. apart on center. Both shear and moment strengths are necessary to redirect a vehicle. Subsequently, both the shear and the overturning moment capacities of the original barrier must be achieved in an epoxy adhesive anchorage design. The Wisconsin Standard Sloped Face Parapet 'LF' bridge rail was selected as the baseline design because it is preferred on most state and interstate highway bridges [76] and it consisted of upside down U-shaped, epoxy coated no. 5 stirrups with a hooked end spaced at 8 in. (203 mm) on center. Figure 11 shows a cross-section of the barrier while detailed drawings and static calculations of the strength of this bridge rail are shown in Appendix B.

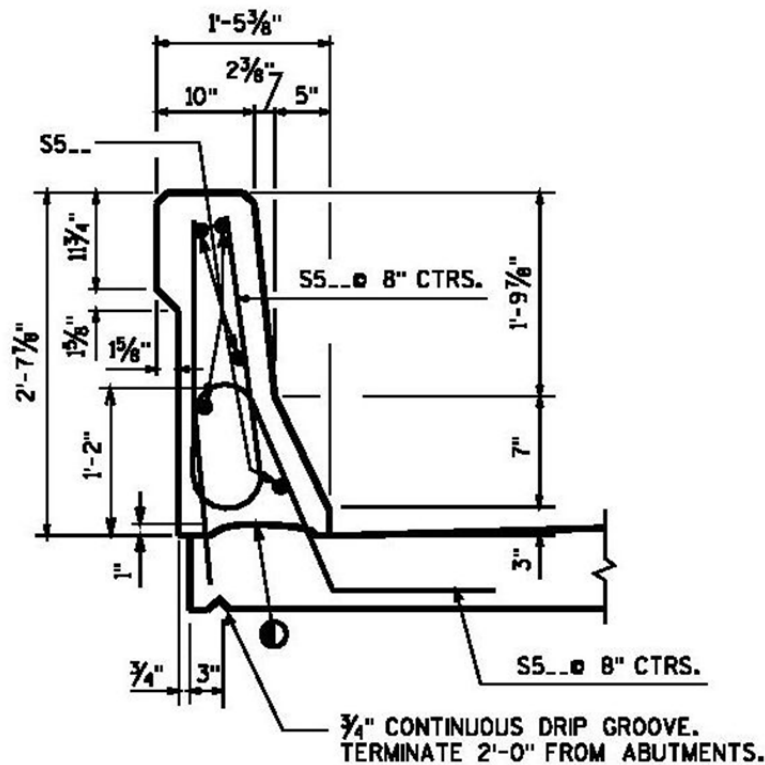


Figure 11. Wisconsin Sloped Face Parapet 'LF' Cross-Sectional Drawing [70]

The overturning moment capacity of the Wisconsin Sloped Face Parapet 'LF' bridge rail is determined by the tensile force in the hooked end of the stirrup and the bearing force of the barrier on the edge of the concrete slab as well as the torsional resistance of the bridge rail section. Calculation of the bridge railing torsional resistance contribution to the overturning moment is difficult to resolve. As such, it is viable to conservatively assume that the entire overturning moment must be resisted by the barrier anchorage. Therefore, the tensile force of the hooked end of the anchor essentially determines the full moment capacity. The shear capacity of the anchorage is distributed to the hooked end and the straight embedded end. The shear capacity of the straight embedded end is limited close to the edge of the concrete and the potential for the concrete breakout in shear. The shear and moment capacities of a single no. 5 stirrup were calculated and then normalized by dividing by the anchor spacing to determine the capacities as forces per length of barrier. Utilizing the calculations shown in Appendix B, the shear and moment strengths of the barrier were found to be 19.13 k/ft and 13.85 k-ft/ft (279.2 kN/m and 61.6 kN-m/m) respectively. Alternatively, a yield line analysis could be completed to verify the strength of a barrier.

3.3 Tensile Failure Modes

Epoxy bonded anchors have three main modes of failure in tension. They are: steel rupture, full concrete cone breakout, and pullout of the adhesive core accompanied by a partial cone breakout. Within the pullout of the adhesive core failure mode, bond failure can occur at the epoxy-concrete interface, the epoxy-anchor interface, or both the epoxy-concrete and the epoxy-anchor interfaces. Since most state's DOTs prefer to have a protective epoxy coating on the reinforcing bars, the epoxy-anchor interface failure is actually a failure between the protective epoxy coating and the epoxy adhesive. A summary of the failure modes is shown in Figure 12.

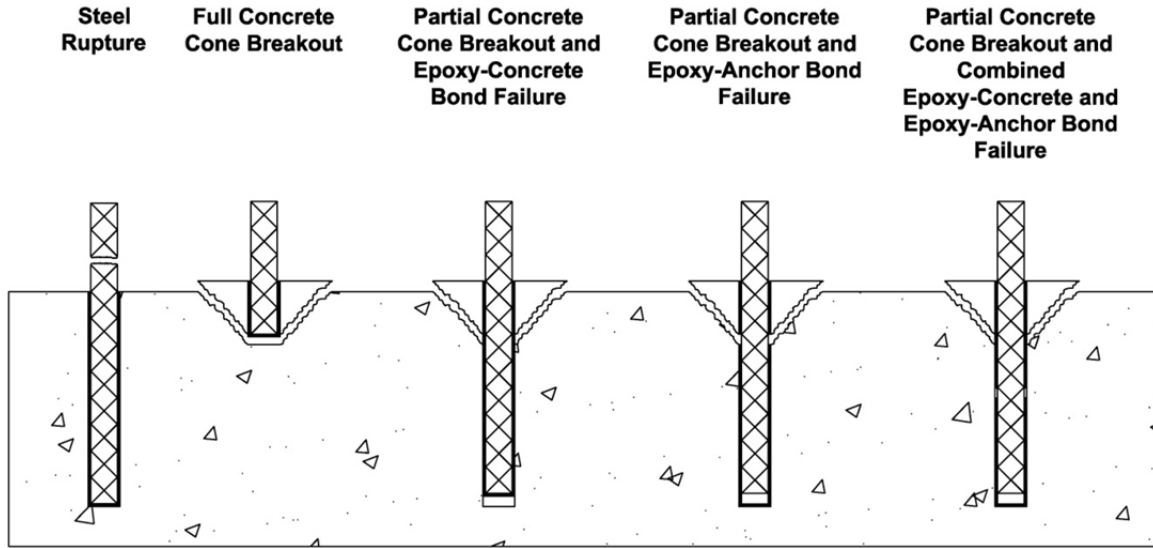


Figure 12. Failure Modes for Epoxy Anchors Loaded in Tension

3.4 Tensile Design Models

Three common models that can be used to predict the tensile capacity of adhesive anchors are a uniform bond stress distribution, an elastic bond stress distribution, and a concrete cone failure. Many of the proposed procedures (as outlined in Chapter 2) use a combination of these failure models to better describe the failure mechanisms present and attempt to improve the accuracy of the solution. Several of the models discussed in the literature review, as well as additional procedures were proposed and compared to test data obtained from the epoxy manufacturer, Hilti.

3.4.1 Steel Rupture Model

The steel rupture model is a function of the cross-sectional area of the anchor (A_s) and the ultimate strength of the anchor steel (f_u), shown in Equation (21). This is the commonly used equation to calculate the tensile rupture strength of steel materials. This failure mode is expected when there is sufficient embedment depth to preclude concrete breakout or bond failure.

$$N_n = A_s f_u \quad (21)$$

3.4.2 Concrete Cone Model

The concrete cone model is generally only valid for adhesive anchors with shallow embedment depths because the concrete breakout capacity is lower than the bond pullout capacity only at short embedment depths. However, most of the failure modes observed in previous testing had a shallow concrete cone that formed near the surface of the concrete. For deeper embedment depths, the fracture area of the concrete cone increases significantly, eventually reaching a transition from a cone failure to a simultaneous cone and bond failure.

The concrete cone model for cast-in-place and post-installed mechanical anchors vary significantly from the concrete cone model for adhesive anchors. This is because of the inherent differences between the load transfers for the different systems. A cast-in-place anchor generally has a stud or a bend at the embedded end of the anchor which causes most of the load to be transferred at the bottom of the anchor. The end of the anchor cannot slip so a full concrete cone is pulled out with a height equal to the embedment depth of the anchor. Similarly, a post-installed mechanical anchor transfers the load by a bearing force near the bottom of the anchor that is obtained by the expansion of the anchor.

Conversely, with adhesive anchors, the load is distributed along the bonded area and there is little stress concentration at the bottom of the anchor. Because the diameter of the anchor is relatively uniform along the entire embedment depth, there is a relatively low mechanical interlock between the anchor and the concrete compared to that of cast-in-place or post-installed mechanical anchors. This allows adhesive anchors to slip out of the hole before a full concrete cone can develop and usually only a shallow concrete cone forms near the top.

The concrete model assumed that the strength of the pullout capacity of all tests would be controlled by the formation of a concrete cone and that the concrete cone was the only component of the system that contributed to the pullout capacity. The calibration coefficient in Equation (4) was modified so that English units could be utilized which resulted in Equation (22) shown below.

$$N_n = 11.08h_{ef}^2\sqrt{f'_c} \quad (22)$$

The procedure used to convert Equation (4) to English units is shown in Appendix C. Note that in Equation (22), h_{ef} should use units of inches and f'_c should use units of pounds per square inch.

3.4.3 Full Uniform Bond Stress Model

The uniform bond stress model assumes that the stress is transferred evenly across the entire bonded area by an average uniform bond stress. The average uniform bond stress value is calculated based on previous test data for the particular adhesive and anchor size, and can be calculated as the failure load divided by the bonded area. The mechanics of this model are very basic as the only required parameters are the average uniform bond stress and the bonded area. This model has been used as the basis for many adhesive anchor design procedures including ICC-ES AC308 and ACI 318-11. Studies have shown that this model accurately predicts the tensile capacities of adhesive anchors for short to medium embedment depths. This model generally over predicts strength values for anchors with deep embedment depths. Short depths include anchors with less than 4 in. (102 mm) of embedment, medium depths are between 4 and 8 in. (102 and 203 mm), and deep embedment depths are considered greater than 8 in. (203 mm).

This model calculated the pullout strength by multiplying the average uniform bond stress by the bond area obtained from the full embedment depth of the anchor. The equation used

to calculate the pullout capacity for the full uniform bond model is shown in Equation (23) below. This model did not take into account the effect of a concrete cone formation. Equation (23) was used to predict the pullout strength for every test in the database herein.

$$N_n = \tau_0 \pi d_0 h_{ef} \quad (23)$$

3.4.4 Cone or Full Uniform Bond Model

The height of the concrete cone was first estimated by a modified version of Equation (3), where English units of inches and pounds were utilized. The resulting equation is shown below.

$$h_{cone} = \frac{\tau_0 \pi d_0}{22.16 \sqrt{f'_c}} \quad (24)$$

Two limit states of either a concrete cone failure or a full uniform bond failure were implemented based on which failure mode was likely to govern. If the estimated height of the concrete cone calculated by Equation (24) was greater than or equal to the total embedment depth, Equation (22) was utilized. Otherwise, the uniform bond stress Equation (23) was used to calculate the pullout capacity.

3.4.5 Cone or Partial Uniform Bond with Calculated Cone Height

It was suggested that the pullout capacity of an adhesive bonded anchor could be accurately predicted by the calculated strength of a partially bonded anchor neglecting the concrete cone [8, 17]. This model utilized Equation (22) when the cone height predicted by Equation (24) was greater than the embedment depth. Otherwise a partial uniform bond stress model was used. Recall that the capacity of a partially bonded anchor is given by the following equation.

$$N_n = \tau_0 \pi d_0 (h_{ef} - h_{cone}) \quad (25)$$

3.4.6 Cone or Partial Uniform Bond with Assumed Cone Height

Equation (24) did not agree with the observations made by Collins, Klingner, and Polyzois [9] that the height of the concrete cone decreased with an increase in embedment depth, and the calculated heights of the cone were greater than the observed heights noted in previous studies [8, 9]. Therefore, the accuracy of Equations (3) and (24) were questioned. In lieu of a better equation to predict the height of the concrete cone, the cone height was assumed to be equal to 2 in. (51 mm) in all cases as recommended by Doerr and Klingner [8]. The procedure in Section 3.4.5 was modified with h_{cone} equal to 2 in. (51 mm) for all cases.

3.4.7 Cone or Cone Plus Partial Uniform Bond Model with Calculated Cone Height

This model was similar to the one proposed by Cook [10] except that the equations were converted to English units and the elastic bond stress equation was not utilized because of the lack of available data for the maximum bond stress and the adhesive stiffness parameter. When the height of the concrete cone predicted by Equation (24) was greater than or equal to the embedment depth of the anchor, the concrete cone Equation (22) was used. Otherwise, a modified version of Equation (5), which allows the input of English units of inches and pounds, was used. This equation is shown below.

$$N_n = \tau_0 \pi d_0 (h_{ef} - h_{cone}) + 11.08 h_{cone}^2 \sqrt{f'_c} \left[\frac{7.94 \sqrt{d_0} - (h_{ef} - h_{cone})}{7.94 \sqrt{d_0}} \right] \quad (26)$$

3.4.8 Cone or Cone Plus Partial Uniform Bond Model with Assumed Cone Height

Again, due to the questionable accuracy of Equations (3) and (24), the height of the concrete cone was assumed to be 2 in. (51 mm) to test this model with a potentially more accurate concrete cone height. The procedure presented in section 3.4.7 was repeated with h_{cone} taken to be 2 in (51 mm).

3.4.9 Modified Cone or Cone Plus Partial Uniform Bond Model with Assumed Cone Height

The procedure presented in section 3.4.8 was repeated with the last bracketed term in Equation (26) dropped out of the equation. Occasionally, the elastic bond stress model is not considered due to the lack of the required parameters. Therefore, this term is not needed. The resulting equation is shown below in Equation (27).

$$N_n = \tau_0 \pi d_0 (h_{ef} - h_{cone}) + 11.08 h_{cone}^2 \sqrt{f'_c} \quad (27)$$

3.4.10 Elastic Bond Stress Model

The elastic bond stress model theoretically better describes the mechanics of an adhesive anchor than the uniform bond stress model. It also satisfies both the compatibility of equilibrium and displacements at the anchor-adhesive interface while the uniform bond stress model only satisfies equilibrium [11]. The derivation of this model is obtained by setting the net energy of the adhesive anchor system equal to the total internal strain energy minus the external energy. A drawing of the adhesive anchor with the geometric variables is shown in Figure 13.

The internal energy in the steel (U_s) is given by Equation (28) where σ is the axial stress in the steel, ε is the axial strain in the steel, and h_{ef} is the embedment depth of the anchor.

$$U_s = \frac{1}{2} \int_0^{h_{ef}} \int_A \sigma \varepsilon dA dy \quad (28)$$

If the axial displacement of the anchor is given by the function $u(y)$, then the strain is calculated as the first derivative of the displacement function.

$$\varepsilon = \frac{du(y)}{dy} = u' \quad (29)$$

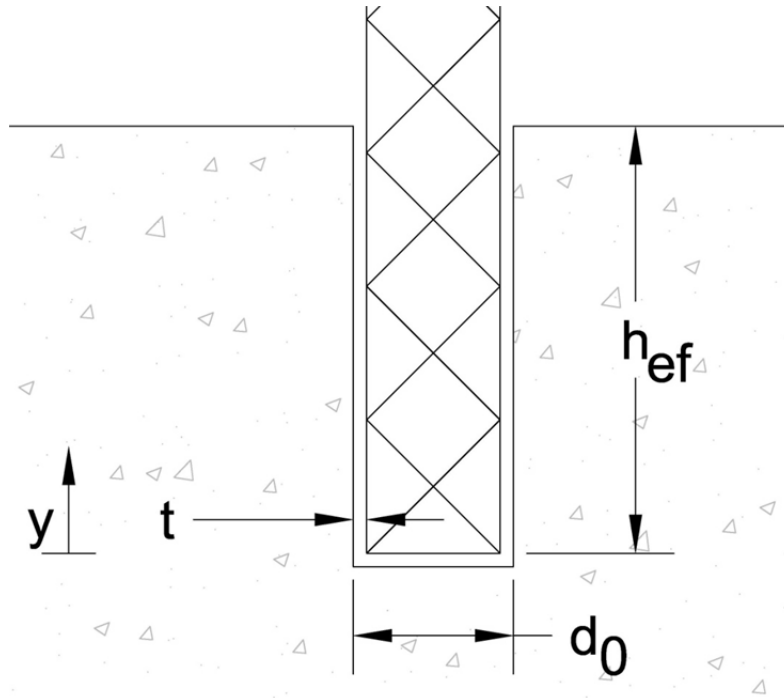


Figure 13. Adhesive Anchor Used to Develop the Elastic Model

By assuming a linear relationship between the stress and strain, the axial stress can be determined by Hook's law as the modulus of elasticity of the steel (E_s) times the strain.

$$\sigma = E_s \varepsilon \quad (30)$$

By combining Equations (29) and (30), the stress can be expressed by Equation (31).

$$\sigma = E_s u' \quad (31)$$

The area of the anchor can be assumed to be constant throughout the embedment depth, so the integral over the area can be reduced to the cross-sectional area of the anchor steel (A_s).

$$\int_A dA = A_s \quad (32)$$

By substituting Equations (29) , (31), and (32) into Equation (28), the internal energy of the steel is given by Equation (33).

$$U_s = \frac{1}{2} \int_0^{h_{ef}} E_s A_s (u')^2 dy \quad (33)$$

The internal energy of the adhesive (U_a) is given by Equation (34) where τ is the shear stress in the adhesive and γ is the shear strain in the adhesive.

$$U_a = \frac{1}{2} \int_0^{h_{ef}} \int_A \tau \gamma dA dy \quad (34)$$

By assuming an elastic response by the adhesive, the shear stress can be determined by Hook's law in shear as the shear modulus of elasticity of the adhesive (G_a) times the shear strain.

$$\tau = G_a \gamma \quad (35)$$

The shear strain is defined as the axial displacement divided by the thickness of the adhesive layer (t).

$$\gamma = \frac{u}{t} \quad (36)$$

By combining Equations (35) and (36), the shear stress can be calculated by Equation (37).

$$\tau = \frac{G_a u}{t} \quad (37)$$

The integral over the area in Equation (34) can be approximated by Equation (38) where d_0 is the diameter of the hole.

$$\int_A dA \cong \pi d_0 t \quad (38)$$

By substituting Equations (36), (37), and (38) into Equation (34), the internal energy due to the adhesive is given by Equation (39).

$$U_a = \frac{1}{2} \int_0^{h_{ef}} \frac{G_a d_0 \pi u^2}{t} dy \quad (39)$$

The external energy applied to the system (U_e) is simply the work applied by the load at the top of the anchor. This is given by Equation (40) where N is the applied tensile load at the top of the anchor, and $u(h_{ef})$ is the deflection of the anchor at the concrete surface (the function u evaluated at y equal to h_{ef}).

$$U_e = Nu(h_{ef}) \quad (40)$$

By combining Equations (33), (39), and (40), the net energy of the system (U_{net}) is shown below.

$$U_{net} = U_s + U_a - U_e$$

$$U_{net} = \frac{1}{2} \int_0^{h_{ef}} E_s A_s (u')^2 dy + \frac{1}{2} \int_0^{h_{ef}} \frac{G_a d_0 \pi u^2}{t} dy - Nu(h_{ef}) \quad (41)$$

Based on the principle of minimum total potential energy, the internal energy will approach a minimum value at equilibrium [78]. The resulting second order homogeneous differential equation obtained by minimizing the net energy of the system with respect to the displacement is shown in Equation (42).

$$u'' - \lambda^2 u = 0 \quad (42)$$

The λ^2 variable is an elastic property of the anchor system and is given in terms of the dimensions and material properties of the components, as shown in Equation (43).

$$\lambda^2 = \frac{G_a d_0 \pi}{t E_s A_s} \quad (43)$$

The second order homogeneous differential equation can be put into a more general form as shown in Equation (44) where $a = 1$, $b = 0$, and $c = -\lambda^2$.

$$au'' + bu' + cu = 0 \quad (44)$$

Equation (44) can be solved by finding the roots of the following equation.

$$\begin{aligned}
 ar^2 + br + c &= 0 \\
 &= 1r^2 + 0r + (-\lambda^2) = 0 \\
 &= (r - \lambda)(r + \lambda) = 0 \\
 \therefore r &= \pm \lambda
 \end{aligned} \tag{45}$$

Therefore, the general solution to Equation (44) is shown below.

$$u = c_1 e^{\lambda y} + c_2 e^{-\lambda y} \tag{46}$$

The initial conditions of $u(0) = 1$ and $u'(0) = 0$ are satisfied if $c_1 = c_2 = 1/2$.

Therefore, Equation (46) can be expressed as the following equation.

$$u_1 = \frac{1}{2} e^{\lambda y} + \frac{1}{2} e^{-\lambda y} = \cosh(\lambda y) \tag{47}$$

Similarly, the initial conditions of $u(0) = 0$ and $u'(0) = 1$ are satisfied if $c_1 = 1/2$ and $c_2 = -1/2$. Therefore, Equation (46) can be expressed as the following equation.

$$u_2 = \frac{1}{2} e^{\lambda y} - \frac{1}{2} e^{-\lambda y} = \sinh(\lambda y) \tag{48}$$

Equations (47) and (48) form a fundamental set of solutions, and the general solution to Equation (42) is shown below [79].

$$u(y) = k_1 \cosh(\lambda y) + k_2 \sinh(\lambda y) \tag{49}$$

The first derivative of Equation (49) with respect to y is shown below.

$$u'(y) = k_1 \lambda \sinh(\lambda y) + k_2 \lambda \cosh(\lambda y) \tag{50}$$

By assuming that the epoxy below the bottom of the anchor carries no load, the strain at the bottom of the anchor is equal to zero.

$$\varepsilon(0) = u'(0) = 0 \tag{51}$$

By applying the above boundary condition to Equation (50), the constant k_2 must be equation to zero.

$$k_2 = 0 \quad (52)$$

The second boundary condition is derived from the strain in the anchor steel at the concrete surface. The value of the strain in the anchor at the concrete surface is shown in Equation (53).

$$\varepsilon(h_{ef}) = u'(h_{ef}) = \frac{N}{A_s E_s} \quad (53)$$

By applying Equations (52) and (53) to Equation (50), the constant k_1 can be solved for and is given by Equation (54).

$$k_1 = \frac{N}{A_s E_s \lambda \sinh(\lambda h_{ef})} \quad (54)$$

By substituting the constants k_1 and k_2 into Equation (49), the displacement function is given by Equation (55).

$$u(y) = \frac{N \cosh(\lambda y)}{E_s A_s \lambda \sinh(\lambda h_{ef})} \quad (55)$$

Rearranging the above equation yields the following equation for the applied tensile load.

$$N = u(y) E_s A_s \lambda \frac{\sinh(\lambda h_{ef})}{\cosh(\lambda y)} \quad (56)$$

Since the maximum shear stress (τ_{max}) will occur at the top of the anchor, the shear strain at the top of the anchor can be determined based on the maximum shear stress.

$$\gamma(h_{ef}) = \frac{\tau_{max}}{G_a} = \frac{u(h_{ef})}{t} \quad (57)$$

Rearranging these terms to solve for the axial displacement at the top of the anchor yields the following equation.

$$u(h_{ef}) = \frac{t\tau_{max}}{G_a} \quad (58)$$

Combining Equations (56) and (58), the maximum force at the top of the anchor ($y = h_{ef}$) can be calculated by Equation (59).

$$N_{max} = \frac{t\tau_{max}}{G_a} E_s A_s \lambda \tanh(\lambda h_{ef}) \quad (59)$$

Equation (43) can be rearranged to the following equation.

$$\frac{tE_s A_s}{G_a} = \frac{d_0 \pi}{\lambda^2} \quad (60)$$

By substituting Equation (60) in Equation (59), the maximum tensile load of an adhesive anchor can be expressed as follows.

$$N_{max} = \frac{\tau_{max} d_0 \pi}{\lambda} \tanh(\lambda h_{ef}) \quad (61)$$

However, the λ term is dependent on the diameter of the hole. If the area of the steel is approximated by the area of the hole, then the adhesive stiffness parameter (λ') can be derived by the following procedure.

$$A_s \cong \frac{\pi d_0^2}{4} \quad (62)$$

$$\lambda^2 = \frac{G_a d_0 \pi}{tE_s \frac{\pi d_0^2}{4}} = \frac{4G_a}{tE_s d_0} \quad (63)$$

$$\lambda = \sqrt{\frac{4G_a}{tE_s d_0}} = \frac{1}{\sqrt{d_0}} \sqrt{\frac{4G_a}{tE_s}} = \frac{1}{\sqrt{d_0}} \lambda' \quad (64)$$

$$\therefore \lambda' = \sqrt{\frac{4G_a}{tE_s}} \quad (65)$$

Finally, substituting Equation (64) into Equation (61) yields the equation for the elastic bond stress model that is shown below [8].

$$N_{max} = \frac{\pi\tau_{max}d_0^{1.5}}{\lambda'} \tanh\left(\frac{\lambda'h_{ef}}{\sqrt{d_0}}\right) \quad (66)$$

This equation is limited by that fact that it only accounts for load transfer through the bonded interface. As explained in the literature review, many of the failures observed from prior testing had a concrete cone failure near the concrete surface. The maximum shear stress in Equation (66) will not necessarily be controlled by the maximum shear stress that the adhesive can hold before failure in shear, but could be controlled by the shearing stress at the adhesive-concrete or adhesive-anchor interfaces. This is difficult to determine and could be highly sensitive to installation conditions and the particular adhesive used.

3.5 Shear Design Models

Due to the similar behavior between adhesive, cast-in-place, and post-installed mechanical anchors in shear, the provisions presented in Appendix D of ACI 318-08 appear to be applicable to adhesive anchors. The only significant addition that ICC-ES AC308 provides to ACI 318-08 as a specification for the design of adhesive anchors in shear is a section that computes the nominal pryout strength in shear. This capacity is based on the pryout and breakout strengths of the anchor in tension. The results of Bickel and Shaikh's study indicated that the CCD method was adequate to predict the capacities of adhesive anchors loaded in shear [16].

3.6 Pullout Model Comparisons to Manufacturer Test Data

In order to evaluate the various models to predict the dynamic pullout capacities of epoxy-bonded anchors, several models were compared to test capacities from single anchor pullout tests. The products chosen to use in this study were the Hilti HIT-RE 500 and the Hilti HIT-RE 500-SD adhesive epoxies. The "SD" indicates the epoxy can be used for strength design. The Hilti products showed high anchorage capacities and are available from many suppliers around the country as well as direct sales from Hilti. Comparison of various epoxy

adhesive manufacturers' specified ultimate shear and tensile loads is shown in Appendix A. Further, extensive testing was conducted by ICC-ES to determine the bond stress properties of the Hilti HIT-RE 500-SD epoxy that are needed to implement into the uniform bond stress model contained in ICC-ES AC308. The results from this testing program are contained in the ICC-ES report ESR-2322 [80].

The models described in sections 3.4.2 through 3.4.9 were evaluated and compared to a database of test data from Hilti. For each model investigated, the pullout capacity was calculated based on the adhesive parameters and the physical dimensions of the test specimen. A test-to-predicted capacity ratio was calculated for each data point by dividing the actual capacity obtained from the test data by the calculated capacity determined by the model. For each model, the mean of the test-to-predicted ratios for all data points was used to examine the accuracy. The standard deviation and coefficient of variation (COV) of the mean test-to-predicted ratios were calculated for each model to analyze the precision. Due to the complexities involved with determining the parameters for the elastic bond stress model, only variations of the concrete cone and/or uniform bond stress models were analyzed during this part of the research.

The *2008 Hilti North American Product Technical Guide* specifies a single bond stress value according to ASTM C882-91 for the Hilti HIT-RE 500 epoxy [22]. However, ICC-ES ESR-2322 and the Hilti Technical Guide specify bond strengths that decrease with an increase in anchor diameter for the Hilti HIT-RE 500-SD epoxy [80]. The bond strength value stated in the Hilti Technical Guide for the HIT-RE 500 epoxy was lower than the lowest value for the HIT-RE 500-SD listed in ICC-ES ESR-2322 and the Hilti Technical Guide. All of the models were calculated with both bond stresses, the one specified by the Hilti Technical Guide as well as values from ICC-ES ESR-2322.

3.6.1 Comparison of Proposed Models with Test Data

The calculated pullout capacities and the corresponding mean test-to-predicted pullout capacities ratios for the various models are shown in Appendix D. For each model, a mean test-to-predicted ratio was calculated as well as the standard deviation and coefficient of variation of the mean values. A summary of the mean test-to-predicted pullout capacity ratios and coefficients of the variations for all models are shown in Table 7. Due to the lack of detailed test data, these values are based solely on the ultimate strengths and do not consider whether the proper failure mechanism that was predicted matched that observed from testing.

Most of the models had a slightly better relation to the actual test capacities with the bond stress values contained in ICC-ES ESR-2322. This suggested that the average uniform bond stress is not constant for all anchor sizes and embedment depths. However, the specified bond stress from the Hilti product documentation provided good results that were slightly more conservative than the more detailed bond stress values obtained from ICC-ES ESR-2322.

The full uniform bond model tended to predict strengths much higher than the other models and the testing results. In fact, for the shortest embedment depths, the calculated capacity was usually close to twice the test capacity. This was expected since for short embedment depths, a small cone failure with little or no bond failure is likely to occur. Therefore, the full bond strength is not developed because the concrete fails before the adhesive reaches its maximum limit. For longer embedment depths, this model showed good results.

The concrete cone model was very accurate in estimating the capacities for all anchors as its mean test-to-predicted value was equal to 1.0 with a relatively small coefficient of variation. This model, however, does a poor job of describing the mechanics of the actual failure modes that would be expected to occur.

Table 7. Summary of Model Comparison with Hilti Test Data

Model Type	Bond Stress Specified in Hilti Documentation			Bond Stress Specified In ICC-ES ESR-2322		
	Mean Test-to-Predicted Ratio	Std. Dev. of Mean T/P Ratios	COV of Mean T/P Ratios	Mean Test-to-Predicted Ratio	Std. Dev. of Mean T/P Ratios	COV of Mean T/P Ratios
Full Uniform Bond Model	0.87	0.24	0.27	0.76	0.22	0.29
Concrete Cone Model	1.00	0.19	0.19	1.00	0.19	0.19
Cone or Full Uniform Bond Model	1.04	0.16	0.15	0.98	0.16	0.16
Cone or Cone Plus Partial Uniform Bond Model with Calculated Cone Height	1.45	0.27	0.19	1.36	0.24	0.18
Cone or Cone Plus Partial Uniform Bond Model with Assumed Cone Height	1.25	0.24	0.19	1.13	0.19	0.17
Modified Cone or Cone Plus Partial Uniform Bond Model with Assumed Cone Height	1.17	0.21	0.18	1.06	0.18	0.17
Cone or Partial Uniform Bond with Calculated Cone Height	3.63	8.93	2.46	1.67	0.52	0.31
Cone or Partial Uniform Bond with Assumed Cone Height	1.62	1.01	0.62	1.40	0.78	0.56

The cone or full uniform bond model also did an excellent job of predicting the pullout capacities for all anchors. The mean test-to-predicted values were 1.04 and 0.98 for bond stress values specified by the Hilti product documentation and ICC-ES ESR-2322, respectively. This model also had the smallest coefficient of variation and standard deviation of all the models compared.

The cone or cone plus partial uniform bond with the calculated cone height was conservative for every data point. For shorter embedment depths, the calculated values corresponded to the concrete cone model values which were only slightly below the actual test capacities. For medium to deep embedment depths this model was very conservative.

Theoretically, this model does an adequate job of explaining the failure mechanisms that are expected to be present. However, it does not work with the particular equation used to estimate the concrete breakout strength when combined with the bond stress values input into this model. The error in this model is believed to be attributed to the inaccuracy of Equation (24). As noted previously, this equation was believed to overestimate the height of the concrete cone as compared to previous testing observed from the literature review.

When the cone or cone plus partial uniform bond model was used with an assumed cone height of 2 in. (51 mm), slightly more accurate results were obtained. Perhaps this is because the cone height equation predicts the cone height to be too large, resulting in an overestimation of the strength contributed by the concrete breakout. With a smaller cone height the influence of the bond stress has a greater contribution to the overall capacity, especially for deeper embedment depths.

The modified cone or cone plus partial uniform bond model showed good results that were slightly conservative. The average test-to-predicted ratio was 1.05 when the bond stress values from ICC-ES ESR-2322 were used. The results were slightly less accurate than the cone or full uniform bond model, but the modified cone or cone plus partial uniform bond model better describes the actual failure modes that would be expected to be present.

Both the cone or partial bond models calculated capacities that were quite conservative. These models also became very unstable if the calculated or assumed height of the concrete cone was slightly less than the embedment depth. This is because when the embedment depth was slightly more than the cone height, only a very small bond area was considered to develop the capacity of the anchor.

3.7 Creep Consideration

As discussed in the literature review, all qualified products approved by ICC-ES AC308 or ACI 355.4-11 are required to be tested and meet creep criteria. Since epoxy is a visco-plastic material, creep of the anchors would only occur due to long-term sustained tensile loading. Bridge railings and barriers are supported vertically by the bridge deck so there is not any long-term sustained tensile loading in the anchors. An impact of a crash on the barrier would not allow a long enough duration load to induce creep behavior of the anchors. Therefore, creep of the anchors does not need to be a design consideration when using epoxy adhesive anchors in bridge rail and temporary barrier anchorages.

3.8 Discussion

The cone or full uniform bond model showed a high correlation to test data obtained from the manufacturer for static loading conditions. This model proved to be the most accurate and stable for all embedment depths while providing a reasonable prediction of the expected failure mode. Therefore, a limit state design of either a concrete cone breakout or a full uniform bond failure was selected for further development. For this method, two failure strengths would be calculated and the lower of the two failure modes would be the governing strength. However, in bridge rail applications, the cone model is not likely to be the governing design consideration due the fact that very short embedment depths will not be utilized and a bond failure mode will most likely govern in most cases. Further, the manufacturers' specifications provide the bond stress values for the epoxies that can be easily and quickly implemented into the full uniform bond model. The elastic model solution appeared to show validity based on the energy method of analysis. However, the complex parameters required would not be readily available without additional testing for each product.

4 EPOXY ANCHOR DYNAMIC TESTING

4.1 Purpose

Dynamic bogie tests were conducted on epoxy adhesive anchors to determine their capacities under dynamic loads in both shear and tension. Both ASTM A775 epoxy-coated and plain black ASTM A615 Grade 60 steel reinforcing bars were tested to investigate how protective coatings affect the strength of the anchor. Dual anchor tensile tests were also conducted to determine if closely spaced anchors experienced a reduction in tensile capacity. Finally, ASTM A307 threaded rods were tested to evaluate the potential for epoxy adhesive anchors for use with current portable concrete barrier tie-down designs.

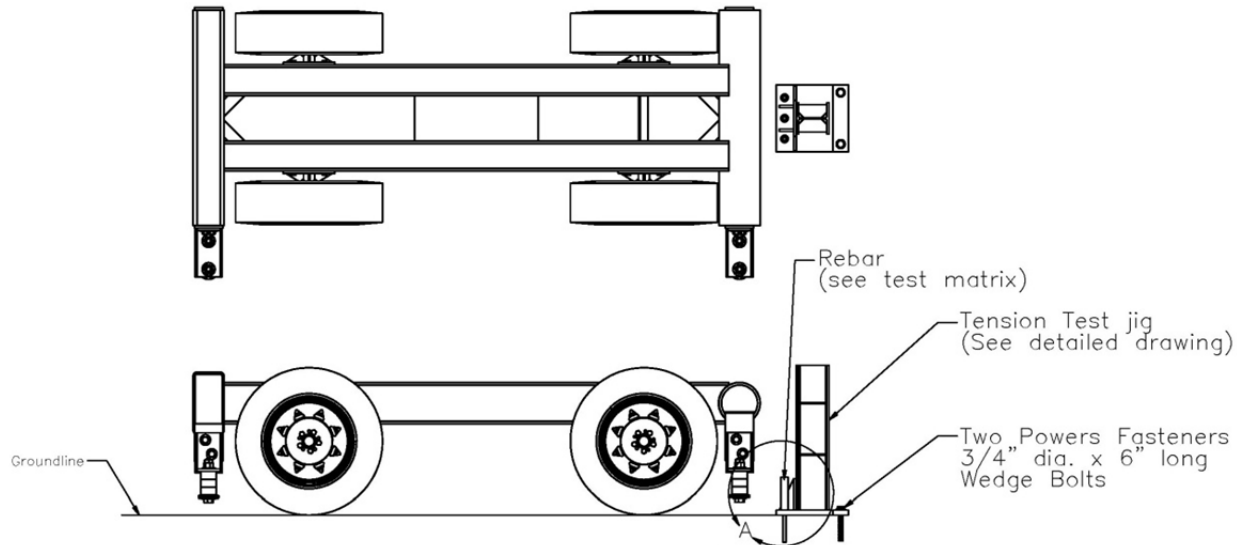
4.2 Scope

The test setup drawings for test nos. WEAB-1 through WEAB-16 are shown in Figures 14 and 15. Detailed test setup drawings for all tests are shown in Appendix F. The test matrix is shown in or blow through the bottom of the deck. Material specifications sheets are shown in Appendix G. Material specifications were not available for the ASTM A307 threaded rods.

Table 8. Custom designed test jigs, as explained in section 4.4.2, were used to transfer the momentum of the bogie vehicle into dynamic forces on the anchors. The target impact conditions were 10 mph (16.09 km/h) for single anchor tests and 15 mph (24.14 km/h) for double anchor tests. All tests were conducted in an unreinforced concrete slab with an unconfined compressive strength of 6,454 psi (44.50 MPa) according to concrete cylinder testing. The anchor holes were constructed using a carbide-tipped concrete bit and a rotary hammer drill. The holes were clean by repeated brushing and blowing compressed air into the hole according to the manufacturer's specifications. The test specimens were embedded to a depth of 5- $\frac{1}{4}$ in. (133 mm) for all of the component tests. This depth was chosen as it was the maximum depth allowable for an 8-in. (203-mm) thick bridge deck that would ensure that the installation drill hole would not damage

Epoxy Anchor Rebar Bogie Testing—Tensile Test Setup

1. Bogie No. 3 – Small Bogie with standard round impact head
2. Speed = 15 mph
3. One high-speed digital camera perpendicular
4. One high-speed digital camera perpendicular zoomed in on the tensile test jig and rebar.
5. JVC digital video
6. DTS and EDR-3
7. Note any installation issues or problems in fieldbook.
8. Note failure mode in fieldbook.
9. Each test must be at least 2' from any previous test anchor holes to prevent anchor spacing and edge spacing issues from affecting results.
10. Kick plate anchors must be replaced each test.
11. Epoxy and epoxy-coated rebar will be donated.
12. Before installation of anchors, measure the bar deformation rib height as well as the epoxy-coating thickness.
13. Epoxy used for first round of testing will be Hilti HIT-RE 500.

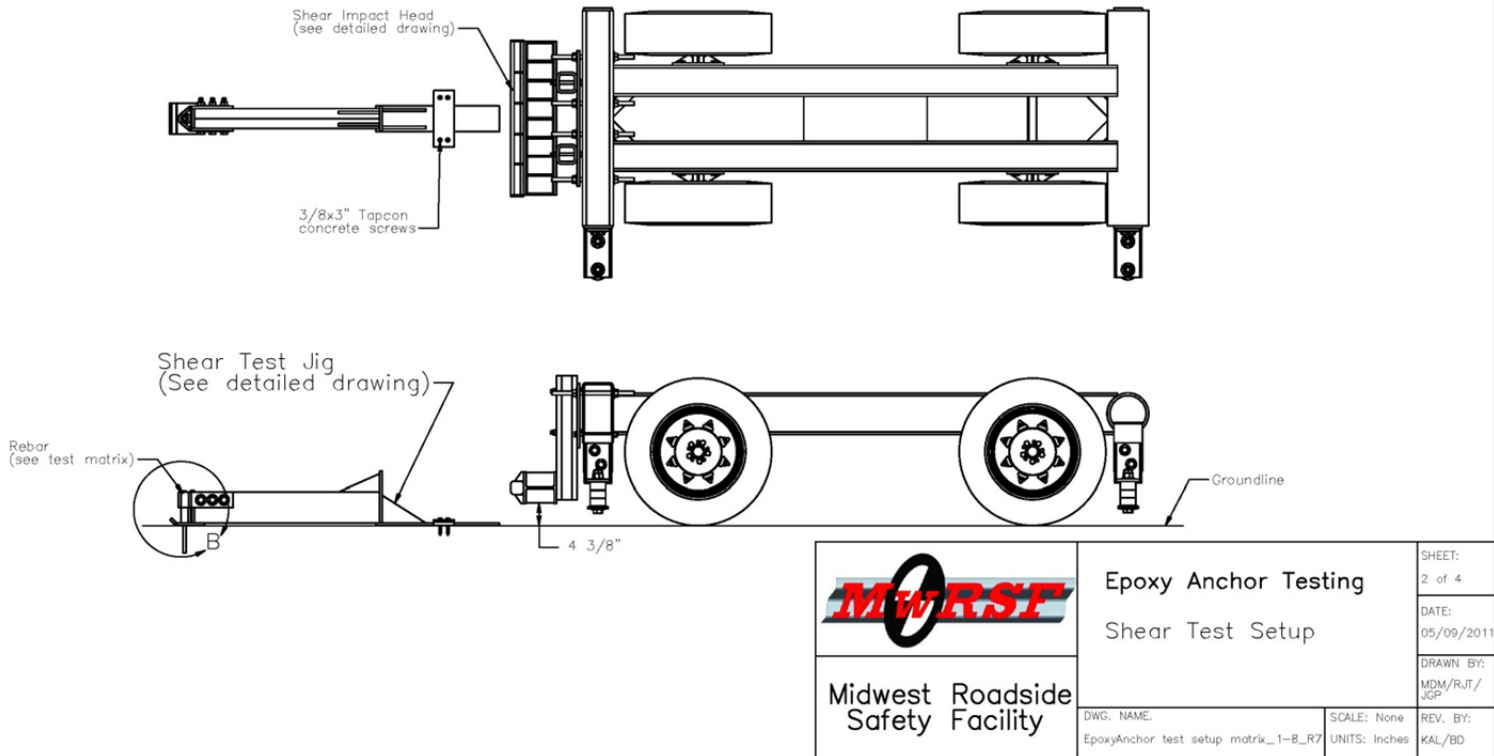


 Midwest Roadside Safety Facility	Epoxy Anchor Testing Tension Test Setup	SHEET: 1 of 4
		DATE: 05/09/2011
	DWG. NAME: EpoxyAnchor test setup matrix_1-8_R7	DRAWN BY: MDM/RJT/ JGP
	SCALE: None UNITS: Inches	REV. BY: KAL/BD

Figure 14. Tension Test Setup, Test Nos. WEAB-1 Through WEAB-4, WEAB-7 and WEAB-8

Epoxy Anchor Rebar Bogie Testing—Shear Test Setup

1. Bogie No. 3 – Small Bogie with Shear Impact Head
2. Speed = 10 mph
3. One high-speed digital camera perpendicular
4. One high-speed digital camera perpendicular zoomed in on the shear test jig and rebar.
5. JVC digital video
6. DTS and EDR-3
7. Note any installation issues or problems in fieldbook.
8. Note failure mode in fieldbook.
9. Each test must be at least 2' from any previous test anchor holes to prevent anchor spacing and edge spacing issues from affecting results.
10. Epoxy and epoxy-coated rebar will be donated.
11. Before installation of anchors, measure the bar deformation rib height as well as the epoxy coating thickness.
12. Tapcon concrete screws need to be replaced after each test.
13. Epoxy used for first round of testing will be Hilti HIT-RE 500.




 Midwest Roadside Safety Facility	Epoxy Anchor Testing Shear Test Setup	SHEET: 2 of 4
	DWG. NAME: EpoxyAnchor test setup matr_k_1-8_R7	SCALE: None UNITS: Inches
		REV. BY: KAL/BD

Figure 15. Shear Test Setup, Test Nos. WEAB-5 and WEAB-6

or blow through the bottom of the deck. Material specifications sheets are shown in Appendix G. Material specifications were not available for the ASTM A307 threaded rods.

Table 8. Dynamic Bogie Test Matrix

Test No.	Test Type	Bar Size, US (Metric)	Bar Coating	Epoxy Type	Spacing	Target Bogie Speed, mph (km/h)	Bogie Weight, lb (kg)	Steel Type	Ultimate Steel Strength, ksi (Mpa)
WEAB-1	Tensile	#5 (#16)	None	Hilit HIT-RE 500	Single	10.00 (16.09)	1,485 (674)	ASTM A615, Grade 60	103,937 (717)
WEAB-2	Tensile	#5 (#16)	None	Hilit HIT-RE 500	Single	10.00 (16.09)	1,485 (674)	ASTM A615, Grade 60	103,937 (717)
WEAB-3	Tensile	#5 (#16)	Epoxy	Hilit HIT-RE 500	Single	10.00 (16.09)	1,485 (674)	ASTM A615, Grade 60	103,937 (717)
WEAB-4	Tensile	#5 (#16)	Epoxy	Hilit HIT-RE 500	Single	10.00 (16.09)	1,485 (674)	ASTM A615, Grade 60	103,937 (717)
WEAB-5	Shear	#5 (#16)	Epoxy	Hilit HIT-RE 500	Single	10.00 (16.09)	1,735 (787)	ASTM A615, Grade 60	103,937 (717)
WEAB-6	Shear	#5 (#16)	Epoxy	Hilit HIT-RE 500	Single	10.00 (16.09)	1,735 (787)	ASTM A615, Grade 60	103,937 (717)
WEAB-7	Tensile	#5 (#16)	Epoxy	Hilit HIT-RE 500	2 @ 8 in. (2 @ 203 mm)	15.00 (24.14)	1,485 (674)	ASTM A615, Grade 60	103,937 (717)
WEAB-8	Tensile	#5 (#16)	Epoxy	Hilit HIT-RE 500	2 @ 8 in. (2 @ 203 mm)	15.00 (24.14)	1,485 (674)	ASTM A615, Grade 60	103,937 (717)
WEAB-9	Tensile	#6 (#19)	Epoxy	Hilit HIT-RE 500-SD	Single	15.00 (24.14)	1,727 (783)	ASTM A615, Grade 60	100,400 (692)
WEAB-10	Tensile	#6 (#19)	Epoxy	Hilit HIT-RE 500-SD	Single	15.00 (24.14)	1,727 (783)	ASTM A615, Grade 60	100,400 (692)
WEAB-11	Tensile	#6 (#19)	Epoxy	Hilit HIT-RE 500-SD	2 @ 8 in. (2 @ 203 mm)	15.00 (24.14)	1,727 (783)	ASTM A615, Grade 60	100,400 (692)
WEAB-12	Tensile	#6 (#19)	Epoxy	Hilit HIT-RE 500-SD	2 @ 8 in. (2 @ 203 mm)	15.00 (24.14)	1,727 (783)	ASTM A615, Grade 60	100,400 (692)
WEAB-13	Shear	#6 (#19)	Epoxy	Hilit HIT-RE 500-SD	Single	10.00 (16.09)	1,736 (787)	ASTM A615, Grade 60	100,400 (692)
WEAB-14	Tensile	1 1/8 in. (29 mm)	None	Hilit HIT-RE 500-SD	Single	15.00 (24.14)	1,505 (682)	ASTM A307	60,000* (414)*
WEAB-15	Shear	1 1/8 in. (29 mm)	None	Hilit HIT-RE 500-SD	Single	10.00 (16.09)	1,741 (790)	ASTM A307	60,000* (414)*
WEAB-16	Tensile	#6 (#19)	None	Hilit HIT-RE 500-SD	Single	15.00 (24.14)	1,723 (782)	ASTM A615, Grade 60	100,400 (692)

*Based on rated material capacities, not actual capacities

4.3 Test Facility

The testing facility is located at the Lincoln Air Park on the northwest side of the Lincoln Municipal Airport and is approximately 5 miles (8.0 km) northwest of the University of Nebraska-Lincoln.

4.4 Equipment and Instrumentation

4.4.1 Accelerometers

Two environmental shock and vibration sensor/recorder systems were used to measure the accelerations in the longitudinal direction for test nos. WEAB-1 through WEAB-16. All of the accelerometers were mounted near the center of gravity of the bogie.

The first accelerometer system was a two-arm piezoresistive accelerometer system manufactured by Endevco of San Juan Capistrano, California. The accelerometer was used to measure the longitudinal accelerations at a sample rate of 10,000 Hz. The accelerometer was configured and controlled using a system developed and manufactured by Diversified Technical Systems, Inc. (DTS) of Seal Beach, California. More specifically, data was collected using a DTS Sensor Input Module (SIM), Model TDAS3-SIM-16M. The SIM was configured with 16 MB SRAM and 8 sensor input channels to 250 kB SRAM/channel. The SIM was mounted on a TDAS3-R4 module rack. The module rack was configured with isolated power/event/communications, 10BaseT Ethernet and RS232 communication, and an internal backup battery. Both the SIM and module rack were crashworthy. The “DTS TDAS Control” computer software program and a customized Microsoft Excel worksheet were used to analyze and plot the accelerometer data. For test nos. WEAB-10 through WEAB-15, two longitudinal accelerometers were utilized with the DTS unit.

The second system, Model EDR-3, was a triaxial piezoresistive accelerometer system manufactured by IST of Okemos, Michigan. The EDR-3 was configured with 256 kB of RAM, a range of ± 200 g's, a sample rate of 3,200 Hz, and a 1,120 Hz low-pass filter. The “DynaMax 1 (DM-1)” computer software program and a customized Microsoft Excel worksheet were used to analyze and plot the accelerometer data.

4.4.2 Test Jigs

Two test jigs were utilized in the bogie tests to apply either shear or tensile loads to the anchors. The tensile jig design consisted of a 28-in. (711-mm) long W6x25 (W152x37.2) I-beam welded to a 1-in. (25-mm) thick base plate. The reinforcing bar anchors were held by Erico Lenton LOCK or Dayton Bar Lock mechanical reinforcing bar splices that were installed on the reinforcing bars above the base plate. The center connecting pin was removed to allow the use of more bolts to grip the reinforcing bar. Hex nuts were used for tests that involved threaded rod. A kick plate was attached to the concrete slab on the non-impact side of the test jig to provide shear resistance and allow the jig to rotate, thus, putting a tensile load on the anchors. A schematic drawing of the tensile jig is shown in Figure 16.

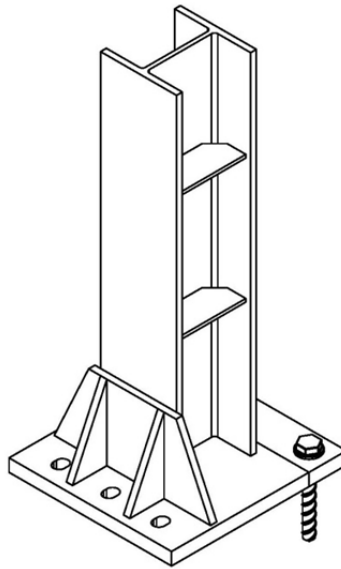


Figure 16. Tensile Jig

The shear jig consisted of two 3-ft (0.91-m) long, C6x8.2 (C152x12.2) channels welded to a metal sled plate on the front end and an impact plate on the rear end. The anchors were held by Erico Lenton LOCK or Dayton Bar Lock mechanical reinforcing bar splices that were installed on top of the sled plate on the front end of the test jig. A metal strap was wrapped

around the reinforcing bar splices to attach the anchors to the jig and prevent rotation of the anchors upon impact. The center connection pin was removed to allow the use of more bolts to grip the reinforcing bar. Hex nuts were used for tests that involved threaded rod. The impact plate was welded to the channels with ½-in. (12.7-mm) stiffener plates and a long metal guidance plate was welded to the rear end of the channels. A metal plate was screwed to the concrete above the guidance plate to prevent the jig from yawing or lifting off the concrete surface. Calculations that estimated the maximum loads that would be applied to the test jigs are shown in Appendix E. Analytical design calculations and detailed drawings of the test jigs are shown in Appendix E. The test jigs were modified accordingly to accommodate larger anchors for test nos. WEAB-9 through WEAB-16. A schematic drawing of the shear jig is shown in Figure 17.

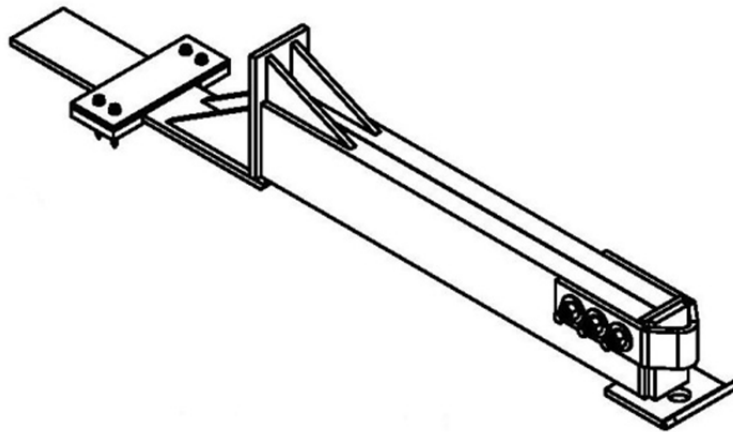


Figure 17. Shear Jig

4.4.3 Bogie

The dynamic bogie tests were conducted using a corrugated beam guardrail to guide the tires of the bogie vehicle. A pickup was used to push the bogie vehicle to the required impact velocity. After reaching the target velocity, the push vehicle braked allowing the bogie to be free rolling as it came off the track. For the tension tests, the bogie head impacted the test jig at an

impact height of approximately 21 5/8 in. (549 mm). This caused the tension jig to rotate applying a vertical pullout force to the anchors. For the shear tests, the bogie head impacted the test jig at an impact height of approximately 7 3/8 in. (187 mm). The bogie impact load was transferred to the anchor as the shear jig translated along the concrete surface.

A rigid frame bogie was used to impact the test jigs. For the tensile tests, the bogie head was constructed of an 8-in. (203-mm) diameter, 1/2-in. (13-mm) thick standard steel pipe, with 3/4-in. (19-mm) neoprene belting wrapped around the pipe to prevent local damage to the post from the impact. The height of impact for the tensile test was 21.66 in. (550 mm). A variable height, detachable steel impact head was used in the shear tests. The shear impact head had an impact height of approximately 7 5/16 in. (186 mm) from the ground surface. A 3/4 in. (19-mm) neoprene pad was attached to the impact plate of the shear jig. Pictures of the tensile and shear bogie test setups are shown in Figures 18 and 19.



Figure 18. Tensile Test Setup



Figure 19. Shear Test Setup

4.4.4 Pressure Tape Switches

Three pressure tape switches were placed near the end of the bogie track and were used to determine the speed of the bogie before impact. The switches were spaced at approximately 18 in. (457 mm) for test nos. WEAB-1 through WEAB-8 and 39.37 in. (1 m) for test nos. WEAB-9 through WEAB-16. As the right-front tire of the bogie passed over each tape switch, a strobe light was fired sending an electronic timing signal to the data acquisition system. The system recorded the signals and the time each occurred. The speed was then calculated using the spacing between the sensors and the time between the signals. Strobe lights and high-speed video analysis are used only as a backup in the event that vehicle speeds cannot be determined from the electronic data.

4.4.5 Digital Cameras

Two AOS VITcam high-speed digital video cameras and one JVC digital video camera were used to document each test. The AOS high-speed camera had a frame rate of 500 frames per second and the JVC digital video camera had a frame rate of 29.97 frames per second. All the

cameras were placed laterally from the test jig, with a view perpendicular to the bogie's direction of travel. A Nikon D50 digital still camera was also used to document pre- and post-test conditions for all tests.

4.4.6 Data Processing

The electronic accelerometer data obtained in dynamic testing was filtered using the SAE Class 60 Butterworth filter conforming to the SAE J211/1 specifications [81]. The pertinent acceleration signal was extracted from the bulk of the data signals. The processed acceleration data was then multiplied by the mass of the bogie to get the impact force using Newton's Second Law. Next, the acceleration trace was integrated to find the change in velocity versus time. Initial velocity of the bogie, calculated from the pressure tape switch data, was then used to determine the bogie velocity, and the calculated velocity trace was integrated to find the bogie's displacement. This displacement is also the displacement of the test jig at the impact location. Combining the previous results, a force vs. deflection curve was plotted for each test. Finally, integration of the force vs. deflection curve provided the energy vs. deflection curve for each test.

The anchor force for the tensile tests was determined by summing the moments about the reaction point of the test jig and solving for the anchor force. The reaction point was estimated to be the end of the base plate on the non-impact side. This was selected because after a slight rotation of the test jig, only that point would be in contact with the concrete and only a point force would be applied to the jig at this point. Therefore, the anchor force was calculated as the bogie force multiplied by the ratio of the vertical distance to the horizontal distance from the reaction point to the bogie force. A free body diagram of the forces associated with the tension test jig is shown in Figure 20.

The anchor force for the shear jig was calculated as a sum of the forces in the horizontal direction. The frictional forces of the jig sliding on the concrete were neglected so the anchor force was assumed equivalent to the bogie force from the accelerometer data.

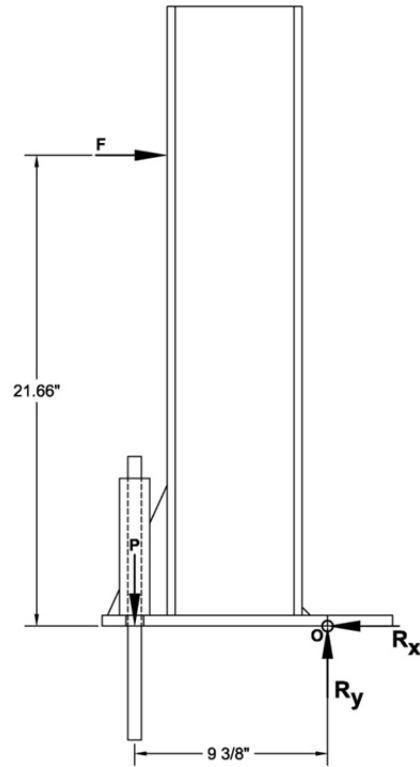


Figure 20. Free Body Diagram of the Tension Test Jig

5 DYNAMIC TESTING RESULTS AND DISCUSSION

5.1 Dynamic Testing Results

A series of 16 dynamic bogie tests were conducted on various epoxy adhesive anchors to determine the shear and tensile capacities. Test nos. WEAB-1 through WEAB-8 utilized no. 5 ASTM A615 Grade 60 deformed reinforcing bars and test nos. WEAB-9 through WEAB-13 and WEAB-16 utilized no. 6 ASTM A615 Grade 60 deformed reinforcing bars. Test nos. WEAB-14 and WEAB-15 utilized 1 1/8 in. (29 mm) diameter ASTM A307 threaded rod. Both tension and shear tests were conducted for each type of anchor. Duel anchor tension tests were also conducted for the reinforcing bar anchors to determine the effects of closely spaced anchors. The test specimens were embedded to a depth of 5-1/4 in. (133 mm) for all of the component tests. The results for test nos. WEAB-1 through WEAB-16 are described in the following sections.

5.1.1 Test No. WEAB-1

For test no. WEAB-1, a single, uncoated no. 5 ASTM A615 Grade 60 deformed reinforcing bar was loaded in tension. The bogie impacted the test jig at a speed of 9.78 mph (15.74 km/h). The anchor experienced necking and fractured approximately 1 ¼ in. (32 mm) above the concrete surface. A concrete cone of approximately 4 to 5 in. (102 to 127 mm) in diameter by 1 in. (25 mm) deep spalled off from the concrete surface. The concrete cone was split into several small pieces that were disengaged from the anchor. The maximum tensile load observed was 38.8 kips (172.6 kN) according to the EDR-3 data and 37.9 kips (168.6 kN) according to the DTS data. Pre- and post-test photographs are shown in Figure 21. A plot of the force versus time history is shown in Figure 22. Sequential photographs are shown in Figure 23.



Pre-Test



Post-Test

Figure 21. Pre- and Post-Test Photographs, Test No. WEAB-1

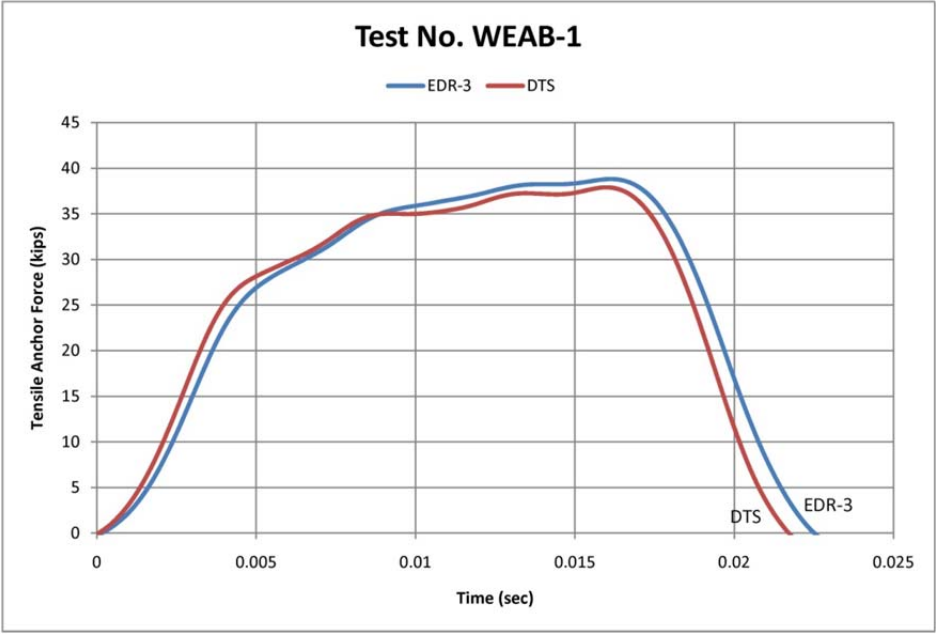


Figure 22. Force vs. Time, Test No. WEAB-1

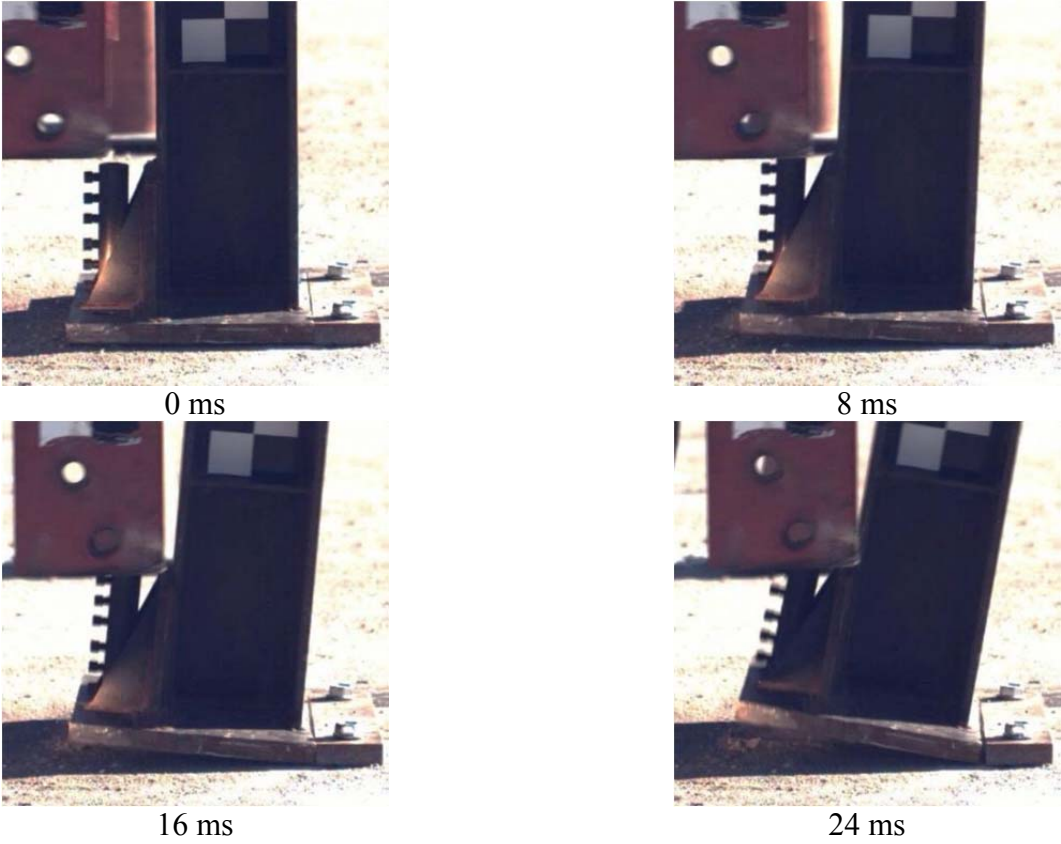


Figure 23. Sequential Photographs, Test No. WEAB-1

5.1.2 Test No. WEAB-2

For test no. WEAB-2, a single, uncoated no. 5 ASTM A615 Grade 60 deformed reinforcing bar was loaded in tension. The bogie impacted the test jig at a speed of 10.40 mph (16.74 km/h). The anchor experienced necking and fractured approximately 1 ¼ in. (32 mm) above the concrete surface. A concrete cone of approximately 3 in. (76 mm) in diameter by ¾ in. (19 mm) deep spalled off from the concrete surface. The concrete cone was split into several small pieces that were disengaged from the anchor. The maximum tensile load observed was 39.8 kips (177.2 kN) according to the EDR-3 data and 38.9 kips (173.2 kN) according to the DTS data. Pre- and post-test photographs are shown in Figure 24. A plot of the force versus time history is shown in Figure 25. Sequential photographs are shown in Figure 26.



Pre-Test



Post-Test

Figure 24. Pre- and Post-Test Photographs, Test No. WEAB-2

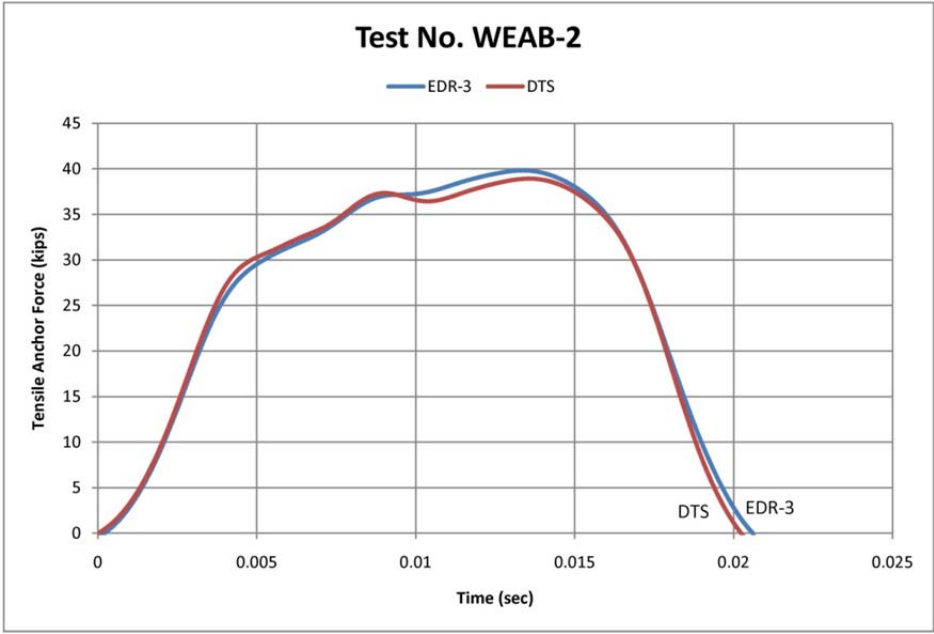


Figure 25. Force vs. Time, Test No. WEAB-2

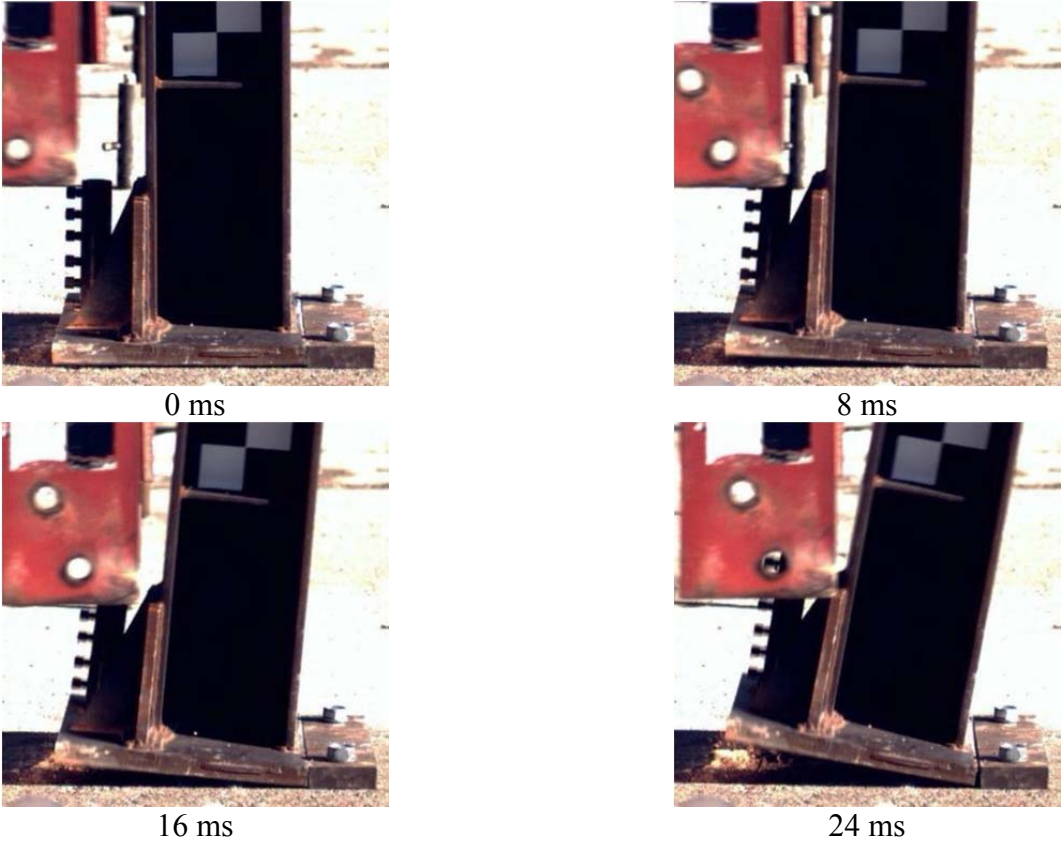


Figure 26. Sequential Photographs, Test No. WEAB-2

5.1.3 Test No. WEAB-3

For test no. WEAB-3, a single, epoxy-coated no. 5 ASTM A615 Grade 60 deformed reinforcing bar was loaded in tension. The bogie impacted the test jig at a speed of 9.47 mph (15.24 km/h). The anchor experienced necking and fractured approximately 3 in. (76 mm) above the concrete surface. A concrete cone of approximately 3 ½ in. (89 mm) in diameter by ½ in. (13 mm) deep spalled off from the concrete surface. The concrete cone was split into several small pieces that were bonded to the anchor. The maximum tensile load observed was 35.1 kips (156.2 kN) according to the EDR-3 data and 34.9 kips (155.1 kN) according to the DTS data. The fracture occurred at a localized minimum cross-sectional area that was created from one of the coupler screws. Therefore, the maximum force was governed by an area less than that of a no. 5 (metric no. 16) reinforcing bar. Pre- and post-test photographs are shown in Figure 27. A plot of the force versus time history is shown in Figure 28. Sequential photographs are shown in Figure 29.



Pre-Test



Post-Test

Figure 27. Pre- and Post-Test Photographs, Test No. WEAB-3

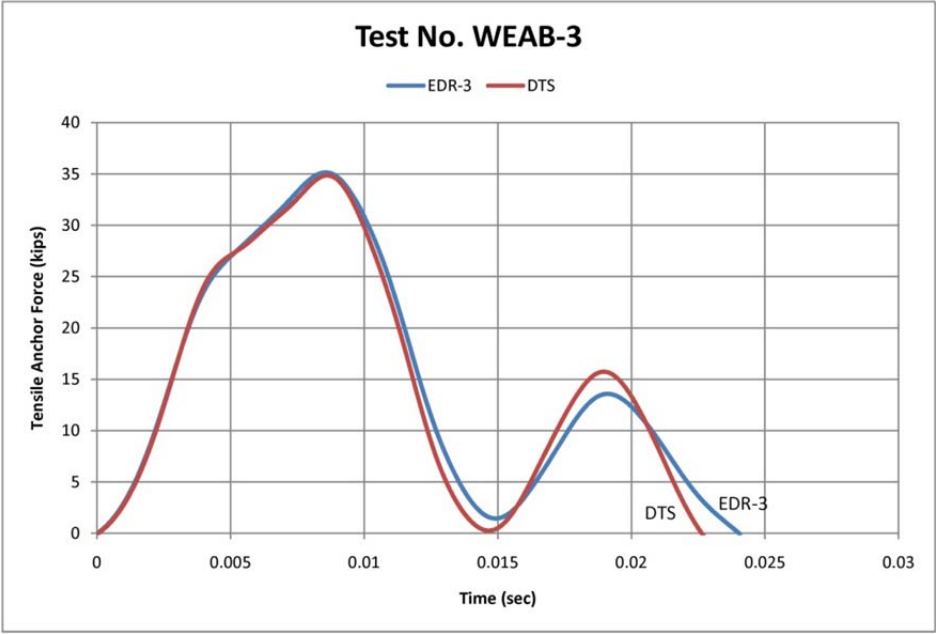


Figure 28. Force vs. Time, Test No. WEAB-3

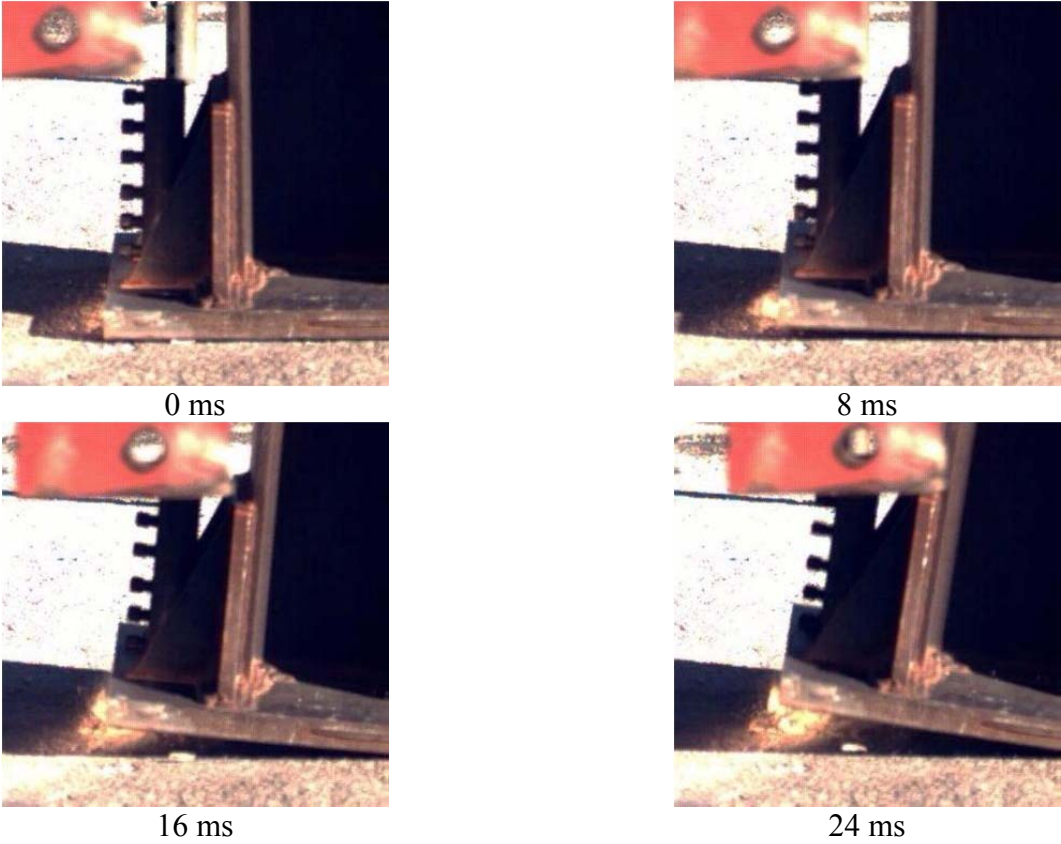


Figure 29. Sequential Photographs, Test No. WEAB-3

5.1.4 Test No. WEAB-4

For test no. WEAB-4, a single, epoxy-coated no. 5 ASTM A615 Grade 60 deformed reinforcing bar was loaded in tension. The bogie impacted the test jig at a speed of 8.86 mph (14.26 km/h). The anchor experienced necking and fractured approximately 2 in. (51 mm) below the concrete surface. A concrete cone of approximately 3 ¾ in. (95 mm) in diameter by 7/8 in. (22 mm) deep spalled off from the concrete surface. The concrete cone was split into several small pieces that were disengaged from the anchor. The maximum tensile load observed was 36.8 kips (163.8 kN) according to the EDR-3 data and 35.1 kips (156.0 kN) according to the DTS data. Pre- and post-test photographs are shown in Figure 30. A plot of the force versus time history is shown in Figure 31. Sequential photographs are shown in Figure 32.



Pre-Test



Post-Test

Figure 30. Pre- and Post-Test Photographs, Test No. WEAB-4

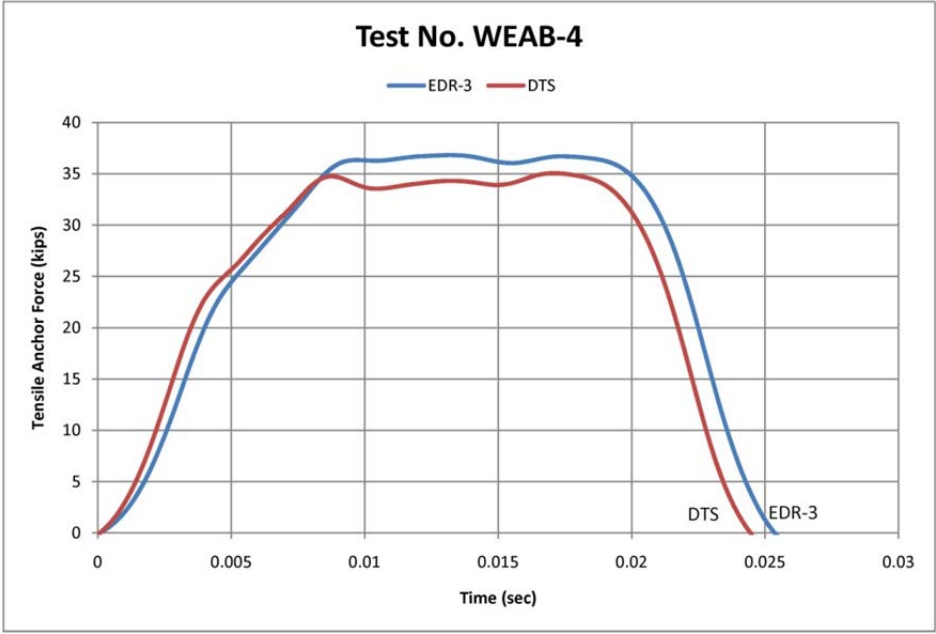


Figure 31. Force vs. Time, Test No. WEAB-4

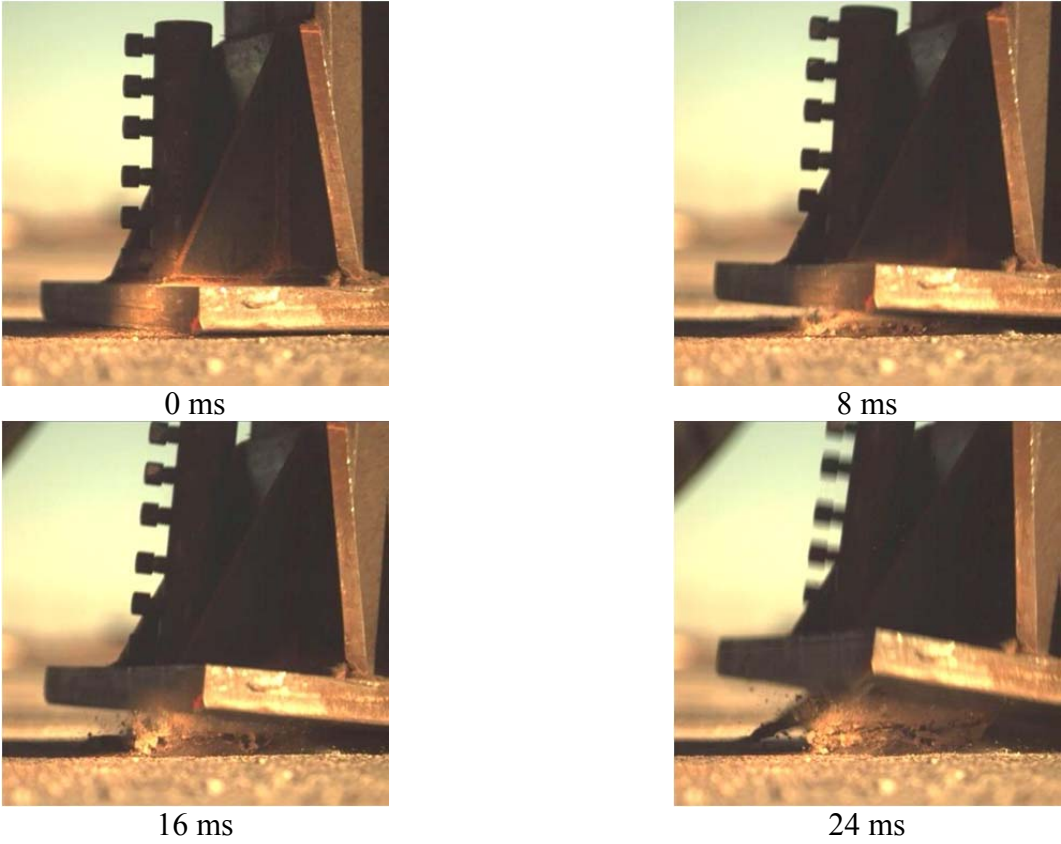


Figure 32. Sequential Photographs, Test No. WEAB-4

5.1.5 Test No. WEAB-5

For test no. WEAB-5, a single, epoxy-coated no. 5 ASTM A615 Grade 60 deformed reinforcing bar was loaded in shear. The bogie impacted the test jig at a speed of 9.64 mph (15.51 km/h). The anchor sheared off at the concrete surface. The maximum shear load observed was 25.7 kips (114.4 kN) according to the EDR-3 data and 32.4 kips (144.0 kN) according to the DTS data. Pre- and post-test photographs are shown in Figure 33. A plot of the force versus time history is shown in Figure 34. Sequential photographs are shown in Figure 35.



Pre-Test



Post-Test

Figure 33. Pre- and Post-Test Photographs, Test No. WEAB-5

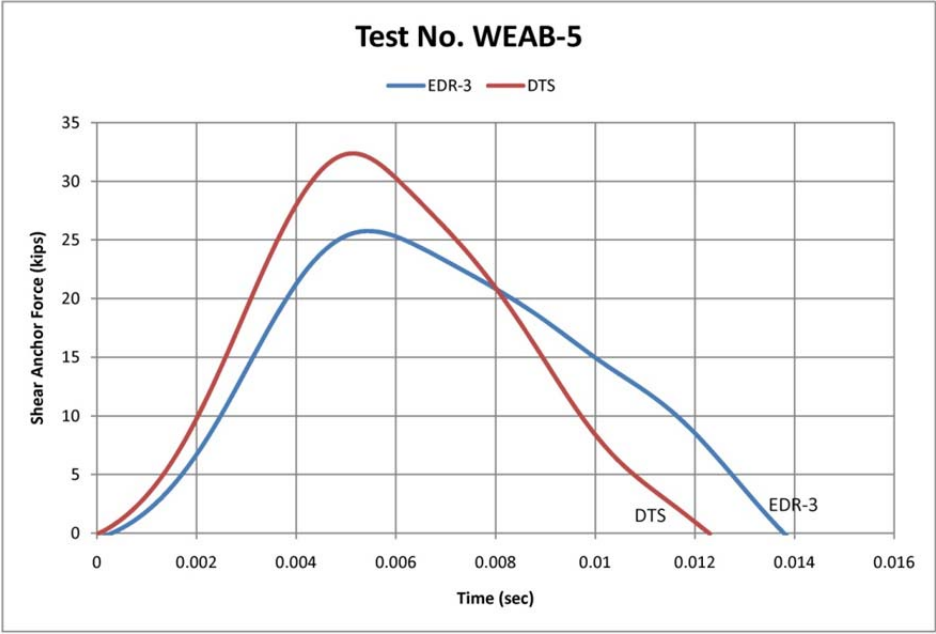


Figure 34. Force vs. Time, Test No. WEAB-5

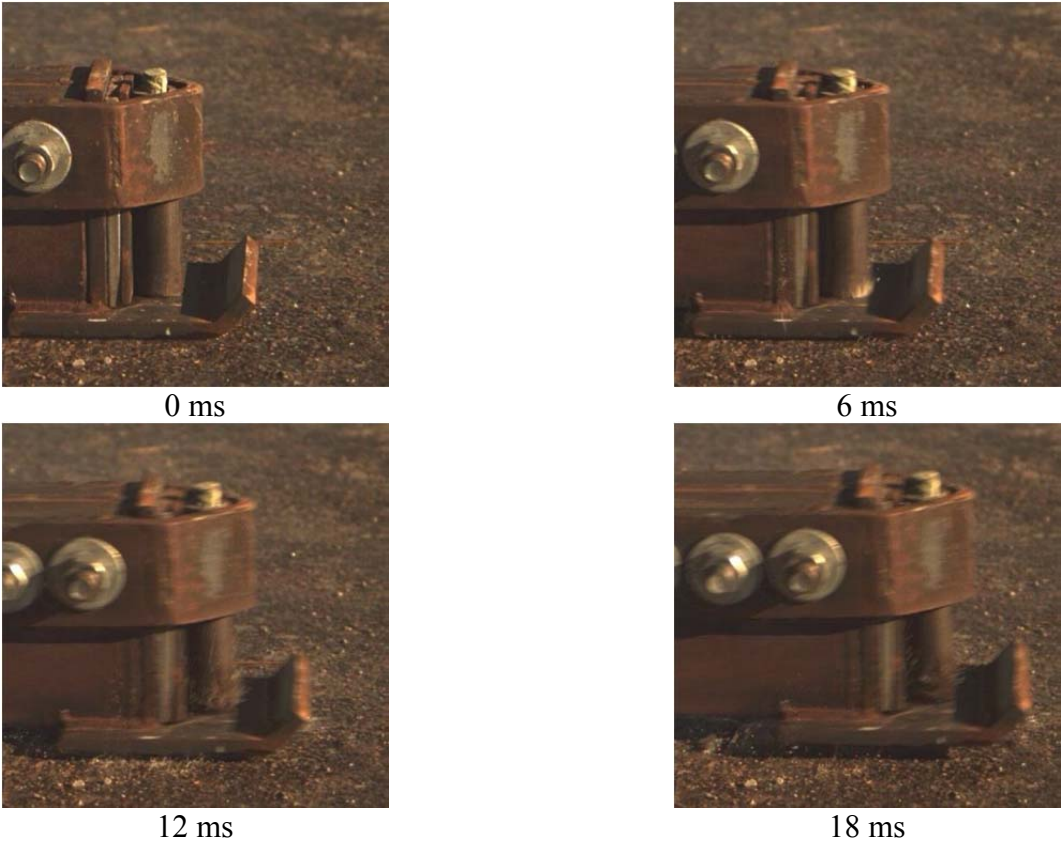


Figure 35. Sequential Photographs, Test No. WEAB-5

5.1.6 Test No. WEAB-6

For test no. WEAB-6, a single, epoxy-coated no. 5 ASTM A615 Grade 60 deformed reinforcing bar was loaded in shear. The bogie impacted the test jig at a speed of 9.71 mph (15.62 km/h). The anchor sheared off at the concrete surface. There was a 1/8 in. (3 mm) gap between the epoxy-coated anchor and the edge of the concrete hole on the impact side. The maximum shear load observed was 23.7 kips (105.6 kN) according to the EDR-3 data and 28.4 kips (126.4 kN) according to the DTS data. Pre- and post-test photographs are shown in Figure 36. A plot of the force versus time history is shown in Figure 37. Sequential photographs are shown in Figure 38.



Pre-Test



Post-Test

Figure 36. Pre- and Post-Test Photographs, Test No. WEAB-6

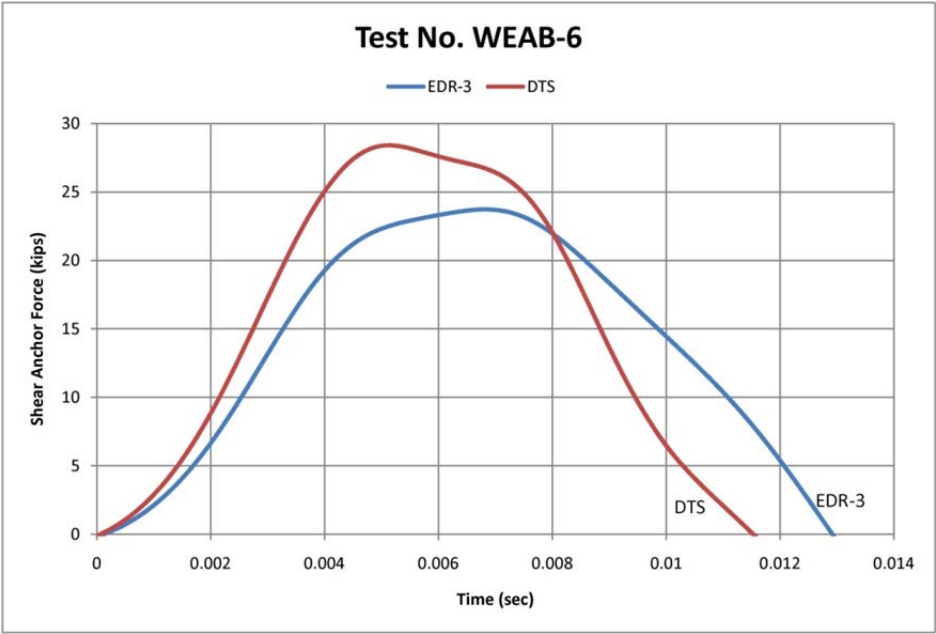


Figure 37. Force vs. Time, Test No. WEAB-6

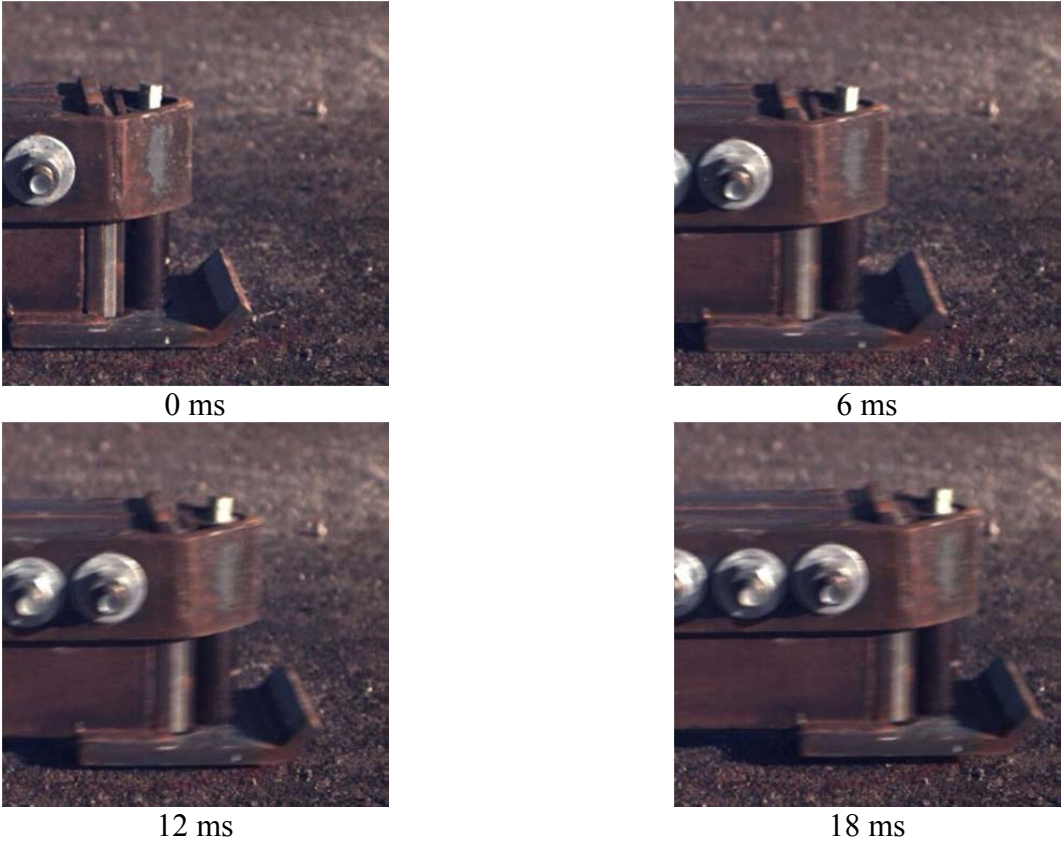


Figure 38. Sequential Photographs, Test No. WEAB-6

5.1.7 Test No. WEAB-7

For test no. WEAB-7, two, epoxy-coated no. 5 ASTM A615 Grade 60 deformed reinforcing bars spaced 8 in. (203 mm) apart were loaded in tension. The bogie impacted the test jig at a speed of 16.64 mph (26.78 km/h). One of the anchors fractured 2 1/8 in. (54 mm) below the concrete surface and was accompanied by a concrete cone breakout of 5 in. (127 mm) in diameter by 1 1/4 in. (32 mm) deep. Detachment of the epoxy coating on this anchor was observed at locations that were bonded to the concrete. The other anchor pulled out of the concrete and was accompanied by a concrete cone breakout of 6 in. (152 mm) diameter by 1 1/4 in. (32 mm) deep. Slight flaking of the epoxy coating was observed on the anchor that pulled out. It appeared that the pullout occurred due to disengagement of the adhesive from the epoxy coating of the rebar. Both reinforcing bars were slightly bent. The maximum tensile load observed was 73.8 kips (328.3 kN) according to the EDR-3 data and 73.8 kips (328.3 kN) according to the DTS data. Pre- and post-test photographs are shown in Figure 39. Pictures of the anchors are shown in Figure 40. A plot of the force versus time history is shown in Figure 41. Sequential photographs are shown in Figure 42.



Pre-Test



Post-Test

Figure 39. Pre- and Post-Test Photographs, Test No. WEAB-7



Figure 40. Post-Test Anchor Photographs, Test No. WEAB-7

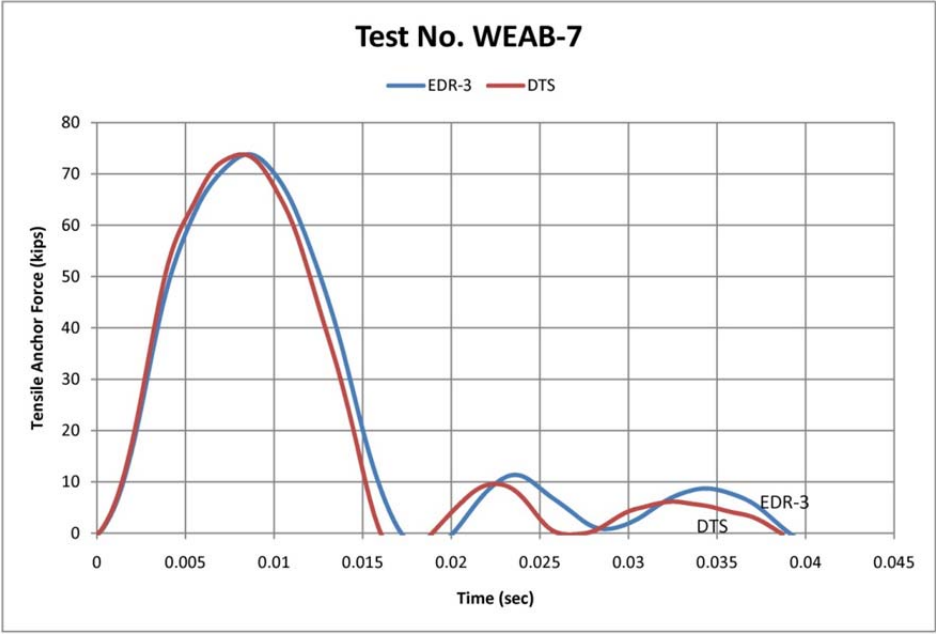


Figure 41. Force vs. Time, Test No. WEAB-7

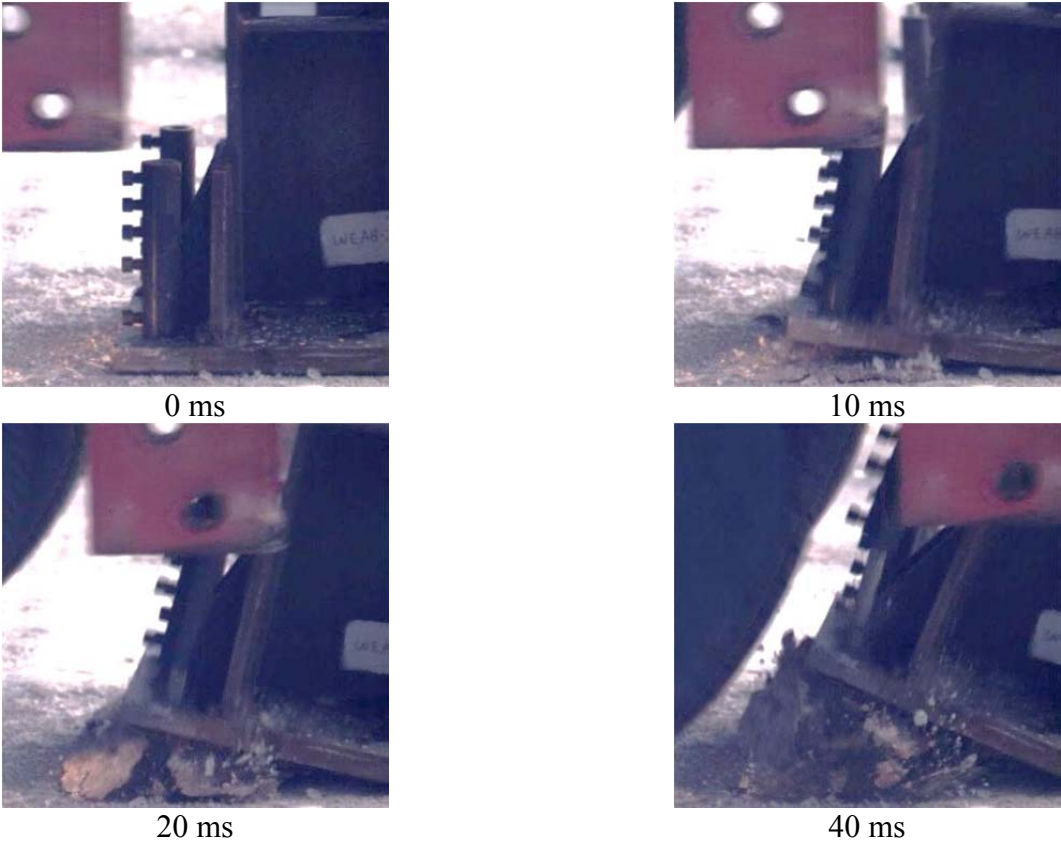


Figure 42. Sequential Photographs, Test No. WEAB-7

5.1.8 Test No. WEAB-8

For test no. WEAB-8, two, epoxy-coated no. 5 ASTM A615 Grade 60 deformed reinforcing bars spaced 8 in. (203 mm) apart were loaded in tension. The bogie impacted the test jig at a speed of 14.05 mph (22.61 km/h). Both anchors pulled out of the concrete. The concrete breakout area was approximately 29 in. (737 mm) long by 24 in. (610 mm) wide by 4 in. (102 mm) deep at the anchor hole locations. It was suspected that the failure area was larger than observed in previous testing due to potential existing damage to the aged concrete. Bond failures were present on both the epoxy-anchor and the epoxy-concrete interfaces. The epoxy adhesive was attached to the anchor for the bottom 4 in. (102 mm) of both reinforcing bars. Both reinforcing bars were slightly bent. The maximum tensile load observed was 72.6 kips (323.1 kN) according to the EDR-3 data and 72.4 kips (322.1 kN) according to the DTS data. Pre- and post-test photographs are shown in Figure 43. Pictures of the pulled-out anchors are shown in Figure 44. A plot of the force versus time history is shown in Figure 45. Sequential photographs are shown in Figure 46.



Pre-Test



Post-Test

Figure 43. Pre- and Post-Test Photographs, Test No. WEAB-8



Figure 44. Post-Test Anchor Photographs, Test No. WEAB-8

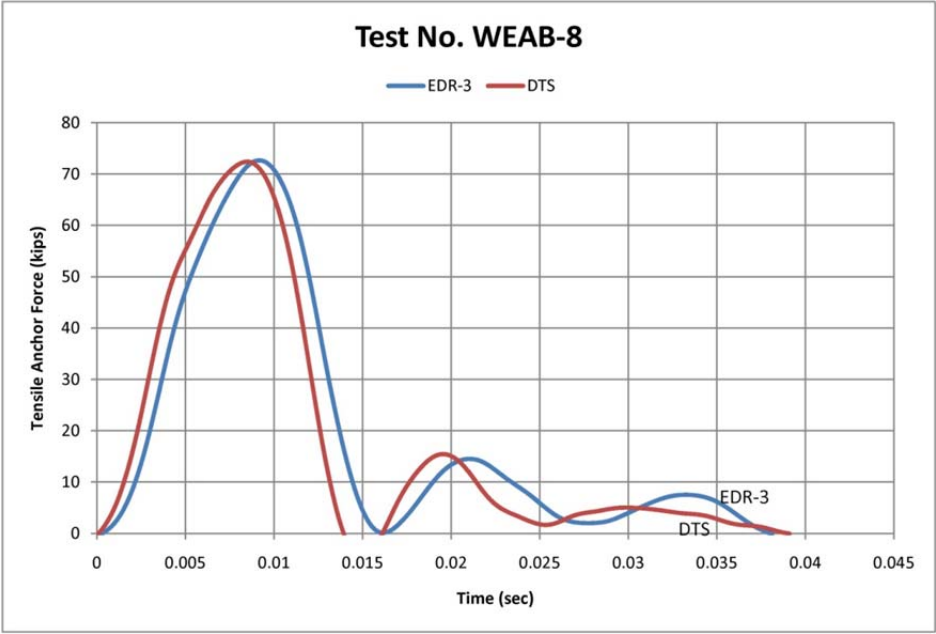


Figure 45. Force vs. Time, Test No. WEAB-8

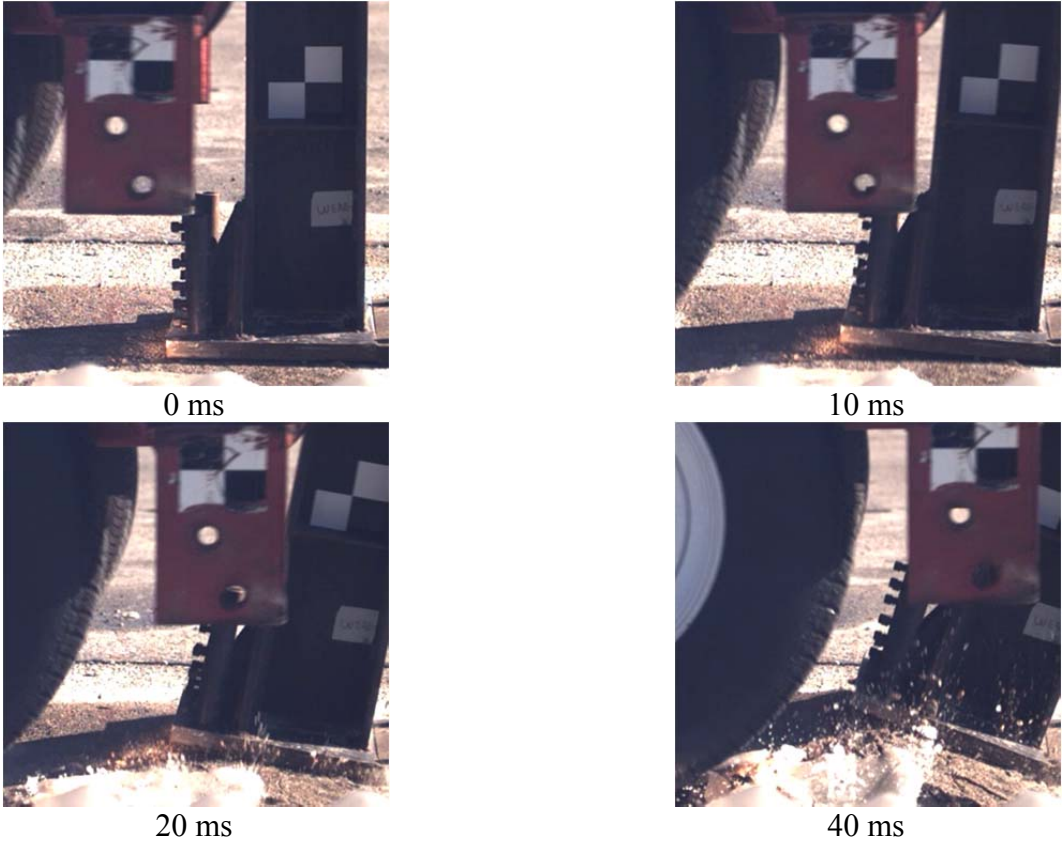
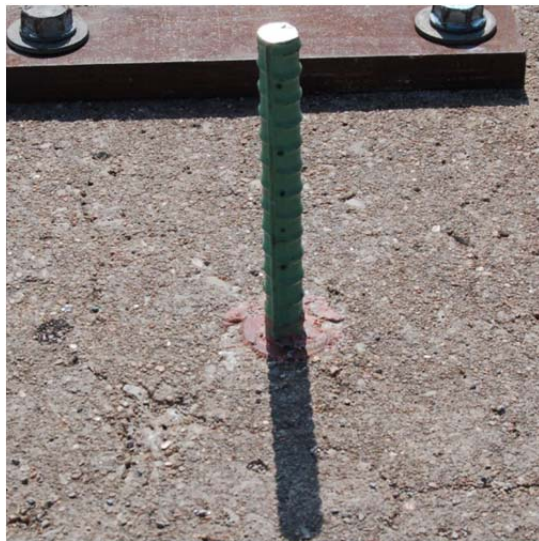


Figure 46. Sequential Photographs, Test No. WEAB-8

5.1.9 Test No. WEAB-9

For test no. WEAB-9, a single, epoxy-coated no. 6 ASTM A615 Grade 60 deformed reinforcing bar was loaded in tension. The bogie impacted the test jig at a speed of 14.23 mph (22.90 km/h). The anchor pulled out of the concrete hole and still had some epoxy adhesive attached on the bottom half of the embedded anchor length. There was not any flaking of the protective epoxy coating of the anchor. A concrete cone of approximately 3 ½ in. (89 mm) in diameter by ½ in. (13 mm) deep broke out and small concrete chucks were scattered around the anchor area. The maximum tensile load observed was 41.0 kips (182.3 kN) according to the EDR-3 data and 41.6 kips (185.2 kN) according to the DTS data. Pre- and post-test photographs are shown in Figure 47. A picture of the pulled out anchor is shown in Figure 48. A plot of the force versus time history is shown in Figure 49. Sequential photographs are shown in Figure 50.



Pre-Test



Post-Test

Figure 47. Pre- and Post-Test Photographs, Test No. WEAB-9



Figure 48. Post-Test Anchor Photograph, Test No. WEAB-9

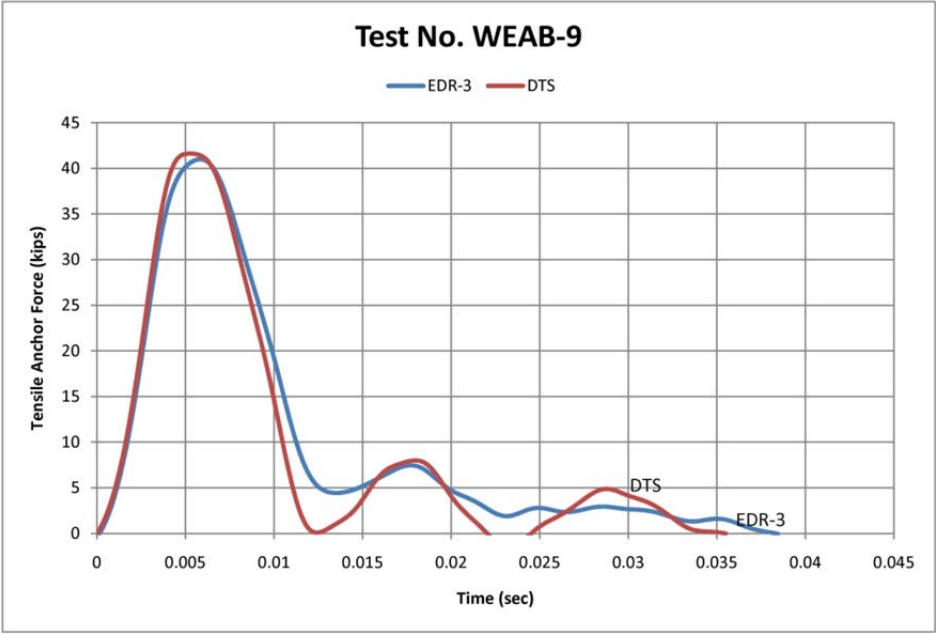


Figure 49. Force vs. Time, Test No. WEAB-9

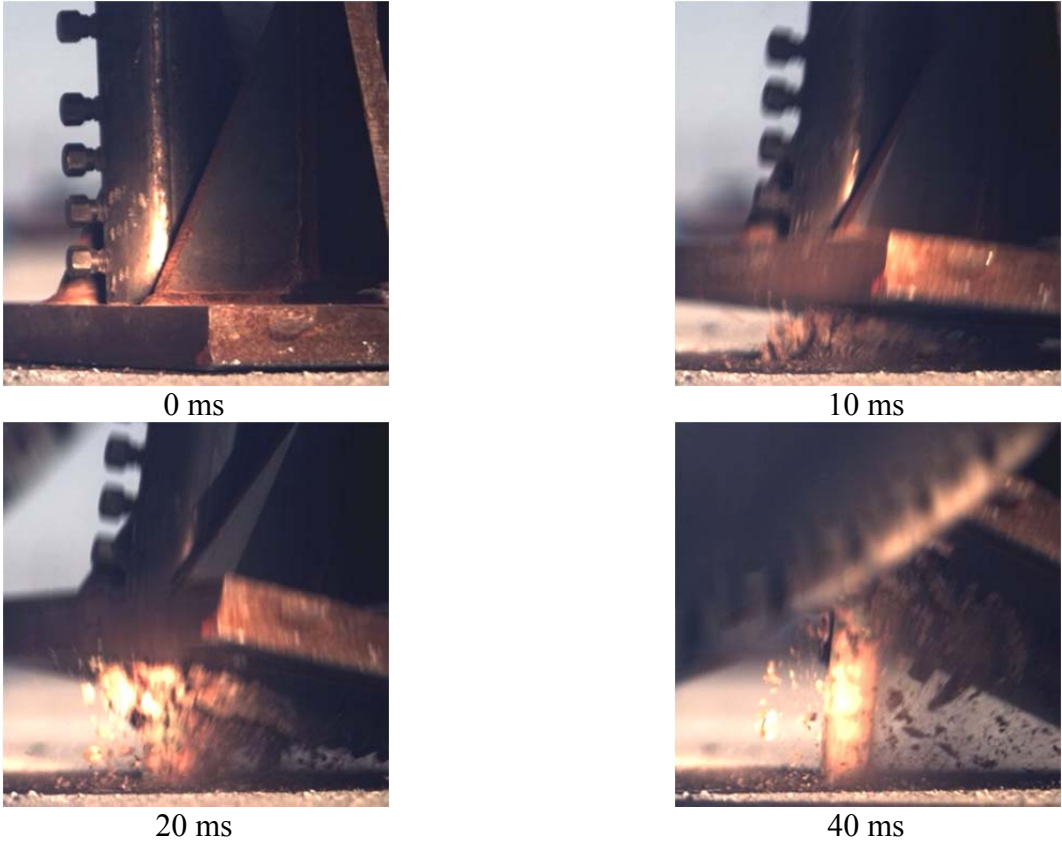


Figure 50. Sequential Photographs, Test No. WEAB-9

5.1.10 Test No. WEAB-10

For test no. WEAB-10, a single, epoxy-coated no. 6 ASTM A615 Grade 60 deformed reinforcing bar was loaded in tension. The bogie impacted the test jig at a speed of 15.73 mph (25.31 km/h). The anchor pulled out of the concrete hole and very little epoxy adhesive was still bonded to the anchor. There was a significant amount of the protective epoxy coating removed from the anchor at the middle 1/3 of the embedded portion. A concrete cone of approximately 4 ½ in. (114 mm) diameter by 1 in. (25 mm) deep broke out and small concrete chunks were scattered around the anchor area. The maximum tensile load observed was 42.7 kips (189.9 kN) according to the EDR-3 data, 44.2 kips (196.5 kN) according to the DTS no. 1 data, and 44.4 kips (197.3 kN) according to the DTS no. 2 data. Pre- and post-test photographs are shown in Figure 51. A picture of the pulled out anchor is shown in Figure 52. A plot of the force versus time history is shown in Figure 53. Sequential photographs are shown in Figure 54.



Pre-Test



Post-Test

Figure 51. Pre- and Post-Test Photographs, Test No. WEAB-10



Figure 52. Post-Test Anchor Photograph, Test No. WEAB-10

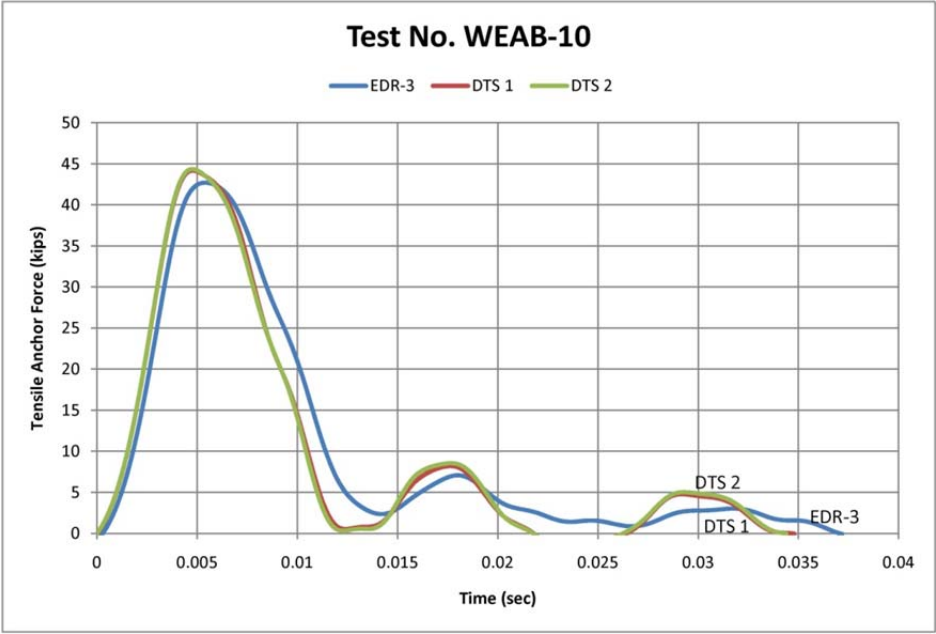


Figure 53. Force vs. Time, Test No. WEAB-10

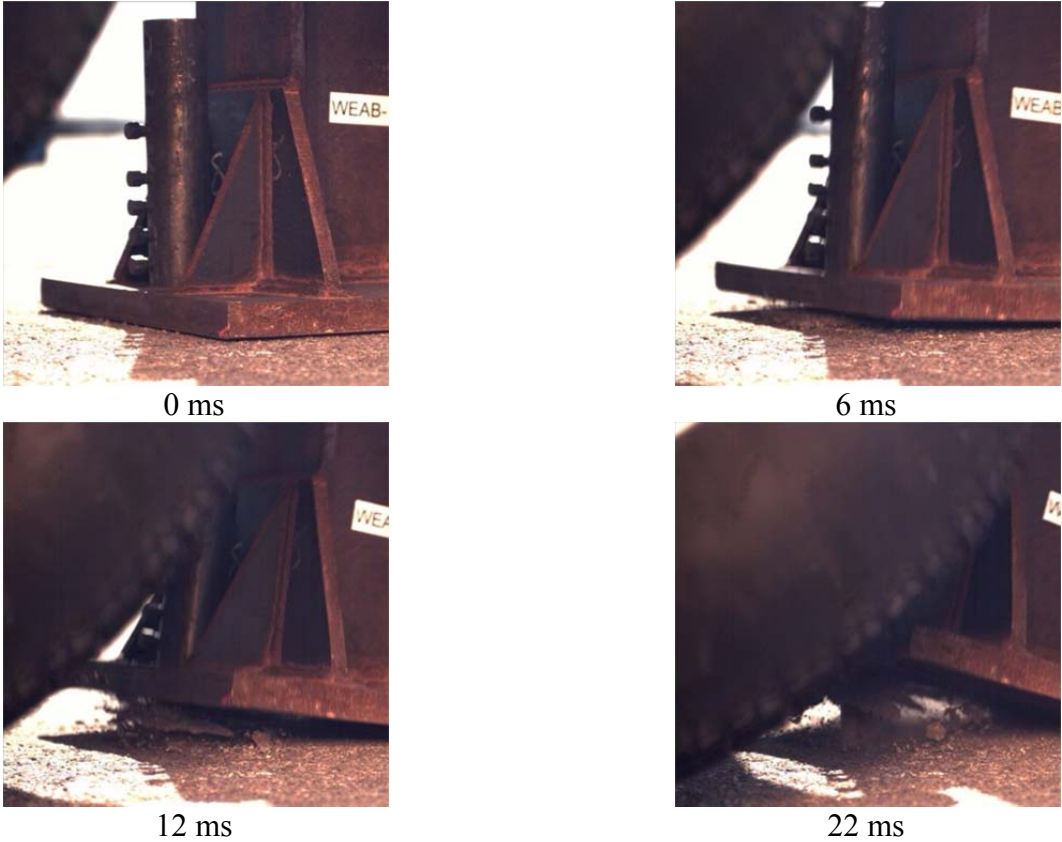


Figure 54. Sequential Photographs, Test No. WEAB-10

5.1.11 Test No. WEAB-11

For test no. WEAB-11, two epoxy-coated no. 6 ASTM A615 Grade 60 deformed reinforcing bars spaced 8 in. (203 mm) apart were loaded in tension. The bogie impacted the test jig at a speed of 15.11 mph (24.32 km/h). The anchors pulled out of the concrete holes and still had most of the epoxy adhesive still bonded to the anchors. The concrete breakout surface was approximately 14 in. (356 mm) by long by 16 in. (406 mm) wide. The maximum depths of the concrete breakout surface were 2 3/4 in. (70 mm) and 3 in. (76 mm), respectively, at the locations of the two anchor holes. The maximum tensile load observed was 60.9 kips (270.8 kN) according to the EDR-3 data, 60.5 kips (269.1 kN) according to the DTS no. 1 data, and 60.6 kips (269.5 kN) according to the DTS no. 2 data. Pre- and post-test photographs are shown in Figure 55. Pictures of the pulled out anchors are shown in Figure 56. A plot of the force versus time history is shown in Figure 57. Sequential photographs are shown in Figure 58.



Pre-Test



Post-Test

Figure 55. Pre- and Post-Test Photographs, Test No. WEAB-11



Figure 56. Post-Test Anchor Photograph, Test No. WEAB-11

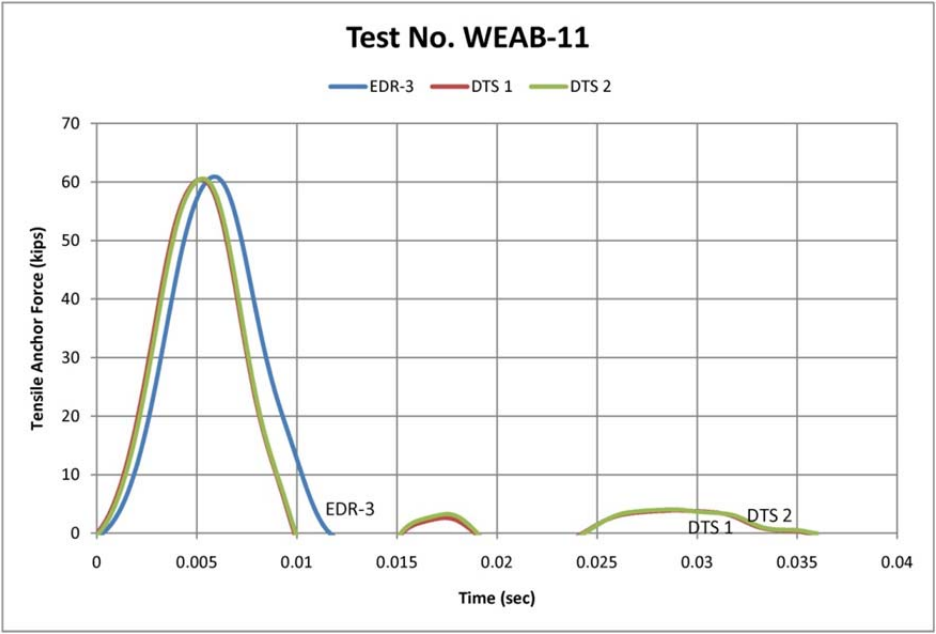


Figure 57. Force vs. Time, Test No. WEAB-11

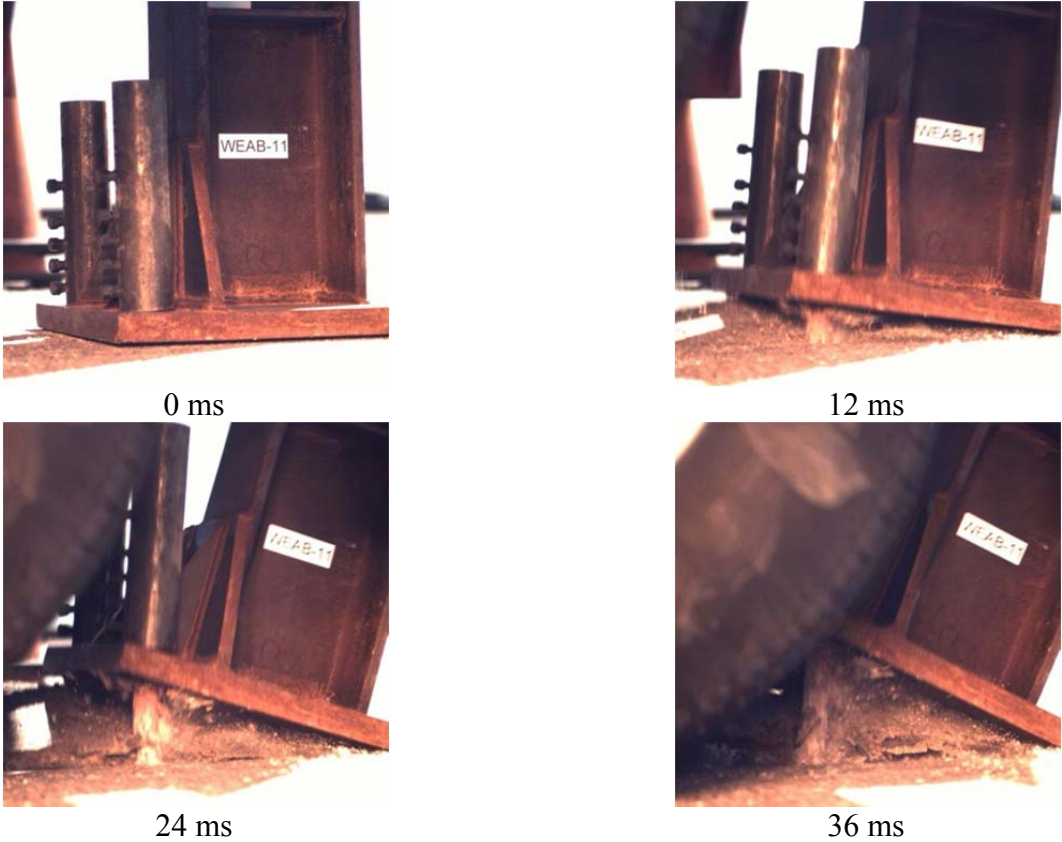


Figure 58. Sequential Photographs, Test No. WEAB-11

5.1.12 Test No. WEAB-12

For test no. WEAB-12, two epoxy-coated no. 6 ASTM A615 Grade 60 deformed reinforcing bars spaced 8 in. (203 mm) apart were loaded in tension. The bogie impacted the test jig at a speed of 15.08 mph (24.27 km/h). The anchors pulled out of the concrete. Anchor no. 1 had some epoxy adhesive still attached to the middle 1/3 of the embedment length and a significant amount of the epoxy coating had flaked off the bottom 1/3 of the embedded length. Anchor no. 2 had some epoxy adhesive still attached on the top 1/3 of the embedded length and most of the protective epoxy coating was flaked away for the bottom 1/2 of the embedded length. Two separate concrete cone breakouts occurred. The cone size for anchor no. 1 was approximately 6 1/2 in. (165 mm) in diameter by 2 in. (51 mm) deep while the cone size for anchor no. 2 was approximately 4 in. (102) in diameter by 1 1/2 in. (38 mm) deep. The maximum tensile load observed was 75.7 kips (336.6 kN) according to the EDR-3 data, 75.7 kips (336.0 kN) according to the DTS no. 1 data, and 75.5 kips (335.7 kN) according to the DTS no. 2 data. Pre- and post-test photographs are shown in Figure 59. Pictures of the pulled out anchors are shown in Figure 60. A plot of the force versus time history is shown in Figure 61. Sequential photographs are shown in Figure 62.



Pre-Test



Post-Test

Figure 59. Pre- and Post-Test Photographs, Test No. WEAB-12



Figure 60. Post-Test Anchor Photograph, Test No. WEAB-12

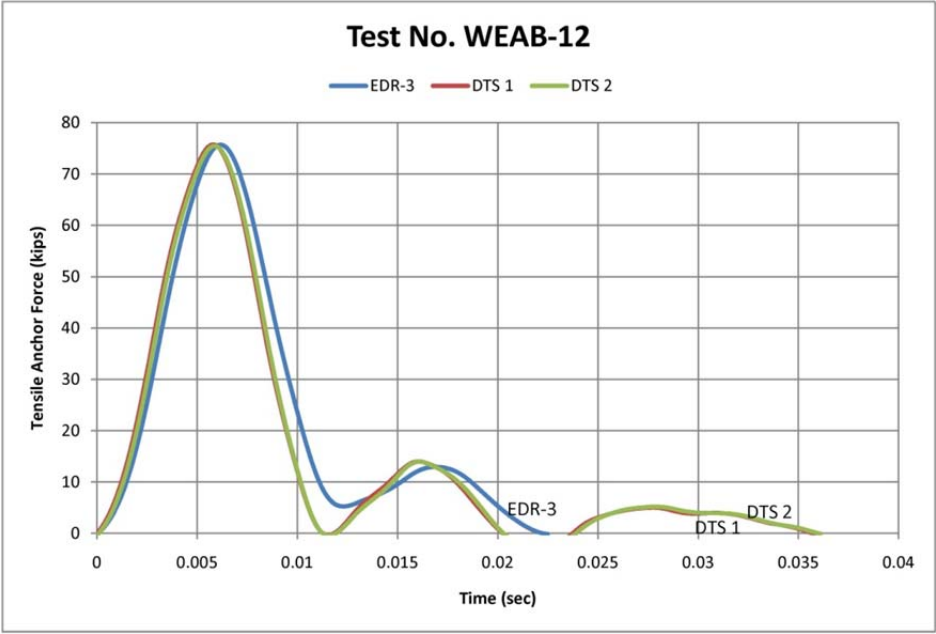


Figure 61. Force vs. Time, Test No. WEAB-12

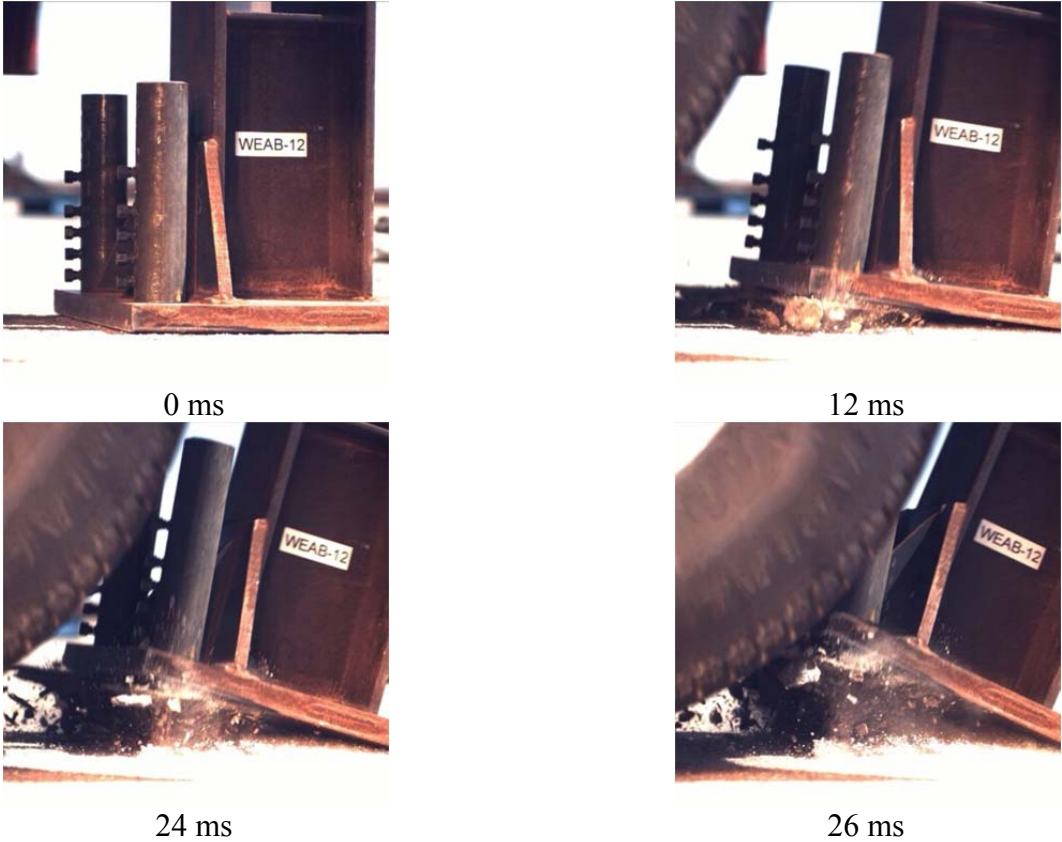


Figure 62. Sequential Photographs, Test No. WEAB-12

5.1.13 Test No. WEAB-13

For test no. WEAB-13, a single, epoxy-coated no. 6 ASTM A615 Grade 60 deformed reinforcing bar was loaded in shear. The bogie impacted the test jig at a speed of 9.98 mph (16.06 km/h). The anchor sheared off at the concrete surface. There was a 3/8 in. (10 mm) gap between the epoxy-coated anchor and the edge of the concrete hole on the impact side. A small amount of concrete dust and particles were loose on the non-impact side of the anchor. The maximum shear load observed was 32.1 kips (142.9 kN) according to the EDR-3 data, 29.6 kips (131.9 kN) according to the DTS no.1 data, and 28.4 kips (126.4 kN) according to the DTS no. 2 data. Pre- and post-test photographs are shown in Figure 63. A plot of the force versus time history is shown in Figure 64. Sequential photographs are shown in Figure 65.



Pre-Test



Post-Test

Figure 63. Pre- and Post-Test Photographs, Test No. WEAB-13

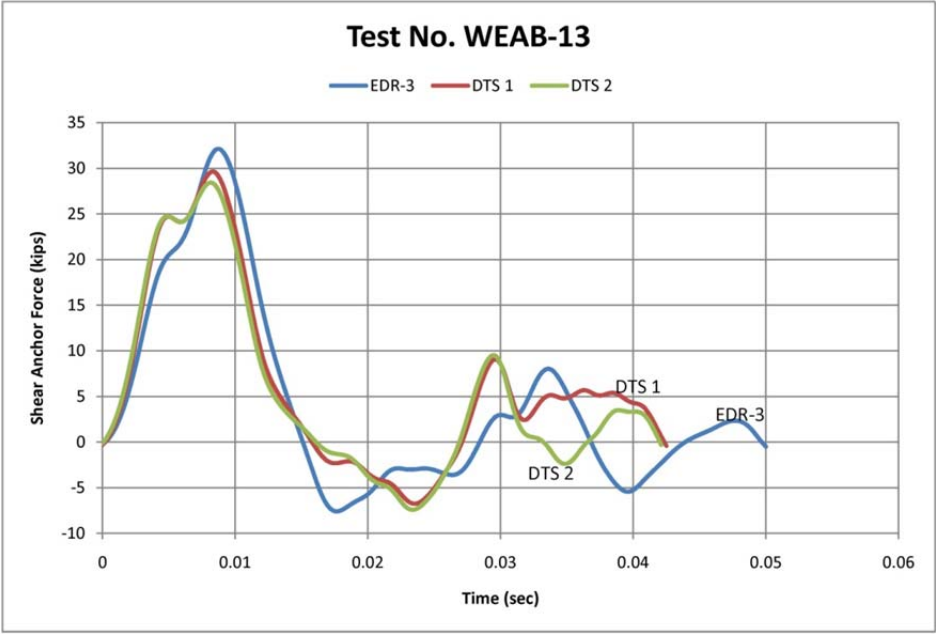


Figure 64. Force vs. Time, Test No. WEAB-13

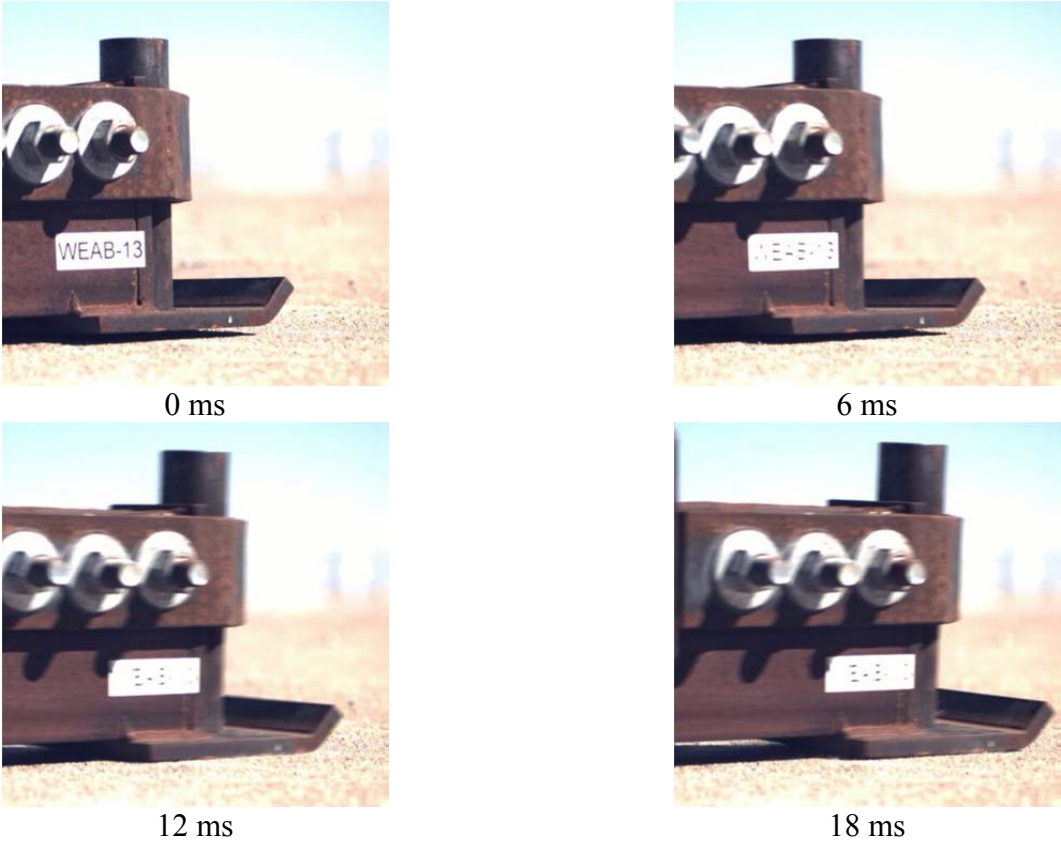


Figure 65. Sequential Photographs, Test No. WEAB-13

5.1.14 Test No. WEAB-14

For test no. WEAB-14, a single, 1 1/8 in. (29 mm) diameter ASTM A307 threaded rod was loaded in tension. The bogie impacted the test jig at a speed of 15.19 mph (24.45 km/h). The anchor pulled out of the concrete hole and had most of the epoxy adhesive still attached on the bottom 2/3 of the embedded length. A concrete cone of approximately 15 in. (381 mm) in diameter by 2 3/4 in. (70 mm) deep broke out and concrete chunks were scattered around the anchor area. The maximum tensile load observed was 43.7 kips (194.5 kN) according to the EDR-3 data, 46.7 kips (207.8 kN) according to the DTS no. 1 data, and 45.5 kips (202.3 kN) according to the DTS no. 2 data. Pre- and post-test photographs are shown in Figure 66. A picture of the pulled out anchor is shown in Figure 67. A plot of the force versus time history is shown in Figure 68. Sequential photographs are shown in Figure 69.



Pre-Test



Post-Test

Figure 66. Pre- and Post-Test Photographs, Test No. WEAB-14



Figure 67. Post-Test Anchor Photograph, Test No. WEAB-14

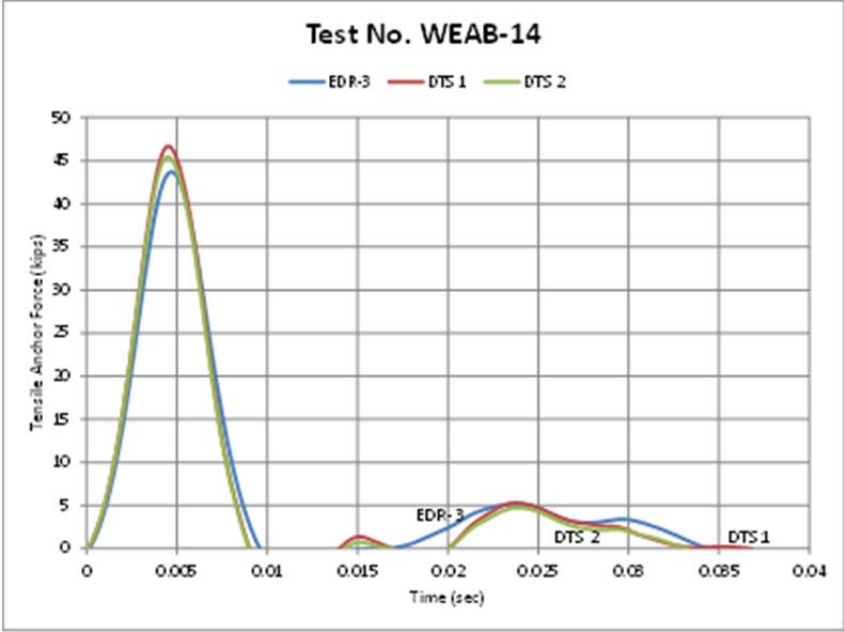


Figure 68. Force vs. Time, Test No. WEAB-14

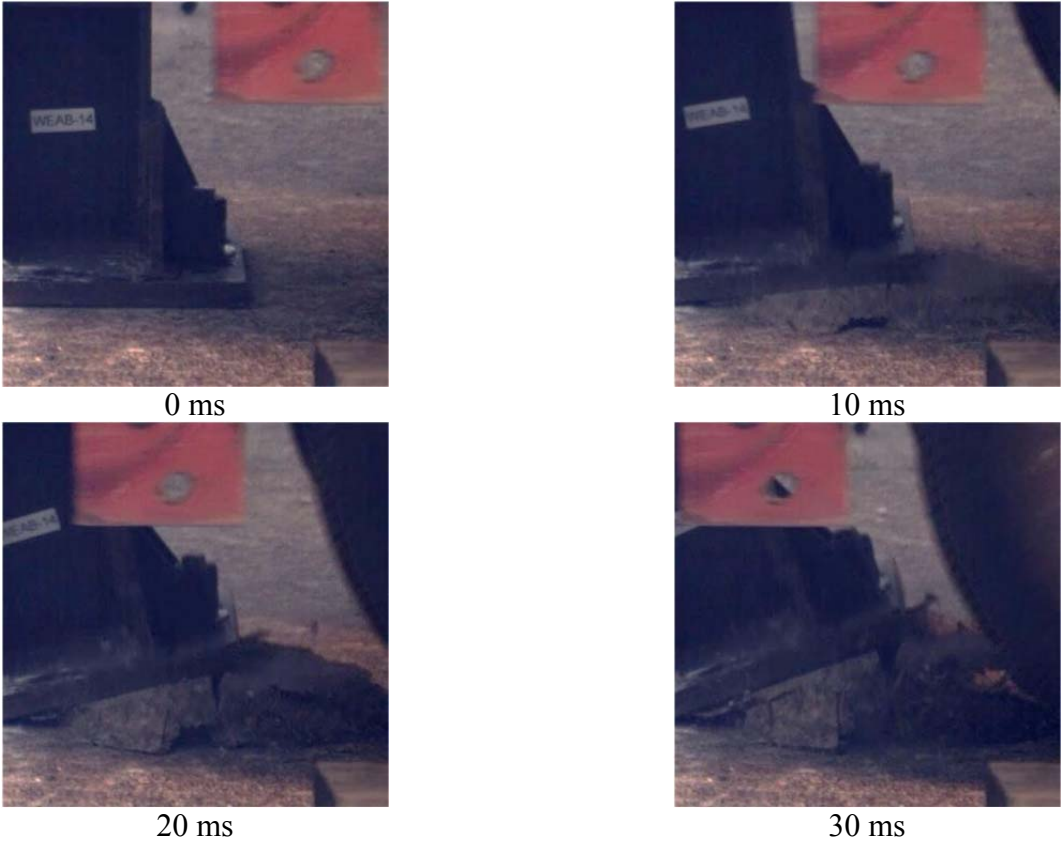


Figure 69. Sequential Photographs, Test No. WEAB-14

5.1.15 Test No. WEAB-15

For test no. WEAB-15, a single, 1 1/8 in. (29 mm) diameter ASTM A307 threaded rod was loaded in shear. The bogie impacted the test jig at a speed of 9.28 mph (14.93 km/h). The welds on the bogie head fractured before the anchor failed. The anchor experienced plastic deformation and bent to an angle of 6 degrees from the vertical direction. A slight shear fracture surface started to form on the impact side of the anchor. The maximum shear load observed was 43.7 kips (194.2 kN) according to the EDR-3 data, 39.1 kips (173.8 kN) according to the DTS no. 1 data, and 39.2 kips (174.3 kN) according to the DTS no. 2 data. Pre- and post-test photographs are shown in Figure 70. A plot of the force versus time history is shown in Figure 71. Sequential photographs are shown in Figure 72.



Pre-Test



Post-Test

Figure 70. Pre- and Post-Test Photographs, Test No. WEAB-15

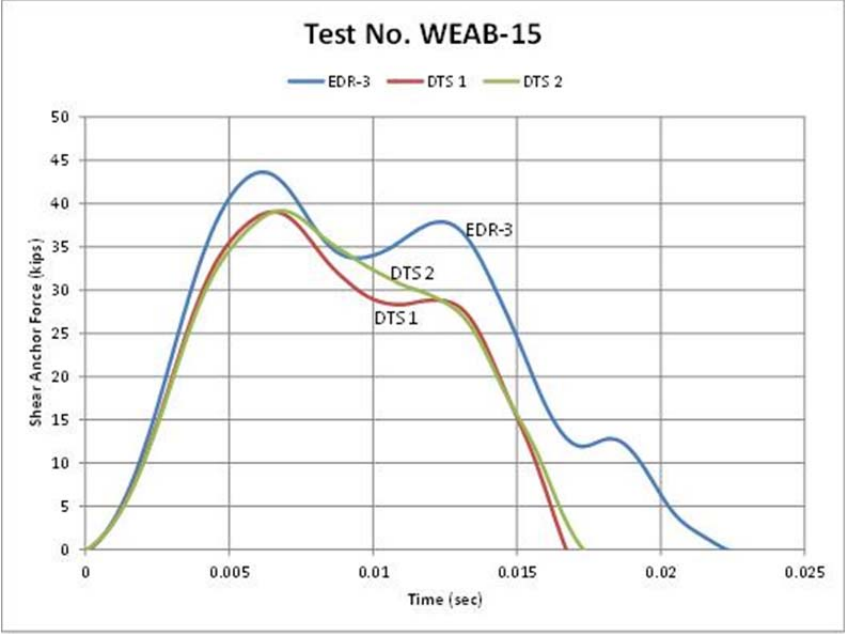


Figure 71. Force vs. Time, Test No. WEAB-15

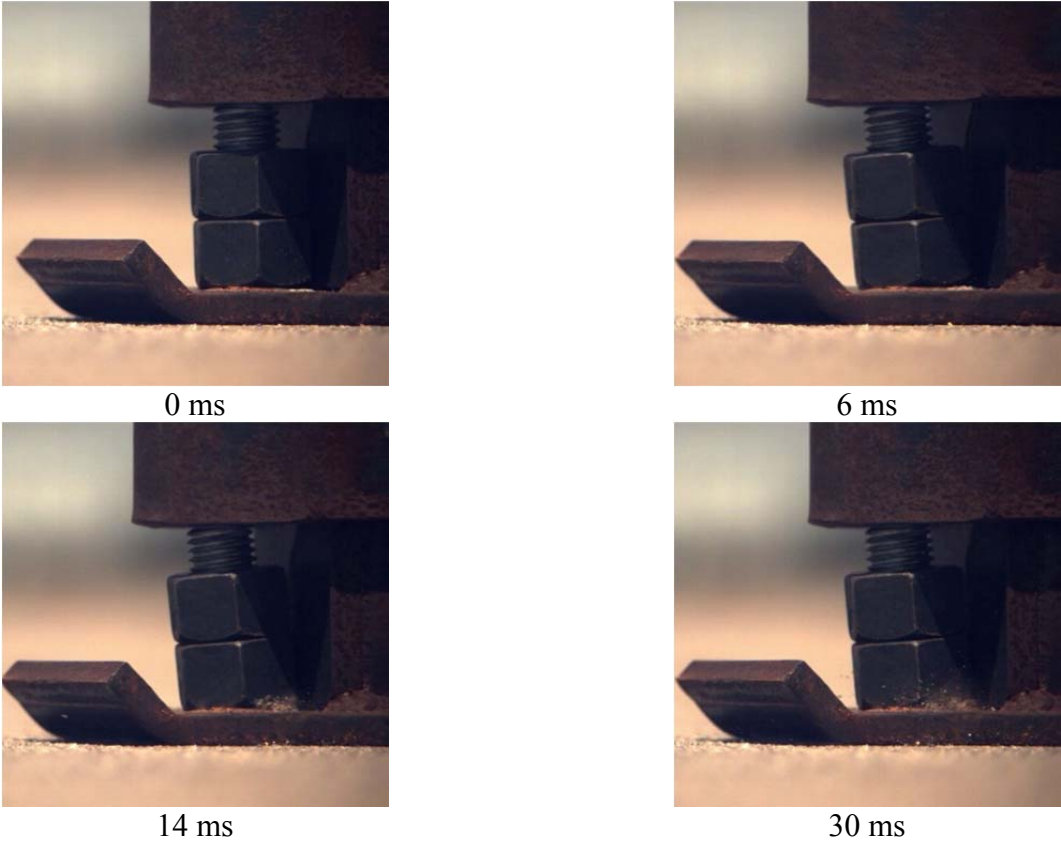


Figure 72. Sequential Photographs, Test No. WEAB-15

5.1.16 Test No. WEAB-16

For test no. WEAB-16, a single, uncoated no. 6 ASTM A615 Grade 60 deformed reinforcing bar was loaded in tension. The bogie impacted the test jig at a speed of 15.90 mph (25.58 km/h). The anchor pulled out of the concrete hole and had a small amount of epoxy still attached on the bottom 3 in. (76 mm) of the embedded length. A concrete cone of approximately 6 in. (152 mm) in diameter by 1 ¼ in. (32 mm) deep broke out and small concrete chunks were scattered around the anchor area. The maximum tensile load observed was 49.6 kips (220.4 kN) according to EDR-3 data, 47.0 kips (209.2 kN) according to DTS no. 1 data, and 45.2 kips (200.9 kN) according to DTS no. 2 data. Pre- and post-test photographs are shown in Figure 73. A picture of the pulled out anchor is shown in Figure 74. A plot of the force versus time history is shown in Figure 75. Sequential photographs are shown in Figure 76.



Pre-Test



Post-Test

Figure 73. Pre- and Post-Test Photographs, Test No. WEAB-16



Figure 74. Post-Test Anchor Photograph, Test No. WEAB-16

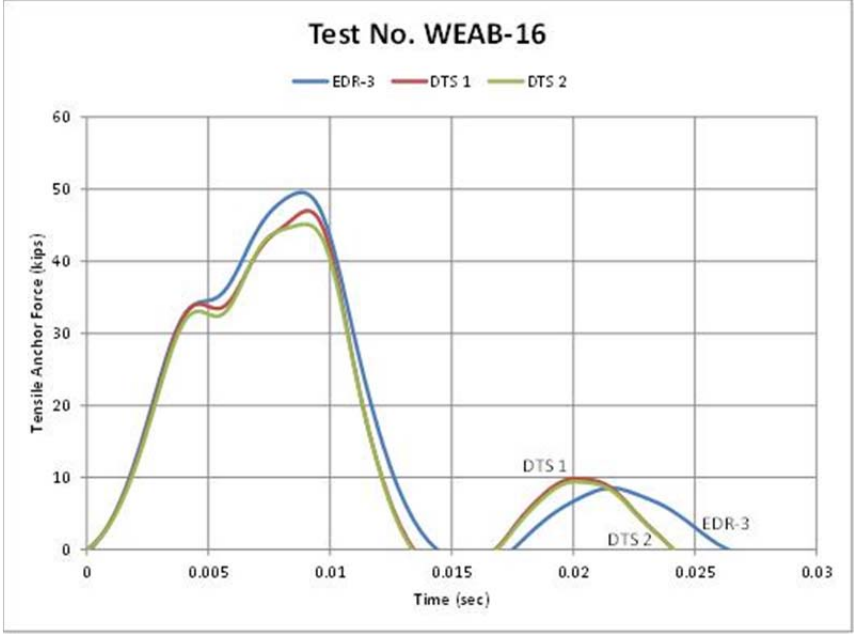


Figure 75. Force vs. Time, Test No. WEAB-16

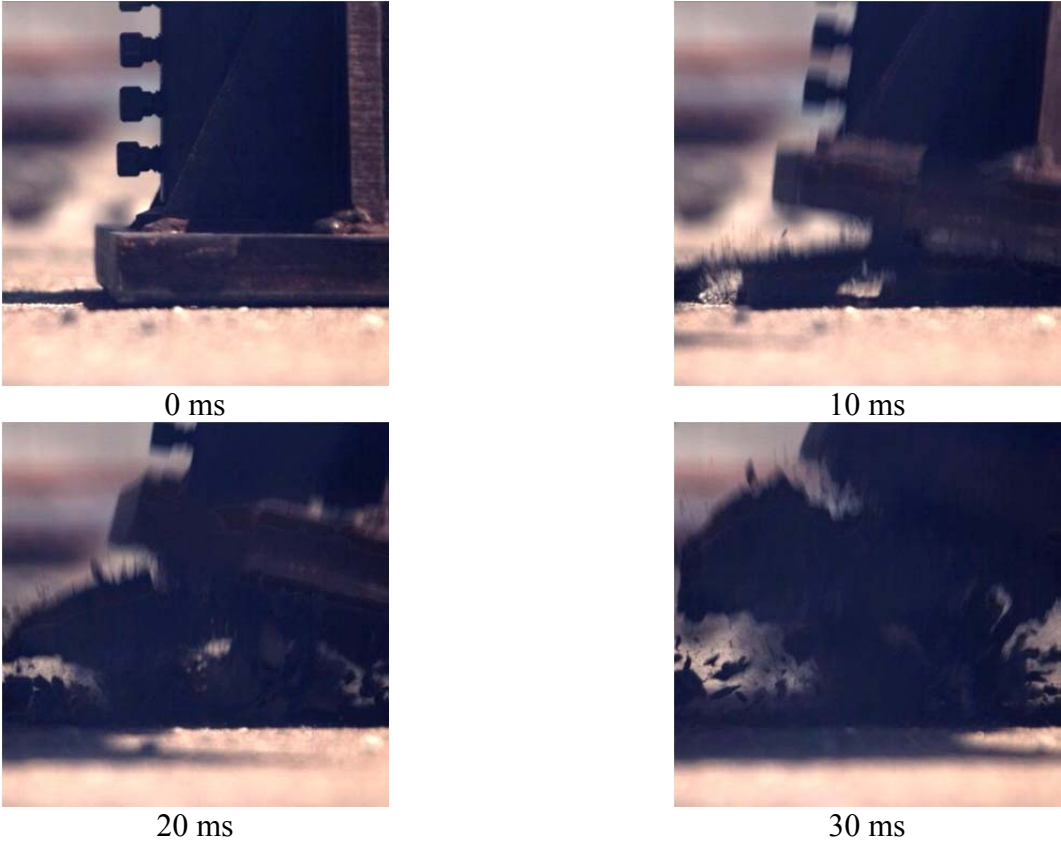


Figure 76. Sequential Photographs, Test No. WEAB-16

5.2 Discussion of Results

The dynamic bogie tests were used to establish criteria for the increase in load capacity based on dynamic loading, the effects of using epoxy-coated reinforcing bars, and the effects of groups of anchors located in close proximity to each other. The anchors were embedded 5 ¼ in. (133 mm) for all tests to allow for use in an 8-in. (203-mm) thick bridge deck without potentially damaging the underside during installation. Most of the tests were conducted with either no. 5 or 6 ASTM A615 Grade 60 reinforcing bars because those were the most commonly used anchor bar detailed in the state standard bridge railings (see Tables 5 and 6). Tension and shear tests were also conducted on 1 1/8 in. (29 mm) ASTM A307 threaded rods, the anchorage used in the bolt-through tie-down system for the F-shape temporary concrete barrier developed by MwRSF [41]. The results for test nos. WEAB-1 through WEAB-16 are shown in Table 9. Note that the failure modes listed in Table 9 were listed as steel fracture, concrete breakout, or adhesive bond failure depending on the mode of failure observed in the testing. Concrete fracture was noted if the concrete cone depth observed in the testing was greater than or equal to 2 in (51 mm). This concrete cone depth was consistent with concrete failure modes discussed in Chapters 2 and 3.

For the no. 5 epoxy-coated reinforcing bar tension tests, the average maximum loads were 35.60 kips (159.9 kN) and 73.2 kips (325.5 kN), respectively, for single and double anchors spaced 8 in. (203 mm) apart. Test no. WEAB-3 was not considered since the anchor failed at a localized minimum area of the coupler screw. Therefore, the failure load was representative of the reduced cross-sectional area of a no. 5 reinforcing bar rather than the full cross-sectional area. For the single anchor tensile tests of no. 5 rebar, the primary failure mode was steel rupture. The true strength of the bond failure mode would have been higher than the failure load observed. There was not a reduction in the average force per anchor when comparing single no. 5 and double no. 5 reinforcing bars spaced 8 in. (203 mm) apart, but the failure modes

Table 9. Dynamic Bogie Testing Summary

Test No.	Test Type	Bar Coating	Bar Size, US (Metric)	Spacing	Bogie Speed, mph (km/h)	Max Anchor Load EDR-3, kips (kN)	Max Anchor Load DTS 1, kips (kN)	Max Anchor Load DTS 2, kips (kN)	Failure Mode
WEAB-1	Tensile	None	#5	Single	9.78 (15.74)	38.80 (172.60)	37.91 (168.62)		Steel fracture
WEAB-2	Tensile	None	#5	Single	10.40 (16.74)	39.83 (177.19)	38.94 (173.20)		Steel fracture
WEAB-3	Tensile	Epoxy	#5	Single	9.47 (15.24)	35.12 (156.23)	34.86 (155.07)		Steel fracture in coupler
WEAB-4	Tensile	Epoxy	#5	Single	8.86 (14.26)	36.83 (163.83)	35.07 (155.98)		Steel fracture
WEAB-5	Shear	Epoxy	#5	Single	9.64 (15.51)	25.72 (114.43)	32.38 (144.02)		Steel fracture
WEAB-6	Shear	Epoxy	#5	Single	9.71 (15.62)	23.73 (105.57)	28.41 (126.39)		Steel fracture
WEAB-7	Tensile	Epoxy	#5	2 @ 8 in. (2 @ 203 mm)	16.64 (26.78)	73.80 (328.30)	73.80 (328.28)		Steel fracture/adhesive bond failure
WEAB-8	Tensile	Epoxy	#5	2 @ 8 in. (2 @ 203 mm)	14.05 (22.61)	72.64 (323.14)	72.41 (322.10)		Concrete breakout/adhesive bond failure
WEAB-9	Tensile	Epoxy	#6	Single	14.23 (22.91)	40.99 (182.34)	41.63 (185.18)		Adhesive bond failure
WEAB-10	Tensile	Epoxy	#6	Single	15.73 (25.31)	42.69 (189.90)	44.16 (196.45)	44.35 (197.30)	Adhesive bond failure
WEAB-11	Tensile	Epoxy	#6	2 @ 8 in. (2 @ 203 mm)	15.11 (24.32)	60.88 (270.80)	60.48 (269.05)	60.58 (269.46)	Concrete breakout/adhesive bond failure
WEAB-12	Tensile	Epoxy	#6	2 @ 8 in. (2 @ 203 mm)	15.08 (24.26)	75.66 (336.55)	75.74 (336.90)	75.48 (335.74)	Concrete breakout/adhesive bond failure
WEAB-13	Shear	Epoxy	#6	Single	9.98 (16.07)	32.13 (142.90)	29.64 (131.87)	28.42 (126.44)	Steel fracture
WEAB -14	Tensile	None	1 1/8 in. (29 mm)	Single	15.19 (24.45)	43.73 (194.51)	46.71 (207.77)	45.47 (202.28)	Concrete breakout/adhesive bond failure
WEAB-15	Shear	None	1 1/8 in. (29 mm)	Single	9.28 (14.93)	43.65 (194.15)	39.06 (173.76)	39.19 (174.34)	Bogie head failure
WEAB-16	Tensile	None	#6	Single	15.90 (25.58)	49.56 (220.43)	47.02 (209.15)	45.15 (200.85)	Adhesive bond failure

demonstrated in the dual anchor tests were different than the single anchor tests. This would indicate that the spacing was affecting the anchor performance.

For the no. 6 epoxy-coated reinforcing bar tension tests, the average pullout loads were 42.8 kips (190.2 kN) and 68.1 kips (303.1 kN), respectively, for single and dual anchors spaced 8 in. (203 mm) apart. This suggested that there is a 20 percent decrease in capacity for groups of anchors spaced 8 in. (203 mm) apart. Unlike the test with the no. 5 reinforcing bars, the failure mode for no. 6 reinforcing bars consisted of the pullout of the adhesive core accompanied by a small concrete cone breakout. The steel failure mode is more desirable than the bond failure mode in bridge rail applications because it will limit the damage to the bridge deck. Also, fracturing of the steel is more ductile and will allow for increased energy absorption of the barrier upon impact. It should also be noted that the test configuration used in these component tests only evaluated the effect of two adjacent anchors loaded simultaneously. The reduction of capacity for closely spaced anchors is related to the area of concrete resisting the applied load surrounding each anchor. For the testing conducted herein, the overlapping areas of concrete loading were only present on the concrete region between the two anchors. Actual bridge rail anchors would likely have more than two adjacent anchors loaded simultaneously. The loading of several adjacent anchors would be expected to increase the influence of the reduced anchor spacing on adjacent anchors and further reduce anchor capacity as compared to the reductions observed in this component testing.

The shear reinforcing bar tests confirmed that the steel failure mode would control with no. 5 and 6 bars with at least 5 ¼ in. (133 mm) embedment and located sufficiently far away from the deck edge to prevent concrete breakout. The effect of edge distance on anchor capacity is affected by adhesive strength, anchor size, concrete strength, and embedment depth. Further discussion of edge effects and methods for calculating them are discussed in Chapter 8.

It was also evident that the protective epoxy coating of the anchors affected the ultimate bond strength. The average dynamic pullout load from uncoated no. 6 reinforcing bars was 47.2 kips (210.1 kN) while the average dynamic pullout load from ASTM A615 Grade 60 epoxy coated no. 6 reinforcing bars was 42.8 kips (190.2). Therefore, approximately a 9 percent decrease in bond strength was observed when the reinforcing bars had a protective epoxy coating according to ASTM A775 standards.

In order to allow for an alternative anchorage design for the tie-down F-shape temporary concrete barrier developed by MwRSF, the epoxy adhesive anchorage needed to be able to develop the nominal ultimate strength of the 1 1/8 in. (29 mm) diameter ASTM A307 threaded rod anchors. The ultimate strengths of the A307 rods were determined from simple principles of mechanics of materials. The ultimate stress (σ_u) of the A307 rods was specified to be 60 ksi (414 MPa) and the cross-sectional area (A) for a 1 1/8 in. (29 mm) diameter threaded rod is 0.763 in.² (492 mm²). The equations used to calculate the ultimate tension (P_u) and shear capacities (V_u) are shown in Equations (67) and (68), respectively. Note that the shear capacity was calculated using Von Mises criteria.

$$P_u = \sigma_u A \quad (67)$$

$$V_u = \frac{\sigma_u A}{\sqrt{3}} \quad (68)$$

The ultimate tension and shear capacities were calculated to be 45.9 kips (203.6 kN) and 26.4 kips (117.6 kN), respectively. The average ultimate tension and shear loads observed from the dynamic testing program of the 1 1/8 in. (29 mm) diameter A307 rods were 45.3 kips (201.5 kN) and 40.6 kips (180.8 kN), respectively. The failure mode in tension consisted of a pullout of the adhesive core accompanied by a 2 3/4 in. (70 mm) deep concrete cone breakout. The ultimate shear value obtained during the component test is an estimated minimum value because the

anchor did not fail in the test and the load was governed by the equipment. Nonetheless, the ultimate shear capacity was determined to be far greater than the nominal shear capacity of the anchor and the ultimate tension capacity was within one percent of the nominal tension capacity for the concrete strength in the component tests. Therefore, the anchorage design with 5 ¼ in. (133 mm) embedment depth utilizing the Hilti HIT-RE 500-SD epoxy adhesive was considered an adequate alternative anchorage design for the 1 1/8 in. (29 mm) diameter A307 rods used in the tie-down temporary concrete barrier developed by MwRSF because the tested capacities met the nominal capacities of the anchorages used in the full-scale crash test. However, the failure in the tension test created significant concrete damage. This concrete damage would be expected to occur to the bridge decks of real-world installations during severe, high-energy impacts. In addition, the compressive strength of the concrete used in these component tests may be higher than the typical strength of concrete bridge decks. Thus, some decrease in the capacity of the anchors would be expected for lower strength concrete. This decrease in strength would likely be offset to some extent by the presence of reinforcing steel in the bridge deck. Thus, it is believed that using the A307 rod with Hilti HIT-RE 500 or Hilti HIT-RE 500 SD epoxy adhesive with a 5 ¼-in. embedment depth should provide similar anchorage to the tested system, but some increased deflection and increased deck damage may result. It should also be noted that epoxy adhesive manufacturer recommendations for torque requirements on threaded anchors should be closely followed for these types of anchors to prevent concerns for anchor creep and associated reductions in anchor capacity.

The testing described herein was conducted using a single type of adhesive manufactured by Hilti. This was done to provide consistent and comparable test results for use in the research effort. Chapters 8 and 9 will apply the results from this testing to calculation methods for epoxy

adhesive anchors. The resulting calculation methods should be applicable to other epoxy adhesives with different bond strengths.

6 EPOXY ANCHOR STATIC TESTING

6.1 Purpose

Static tension testing of an epoxy adhesive anchor was also conducted as part of the research effort. The purpose of the static tension test was to determine the relationship of the static pullout capacity to the dynamic pullout capacity. Static bond strength data was available from the manufacturer's published specifications. However, by conducting a static test in the same concrete slab and utilizing similar testing methods, a more accurate comparison could be obtained. Also, data from the manufacturer's published specifications was not the average true ultimate strength values, but were based on the 5 percent fractile strengths as required by ICC-ES AC308 [5]. Further, the epoxy manufacturer could also impose safety factors to ensure an increase in reliability.

6.2 Scope

The conditions for the static testing (i.e. concrete slab, epoxy adhesive, bar size, test jig) were identical to the dynamic bogie test no. WEAB-16. This was done to minimize the effects of other variables affecting the test results and to get an accurate comparison of load capacity based on loading rate.

6.3 Test Setup

The static test utilized an uncoated, deformed no. 6, ASTM A615 grade 60 steel reinforcing bar that was embedded 5 ¼ in. (133 mm) into an unreinforced concrete slab and bonded by the Hilti HIT-RE 500-SD epoxy adhesive. The anchor hole was constructed using a carbide-tipped concrete bit and a rotary hammer drill. The concrete slab had an average unconfined compressive strength of 6,454 psi (44.50 MPa), as determined from concrete cylinder testing. Material strength specification sheets are shown in Appendix G.

The tensile jig used in the dynamic bogie testing was modified by cutting a hole in the web of the W-beam, which allowed a chain to be attached to the jig at the same height used in the dynamic testing. Two load cells assembled in series were then connected to the chain that was attached to the test jig on one end and a hydraulic ram on the other. The hydraulic ram was supported by wood blocking at approximately the chain mounting height to ensure a perpendicular connection to the test jig. The rear end of the hydraulic ram was then secured to a rigid anchor which was bolted to the concrete slab. The test setup drawing for the static tensile test is shown in Figure 77. Detailed drawings are shown in Appendix F.

6.4 Test Facility

The testing facility is located at the Lincoln Air Park on the northwest side of the Lincoln Municipal Airport and is approximately 5 miles (8.0 km) northwest of the University of Nebraska-Lincoln.

6.5 Equipment and Instrumentation

6.5.1 Load Cells

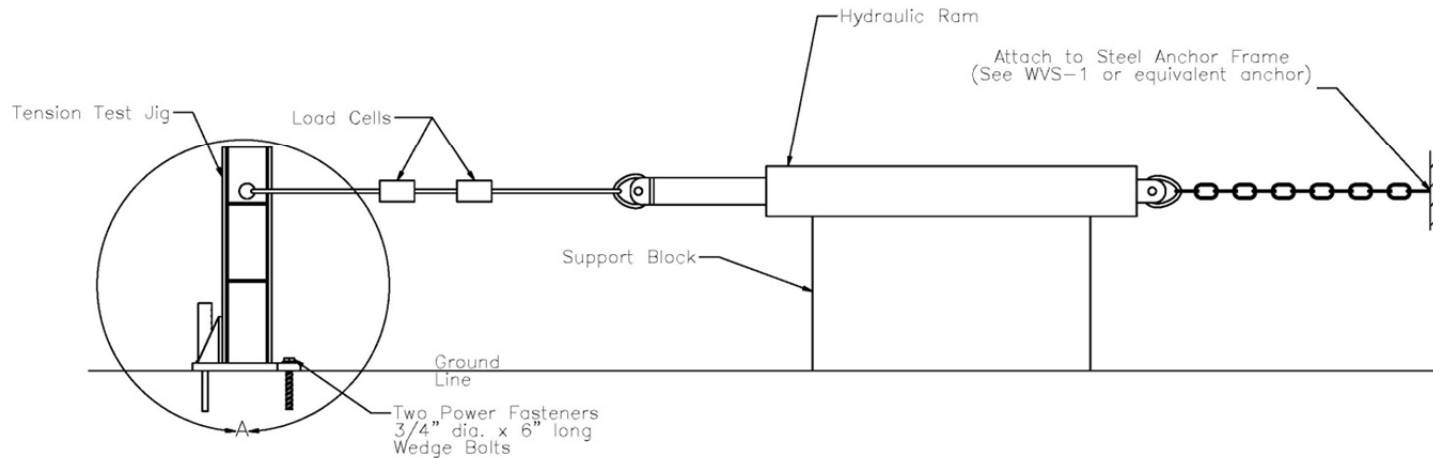
Two load cells were placed in series with the test apparatus to measure the force exerted on the test jig until failure of the anchor. The load cells were placed in tension between the test jig and the hydraulic ram. The load cells were manufactured by Transducer Techniques and conformed to model no. TLL-50K with a load range up to 50,000 lb (222.4 kN). During testing, output voltage signals were sent from the load cells to a Keithly Metrabyte DAS-1802HC data acquisition board, acquired with Test Point software, and stored permanently on a personal computer. The data collection rate for the load cells was 10,000 samples per second (10,000 Hz).

6.5.2 Hydraulic Ram

The hydraulic ram model used was the SAE-9436 manufactured by Prince Manufacturing Corporation of North Sioux City, South Dakota. It had a 36 in. (914 mm) stroke and a 4 in. (102

Epoxy Anchor Rebar Static Testing—Tensile Test Setup

1. Hydraulic Ram
2. One high-speed digital camera perpendicular
3. One high-speed digital camera perpendicular zoomed in on the tensile test jig and rebar.
4. JVC digital video
5. Two Load Cells
6. Note any installation issues or problems in fieldbook.
7. Note failure mode in fieldbook.
8. Each test must be at least 2' from any previous test anchor holes to prevent anchor spacing and edge spacing issues from affecting results.
9. Kick plate anchors must be replaced each test.
10. Before installation of anchors, measure the bar deformation rib height.
11. Anchors must be installed while the concrete temperature remains above 45° during curing time for the epoxy. If required, heat the concrete to the desired temperature.
12. Anchors are to be installed in same concrete slabs as used in test nos. WEAB 1–15.
13. Epoxy used for fourth round of testing will be Hilti HIT-RE 500-SD.




 Midwest Roadside Safety Facility	Epoxy Anchor Testing Static Test Setup	SHEET: 1 of 3
	DWG. NAME: EpoxyAnchor test setup matrix_17_R1	SCALE: None UNITS: Inches
		REV. BY: BJD

Figure 77. Tension Test Setup, Test No. WEAB-17

mm) diameter bore. An external pump was used to push hydraulic fluid into the hydraulic cylinder.

6.5.3 Test Jig

The tensile test jig used in the dynamic bogie testing was modified by cutting a hole in the web of the W-section post to allow a chain to be attached. The center of the hole had a mounting height of approximately 24 ½ in. (622 mm) from the concrete slab surface. For more details on the design of the tensile test jig refer to Section 4.4.2 or Appendix E. A picture of the test setup is shown in Figure 78.



Figure 78. Static Test Setup

6.5.4 Digital Cameras

Two AOS VITcam high-speed digital video cameras and one JVC digital video camera were used to document the test. The AOS high-speed camera had a frame rate of 120 frames per second and the JVC digital video camera had a frame rate of 29.97 frames per second. All the cameras were placed laterally from the test jig, with a view perpendicular to the hydraulic ram's direction of travel. A Nikon D50 digital still camera was also used to document pre- and post-test conditions for all tests.

6.5.5 Data Processing

The anchor force for the tensile test was determined by summing the moments about the reaction point of the test jig and solving for the anchor force. However, the applied load height for the static testing was 24 ½ in. (622 mm). For details about the calculation of the anchor force from the applied force to the test jig, refer to Section 4.4.6.

7 STATIC TESTING RESULTS AND DISCUSSION

7.1 Results

7.1.1 Test No. WEAB-17

For test no. WEAB-17, the hydraulic ram applied an increasing load for approximately 18 seconds until failure of the anchor. The anchor pulled out of the concrete hole and most of the epoxy adhesive was still attached to the reinforcing bar. A concrete cone of approximately 10 to 12 in. (254 to 305 mm) in diameter by 2 in. (51 mm) deep broke out and was still attached to the reinforcing bar. The maximum tensile load observed was 45.2 kips (201.1 kN) according to load cell no. 1 data and 43.7 kips (194.3 kN) according to load cell no. 2. Pre- and post-test photographs are shown in Figure 79. A plot of the force versus time history is shown in Figure 80. Sequential photographs are shown in Figure 81. A picture of the pulled out anchor is shown in Figure 82.



Pre-Test



Post-Test

Figure 79. Pre- and Post-Test Photographs, Test No. WEAB-17

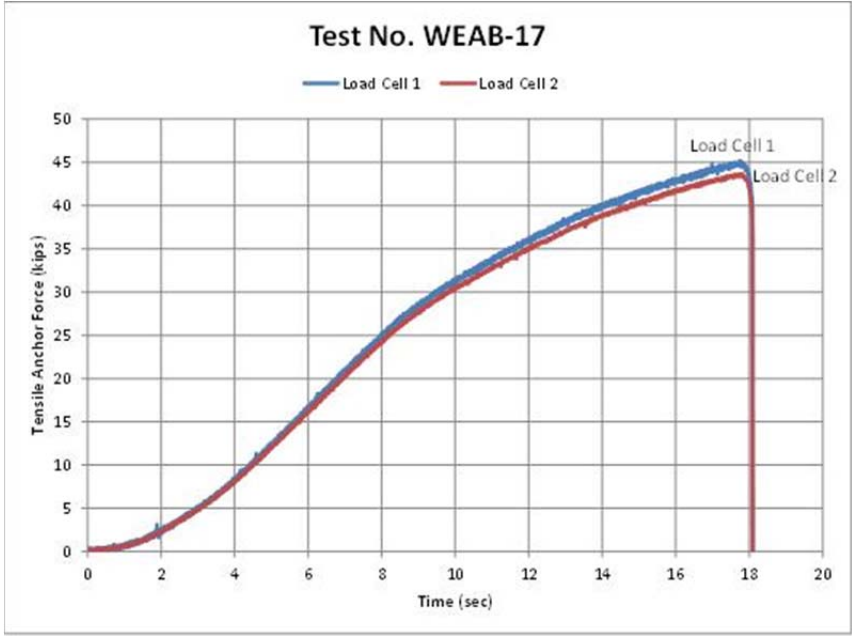


Figure 80. Force vs. Time, Test No. WEAB-17

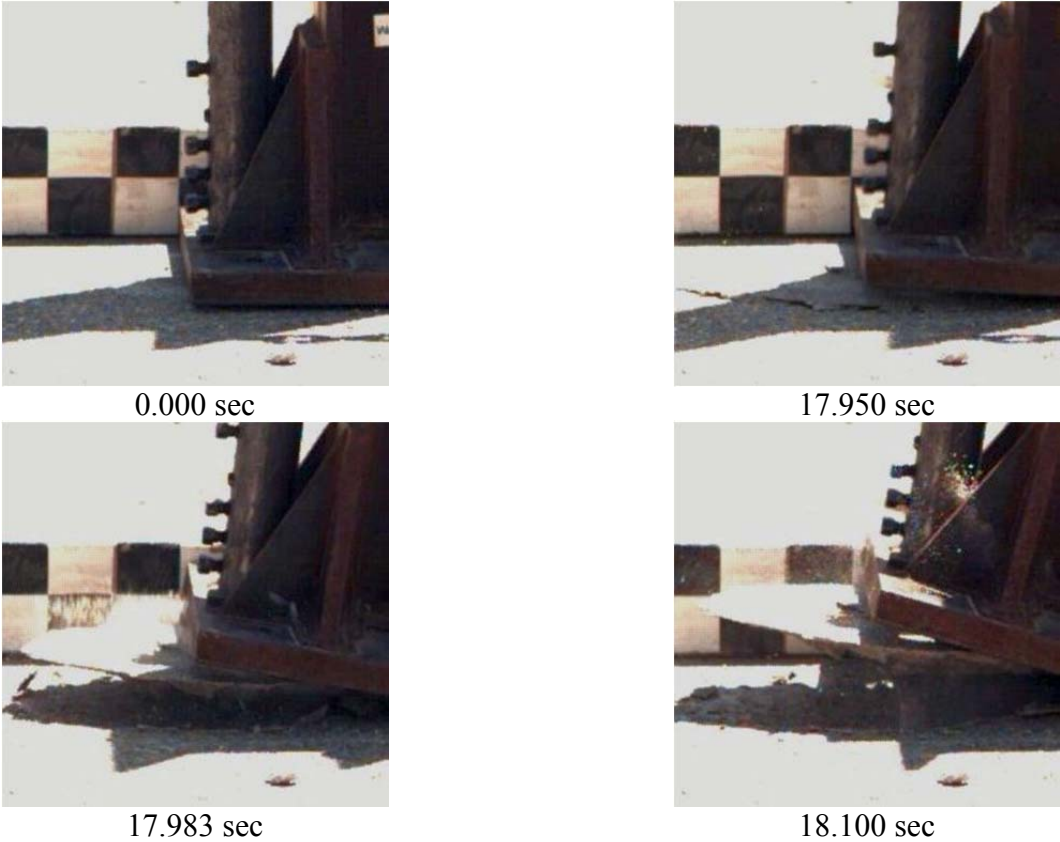


Figure 81. Sequential Photographs, Test No. WEAB-17



Figure 82. Post-Test Anchor Photograph, Test No. WEAB-17

7.2 Discussion

The average static pullout strength from the two load cell recordings from test no. WEAB-17 was 44.5 kips (198 kN). The failure mode observed in test no. WEAB-17 was a combination of concrete breakout and adhesive bond failure. Recall, the average dynamic pullout strength from processed accelerometer data from test no. WEAB-16 was 47.2 kips (210 kN).

The dynamic increase factor for the bond strength failure mode was not able to be determined based on the available data due to several reasons. First, the static and dynamic testing of the no. 6 rebar in test nos. WEAB-16 and WEAB17 demonstrated different failure modes, as noted previously. Test no. WEAB-16 displayed an adhesive bond failure when loading the rebar under a dynamic tensile load, while test no. WEAB-17 displayed a combined failure mode of both the adhesive bond and concrete breakout. The disparity in the failure modes of the two tests makes it impossible to accurately compare the bond strengths. A second factor that prevented the determination of a dynamic increase factor was the relative load rates of the tests. While the dynamic load rate used in test no. WEAB-16 was acceptable, the static load rate chosen was not sufficiently slow to allow for determination of an increase factors. ACI 355.4-11, *Qualification of Post-Installed Adhesive Anchors in Concrete*, which became available following the testing described herein, recommends following ASTM E488, *Standard Test Methods for Strength of Anchors in Concrete Elements* [83], procedures for evaluation of adhesive anchor capacities. The load rate for static testing is defined by these documents as application of an initial load up to 5 percent of the estimated maximum load capacity of the anchorage system to be tested in order to bring all members into full bearing, and subsequent increase of the load or displacement so that peak load occurs after 1 to 3 minutes from the start of testing. The equipment used to load the adhesive anchor in test no. WEAB-17 was not capable of delivering the very slow load rates recommended in the ACI and ASTM specifications. Thus, test no.

WEAB-17 represents a quasi-static load rate which is much lower than the dynamic test conducted in test no. WEAB-16, but the load rate is not sufficiently low to use for determination of the dynamic increase factor.

Hilti does provide a recommended 40 percent increase in the listed bond strength for the HIT RE-500 SD adhesive for short duration or dynamic loading. It should be noted that this dynamic increase factor was lower than values recommended by existing literature. Berra and Solomos reported that the dynamic capacity of post-installed anchors to range from 1.59 to 2.39 times as high as those predicted from static loading conditions and that a dynamic increase factor of 1.25, as permitted in ACI 349-97, was reasonable for chemical adhesive anchors [19]. However, the static values used in that study were based on predictive equations from ACI and the CCD method and not true analysis or actual test data. A dynamic increase factor of 1.2 was suggested by Braimah, Constestabile and Guilbeault [20].

8 EVALUATION OF ADHESIVE ANCHOR MODELS

8.1 Adhesive Anchor Models

In order to evaluate potential models for determining the capacity of epoxy adhesive anchors for attachment of concrete barriers to bridge decks, comparisons were made between the data produced in the component testing conducted in this study and the most promising models for estimation of the anchor capacities. In Chapter 3, the researchers reviewed and compared analytical models for determination of the shear and tensile capacities for epoxy adhesive anchors. The analysis in Chapter 3 concluded that the shear capacities for epoxy adhesive anchors were best determined based on the models presented in Appendix D of ACI 318-08 due to the similar behavior between adhesive, cast-in-place, and post-installed mechanical anchors in shear. For estimation of tensile capacities of epoxy adhesive anchors, it was recommended that the cone or full uniform bond model be used for estimation of anchor tensile capacity due to its high correlation to test data obtained from the manufacturer for static loading conditions. This model also proved to be the most accurate and stable for all embedment depths while providing a reasonable prediction of the expected failure mode.

Following the analysis done in Chapter 3, a more recent revision of the ACI code, ACI 318-11 [84], was released. ACI 318-11 included guidance for the design of post-installed adhesive anchors that was not available in the ACI 318-08. It was believed that the ACI 318-11 guidance should be included as part of this research as well due to the widespread use and accessibility of the ACI code.

Several differences exist between the adhesive anchor procedures in ACI 318-11 and the procedures detailed in Chapter 3. With respect to calculation of the tensile capacity of post-installed adhesive anchors, ACI 318-11 and the cone or full uniform bond model differ in both the methodology for the determination of the failure modes as well as the methods for

calculating anchor capacity. ACI 318-11 proposes five failure modes for post-installed anchors in tension. These failure modes include, steel fracture, adhesive bond failure, concrete breakout, pullout of post-installed expansion and undercut anchors, and concrete side-face blowout of headed anchors in tension. The latter two failure modes clearly don't apply for epoxy adhesive anchors and can be neglected. ACI 318-11 selects the failure mode for the post-installed anchor by calculating the tensile load capacity for all of the possible failure modes and selecting the lowest magnitude failure load as the primary failure mode. The selection of the failure mode for the cone or full uniform bond model differs in that equations are used to estimate the depth of the concrete cone based on anchor size and embedment and the estimated cone height then determines if the failure mode is an adhesive bond or concrete breakout failure mode. After the failure mode is selected, the appropriate equation is applied to determine the estimated load. Steel capacity is calculated separately for the cone or full uniform bond model and compared with the concrete or bond failure to determine the limiting failure mode. Thus, ACI-318-11 and cone or full uniform bond model may potentially indicate different tensile failure modes when used to evaluate post-installed adhesive anchors.

In addition to the differences in the determination of tensile failure mode, the cone or full uniform bond model and ACI 318-11 use slightly different equations to calculate the tensile capacity for the concrete and bond failure modes. A comparison of the ACI 318-11 and the cone or full uniform bond model equations for calculating the anchor capacity for each failure mode are shown in Table 10. Note that the equations shown in Table 10 do not include any additional modification factors such as dynamic increase factors, reduction factors, or epoxy coating factors. The calculation of the steel capacity is identical for the cone or full uniform bond model and ACI 318-11. Calculation of concrete breakout capacity differs slightly in both the constant coefficients used in the equations and the exponent power of the h_{ef} term. The adhesive bond

capacity calculation of the two methods varies only by the use of the hole diameter, d_o , for the cone or full uniform bond model versus the use of the anchor diameter, d_a , in ACI 318-11. λ_a is a modification factor for lightweight concrete that is equal to 1 for normal weight concrete and does not affect the equations. τ_0 and τ_{cr} are both represent the nominal bond stress for the adhesive based on the published data. Based on these comparisons, one would expect that the two methods would produce similar steel and adhesive bond capacities, but may predict significantly different concrete breakout capacity.

Table 10. Comparison of Tensile Capacity Calculations for ACI 318-11 and the Cone or Full Uniform Bond Model

Failure Mode	Cone or Full Uniform Bond Model	ACI 318-11	Comments
Steel Fracture	$N_n = A_s f_u$	$N_{sa} = A_{se} N f_{uta}$	Identical
Concrete Breakout	$N_n = 11.08 h_{ef}^2 \sqrt{f'_c}$	$N_b = k_c \lambda_a \sqrt{f'_c} h_{ef}^{1.5}$	The methods use different exponent power for the h_{ef} term and the constant coefficients vary.
Adhesive Bond Failure	$N_n = \tau_0 \pi d_o h_{ef}$	$N_{ba} = \lambda_a \tau_{cr} \pi d_a h_{ef}$	ACI 318-11 uses the anchor diameter, d_a , rather than the hole diameter, d_o .

As noted in Chapter 3, the provisions presented in Appendix D of ACI 318-08 for calculation of shear capacity of concrete anchors appeared to be applicable to adhesive anchors, due to the similar behavior between adhesive, cast-in-place, and post-installed mechanical

anchors in shear. These provisions have remained the same in ACI 318-11 and are currently the best methods for evaluation of post-installed adhesive anchors loaded in shear.

In subsequent sections, the above tensile and shear procedures for post-installed adhesive anchors will be applied to the component testing conducted as part of this research to help determine the best models for design.

8.2 Comparison of Tension Calculation Procedures for Post-Installed Adhesive Anchors

Comparison of the ACI 318-11 and the cone or full uniform bond model calculation procedures for post-installed adhesive anchors was performed in three variations. First, the methods were used to calculate the anchor capacities and failure modes for the tension component tests conducted in the study without any modification or strength reduction factors, using listed bond strengths from the manufacturer, and using actual as-tested material properties for the concrete and steel anchors. A second analysis was performed with both methods where modification factors were applied for dynamic strength increases, epoxy coating effects were added, and as-tested material properties for concrete and steel were applied. A third comparison was then performed using appropriate modification and strength reduction factors as well as nominal published material strengths to represent the methods used for design of a post-installed anchorage. Details of these comparisons and the results are discussed in subsequent sections. The comparisons were conducted by using both methods to calculate the failure mode and capacity of the post-installed adhesive anchors for all of the tension tests in the WEAB series of component testing detailed previously. Test nos. WEAB-3 and WEAB-17 were omitted from the comparisons because test no. WEAB-3 failed due to the effect of the coupler on the rebar and test no. WEAB-17 was a quasi-static test used only for help in determining a dynamic increase factor for bond strength.

8.2.1 Non-Factored, As-Tested Materials Comparison

The first comparison of the ACI 318-11 and the cone or full uniform bond model procedures for post-installed adhesive anchors was limited to determination of the failure modes and anchor capacities for both methods without using any modification or reduction factors, applying as-tested material properties for the steel and concrete, and using the bond strength for Hilti HIT-RE 500 SD listed in the Hilti technical guide. This comparison was intended to compare both methods using the best material data available without incorporating dynamic increase factors for the steel, epoxy adhesive, and concrete or using reduction factors. Modification factors for anchor spacing and edge distance found in ACI 318-11 were applied to the cone or full uniform bond model in order to provide a consistent comparison, as these factors were not part of the development of that model. Note that all of the equations shown below are in US Custom units.

For the cone or full uniform bond model, equation (69) was used to determine the height of the concrete cone and the failure mode. If the estimated height of the concrete cone calculated by Equation (69) was greater than or equal to the embedment depth, concrete cone and breakout was predicted and Equation (71) was utilized. Otherwise adhesive failure is predicted, and the uniform bond stress Equation (72) was used to calculate the pullout capacity. The predicted capacity for concrete breakout or adhesive bond failure was then compared to the steel fracture capacity of the anchor in equation (70) to determine the limiting failure mode. In equation (70), A_s is the effective cross-sectional area of the anchor in tension and f_u is the ultimate tensile stress of the anchor. In equation (71), f_c' is the unconfined compressive strength of the concrete, h_{ef} is the embedment depth of the anchor, $\psi_{ed,N}$ is a reduction factor for anchor edge distance, $\psi_{cp,N}$ is a factor for cracked concrete, and $\frac{A_{Nc}}{A_{Nco}}$ is the reduction factor for anchor spacing, as

detailed in ACI 381-11. In equation (72), τ_o is the static bond stress, d_o is the diameter of the hole, h_{ef} is the embedment depth of the anchor, $\psi_{ed,Na}$ is a reduction factor for anchor edge distance, $\psi_{cp,Na}$ is a factor for cracked concrete, and $\frac{A_{Na}}{A_{Na0}}$ is the spacing factor, as detailed in ACI 381-11.

$$h_{cone} = \frac{\tau_o \pi d_o}{22.16 \sqrt{f'_c}} \quad (69)$$

$$N_n = A_s f_u \quad (70)$$

$$N_n = 11.08 h_{ef}^2 \sqrt{f'_c} \psi_{ed,N} \psi_{cp,N} \frac{A_{Nc}}{A_{Nco}} \quad (71)$$

Where:

$$\psi_{ed,N} = \begin{cases} 1.00 & \text{if } c_a \geq 1.5 h_{ef} \\ 0.7 + 0.3 \frac{c_{a,min}}{1.5 h_{ef}} & \text{if } c_a < 1.5 h_{ef} \end{cases}$$

$$\psi_{cp,N} = \begin{cases} 1.00 & \text{for uncracked concrete where } c_{a,min} \geq c_{ac} \\ \frac{c_{a,min}}{c_{ac}} & \text{for cracked concrete where } c_{a,min} < c_{ac} \end{cases}$$

$$N_n = \tau_o \pi d_o h_{ef} \psi_{ed,Na} \psi_{cp,Na} \frac{A_{Na}}{A_{Na0}} \quad (72)$$

Where:

$$\psi_{ed,Na} = \begin{cases} 1.00 & \text{if } c_a \geq c_{Na} \\ 0.7 + 0.3 \frac{c_{a,min}}{c_{Na}} & \text{if } c_a < c_{Na} \end{cases}$$

$$\psi_{cp,Na} = \begin{cases} 1.00 & \text{for uncracked concrete where } c_{a,min} \geq c_{ac} \\ \frac{c_{a,min}}{c_{ac}} & \text{for cracked concrete where } c_{a,min} < c_{ac} \end{cases}$$

For the ACI 318-11 method, three equations were used to determine the capacity of the post-installed adhesive anchors for three separate failure modes: steel fracture, concrete breakout, and adhesive bond failure. The lowest calculated capacity of the three failure modes

was then selected as the anchor capacity. The ACI 318-11 equations used in this comparison for steel fracture, concrete breakout, and adhesive bond failure are shown in equations (73), (74), and (75), respectively. In equation (73), $A_{se,N}$ is the effective cross-sectional area of the anchor in tension and f_{uta} is the ultimate tensile stress of the anchor. In equation (74), k_c is a coefficient that is equal to 24 based on the ACI 355.4 evaluation of Hilti HIT-RE 500 SD post-installed adhesive anchors, λ_a is a modification factor for lightweight concrete, f_c' is the unconfined compressive strength of the concrete, h_{ef} is the embedment depth of the anchor, $\psi_{ed,N}$ is a reduction factor for anchor edge distance, $\psi_{c,N}$ is a factor for concrete cracking under service loads, $\psi_{cp,N}$ is a factor for cracked concrete, and $\frac{A_{Nc}}{A_{Nco}}$ is the reduction factor for anchor spacing, as detailed in ACI 381-11. In equation (75), λ_a is a modification factor for lightweight concrete, τ_{cr} is the static bond stress, d_a is the diameter of the anchor, h_{ef} is the embedment depth of the anchor, $\psi_{ed,Na}$ is a reduction factor for anchor edge distance, $\psi_{cp,Na}$ is a factor for cracked concrete, and $\frac{A_{Na}}{A_{Na0}}$ is the spacing factor, as detailed in ACI 381-11.

$$N_{sa} = A_{se,N}f_{uta} \quad (73)$$

$$N_b = k_c\lambda_a\sqrt{f_c'}h_{ef}^{1.5}\psi_{ed,N}\psi_{c,N}\psi_{cp,N}\frac{A_{Nc}}{A_{Nco}} \quad (74)$$

Where:

$$\psi_{ed,N} = \begin{cases} 1.00 & \text{if } c_a \geq 1.5h_{ef} \\ 0.7 + 0.3 \frac{c_{a,min}}{1.5h_{ef}} & \text{if } c_a < 1.5h_{ef} \end{cases}$$

$$\psi_{c,N} = \begin{cases} 1.00 & \text{for } k_c \text{ determined from ACI 355.4 evaluation} \\ 1.25 & \text{for cast in anchors} \\ 1.40 & \text{for post – installed anchors where } k_c = 17 \end{cases}$$

$$\psi_{cp,N} = \begin{cases} 1.00 & \text{for uncracked concrete where } c_{a,min} \geq c_{ac} \\ \frac{c_{a,min}}{c_{ac}} & \text{for cracked concrete where } c_{a,min} < c_{ac} \end{cases}$$

$$N_{ba} = \lambda_a \tau_{cr} \pi d_a h_{ef} \psi_{ed,Na} \psi_{cp,Na} \frac{A_{Na}}{A_{Na0}} \quad (75)$$

Where:

$$\psi_{ed,Na} = \begin{cases} 1.00 & \text{if } c_a \geq c_{Na} \\ 0.7 + 0.3 \frac{c_{a,min}}{c_{Na}} & \text{if } c_a < c_{Na} \end{cases}$$

$$\psi_{cp,Na} = \begin{cases} 1.00 & \text{for uncracked concrete where } c_{a,min} \geq c_{ac} \\ \frac{c_{a,min}}{c_{ac}} & \text{for cracked concrete where } c_{a,min} < c_{ac} \end{cases}$$

The comparison of the ACI 318-11 and the cone or full uniform bond models is shown in Table 11. Results from the comparison demonstrate that both methods struggled to predict the correct failure mode and significantly under predicted the capacities of the post-installed adhesive anchors in the WEAB test series. However, it should be noted that this comparison did not include dynamic increase factors for the steel, concrete, or epoxy adhesive. The addition of these modification factors was expected to provide an improved prediction of both failure mode and capacity.

Table 11. Comparison of ACI 318-11, Cone or Full Uniform Bond Model, and WEAB Testing - Non-Factored and As-Tested Materials

Test No.	Test Article	Actual Failure Mode	Average Actual Load (kips)	Cone or Uniform Bond			ACI 318-11			
				Failure Mode	Capacity (kips)	Test-to-Predicted Ratio	Failure Mode	Capacity (kips)	Test-to-Predicted Ratio	
WEAB-1	#5 bar uncoated	Steel Fracture	38.35	Bond Failure	26.5	1.45	Bond Failure	22.1	1.74	
WEAB-2	#5 bar uncoated	Steel Fracture	39.38	Bond Failure	26.5	1.49	Bond Failure	22.1	1.78	
WEAB-4	#5 bar epoxy coated	Steel Fracture	35.95	Bond Failure	26.5	1.36	Bond Failure	22.1	1.63	
WEAB-7	2 #5 bars @ 8" epoxy coated	Steel Fracture/ Bond Failure	73.80	Bond Failure	38.6	1.91	Bond Failure	32.2	2.29	
WEAB-8	2 #5 bars @ 8" epoxy coated	Concrete Breakout/ Bond Failure	72.53	Bond Failure	38.6	1.88	Bond Failure	32.2	2.25	
WEAB-9	#6 bar epoxy coated	Bond Failure	41.31	Bond Failure	29.8	1.38	Concrete Breakout	23.2	1.78	
WEAB-10	#6 bar epoxy coated	Bond Failure	43.74	Bond Failure	29.8	1.47	Concrete Breakout	23.2	1.89	
WEAB-11	2 #6 bars @ 8" epoxy coated	Concrete Breakout/ Bond Failure	60.65	Bond Failure	41.4	1.46	Concrete Breakout	34.8	1.74	
WEAB-12	2 #6 bars @ 8" epoxy coated	Concrete Breakout/ Bond Failure	75.62	Bond Failure	41.4	1.83	Concrete Breakout	34.8	2.17	
WEAB-14	1½" A307 rod uncoated	Concrete Breakout/ Bond Failure	45.30	Bond Failure	39.3	1.15	Concrete Breakout	23.2	1.95	
WEAB-16	#6 bar uncoated	Bond Failure	47.24	Bond Failure	29.8	1.58	Concrete Breakout	23.2	2.04	
						Average Test / Predicted =	1.54	Average Test / Predicted =		1.93

8.2.2 Factored, As-Tested Comparison

The second comparison between the ACI 318-11 and the cone or full uniform bond model procedures for post-installed adhesive anchors applied dynamic increase factors for the steel, concrete, and epoxy adhesive in order to evaluate if the increase factors would improve the model predictions for failure mode and capacity. Both models were still applied using as-tested material properties for the steel and concrete. Modification factors for dynamic loading and concrete strength were also applied to the bond strength for Hilti HIT-RE 500 SD. The determination of the modification factors for each material is detailed below. Modification factors for anchor spacing and edge distance found in ACI 318-11 were applied to the cone or full uniform bond model in order to provide a consistent comparison, as these factors were not part of the development of that model. Note that all of the equations shown below are in US Custom units.

The dynamic magnification factor for the steel rebar was determined by comparison of the calculated ultimate strength of the rebar based on the as-tested ultimate strength and cross-sectional area of the no. 5 rebar and the dynamic fracture loads obtained from component test nos. WEAB -1, WEAB-2, and WEAB-4, as shown in Table 12. The ratio of the tested to calculated fracture loads was determined and the average increase was chosen as the dynamic increase factor (DIF). The resulting DIF for steel was found to be 1.18.

Table 12. Determination of Dynamic Increase Factor for ASTM A615 Grade 60 Steel Rebar

Test No.	Actual Load (kips)	Steel Fracture Strength (kips)	Test-to-Predicted Ratio
		$N_s = A_s f_{uta}$	
WEAB-1	38.35	32.22	1.19
WEAB-2	39.38	32.22	1.22
WEAB-4	35.95	32.22	1.12
Average Test / Predicted=			1.18

Determination of the DIF for the concrete was done using a similar methodology to the increase factor for the steel rebar. Concrete breakout strengths were calculated for test nos. WEAB-8, WEAB-11, WEAB-12, and WEAB-14 with both the ACI 318-11 and the cone and full uniform bond models. The calculated concrete breakout strengths were then compared with the measured dynamic concrete breakout loads for those tests, as shown in Table 13. The average test to predicted ratio was found to be 1.88 when using the cone or uniform bond method and 1.99 when using the ACI 318-11 method.

Table 13. Determination of Dynamic Increase Factor for Concrete Fracture

Test No.	Actual Load (kips)	Concrete Breakout Strength <i>Cone or Bond Model</i> (kips)	Test-to-Predicted Ratio	Concrete Breakout Strength <i>ACI 318-11</i> (kips)	Test-to-Predicted Ratio
		$N_b = 11.08 * h_{ef}^2 \sqrt{f_c} A_{nc} / A_{nco}$		$N_b = 24 * h_{ef}^{1.5} \sqrt{f_c} A_{nc} / A_{nco}$	
WEAB-8	72.5	36.80	1.97	34.79	2.08
WEAB-11	60.6	36.80	1.65	34.79	1.74
WEAB-12	75.6	36.80	2.05	34.79	2.17
WEAB-14	45.3	24.53	1.85	23.19	1.95
Average Test / Predicted=			1.88	Average Test / Predicted=	1.99

In order to check the validity of the ratios determined in Table 13, the DIF for concrete fracture was also estimated through calculation of the strain rate applied during the WEAB testing and using the strain rate to determine the DIF through previously published analytical

methods. Determination of strain rates from the dynamic testing proved difficult to ascertain. Thus, upper and lower bounds for the estimated strain rates were determined in order to bracket the calculated DIF for concrete fracture using the CEB model code [85]. The DIF calculated from the CEB model code using the estimated upper and lower strain rates showed that the 1.88 and 1.99 DIFs determined above fell in the mid-range of the DIFs determined from the upper and lower bounds of the estimated strain rate. Thus, the DIFs for concrete fracture shown in Table 13 seemed reasonable.

In summary, two methods were used to evaluate the concrete DIF in order to build confidence. As the DIF values from the two methods were relatively close, the researchers chose the more conservative of the two values due to the limited amount of data in this project. In addition, while the DIF's were calculated using both the ACI 318-11 and the cone and full uniform bond models, there was no reason that the lower, more conservative DIF value cannot be used with the ACI calculation methods. For the purposes of calculating the concrete breakout strength in the ACI 318-11 and the cone or full uniform bond model, the lower DIF value of 1.88 was chosen for the analysis as it was the more conservative of the two estimates.

Determination of a DIF for the adhesive bond from the component testing conducted in this research proved difficult, as noted in Chapter 7. The researchers were unable to calculate a DIF due to issues with varying failure modes in the static and dynamic tests and the inability to test at the recommended static strain rate. The Hilti technical guide recommends 40 percent increase in the listed bond strength for the HIT-RE 500 SD adhesive for short duration or dynamic loading. In addition, Hilti also recommends a 6 percent increase in the bond strength for concrete strengths between 4,500 psi and 6,500 psi. Thus, modification factors of 1.06 and 1.40 were applied to the adhesive bond strength to account for dynamic loading and increased concrete strength, respectively. The adhesive bond strength was also modified based on the

presence of epoxy coated rebar. As noted in Chapter 5, the effect of epoxy coating on an anchor relative to plain black steel anchors was found to result in a reduction of 9 percent. To be conservative, a 10 percent reduction was used in the suggested models.

For the cone or full uniform bond model, equation (69) was used again to determine the height of the concrete cone and the failure mode. If the estimated height of the concrete cone calculated by Equation (69) was greater than or equal to the embedment depth, concrete cone and breakout was predicted and Equation (77) was utilized. Otherwise adhesive failure is predicted, and the uniform bond stress Equation (78) was used to calculate the pullout capacity. The predicted capacity for concrete breakout or adhesive bond failure was then compared to the steel fracture capacity of the anchor in equation (76) to determine the limiting failure mode. In equation (76), A_s is the effective cross-sectional area of the anchor in tension, f_u is the ultimate tensile stress of the anchor, and $\psi_{sd,N}$ is the DIF for steel. In equation (77), f_c' is the unconfined compressive strength of the concrete, h_{ef} is the embedment depth of the anchor, $\psi_{cd,N}$ is the DIF for the concrete breakout, $\psi_{ed,N}$ is a reduction factor for anchor edge distance, $\psi_{cp,N}$ is a factor for cracked concrete, and $\frac{A_{Nc}}{A_{Nco}}$ is the reduction factor for anchor spacing, as detailed in ACI 381-11. In equation (78), τ_o is the static bond stress, d_o is the diameter of the hole, h_{ef} is the embedment depth of the anchor, $\psi_{bd,N}$ is the DIF for the adhesive bond, $\psi_{bc,N}$ is the concrete strength increase factor, $\psi_{ep,N}$ is the anchor coating factor, $\psi_{ed,Na}$ is a reduction factor for anchor edge distance, $\psi_{cp,Na}$ is a factor for cracked concrete, and $\frac{A_{Na}}{A_{Na0}}$ is the spacing factor, as detailed in ACI 381-11.

$$N_n = A_s f_u \psi_{sd,N} \quad (76)$$

Where:

$$\psi_{sd,N} = \begin{cases} 1.00 & \text{for static loading} \\ 1.18 & \text{for dynamic loading} \end{cases}$$

$$N_n = 11.08h_{ef}^2\sqrt{f'_c}\psi_{cd,N}\psi_{ed,N}\psi_{cp,N}\frac{A_{Nc}}{A_{Nco}} \quad (77)$$

Where:

$$\psi_{cd,N} = \begin{cases} 1.00 & \text{for static loading} \\ 1.88 & \text{for dynamic loading} \end{cases}$$

$$\psi_{ed,N} = \begin{cases} 1.00 & \text{if } c_a \geq 1.5h_{ef} \\ 0.7 + 0.3\frac{c_{a,min}}{1.5h_{ef}} & \text{if } c_a < 1.5h_{ef} \end{cases}$$

$$\psi_{cp,N} = \begin{cases} 1.00 & \text{for uncracked concrete where } c_{a,min} \geq c_{ac} \\ \frac{c_{a,min}}{c_{ac}} & \text{for cracked concrete where } c_{a,min} < c_{ac} \end{cases}$$

$$N_n = \tau_0\pi d_0 h_{ef}\psi_{bd,N}\psi_{bc,N}\psi_{ep,N}\psi_{ed,Na}\psi_{cp,Na}\frac{A_{Na}}{A_{Na0}} \quad (78)$$

Where:

$$\psi_{bd,N} = \begin{cases} 1.00 & \text{for static loading} \\ 1.40 & \text{for dynamic loading} \end{cases}$$

$$\psi_{bc,N} = \begin{cases} 1.00 & \text{for } 2,500 \text{ psi} < f'_c < 4,500 \text{ psi} \\ 1.06 & \text{for } 4,500 \text{ psi} < f'_c < 6,500 \text{ psi} \\ 1.08 & \text{for } 6,500 \text{ psi} < f'_c < 8,500 \text{ psi} \end{cases}$$

$$\psi_{ep,N} = \begin{cases} 1.00 & \text{for black steel rods} \\ 0.90 & \text{for epoxy coated rods} \end{cases}$$

$$\psi_{ed,Na} = \begin{cases} 1.00 & \text{if } c_a \geq c_{Na} \\ 0.7 + 0.3\frac{c_{a,min}}{c_{Na}} & \text{if } c_a < c_{Na} \end{cases}$$

$$\psi_{cp,Na} = \begin{cases} 1.00 & \text{for uncracked concrete where } c_{a,min} \geq c_{ac} \\ \frac{c_{a,min}}{c_{ac}} & \text{for cracked concrete where } c_{a,min} < c_{ac} \end{cases}$$

For the ACI 318-11 method, three equations were used to determine the capacity of the post-installed adhesive anchors for three separate failure modes: steel fracture, concrete breakout, and adhesive bond failure. The lowest calculated capacity of the three failure modes was then selected as the anchor capacity. The ACI 318-11 equations used in this comparison for steel fracture, concrete breakout, and adhesive bond failure are shown in equations (79), (80), and (81), respectively. In equation (79), $A_{se,N}$ is the effective cross-sectional area of the anchor in tension, f_{uta} is the ultimate tensile stress of the anchor, and $\psi_{sd,N}$ is the DIF for the steel. In equation (80), k_c is a coefficient that is equal to 24 based on the ACI 355.4 evaluation of Hilti HIT-RE 500 SD post-installed adhesive anchors, λ_a is a modification factor for lightweight concrete, f_c' is the unconfined compressive strength of the concrete, h_{ef} is the embedment depth of the anchor, $\psi_{cd,N}$ is the DIF for the concrete breakout, $\psi_{ed,N}$ is a reduction factor for anchor edge distance, $\psi_{c,N}$ is a factor for concrete cracking under service loads, $\psi_{cp,N}$ is a factor for cracked concrete, and $\frac{A_{Nc}}{A_{Nco}}$ is the reduction factor for anchor spacing, as detailed in ACI 381-11. In equation (81), λ_a is a modification factor for lightweight concrete, τ_{cr} is the static bond stress, d_a is the diameter of the anchor, h_{ef} is the embedment depth of the anchor, $\psi_{bd,N}$ is the DIF for the adhesive bond, $\psi_{bc,N}$ is the concrete strength increase factor, $\psi_{ep,N}$ is the anchor coating factor, $\psi_{ed,Na}$ is a reduction factor for anchor edge distance, $\psi_{cp,Na}$ is a factor for cracked concrete, and $\frac{A_{Na}}{A_{Na0}}$ is the spacing factor, as detailed in ACI 381-11.

$$N_{sa} = A_{se,N} f_{uta} \psi_{sd,N} \quad (79)$$

Where:

$$\psi_{sd,N} = \begin{cases} 1.00 & \text{for static loading} \\ 1.18 & \text{for dynamic loading} \end{cases}$$

$$N_b = k_c \lambda_a \sqrt{f'_c} h_{ef}^{1.5} \psi_{cd,N} \psi_{ed,N} \psi_{c,N} \psi_{cp,N} \frac{A_{Nc}}{A_{Nco}} \quad (80)$$

Where:

$$\psi_{cd,N} = \begin{cases} 1.00 & \text{for static loading} \\ 1.88 & \text{for dynamic loading} \end{cases}$$

$$\psi_{ed,N} = \begin{cases} 1.00 & \text{if } c_a \geq 1.5h_{ef} \\ 0.7 + 0.3 \frac{c_{a,min}}{1.5h_{ef}} & \text{if } c_a < 1.5h_{ef} \end{cases}$$

$$\psi_{c,N} = \begin{cases} 1.00 & \text{for } k_c \text{ determined from ACI 355.4 evaluation} \\ 1.25 & \text{for cast in anchors} \\ 1.40 & \text{for post - installed anchors where } k_c = 17 \end{cases}$$

$$\psi_{cp,N} = \begin{cases} 1.00 & \text{for uncracked concrete where } c_{a,min} \geq c_{ac} \\ \frac{c_{a,min}}{c_{ac}} & \text{for cracked concrete where } c_{a,min} < c_{ac} \end{cases}$$

$$N_{ba} = \lambda_a \tau_{cr} \pi d_a h_{ef} \psi_{bd,N} \psi_{bc,N} \psi_{ep,N} \psi_{ed,Na} \psi_{cp,Na} \frac{A_{Na}}{A_{Na0}} \quad (81)$$

Where:

$$\psi_{bd,N} = \begin{cases} 1.00 & \text{for static loading} \\ 1.40 & \text{for dynamic loading} \end{cases}$$

$$\psi_{bc,N} = \begin{cases} 1.00 & \text{for } 2,500 \text{ psi} < f'_c < 4,500 \text{ psi} \\ 1.06 & \text{for } 4,500 \text{ psi} < f'_c < 6,500 \text{ psi} \\ 1.08 & \text{for } 6,500 \text{ psi} < f'_c < 8,500 \text{ psi} \end{cases}$$

$$\psi_{ep,N} = \begin{cases} 1.00 & \text{for black steel rods} \\ 0.90 & \text{for epoxy coated rods} \end{cases}$$

$$\psi_{ed,Na} = \begin{cases} 1.00 & \text{if } c_a \geq c_{Na} \\ 0.7 + 0.3 \frac{c_{a,min}}{c_{Na}} & \text{if } c_a < c_{Na} \end{cases}$$

$$\psi_{cp,Na} = \begin{cases} 1.00 & \text{for uncracked concrete where } c_{a,min} \geq c_{ac} \\ \frac{c_{a,min}}{c_{ac}} & \text{for cracked concrete where } c_{a,min} < c_{ac} \end{cases}$$

Analysis of the ACI 318-11 and the cone or full uniform bond models with modification factors for the steel, concrete, and adhesive demonstrated a much improved performance over the models without modification factors, as shown in Table 14. Results from the comparison found that both methods were capable of identifying the correct failure modes for most of the WEAB tests. The cone or uniform bond model identified the correct failure mode or one of the two combined failure modes for every test except for test no. WEAB-4. The ACI 318-11 procedures also identified the appropriate failure mode for the majority of the testing, but the method proved to be conservative when predicting steel failure as seen in the calculations for test nos. WEAB-1, WEAB-2, and WEAB-4.

Table 14. Comparison of ACI 318-11, Cone or Full Uniform Bond Model, and WEAB Testing - Factored and As-Tested Materials

Test No.	Test Article	Actual Failure Mode	Average Actual Load (kips)	Cone or Uniform Bond			ACI 318-11			
				Failure Mode	Capacity (kips)	Test-to-Predicted Ratio	Failure Mode	Capacity (kips)	Test-to-Predicted Ratio	
WEAB-1	#5 bar uncoated	Steel Fracture	38.35	Steel Fracture	38.0	1.01	Bond Failure	32.8	1.17	
WEAB-2	#5 bar uncoated	Steel Fracture	39.38	Steel Fracture	38.0	1.04	Bond Failure	32.8	1.20	
WEAB-4	#5 bar epoxy coated	Steel Fracture	35.95	Bond Failure	35.4	1.02	Bond Failure	29.5	1.22	
WEAB-7	2 #5 bars @ 8" epoxy coated	Steel Fracture/ Bond Failure	73.80	Bond Failure	51.6	1.43	Bond Failure	43.0	1.72	
WEAB-8	2 #5 bars @ 8" epoxy coated	Concrete Breakout/ Bond Failure	72.53	Bond Failure	51.6	1.41	Bond Failure	43.0	1.69	
WEAB-9	#6 bar epoxy coated	Bond Failure	41.31	Bond Failure	39.8	1.04	Bond Failure	34.1	1.21	
WEAB-10	#6 bar epoxy coated	Bond Failure	43.74	Bond Failure	39.8	1.10	Bond Failure	34.1	1.28	
WEAB-11	2 #6 bars @ 8" epoxy coated	Concrete Breakout/ Bond Failure	60.65	Bond Failure	55.3	1.10	Bond Failure	47.4	1.28	
WEAB-12	2 #6 bars @ 8" epoxy coated	Concrete Breakout/ Bond Failure	75.62	Bond Failure	55.3	1.37	Bond Failure	47.4	1.59	
WEAB-14	1 1/8" A307 rod uncoated	Concrete Breakout/ Bond Failure	45.30	Concrete Breakout	46.1	0.98	Concrete Breakout	43.6	1.04	
WEAB-16	#6 bar uncoated	Bond Failure	47.24	Bond Failure	44.3	1.07	Bond Failure	37.9	1.24	
Average Test / Predicted =						1.14	Average Test / Predicted =			1.33

Both models also proved reasonably accurate for prediction of anchor capacity. The cone or uniform bond model was the more accurate of the two models, and the anchor capacities predicted with this model correlated well with the majority of the testing except for test nos. WEAB-7, WEAB-8, and WEAB-12. These tests involved dual anchors and suggest that the reduction factors for anchor spacing on concrete breakaway and adhesive bond capacity are quite conservative. The ACI 318-11 procedures predicted values that were slightly more conservative across the board, but the predicted loads were still within 33 percent of the tested loads on average. ACI 318-11 procedures also demonstrated significant under prediction of the capacity of the dual anchor tests. Thus, it was found that both the ACI 318-11 and the cone or full uniform bond models were capable of correctly predicting the majority of the failure modes and anchor capacities when compared with the WEAB test series when proper modification factors for the steel, concrete, and adhesive models were applied. Overall, the ACI 318-11 procedure was the more conservative of the two approaches.

8.2.3 Design Comparison

The final comparison between the ACI 318-11 and the cone or full uniform bond model procedures for post-installed adhesive anchors was conducted using published, nominal values for steel and concrete material properties, the dynamic modification factors for steel, concrete, and adhesive noted in Section 8.2.2, and appropriate strength reduction factors. This comparison was conducted in order to evaluate both models' predictions for failure mode and capacity when using a standard design approach. Strength reduction factors (ϕ) for both models were determined based on the recommended reduction factors in Appendix D of ACI 318-11 for consistency. The strength reduction factors for steel, concrete, and adhesive bond capacities were set to 0.75, 0.65, and 0.65 respectively. Modification factors for anchor spacing and edge distance found in ACI 318-11 were applied to the cone or full uniform bond model in order to

provide a consistent comparison, as these factors were not part of the development of that model. Note that all of the equations shown below are in US Custom units.

For the cone or full uniform bond model, equation (69) was again used to determine the height of the concrete cone and the failure mode. If the estimated height of the concrete cone calculated by Equation (69) was greater than or equal to the embedment depth, concrete cone and breakout was predicted and Equation (83) was utilized. Otherwise adhesive failure is predicted, and the uniform bond stress Equation (84) was used to calculate the pullout capacity. The predicted capacity for concrete breakout or adhesive bond failure was then compared to the steel fracture capacity of the anchor in equation (82) to determine the limiting failure mode. In equation (82), ϕ is the strength reduction factor, A_s is the effective cross-sectional area of the anchor in tension, f_u is the ultimate tensile stress of the anchor, and $\psi_{sd,N}$ is the DIF for the steel failure. In equation (83), ϕ is the strength reduction factor, h_{ef} is the embedment depth of the anchor, $\psi_{cd,N}$ is the DIF for concrete breakout, $\psi_{ed,N}$ is a reduction factor for anchor edge distance, $\psi_{cp,N}$ is a factor for cracked concrete, and $\frac{A_{Nc}}{A_{Nco}}$ is the reduction factor for anchor spacing, as detailed in ACI 381-11. In equation (84), ϕ is the strength reduction factor, τ_o is the static bond stress, d_o is the diameter of the hole, h_{ef} is the embedment depth of the anchor, $\psi_{bd,N}$ is the DIF for the adhesive bond, $\psi_{bc,N}$ is the concrete strength increase factor, $\psi_{ep,N}$ is the anchor coating factor, $\psi_{ed,Na}$ is a reduction factor for anchor edge distance, $\psi_{cp,Na}$ is a factor for cracked concrete, and $\frac{A_{Na}}{A_{Na0}}$ is the spacing factor, as detailed in ACI 381-11.

$$N_n = \phi A_s f_u \psi_{sd,N} \quad (82)$$

Where:

$$\psi_{sd,N} = \begin{cases} 1.00 & \text{for static loading} \\ 1.18 & \text{for dynamic loading} \end{cases}$$

$$N_n = \phi 11.08 h_{ef}^2 \sqrt{f'_c} \psi_{cd,N} \psi_{ed,N} \psi_{cp,N} \frac{A_{Nc}}{A_{Nco}} \quad (83)$$

Where:

$$\psi_{cd,N} = \begin{cases} 1.00 & \text{for static loading} \\ 1.88 & \text{for dynamic loading} \end{cases}$$

$$\psi_{ed,N} = \begin{cases} 1.00 & \text{if } c_a \geq 1.5h_{ef} \\ 0.7 + 0.3 \frac{c_{a,min}}{1.5h_{ef}} & \text{if } c_a < 1.5h_{ef} \end{cases}$$

$$\psi_{cp,N} = \begin{cases} 1.00 & \text{for uncracked concrete where } c_{a,min} \geq c_{ac} \\ \frac{c_{a,min}}{c_{ac}} & \text{for cracked concrete where } c_{a,min} < c_{ac} \end{cases}$$

$$N_n = \phi \tau_0 \pi d_0 h_{ef} \psi_{bd,N} \psi_{bc,N} \psi_{ep,N} \psi_{ed,Na} \psi_{cp,Na} \frac{A_{Na}}{A_{Na0}} \quad (84)$$

Where:

$$\psi_{bd,N} = \begin{cases} 1.00 & \text{for static loading} \\ 1.40 & \text{for dynamic loading} \end{cases}$$

$$\psi_{bc,N} = \begin{cases} 1.00 & \text{for } 2,500 \text{ psi} < f'_c < 4,500 \text{ psi} \\ 1.06 & \text{for } 4,500 \text{ psi} < f'_c < 6,500 \text{ psi} \\ 1.08 & \text{for } 6,500 \text{ psi} < f'_c < 8,500 \text{ psi} \end{cases}$$

$$\psi_{ep,N} = \begin{cases} 1.00 & \text{for black steel rods} \\ 0.90 & \text{for epoxy coated rods} \end{cases}$$

$$\psi_{ed,Na} = \begin{cases} 1.00 & \text{if } c_a \geq c_{Na} \\ 0.7 + 0.3 \frac{c_{a,min}}{c_{Na}} & \text{if } c_a < c_{Na} \end{cases}$$

$$\psi_{cp,Na} = \begin{cases} 1.00 & \text{for uncracked concrete where } c_{a,min} \geq c_{ac} \\ \frac{c_{a,min}}{c_{ac}} & \text{for cracked concrete where } c_{a,min} < c_{ac} \end{cases}$$

For the ACI 318-11 method, three equations were used to determine the capacity of the post-installed adhesive anchors for three separate failure modes: steel fracture, concrete breakout, and adhesive bond failure. The lowest calculated capacity of the three failure modes

was then selected as the anchor capacity. The ACI 318-11 equations used in this comparison for steel fracture, concrete breakout, and adhesive bond failure are shown in equations (85), (86), and (87), respectively. In equation (85), ϕ is the strength reduction factor, $A_{se,N}$ is the effective cross-sectional area of the anchor in tension, f_{uta} is the ultimate tensile stress of the anchor, and $\psi_{sd,N}$ is the DIF for the steel failure mode. In equation (86), ϕ is the strength reduction factor, k_c is a coefficient that is equal to 24 based on the ACI 355.4 evaluation of Hilti HIT-RE 500 SD post-installed adhesive anchors, λ_a is a modification factor for lightweight concrete, f_c' is the unconfined compressive strength of the concrete, h_{ef} is the embedment depth of the anchor, $\psi_{cd,N}$ is the DIF for concrete breakout, $\psi_{ed,N}$ is a reduction factor for anchor edge distance, $\psi_{c,N}$ is a factor for concrete cracking under service loads, $\psi_{cp,N}$ is a factor for cracked concrete, and $\frac{A_{Nc}}{A_{Nco}}$ is the reduction factor for anchor spacing, as detailed in ACI 381-11. In equation (87), ϕ is the strength reduction factor, λ_a is a modification factor for lightweight concrete, τ_{cr} is the static bond stress, d_a is the diameter of the anchor, h_{ef} is the embedment depth of the anchor, $\psi_{bd,N}$ is the DIF for the adhesive bond, $\psi_{bc,N}$ is the concrete strength increase factor, $\psi_{ep,N}$ is the anchor coating factor, $\psi_{ed,Na}$ is a reduction factor for anchor edge distance, $\psi_{cp,Na}$ is a factor for cracked concrete, and $\frac{A_{Na}}{A_{Na0}}$ is the spacing factor, as detailed in ACI 381-11.

$$N_{sa} = \phi A_{se,N} f_{uta} \psi_{sd,N} \quad (85)$$

Where:

$$\psi_{sd,N} = \begin{cases} 1.00 & \text{for static loading} \\ 1.18 & \text{for dynamic loading} \end{cases}$$

$$N_{cb} = \phi k_c \lambda_a \sqrt{f_c'} h_{ef}^{1.5} \psi_{cd,N} \psi_{ed,N} \psi_{c,N} \psi_{cp,N} \frac{A_{Nc}}{A_{Nco}} \quad (86)$$

Where:

$$\psi_{cd,N} = \begin{cases} 1.00 & \text{for static loading} \\ 1.88 & \text{for dynamic loading} \end{cases}$$

$$\psi_{ed,N} = \begin{cases} 1.00 & \text{if } c_a \geq 1.5h_{ef} \\ 0.7 + 0.3 \frac{c_{a,min}}{1.5h_{ef}} & \text{if } c_a < 1.5h_{ef} \end{cases}$$

$$\psi_{c,N} = \begin{cases} 1.00 & \text{for } k_c \text{ determined from ACI 355.4 evaluation} \\ 1.25 & \text{for cast in anchors} \\ 1.40 & \text{for post – installed anchors where } k_c = 17 \end{cases}$$

$$\psi_{cp,N} = \begin{cases} 1.00 & \text{for uncracked concrete where } c_{a,min} \geq c_{ac} \\ \frac{c_{a,min}}{c_{ac}} & \text{for cracked concrete where } c_{a,min} < c_{ac} \end{cases}$$

$$N_{ba} = \phi \lambda_a \tau_{cr} \pi d_a h_{ef} \psi_{bd,N} \psi_{bc,N} \psi_{ep,N} \psi_{ed,Na} \psi_{cp,Na} \frac{A_{Na}}{A_{Na0}} \quad (87)$$

Where:

$$\psi_{bd,N} = \begin{cases} 1.00 & \text{for static loading} \\ 1.40 & \text{for dynamic loading} \end{cases}$$

$$\psi_{bc,N} = \begin{cases} 1.00 & \text{for } 2,500 \text{ psi} < f'c < 4,500 \text{ psi} \\ 1.06 & \text{for } 4,500 \text{ psi} < f'c < 6,500 \text{ psi} \\ 1.08 & \text{for } 6,500 \text{ psi} < f'c < 8,500 \text{ psi} \end{cases}$$

$$\psi_{ep,N} = \begin{cases} 1.00 & \text{for black steel rods} \\ 0.90 & \text{for epoxy coated rods} \end{cases}$$

$$\psi_{ed,Na} = \begin{cases} 1.00 & \text{if } c_a \geq c_{Na} \\ 0.7 + 0.3 \frac{c_{a,min}}{c_{Na}} & \text{if } c_a < c_{Na} \end{cases}$$

$$\psi_{cp,Na} = \begin{cases} 1.00 & \text{for uncracked concrete where } c_{a,min} \geq c_{ac} \\ \frac{c_{a,min}}{c_{ac}} & \text{for cracked concrete where } c_{a,min} < c_{ac} \end{cases}$$

Analysis of the ACI 318-11 and the cone or full uniform bond models using standard design input is shown in Table 15. Results from this comparison found that both methods were capable of identifying the correct failure modes for most of the WEAB test series when using

available design data and appropriate strength reduction factors. The cone or uniform bond model identified the correct failure mode or one of the two combined failure modes for every test except for test no. WEAB-4. The ACI 318-11 procedures also identified the appropriate failure mode for the majority of the testing, but the method proved to be conservative when predicting steel failure as seen in the calculations for test nos. WEAB-1, WEAB-2, and WEAB-4. Comparison of the ACI 318-11 and the cone or full uniform bond predicted load values found that both models were very conservative for predicted load when using design data. The results of this comparison were somewhat expected as the use of strength reduction factors and published material strength data would tend to reduce the predicted load while having little effect on the failure modes. These results indicated that either model could be applied for the design of post-installed adhesive anchors, but they would tend to be very conservative.

Table 15. Comparison of ACI 318-11, Cone or Full Uniform Bond Model, and WEAB Testing – Design Data

Test No.	Test Article	Actual Failure Mode	Average Actual Load (kips)	Cone or Uniform Bond			ACI 318-11			
				Failure Mode	Capacity (kips)	Test-to-Predicted Ratio	Failure Mode	Capacity (kips)	Test-to-Predicted Ratio	
WEAB-1	#5 bar uncoated	Steel Fracture	38.35	Steel Fracture	24.7	1.55	Bond Failure	21.3	1.80	
WEAB-2	#5 bar uncoated	Steel Fracture	39.38	Steel Fracture	24.7	1.60	Bond Failure	21.3	1.85	
WEAB-4	#5 bar epoxy coated	Steel Fracture	35.95	Bond Failure	23.0	1.56	Bond Failure	19.2	1.88	
WEAB-7	2 #5 bars @ 8" epoxy coated	Steel Fracture/ Bond Failure	73.80	Bond Failure	33.6	2.20	Bond Failure	28.0	2.64	
WEAB-8	2 #5 bars @ 8" epoxy coated	Concrete Breakout/ Bond Failure	72.53	Bond Failure	33.6	2.16	Bond Failure	28.0	2.59	
WEAB-9	#6 bar epoxy coated	Bond Failure	41.31	Bond Failure	25.9	1.60	Bond Failure	22.2	1.86	
WEAB-10	#6 bar epoxy coated	Bond Failure	43.74	Bond Failure	25.9	1.69	Bond Failure	22.2	1.97	
WEAB-11	2 #6 bars @ 8" epoxy coated	Concrete Breakout/ Bond Failure	60.65	Bond Failure	36.0	1.69	Bond Failure	30.8	1.97	
WEAB-12	2 #6 bars @ 8" epoxy coated	Concrete Breakout/ Bond Failure	75.62	Bond Failure	36.0	2.10	Bond Failure	30.8	2.45	
WEAB-14	1½" A307 rod uncoated	Concrete Breakout/ Bond Failure	45.30	Concrete Breakout	28.9	1.57	Concrete Breakout	27.3	1.66	
WEAB-16	#6 bar uncoated	Bond Failure	47.24	Bond Failure	28.8	1.64	Bond Failure	24.7	1.92	
Average Test / Predicted =						1.76	Average Test / Predicted =			2.05

162

8.3 Shear Model

As noted previously in Chapter 3, shear capacities for post-installed adhesive anchors have very similar failure modes and behavior to cast-in-place and post-installed mechanical anchors. The common shear failure modes for these anchors are limited to steel failure, concrete pryout, and concrete breakout of the anchor. Adhesive bond failure is not directly considered, but it is a component of the pryout failure model. ACI 318-11 provides calculation procedures for the determination of the shear capacity of post-installed adhesive anchors. In order to evaluate the performance of these procedures, ACI-318-11 was used to predict the failure mode and capacity of the adhesive anchors in test nos. WEAB-5, WEAB-6, and WEAB-13.

Comparison of the ACI 318-11 shear calculation procedures for post-installed adhesive anchors was performed in three variations. First, the ACI 318-11 was used to calculate the anchor capacities and failure modes for the shear component tests without any modification or reduction factors and using actual, as-tested material properties for concrete and steel. A second analysis was performed where modification factors were applied for dynamic strength increases and as-tested material properties for concrete and steel were applied. A third comparison was then performed using appropriate modification and strength reduction factors as well as nominal published material strengths to represent the methods when used for design of a post-installed anchorage. Details of these comparisons and the results are discussed in subsequent sections.

8.3.1 Non-Factored, As-Tested Materials Comparison

The first comparison of the ACI 318-11 model procedures for post-installed adhesive anchors was limited to determination of the failure modes and anchor capacities without using any modification or reduction factors and applying as-tested material properties for the steel and concrete. This comparison was intended to compare the procedure to the WEAB tests using the

best material data available but without incorporating DIFs for the steel and concrete or strength reduction factors.

In the ACI 318-11 method, three equations were used to determine the capacity of the post-installed adhesive anchors for three separate failure modes: steel fracture, concrete breakout, and concrete pryout. The lowest calculated capacity of the three failure modes was then selected as the anchor capacity. The ACI 318-11 equations used in this comparison for steel fracture, concrete breakout, and concrete pryout are shown in equations (88), (89), and (90), respectively. In equation (88), $A_{se,N}$ is the effective cross-sectional area of the anchor and f_{uta} is the ultimate tensile stress of the anchor. In equation (89), l_e is the load bearing length of the anchor in shear, λ_a is a modification factor for lightweight concrete, d_a is the anchor diameter, c_{a1} is the edge distance along the direction of applied load, c_{a2} is the edge distance perpendicular to the direction of applied load, h_a is the concrete thickness, f_c' is the unconfined compressive strength of the concrete, h_{ef} is the embedment depth of the anchor, $\psi_{ed,V}$ is a reduction factor for anchor edge distance, $\psi_{c,V}$ is a factor for concrete cracking under service loads, $\psi_{h,V}$ is a factor for cracked concrete, and $\frac{A_{Vc}}{A_{Vco}}$ is the reduction factor for anchor spacing, as detailed in ACI 318-11. In equation (90), k_{cp} is a modification factor for embedment depth and N_{cp} is the minimum of the tensile bond and concrete breakout capacity.

$$V_{sa} = 0.6A_{se,N}f_{uta} \quad (88)$$

$$V_{cb} = V_b\psi_{ed,V}\psi_{c,V}\psi_{h,V}\frac{A_{Vc}}{A_{Vco}} \quad (89)$$

Where:

$$V_b = \text{minimum of } \begin{cases} \left(7 \left(\frac{l_e}{d_a}\right)^2 \sqrt{d_a}\right) \lambda_a \sqrt{f'_c} (c_{a1})^{1.5} \\ \text{where } l_e = h_{ef} \text{ and } l_e \leq 8d_a \\ \text{or} \\ 9\lambda_a \sqrt{f'_c} (c_{a1})^{1.5} \end{cases}$$

$$\psi_{ed,v} = \begin{cases} 1.00 \text{ if } c_a \geq 1.5c_{a1} \\ 0.7 + 0.3 \frac{c_{a2}}{1.5c_{a1}} \text{ if } c_a < 1.5c_{a1} \end{cases}$$

$$\psi_{c,v} = \begin{cases} 1.40 \text{ when analysis indicates no cracking at service loads} \\ 1.00 \text{ for anchors in cracked concrete w/o supplemental reinforcement} \\ 1.20 \text{ for anchors in cracked concrete with reinforcement } > \text{ no. 4 bar} \\ 1.40 \text{ for anchors in cracked concrete with reinforcement } > \text{ no. 4 bar} \\ \text{and enclosed within stirrups space not more than 4 in.} \end{cases}$$

$$\psi_{h,v} = \begin{cases} 1.00 \text{ for where } h_a \geq 1.5c_{a1} \\ \sqrt{\frac{1.5c_{a1}}{h_a}} \text{ for cracked concrete where } h_a < 1.5c_{a1} \end{cases}$$

$$V_{cp} = k_{cp} N_{cp} \quad (90)$$

Where:

$$k_{cp} = \begin{cases} 1.00 \text{ for } h_{ef} < 2.5 \text{ in.} \\ 2.00 \text{ for } h_{ef} \geq 2.5 \text{ in.} \end{cases}$$

$$N_{cp} = \text{minimum of } \begin{cases} N_a \text{ in tensile equation D - 3 of ACI 318 - 11} \\ N_{cb} \text{ in tensile equation D - 18 of ACI 318 - 11} \end{cases}$$

The comparison of the ACI 318-11 shear procedures and the applicable WEAB tests is shown in Table 16. Results from the comparison demonstrated that ACI 318-11 predicted the correct failure mode for all the shear tests in the WEAB test series. Because the WEAB testing was conducted in a very large concrete slab, edge distances and slab thickness were very large and essentially prevented concrete breakout from occurring. Similarly, the embedment depth of the tested rebar made pryout highly unlikely as well. Thus, while the correct failure mode was

identified, the ability of ACI 318-11 to correctly predict concrete breakout or pryout failure modes could not be evaluated using the testing in this research. Further testing of shallower anchor embedment and edge effects would be required to evaluate these failure modes.

The predicted load capacity from the analysis found that the ACI-318-11 procedures were fairly conservative and under predicted the strength of the anchor in shear. However, it should be noted that this comparison did not include DIFs for the steel, concrete, or epoxy adhesive. The addition of these modification factors would be expected to provide an improved prediction of anchor capacity.

Table 16. Comparison of ACI 318-11 Shear Procedures and WEAB Testing - Non-Factored and As-Tested Materials

Test No.	Test Article	Actual Failure Mode	Average Actual Load (kips)	ACI 318-11		
				Failure Mode	Capacity (kips)	Test-to-Predicted Ratio
WEAB-5	#5 bar epoxy coated	Steel Fracture	29.05	Steel Fracture	19.33	1.50
WEAB-6	#5 bar epoxy coated	Steel Fracture	26.07	Steel Fracture	19.33	1.35
WEAB-13	#6 bar epoxy coated	Steel Fracture	30.06	Steel Fracture	26.51	1.13
Average Test / Predicted =						1.33

8.3.2 Factored, As-Tested Comparison

The second comparison between the ACI 318-11 procedures for post-installed adhesive anchors loaded in shear and the WEAB series shear tests applied DIFs for the steel, concrete, and epoxy adhesive in order to evaluate if the increase factors would improve the model predictions. The DIFs applied to the materials were the same factors outline in Section 8.2.2. As-tested material properties for the steel and concrete were utilized again as well.

In the ACI 318-11 method, three equations were used to determine the capacity of the post-installed adhesive anchors for three separate failure modes: steel fracture, concrete breakout, and concrete pryout. The lowest calculated capacity of the three failure modes was then selected as the anchor capacity. The ACI 318-11 equations used in this comparison for steel fracture, concrete breakout, and concrete pryout are shown in equations (91), (92), and (93), respectively. In equation (91), $A_{se,N}$ is the effective cross-sectional area of the anchor, f_{uta} is the ultimate tensile stress of the anchor, and $\psi_{sd,V}$ is the DIF for steel. In equation (92), l_e is the load bearing length of the anchor in shear, λ_a is a modification factor for lightweight concrete, d_a is the anchor diameter, c_{a1} is the edge distance along the direction of applied load, c_{a2} is the edge distance perpendicular to the direction of applied load, h_a is the concrete thickness, f_c' is the unconfined compressive strength of the concrete, h_{ef} is the embedment depth of the anchor, $\psi_{cd,V}$ is the DIF for concrete breakout, $\psi_{ed,V}$ is a reduction factor for anchor edge distance, $\psi_{c,V}$ is a factor for concrete cracking under service loads, $\psi_{h,V}$ is a factor for cracked concrete, and $\frac{A_{vc}}{A_{vco}}$ is the reduction factor for anchor spacing, as detailed in ACI 318-11. In equation (93), k_{cp} is a modification factor for embedment depth and N_{cp} is the minimum of the tensile bond and concrete breakout capacity.

$$V_{sa} = 0.6A_{se,Nfuta}\psi_{sd,v} \quad (91)$$

Where:

$$\psi_{sd,v} = \begin{cases} 1.00 & \text{for static loading} \\ 1.18 & \text{for dynamic loading} \end{cases}$$

$$V_{cb} = V_b\psi_{cd,v}\psi_{ed,v}\psi_{c,v}\psi_{h,v}\frac{A_{vc}}{A_{vco}} \quad (92)$$

Where:

$$V_b = \text{minimum of } \begin{cases} \left(7\left(\frac{l_e}{d_a}\right)^2\sqrt{d_a}\right)\lambda_a\sqrt{f'_c}(c_{a1})^{1.5} \\ \text{where } l_e = h_{ef} \text{ and } l_e \leq 8d_a \\ \text{or} \\ 9\lambda_a\sqrt{f'_c}(c_{a1})^{1.5} \end{cases}$$

$$\psi_{cd,v} = \begin{cases} 1.00 & \text{for static loading} \\ 1.88 & \text{for dynamic loading} \end{cases}$$

$$\psi_{ed,v} = \begin{cases} 1.00 & \text{if } c_a \geq 1.5c_{a1} \\ 0.7 + 0.3\frac{c_{a2}}{1.5c_{a1}} & \text{if } c_a < 1.5c_{a1} \end{cases}$$

$$\psi_{c,v} = \begin{cases} 1.40 & \text{when analysis indicates no cracking at service loads} \\ 1.00 & \text{for anchors in cracked concrete w/o supplemental reinforcement} \\ 1.20 & \text{for anchors in cracked concrete with reinforcement } > \text{no. 4 bar} \\ 1.40 & \text{for anchors in cracked concrete with reinforcement } > \text{no. 4 bar} \\ & \text{and enclosed within stirrups space not more than 4 in.} \end{cases}$$

$$\psi_{h,v} = \begin{cases} 1.00 & \text{for where } h_a \geq 1.5c_{a1} \\ \sqrt{\frac{1.5c_{a1}}{h_a}} & \text{for cracked concrete where } h_a < 1.5c_{a1} \end{cases}$$

$$V_{cp} = k_{cp}N_{cp} \quad (93)$$

Where:

$$k_{cp} = \begin{cases} 1.00 & \text{for } h_{ef} < 2.5\text{in.} \\ 2.00 & \text{for } h_{ef} \geq 2.5\text{in.} \end{cases}$$

$$N_{cp} = \text{minimum of } \begin{cases} N_a \text{ in tensile equation D - 3 of ACI 318 - 11} \\ N_{cb} \text{ in tensile equation D - 18 of ACI 318 - 11} \end{cases}$$

The comparison of the ACI 318-11 procedures for post-installed adhesive anchors with DIFs to the applicable WEAB series shear tests is shown in Table 17. Results from the comparison demonstrated that ACI 318-11 predicted the correct failure mode for all the shear tests in the WEAB test series. However, as noted in the previous section, the ability of ACI 318-11 to correctly predict concrete breakout or pryout failure modes could not be evaluated using the testing in this research. The predicted load capacity from the analysis found that the ACI-318-11 procedures produced more accurate and less conservative values when using the DIFs as the average tested-to-predicted ratio dropped from 1.33 to 1.13.

Table 17. Comparison of ACI 318-11 Shear Procedures and WEAB Testing - Factored and As-Tested Materials

Test No.	Test Article	Actual Failure Mode	Average Actual Load (kips)	ACI 318-11		
				Failure Mode	Capacity (kips)	Test-to-Predicted Ratio
WEAB-5	#5 bar epoxy coated	Steel Fracture	29.05	Steel Fracture	22.81	1.27
WEAB-6	#5 bar epoxy coated	Steel Fracture	26.07	Steel Fracture	22.81	1.14
WEAB-13	#6 bar epoxy coated	Steel Fracture	30.06	Steel Fracture	31.28	0.96
Average Test / Predicted =						1.13

8.3.3 Design Comparison

The final comparison between the ACI 318-11 a procedures for post-installed adhesive anchors loaded in shear and the WEAB test series was conducted using published, nominal values for the steel and concrete material properties, the dynamic modification factors for steel, concrete, and adhesive bond noted in Section 8.2.2, and appropriate strength reduction factors. This comparison was conducted in order to evaluate the model's accuracy for predicting failure mode and capacity when using a standard design approach. Strength reduction factors (ϕ) for the concrete and steel equations were determined based on the recommended reduction factors in Appendix D of ACI 318-11. The strength reduction factors for steel and concrete were set to 0.65 and 0.75, respectively.

In the ACI 318-11 method, three equations were used to determine the capacity of the post-installed adhesive anchors for three separate failure modes: steel fracture, concrete breakout, and concrete pryout. The lowest calculated capacity of the three failure modes was then selected as the anchor capacity. The ACI 318-11 equations used in this comparison for steel fracture, concrete breakout, and concrete pryout are shown in equations (91), (92), and (93), respectively. In equation (91), ϕ is the strength reduction factor, $A_{se,N}$ is the effective cross-sectional area of the anchor, f_{uta} is the ultimate tensile stress of the anchor, and $\psi_{sd,V}$ is the DIF for steel. In equation (92), ϕ is the strength reduction factor, l_e is the load bearing length of the anchor in shear, λ_a is a modification factor for lightweight concrete, d_a is the anchor diameter, c_{a1} is the edge distance along the direction of applied load, c_{a2} is the edge distance perpendicular to the direction of applied load, h_a is the concrete thickness, f'_c is the unconfined compressive strength of the concrete, h_{ef} is the embedment depth of the anchor, $\psi_{cd,V}$ is the DIF for concrete breakout, $\psi_{ed,V}$ is a reduction factor for anchor edge distance, $\psi_{c,V}$ is a factor

for concrete cracking under service loads, $\psi_{h,v}$ is a factor for cracked concrete, and $\frac{A_{vc}}{A_{vco}}$ is the reduction factor for anchor spacing, as detailed in ACI 381-11. In equation (93), ϕ is the strength reduction factor, k_{cp} is a modification factor for embedment depth and N_{cp} is the minimum of the tensile bond and concrete breakout capacity.

$$V_{sa} = \phi 0.6 A_{se,N} f_{uta} \psi_{sd,v} \quad (94)$$

Where:

$$\psi_{sd,v} = \begin{cases} 1.00 & \text{for static loading} \\ 1.18 & \text{for dynamic loading} \end{cases}$$

$$V_{cb} = \phi V_b \psi_{cd,v} \psi_{ed,v} \psi_{c,v} \psi_{h,v} \frac{A_{vc}}{A_{vco}} \quad (95)$$

Where:

$$V_b = \text{minimum of} \begin{cases} \left(7 \left(\frac{l_e}{d_a} \right)^2 \sqrt{d_a} \right) \lambda_a \sqrt{f'_c} (c_{a1})^{1.5} \\ \text{where } l_e = h_{ef} \text{ and } l_e \leq 8d_a \\ \text{or} \\ 9 \lambda_a \sqrt{f'_c} (c_{a1})^{1.5} \end{cases}$$

$$\psi_{cd,v} = \begin{cases} 1.00 & \text{for static loading} \\ 1.88 & \text{for dynamic loading} \end{cases}$$

$$\psi_{ed,v} = \begin{cases} 1.00 & \text{if } c_a \geq 1.5c_{a1} \\ 0.7 + 0.3 \frac{c_{a2}}{1.5c_{a1}} & \text{if } c_a < 1.5c_{a1} \end{cases}$$

$$\psi_{c,v} = \begin{cases} 1.40 & \text{when analysis indicates no cracking at service loads} \\ 1.00 & \text{for anchors in cracked concrete w/o supplemental reinforcement} \\ 1.20 & \text{for anchors in cracked concrete with reinforcement } > \text{ no. 4 bar} \\ 1.40 & \text{for anchors in cracked concrete with reinforcement } > \text{ no. 4 bar} \\ & \text{and enclosed within stirrups space not more than 4 in.} \end{cases}$$

$$\psi_{h,v} = \begin{cases} 1.00 & \text{for where } h_a \geq 1.5c_{a1} \\ \sqrt{\frac{1.5c_{a1}}{h_a}} & \text{for cracked concrete where } h_a < 1.5c_{a1} \end{cases}$$

$$V_{cp} = \phi k_{cp} N_{cp} \quad (96)$$

Where:

$$k_{cp} = \begin{cases} 1.00 & \text{for } h_{ef} < 2.5 \text{ in.} \\ 2.00 & \text{for } h_{ef} \geq 2.5 \text{ in.} \end{cases}$$

$$N_{cp} = \text{minimum of } \begin{cases} N_a & \text{in tensile equation D - 3 of ACI 318 - 11} \\ N_{cb} & \text{in tensile equation D - 18 of ACI 318 - 11} \end{cases}$$

The comparison of the ACI 318-11 procedures for post-installed adhesive anchors loaded in shear using standard design input and the applicable WEAB tests is shown in Table 17. Results from the comparison demonstrated that ACI 318-11 again predicted the correct failure mode for all the shear tests in the WEAB test series. However, as noted in the previous sections, the ability of ACI 318-11 to correctly predict concrete breakout or pryout failure modes could not be evaluated from the testing in this research. The predicted load capacity from the analysis found that the ACI-318-11 procedures produced very conservative values when using the strength reduction factors and published material properties. The results of this comparison were expected as the use of strength reduction factors and published material strength data would tend to reduce the predicted load while having little effect on the failure modes. It should be noted that the ACI 318-11 test-to-predicted ratio observed when using design parameters was very similar for both the tensile and shear comparisons. Both the shear and tensile test-to-predicted ratios were 1.98 and 2.05, respectively, which would suggest that the ACI code provides a factor of safety relatively close to two.

Table 18. Comparison of ACI 318-11 Shear Procedures and WEAB Testing – Design Data

Test No.	Test Article	Actual Failure Mode	Average Actual Load (kips)	ACI 318-11		
				Failure Mode	Capacity (kips)	Test-to-Predicted Ratio
WEAB-5	#5 bar epoxy coated	Steel Fracture	29.05	Steel Fracture	12.84	2.26
WEAB-6	#5 bar epoxy coated	Steel Fracture	26.07	Steel Fracture	12.84	2.03
WEAB-13	#6 bar epoxy coated	Steel Fracture	30.06	Steel Fracture	18.22	1.65
Average Test / Predicted =						1.98

175

125

8.4 Discussion of Post-Installed Adhesive Anchor Models

Analytical models for determination of the tensile and shear capacities of post-installed adhesive anchors were compared to the WEAB series of component tests conducted as part of this research effort. Two models, the cone and full uniform bond model and ACI 318-11, were used to predict the tensile failure modes and load capacity of the anchorages. Only the ACI 318-11 procedures were used to predict the failure modes and load capacity of the anchorages when loaded in shear. The predictions of the analytical models were compared while varying the material property input, DIFs, and strength reduction factors in order to determine the feasibility of these models for use in design of post-installed adhesive anchorages.

Review of the tensile model predictions found that both the cone and full uniform bond model and the ACI 318-11 procedures produced overly conservative load values and incorrectly predicted failure modes without accounting for dynamic increases in material strength. When DIFs were included in the analysis, the cone and full uniform bond model predicted the correct failure modes for all of the tests but one, while the ACI 318-11 procedure predicted the correct failure modes for all but three tests. Both methods had some difficulty identifying the steel fracture failure mode. Load capacities determined using DIFs were found to be very close to tested values for both methods with the ACI 318-11 procedures being slightly more conservative. The final comparison of the tensile model predictions compared both models using available, published design data for the material properties, the DIFs, and the strength reduction factors recommended in ACI 318-11. The results from this comparison found that prediction of the failure mode was fairly accurate, but the load capacity predictions were very conservative. The predicted loads for the cone and full uniform bond model and the ACI 318-11 model were 1.76 and 2.05 times higher than the tested loads on average, respectively.

A similar analysis was performed to investigate the prediction of shear failure modes and load capacity using ACI-318-11. Evaluation of the predicted failure mode in shear was limited due to the testing performed in the WEAB test series being solely steel fracture. The embedment depth chosen and the lack of slab edge or thickness effects prevented other failure modes from occurring. Thus, while ACI318-11 correctly predicted steel failure for all of the WEAB tests, it was not possible to determine its effectiveness with respect to predicting either concrete breakout or anchor pry-out failure modes. A need exists to conduct more detailed shear anchor testing to further investigate edge distance and slab thickness effects in order to better understand and quantify the concrete failure in shear. The shear load capacity predicted by ACI 318-11 was reasonably accurate when DIFs were added to the analysis. The load capacity predicted with ACI recommended strength reduction factors was conservative by a factor of 2.

Based on the results of these comparisons, it is recommended that the ACI 318-11 procedure with the proposed dynamic increase factors be utilized for design of post-installed adhesive anchors for concrete barriers. ACI 318-11 is a widely accepted and easily accessible standard that can be implemented by end users. The method provided reasonable results when compared with the WEAB test series. It was found that the use of the proposed dynamic increase factors for concrete breakout, steel fracture, and bond strength determined in this research improved the prediction of the anchor failure modes and capacities. Predicted failure modes were generally accurate in both tension and shear. The ACI 318-11 procedure did not correctly predict steel failure for all of the tensile testing, but it did predict bond failure, which was more conservative for design purposes and should help ensure the desired steel failure mode rather than concrete breakout. Load capacities for the ACI 318-11 procedures were generally quite conservative. Predicted loads generally exceeded test values by a factor of 2 as would be expected for a general purpose building code.

While ACI 318-11 did provide a good model for design of post-installed adhesive anchors for concrete barriers, the implementation of these procedures for design does possess some shortcomings. First, as noted previously, the ability of the ACI 318-11 procedures to predict proper shear failure modes was not verified in this research effort. Similarly, the tensile testing used to for comparison with the design procedures did not incorporate or evaluate edge spacing. Thus, further component testing designed to look specifically a placement of anchors adjacent to the edge and embedment of anchors in thin slabs would be required to fully evaluate failure mode prediction using these procedures. Further research would also be required to evaluate shorter embedment depths that may also affect the failure mode of the anchor. ACI 318-11 also provides some guidance for determining the effect of deck reinforcement on the anchor failure that was not evaluated as part of this effort. Finally, there is concern that the method may be overly conservative in its prediction of anchor load capacities and may limit the design of post-installed adhesive anchorages. Preliminary design calculations seem to indicate that design of a post-installed adhesive anchorage system with the ACI 318-11 procedures would be restrictive. ACI 318-11 will provide designs that meet strength requirements and are more likely to fail in steel fracture due to the conservative nature of the concrete and adhesive bond load calculations. This is generally desired. However, concrete barrier anchorages are generally designed with the requirement that steel fracture be the limiting failure mode in order to provide for increased ductility in the anchorage and prevent damage to the concrete bridge deck. Thus, the conservative calculation of the concrete and bond capacities combined with the requirement to limit the failure mode to steel fracture may potentially lead to designs that are overly conservative. Thus, further research may be desired to determine how overly conservative the design procedures may be through component testing of small sections of bridge rails installed using post-installed adhesive anchors.

9 BRIDGE RAIL ANCHORAGE DESIGN METHODOLOGY

The ACI 318-11 procedures discussed in Chapter 8 provide a means for designing adhesive anchors for use in concrete bridge decks. However, these procedures do not describe how these anchorages are designed in conjunction with a bridge rail section and how to determine if the anchorage and bridge rail combination are adequate for resisting vehicle impact loading without damaging the bridge deck. This chapter will present a methodology for design of the post-installed adhesive anchors in conjunction with a cast-in-place concrete bridge rail, as this is the most common application. Similar design methodologies could be developed for attachment of portable concrete barrier, steel bridge rail, and precast bridge rail designs. However, the design of the attachment of these additional barrier types would largely be dependent on their individual design, and development of design procedures for a wide range of individual barrier types is outside the scope of this research.

In order to design a post-installed adhesive anchorage for a concrete bridge rail several assumptions need to be made. First, it is assumed that there are both front and back rows of anchorage on the barrier. This assumption is generally true for cast in place anchorages as they typically have anchor steel near the front and rear faces of the barrier that pass into the bridge deck. Second, it was assumed that the front and back row of anchors and the transverse steel (stirrups) in the barrier have the same spacing and are tied together prior to casting the barrier. A schematic of the assumed anchorage placement is shown in Figure 83. Third, it is assumed that the front of anchorage near the traffic side face of the barrier develops the tensile load required to develop the overturning moment of the concrete barrier. Fourth, the back row of anchors is assumed to develop the required shear loading of the barrier. Fifth, it is assumed that the bridge deck has adequate tensile, shear and moment capacity for attachment of the bridge railing.

Finally, it is assumed that the bridge deck is not cracked or damaged prior to installation of the epoxy adhesive anchors.

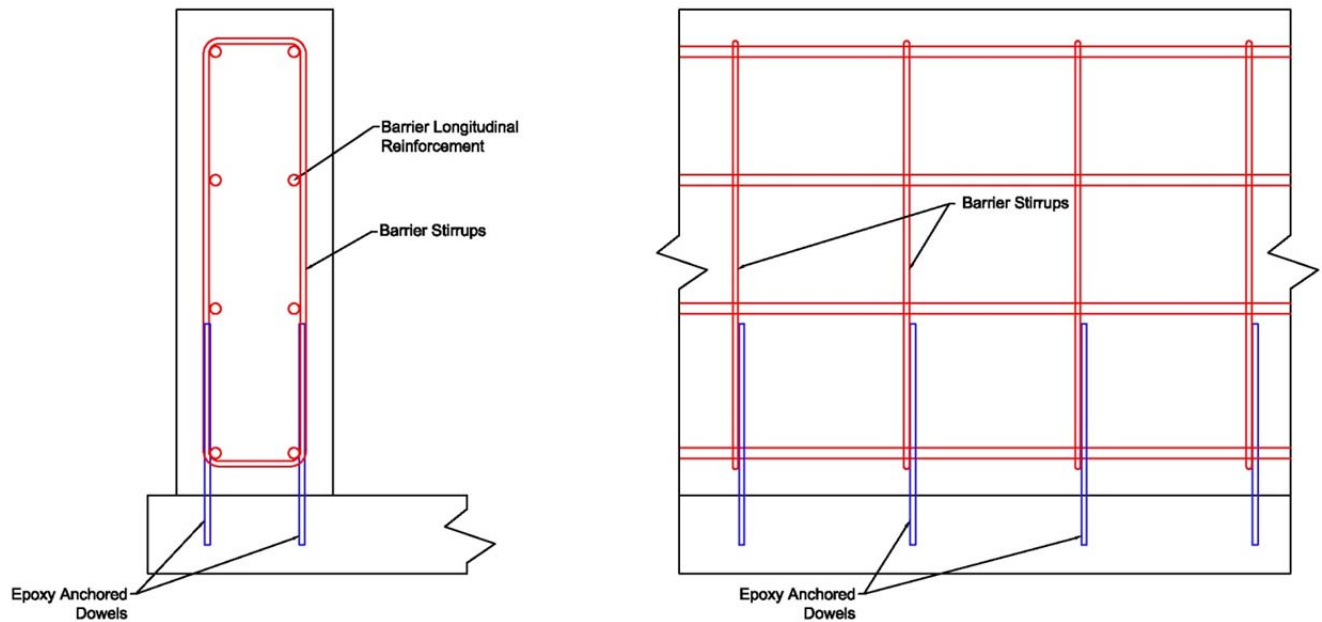


Figure 83. Schematic of Assumed Epoxy Adhesive Anchor Layout

Design of the bridge anchorage using post-installed adhesive anchors would proceed in an iterative design methodology that combines AASHTO LRFD Bridge Design Specifications yield line theory and the ACI 318-11 procedures. There are three design requirements for this design method for epoxy adhesive anchorage of cast-in-place concrete barrier. The first requirement is that the redirective capacity of the barrier calculated via yield line procedures be greater than or equal to the design load. Redirective barrier design loads should be based on the appropriate test level for the barrier in question. The second requirement is that the anchor failure mode for the front row of anchorage be limited to steel fracture. This requirement is necessary because the yield line procedures used to determine the overturning moment capacity, M_c , assume yielding of the reinforcing steel. As such, a similar failure mode must be maintained for

the tension anchors. In addition, requiring the tension steel to yield and fail provides for increased ductility and energy absorption while limiting damage to the bridge deck. The final design requirement is that the shear capacity of the anchorage be at least 65 percent of the lateral design loading over the critical load length, L_{cr} , as calculated from the yield line analysis. Lateral barrier design loads are resisted by a combination of the barrier moment, M_w , inertia, friction, shear capacity of the barrier section, and the shear capacity of the anchorage to the bridge deck. The exact contribution of these components to the total resistive force of the barrier is not clearly defined, but it is believed that assuming a 65 percent contribution from the anchorage to the bridge deck is conservative.

A design methodology for the design of a bridge anchorage using post-installed adhesive anchors is presented below based on the assumptions and design requirements listed above. This design methodology begins with establishing basic parameters for the bridge rail and anchorage. The design of the epoxy adhesive anchorage for cast-in-place barriers is achieved through iteration between the barrier design and the anchorage design to satisfy yield line theory, ACI 318-11, and the design requirements.

1. Establish Barrier Containment Level and Design Load

_____ Test level (NCHRP 350 of MASH)
_____ Design Load

2. Establish Barrier Geometry / Shape

_____ Barrier height
_____ Barrier width
_____ Barrier offset from deck
_____ Anchor edge distance (tensile)
_____ Anchor edge distance (shear)

3. Establish Anchor Variables

_____ Anchor size and strength
_____ Anchor spacing

4. Establish Epoxy Bond and Concrete Variables

_____ Epoxy bond strength
_____ Concrete strength
_____ Embedment depth
_____ Deck thickness

5. Predict Tension Anchor Failure Mode Utilizing ACI 318-11 Procedures

- If steel fracture is predicted mode of failure, go to step 6
- If concrete breakout or epoxy failure is predicted, return to Step 3 or 4

6. Calculate Barrier Overturning Moment Capacity (M_c) based on Variables in Steps 2-3

$$M_c = \underline{\hspace{2cm}}$$

7. Establish Longitudinal Barrier Reinforcement

_____ Longitudinal rebar size
_____ Longitudinal rebar quantity

8. Calculate Barrier Bending Moment Capacity (M_w) based on Variables in Step 7

$$M_w = \underline{\hspace{2cm}}$$

9. Calculate Barrier Capacity utilizing Yield Line Analysis

$$L_{cr} = \underline{\hspace{2cm}}$$
$$\phi R_w = \underline{\hspace{2cm}}$$

- If $\phi R_w \geq$ design load from Step 1, go to Step 10
- If $\phi R_w <$ design load form Step 1, return to Step 8 to strengthen M_w
- If $\phi R_w <$ design load form Step 1 and M_w cannot be increased, return to Step 2 or 3 to reconfigure anchors and strength M_c

10. Calculate Shear Capacity of Each Shear Anchor Utilizing ACI 318-11 Procedures

$$\phi V = \underline{\hspace{2cm}}$$

11. Calculate Number of Anchors in L_{CR}

$$n = L_{cr}/\text{anchor spacing (Step 3)}$$
$$n = \underline{\hspace{2cm}}$$

12. Calculate Total Barrier Shear Capacity

$$\phi V_{barrier} = n\phi V$$
$$\phi V_{barrier} = \underline{\hspace{2cm}}$$

- If $\phi V_{barrier} \geq 0.65 \cdot \text{Design Load}$, design is adequate
- If $\phi V_{barrier} < 0.65 \cdot \text{Design Load}$, return to Step 2 or 3 to increase shear strength

Preliminary design calculations indicate that design of a practical post-installed adhesive anchorage with this methodology would be very conservative due to the nature of the design calculations in yield line theory and ACI 318-11. However, it is believed that the design methodology should err on the conservative side when physical testing is not available to verify the performance of a given bridge rail and anchorage combination. As such, use of the methodology presented herein may potentially require increased longitudinal reinforcement in the bridge rail to better distribute the anchor loads and/or the use of modified anchor size and spacing as compared to current cast-in-place construction. Thus, further research may be desired to determine how overly conservative the design method may be through component testing of small sections of bridge rails installed using post-installed adhesive anchors. In addition, it is believed that more aggressive post-installed adhesive anchorage designs could be developed through the use of full-scale crash testing to verify their performance rather than the conservative design procedures.

10 SUMMARY, CONCLUSIONS, AND RECOMMENDATIONS

10.1 Summary and Conclusions

The objective of this project was to determine if epoxy adhesive anchors could be utilized to anchor concrete barriers to bridge decks and to develop design procedures for implementing epoxy adhesive anchorages into concrete bridge railings. These procedures would allow for more flexibility from a design and construction perspective as the use of epoxy adhesive anchors can simplify construction by eliminating the need for cast-in-place anchors. This research was intended to provide guidance for the installation of precast concrete traffic barriers, cast-in-place barriers, and temporary concrete barriers. Also, this technique would be applicable to permanent barriers, as well as retrofit solutions.

An extensive literature review was conducted to review the common methodologies used to design epoxy adhesive anchors. Most of these studies focused only on static loading conditions. Additionally, cast-in-place anchorages typically used in bridge rail applications require a protective coating against corrosion of either galvanization or the more common epoxy coating. None of the reviewed anchorage studies were conducted with epoxy-coated anchor bars. Several models were analyzed and it was determined that the cone or full uniform bond model was the most accurate and stable for the medium embedment depths associated with bridge rail applications.

A series of 16 dynamic bogie tests and one static test was conducted to investigate the behavior of epoxy adhesive anchors under dynamic load. Most of the anchors tested were no. 5 or no. 6 deformed reinforcing bars, which were the most commonly used anchorages according to a review of the Midwest States Pooled Fund standard plans. Additional dynamic tests were conducted on 1 1/8 in. (29 mm) diameter A307 threaded rods, which was the anchorage required for the F-shape temporary concrete barrier developed by MwRSF. Results from the testing of the

on 1 1/8 in. (29 mm) diameter A307 threaded rods suggested that they can be safely used with Hilti HIT-RE 500 or Hilti HIT-RE 500 SD epoxy adhesive with a 5 1/4-in. embedment depth to anchor the F-shape PCB and reduce deflections, but some increase in deflection and significant damage to the bridge deck is expected in severe impacts.

Following the component testing of epoxy adhesive anchors, comparisons were made between the component tests and analytical models for epoxy adhesive anchors. The cone and full uniform bond model and ACI 318-11 procedures were both compared with the tensile component tests in order to verify their effectiveness. Similarly, the ACI 318-11 procedures were compared with the shear component testing. The comparison parameters between the analytical models and the component tests were varied in order to better evaluate the models against the component tests. First, the models and testing were compared without any modification or reduction factors and using actual, as-tested material properties for concrete and steel. A second analysis was performed where modification factors were applied for dynamic strength increases and as-tested material properties for concrete and steel were applied. A third comparison was then performed using appropriate modification and strength reduction factors as well as nominal published material strengths to represent the methods when used for design of a post-installed anchorage. As part of this analysis, dynamic increase factors for concrete breakout and steel fracture and reduction factors for epoxy rebar coating were proposed based on the component testing.

Review of the comparisons between the analytical models and the tensile component tests found that both the cone and full uniform bond model and ACI 318-11 provided reasonable predictions for the failure mode of the epoxy adhesive anchors, but both were conservative in prediction of design loads. Review of the shear comparisons could not provide as detailed of results due to limitations in the failure modes observed in the component tests, but it was found

that ACI 318-11 provided reasonable yet conservative estimates of the shear capacity of the epoxy adhesive anchors. It was also found that the use of the proposed dynamic increase factors for concrete breakout, steel fracture, and bond strength determined in this research improved the prediction of the anchor failure modes and capacities. It was recommended that the ACI 318-11 procedures be combined with the proposed dynamic increase factors for design of epoxy adhesive anchors based on the performance in these comparisons and its wide accessibility and ease of implementation.

Following the selection of the ACI 318-11 procedures, a design methodology for the use of epoxy adhesive anchors for cast-in-place concrete bridge rails was presented. This method combines yield line analysis and ACI 318-11 to develop acceptable anchor and barrier designs.

10.2 Recommendations

While the ACI 318-11 procedures were found to be the best analytical model for design of post-installed adhesive anchors, the research presented herein does have limitations. As noted previously, the limited number of component tests available in this research prevented investigation of all of the potential failure modes for adhesive anchors. Specifically, anchor pryout and concrete breakout in shear were not evaluated. In addition, the effects of edge distance, slab thickness, anchor spacing, varied anchor embedment, and the effect of reinforcing steel in the concrete slab were not fully treated. As such, the current guidance in ACI 318-11 was used to fill these gaps. As a conservative approach, conventional design procedures from ACI 318-11 were recommended for determination of failure modes and capacities not specifically evaluated in this research.

The component testing conducted as part of this research utilized a Hilti epoxy adhesive. This product was chosen due to its widespread use and the availability of static test data and bond strength data for the adhesive. Thus, all of the calculations and comparisons in the report

are based on the HIT-RE 500 and HIT-RE 500 SD adhesives. It is believed that the use of other adhesives is acceptable with the ACI 318-11 procedures described herein as long as the appropriate material data input is provided. However, it should be noted that different adhesive materials may provide different capacities and failure modes when designing anchorages. It should also be noted that dynamic increase factors may not be available for other adhesives as they were for the Hilti products. Thus, bond strength calculations using adhesives without dynamic load factors may provide lower capacity than those demonstrated by the Hilti adhesives detailed in this research.

The results from this research also suggest that ACI 318-11 may be overly conservative in its prediction of anchor load capacities and may limit the design of post-installed adhesive anchorages. Design of a post-installed adhesive anchorage system with the ACI 318-11 procedures recommended herein will provide designs that meet strength requirements and be more likely to fail in steel fracture due to the conservative nature of the concrete breakout and adhesive bond capacity calculations. However, the conservativeness of the method may lead to anchorage designs that are more restrictive than necessary. Thus, further research may be desired to determine how overly conservative the design procedures may be through physical testing.

10.3 Future Work

The design procedures contained in Chapters 8 and 9 are recommended for use in designing epoxy adhesive anchorages for concrete bridge railings. However, as noted previously, they could be improved through further research to investigate all of the potential failure modes and to limit the conservative nature of the design method. Additional component testing is recommended to fully investigate anchor pryout and concrete breakout in shear, the effects of edge distance, slab thickness, anchor spacing, varied anchor embedment, and the effect of reinforcing steel in the concrete slab. This testing would likely require the construction of a

simulated reinforced bridge deck section. In addition to further research into the failure modes and anchor capacities, it is believed that larger scale component testing of bridge rail sections and full-scale crash testing could be applied to determine the degree of the conservativeness of the proposed design methodology and investigate the use of more aggressive post-installed adhesive anchorage designs.

11 REFERENCES

1. Dickey, B.J., Development of a Design Procedure for Concrete Traffic Barrier Attachments to Bridge Decks Utilizing Epoxy Concrete Anchors, Masters Thesis, University of Nebraska, Lincoln, December 2011.
2. ACI Committee 318, *Building Code Requirements for Structural Concrete (ACI 318-08) and Commentary*, 2008, Farmington Hills, MI, American Concrete Institute, 2009, 409-438.
3. Breen, J.E., Eligehausen, R., Fuchs, Werner., *Concrete Capacity Design (CCD) Approach for Fastening to Concrete*, American Concrete Institute Structural Journal, January-February 1995.
4. American Concrete Institute, *ACI Standard 349-85: Code Requirements for Nuclear Safety Related Concrete Structures, Appendix B – Steel Embedments*, 1985.
5. ICC Evaluation Service, *Acceptance Criteria for Post-Installed Adhesive Anchors in Concrete Elements AC308*, International Code Council, November 2009.
6. Cook, R.A., Davis, T.M., Douglas, E.P., *Adhesive Anchors in Concrete Under Sustained Loading Conditions*, National Cooperative Highway Research Program (NCHRP) Report No. 639, Transportation Research Board, Washington D.C., 2009.
7. Luke, P.C.C., *Strength and Behavior of Rebar Dowels Epoxy Bonded in Hardened Concrete*, Thesis, University of Texas, Austin, TX, May, 1984.
8. Doerr, G.T., Klingner, R.E., *Adhesive Anchors: Behavior and Spacing Requirements*, Report No. 1126-2, Center for Transportation Research, University of Texas, Austin TX, March 1989.
9. Collins, D.M., Klingner, R.E., Polyzois, D., *Load-Deflection Behavior of Cast-in-Place and Retrofit Concrete Anchors Subjected to Static, Fatigue, and Impact Tensile Loads*, Report No. FHWA/TX-89+1126-1, Center for Transportation Research, University of Texas, Austin, TX, February 1989.
10. Cook, R.A., *Behavior of Chemically Bonded Anchors*, Journal of Structural Engineering, American Society of Civil Engineers, September, 1993.
11. Biller, M.H., Cook, R.A., Fagundo, F.E., Richardson, D.E., *Tensile Behavior and Design of Single Adhesive Anchors*, Structures and Materials Research Report No. 91-3, University of Florida, Gainesville, FL, December, 1991.
12. Cook, R.A., Doerr, G.T., Klingner, R.E., *Bond Stress Model for Design of Adhesive Anchors*, American Concrete Institute Structural Journal, September-October, 1993.

13. Cook, R.A., Krishnamurthy, K., McVay, M., *Pullout Simulation of Postinstalled Chemically Bonded Anchors*, Journal of Structural Engineering, New York, New York, September 1996.
14. Cook, R.A., Fuchs, W., Konz, R.C., Kunz, J., *Behavior and Design of Single Adhesive Anchors Under Tensile Load in Uncracked Concrete*, American Concrete Institute Structural Journal, January-February 1998.
15. Appl, J., Cook, R.A., Eligehausen, R., *Behavior and Design of Adhesive Bonded Anchors*, American Concrete Institute Structural Journal, November-December 2006.
16. Bickel, T.S., Shaikh, A.F., *Shear Strength of Adhesive Anchors*, PCI Journal, September-October, 2002.
17. Precast/Prestressed Concrete Institute (PCI) Industry Handbook Committee. (1999). *PCI design handbook: Precast and Prestressed Concrete*, Fifth Ed., PCI. Chigago, IL.
18. Fujikak, K., Ishibashi, T., Mindess, S., Nakayama, J., Sato, H., *Chemically Bonded Anchors Subjected to Rapid Pullout Loading*, American Concrete Institute Materials Journal, May-June 2003.
19. Berra, M., Solomos, G., *Testing of Anchorages in Concrete Under Dynamic Tensile Loading*, Materials and Structures, November 2005.
20. Braimah, A., Constestabile, E., Guilbeault, R., *Behaviour of Adhesive Steel Anchors Under Impulse-Type Loading*, Canadian Journal of Civil Engineering, Ottawa, Ontario, November 2009.
21. Kruger, D., Lin, T., *Engineering Properties of Epoxy Resins Used as Concrete Adhesives*, American Concrete Institute Materials Journal, January-February 1996.
22. Hilti Inc., *2008 Hilti North American Product Technical Guide*, Tulsa, OK, 2008.
23. Adhesives Technology Corp., *HS2000 Technical Data Sheet*, Pompano Beach, FL, July 2009.
24. Adhesives Technology Corp., *Ultrabond 1 Technical Data Sheet*, Pompano Beach, FL, February 2009.
25. Adhesives Technology Corp., *Ultrabond 3 Technical Data Sheet*, Pompano Beach, FL, June 2008.
26. Simpson Strong-Tie Company, Inc., *ET Epoxy-Tie Anchoring Adhesive*, Obtained from web on February 19, 2010, <http://www.simpsonanchors.com/catalog/adhesives/et/>.
27. Power Fasteners Inc., *Power-Fast + Adhesive Injection Systems*, 2009, Obtained from web on February 19, 2010, http://www.powers.com/product_08402.html.

28. Power Fasteners Inc., *T308+ Adhesive Injection System Product Information*, 2009, Obtained from web on February 19, 2010, http://www.powers.com/pdfs/chemical/8503SD_8558SD.pdf.
29. USP Structural Connectors, *CIA-GEL 7000 Epoxy*, Obtained from web on February 19, 2010, http://www.uspconnectors.com/e_ciagel7000.shtml.
30. Yeomans, S.R., *Comparative Studies of Galvanized and Epoxy Coated Steel Reinforcement in Concrete*, Research Report No. R103, Australian Defense Force Academy, Canberra, Australia, February 1991.
31. Clifton, J.R., Mathey, R.G., *Bond of Coated Reinforcing Bars in Concrete*, American Society of Civil Engineers Journal of the Structural Division, January 1976.
32. Jirsa, J.O., Treece, R.A., *Bond Strength of Epoxy-Coated Reinforcing Bars*, American Concrete Institute Materials Journal, March-April 1989.
33. Cleary, D.B., Ramirez, J.A., *Bond Strength of Epoxy-Coated Reinforcement*, American Concrete Institute Materials Journal, March-April 1991.
34. Cusens, A.R., Yu, Z., *Pullout Tests of Epoxy-Coated Reinforcement in Concrete*, Cement and Concrete Composites, 1992.
35. ACI Committee 355, *Qualification of Post-Installed Adhesive Anchors in Concrete (ACI 355.4-11) and Commentary*, 2011, Farmington Hills, MI, American Concrete Institute, August 2011.
36. ACI Committee 318, *Proposed Changes to ACI 318-08 Open for Public Discussion, 318-11 Public Discussion Draft*, Farmington Hills, MI, 2010.
37. Bielenberg, R.W., Faller, R.K., Reid, J.D., Rohde, J.R., Sicking, D.L., *Design and Testing of Tie-Down Systems for Temporary Barriers*, Transportation Research Record No. 1851, Transportation Research Board, National Research Council, Washington D.C., 2003.
38. Bielenberg, B.W., Faller, R.K., Reid, J.D., Holloway, J.C., Rohde, J.R., Sicking, D.L., *Development of a Tie-Down System for Temporary Concrete Barriers*, Final Report to the Midwest State's Regional Pooled Fund, Transportation Research Report No. TRP-03-115-02, Midwest Roadside Safety Facility, University of Nebraska-Lincoln, August 2002.
39. Faller, R.K., Rohde, J.R., Rosson, B.T., Smith, R.P., Addink, K.H., *Development of a TL-3 F-Shape Temporary Concrete Median Barrier*, Final Report to the Iowa Department of Transportation, Project SPR-3(017), Transportation Research Report No. TRP-03-64-96, Midwest Roadside Safety Facility, University of Nebraska-Lincoln, December 1996.
40. Bielenberg, B.W., *Dynamic Component Testing of Potential Alternative Anchors for the F-Shape Concrete Barrier Strap Tie-Down*, Final Report (Letter Report) to the Midwest State's Regional Pooled Fund Program, Transportation Research Report No. TRP-03-182-07, Midwest Roadside Safety Facility, University of Nebraska-Lincoln, April 2007.

41. Polivka, K.A., Faller, R.K., Holloway, J.C., Rohde, J.R., Bielenberg, B.W., Sicking, D.L., *Development and Evaluation of a Tie-Down System for Redesigned F-Shape Concrete Temporary Barrier*, Final Report to the Midwest State's Regional Pooled Fund, Transportation Research Report No. TRP-03-134-03, Project No. SPR-3(o17)-Year 13, Project Code: RPPF-03-06, Midwest Roadside Safety Facility, University of Nebraska-Lincoln, August 2003.
42. Wisconsin Department of Transportation, *Concrete Barrier Temporary Precast*, Standard Detail Drawing 14b7, June 2010, Obtained from web on June 3, 2011, <http://roadwaystandards.dot.wi.gov/standards/fdm/SDD/14b07.pdf>.
43. Polivka, K.A., Bielenberg, R.W., Faller, R.K., Sicking, D.L., Rohde, J.R., Holloway, J.C., *Development of a Steel H-Section Temporary Barrier for Use in Limited Deflection Applications*, Final Report to the Midwest State's Regional Pooled Fund Program, Transportation Research Report No. TRP-03-120-03, Project No. SPR-3(017)-Year 11, Project Code: RPPF-01-01, Midwest Roadside Safety Facility, University of Nebraska-Lincoln, May 2003.
44. Dusel, J.P. Jr., Stoker, J.R., Nordlin, E.F., *Development of a Rebar Dowel Anchorage System for Attaching the California Type 25 Concrete Barrier to Existing Bridges*, Report No. FWHA-CA-TL-79-16, Office of Transportation Laboratory, California Department of Transportation, Sacramento, CA, June 1979.
45. Steves, M.A., Klingner, R.E., Armstrong, K.S., *Response of Highway Barriers to Repeated Impact Loading: Concrete Barriers*, Report No. FHWA/TX-86/69+382-2F, Center for Transportation Research, University of Texas-Austin, November 1985.
46. Holloway, J.C., Faller, R.K., Pfeifer, B.G., Post, E.R., *Performance Level 2 Tests on the Missouri 30-in. New Jersey Shape Bridge Rail*, Final Report to the Missouri Highway and Transportation Department, Transportation Research Report No. TRP-03-27-91, Civil Engineering Department, University of Nebraska-Lincoln, November 1991.
47. Till, R.D., *Analysis of the Bridge Barrier Railing, Type 4; Bridge Barrier Railing, Type 5; and Bridge Railing, Aesthetic Parapet Tube*, Report No. R-1397, Michigan Department of Transportation, July 2001.
48. Polivka, K.A., Faller, R.K., Sicking, D.L., Rohde, J.R., Bielenberg, B.W., Reid, J.D., Coon, B.A., *Performance Evaluation of the Permanent New Jersey Safety Shape Barrier – Update to NCHRP 350 Test No. 4-12 (2214NJ-2)*, Final Report to the National Cooperative Highway Research Program (NCHRP), Transportation Research Board, Transportation Research Report No. TRP-03-178-06, Midwest Roadside Safety Facility, University of Nebraska-Lincoln, October 2006.
49. Buth, C.E, Menges, W.L., Williams, W.F, *Repair/Retrofit Anchorage Designs for Bridge Rails*, Report No. TX-06/0-4823-T1-1, Texas Transportation Institute, Texas A&M University, College Station, TX, March 2007.

50. Gokani, V., Klingner, R.E., Mitchell, G., Picón, R., Tolnai, M., Williamson, E.B., Yang, S., *Design of Retrofit Vehicular Barriers Using Mechanical Anchors*, Report No. FHWA/TX-07/0-4823-CT-1, Center for Transportation Research, University of Texas-Austin, Austin, TX, October 2006.
51. Ross, H.E., Sicking, D.L., Zimmer, R.A., and Michie, J.D., *Recommended Procedures for the Safety Performance Evaluation of Highway Features*, National Cooperative Research Program (NCHRP) Report No. 350, Transportation Research Board, Washington, D.C., 1993.
52. *Standard Specifications for Highway Bridges*. Washington, D.C.: American Association of State Highway and Transportation Officials, 2002. Print.
53. Kennedy, G., Goodchild, C., *Practical Yield Line Design*, Published by the British Cement Association on behalf of the industry sponsors of the Reinforced Concrete Council, British Cement Association Publication No. 97.375, First Edition, Crowthorne, Berkshire, 2003.
54. *AASHTO LRFD Bridge Design Specifications*, American Association of State Highway and Transportation Officials, 4th Edition, Washington D.C., 2007.
55. Noel, J.S., Hirsch, T.J., Buth, C.E., Arnold, A., *Loads on Bridge Railings*, Transportation Research Record No. 796, Transportation Research Board, Washington D.C., 1981.
56. Florida Department of Transportation, *Traffic Railing – (32" F Shape)*, Index No. 420, July 2007, Obtained from web on April 2, 2010, <http://www.dot.state.fl.us/rddesign/rd/rtds/10/420.pdf>.
57. Florida Department of Transportation, *Traffic Railing – (42" F Shape)*, Index No. 425, July 2007, Obtained from web on April 2, 2010, <http://www.dot.state.fl.us/rddesign/rd/rtds/10/425.pdf>.
58. Florida Department of Transportation, *Traffic Railing – (Median 32" F Shape)*, Index No. 421, July 2007, Obtained from web on April 2, 2010, <http://www.dot.state.fl.us/rddesign/rd/rtds/10/421.pdf>.
59. Florida Department of Transportation, *Traffic Railing – (32" Vertical Shape)*, Index No. 423, January 2008, Obtained from web on April 2, 2010, <http://www.dot.state.fl.us/rddesign/rd/rtds/10/423.pdf>.
60. Florida Department of Transportation, *Traffic Railing – (42" Vertical Shape)*, Index No. 422, July 2007, Obtained from web on April 2, 2010, <http://www.dot.state.fl.us/rddesign/rd/rtds/10/422.pdf>.
61. Florida Department of Transportation, *Traffic Railing – (Corral Shape)*, Index No. 424, July 2008, Obtained from web on April 2, 2010, <http://www.dot.state.fl.us/rddesign/rd/rtds/10/424.pdf>.

62. Iowa Department of Transportation, *Barrier Rail –Skewed Stub Abut. With Wing Extensions*, Standard Sheet 1018 (L.A. Skew), March 2010, Obtained from web on April 2, 2010, <http://www.iowadot.gov/bridge/standards/english/EnglishDeckRailBridges.pdf>.
63. Iowa Department of Transportation, *3'-8 Barrier Rail – (R.A.) Skewed Stub Abut. With Wing Extensions*, Standard Sheet 1018C (R.A. Skew), March 2010, Obtained from web on April 2, 2010, <http://www.iowadot.gov/bridge/standards/english/EnglishDeckRailBridges.pdf>.
64. Illinois Department of Transportation, *Deck and Parapet Reinforcement for 34" F Shape Parapet*, Illinois Department of Transportation Bridge Manual, Figure 3.2.4-2, November 2009, Obtained from web on April 2, 2010, http://www.dot.state.il.us/bridges/pdf/Bridge%20Manual_2009.exe.
65. Kansas Department of Transportation, *F4 Barrier Curb (Bridges)*, br184a.dgn, September 2009, Obtained from web on April 2, 2010, http://kart.ksdot.org/StandardDrawings/_us_published_pdfs/br184a.pdf.
66. Kansas Department of Transportation, *32" Kansas Corral Rail R C Haunched Slab (Without Curb)*, br182a.dgn, March 2010, Obtained from web on April 2, 2010, http://kart.ksdot.org/StandardDrawings/_us_published_pdfs/br182a.pdf.
67. Missouri Department of Transportation, *ban01_elev_r.dgn*, February 2010, Obtained from web on April 2, 2010, http://www.modot.mo.gov/business/standard_drawings2/documents/ban01_elev_r_000.pdf.
68. Missouri Department of Transportation, *ban18_type_d_curb_elev.dgn*, February 2010, Obtained from web on April 2, 2010, http://www.modot.mo.gov/business/standard_drawings2/documents/ban18_type_d_curb_el ee_000.pdf.
69. Ohio Department of Transportation, *Bridge Railing Deflector Parapet Type 42"*, BR-1, July 2002, Obtained from web on April 2, 2010, <http://www.dot.state.oh.us/Divisions/HighwayOps/Structures/standard/Bridges/Standard%20DDrawing/br1.pdf>.
70. Wisconsin Department of Transportation, *Sloped Face Parapet 'LF'*, Standard 30.12, January 2010, Obtained from web on April 2, 2010, http://on.dot.wi.gov/dtid_bos/extranet/structures/docs/estandard/w3012.pdf.
71. Wisconsin Department of Transportation, *Sloped Face Parapet 'HF'*, Standard 30.13, January 2010, Obtained from web on April 2, 2010, http://on.dot.wi.gov/dtid_bos/extranet/structures/docs/estandard/w3013.pdf.
72. Wisconsin Department of Transportation, *Sloped Face Parapet "51F"*, Standard 30.20, July 2008, Obtained from web on April 2, 2010, http://on.dot.wi.gov/dtid_bos/extranet/structures/docs/estandard/w3020.pdf.

73. Wisconsin Department of Transportation, *Sloped Face Parapet "B"*, Standard 40.15, July 2008, Obtained from web on April 2, 2010, http://on.dot.wi.gov/dtid_bos/extranet/structures/docs/estandard/w4015.pdf.
74. Wisconsin Department of Transportation, *Vertical Face Parapet 'TX'*, Standard 30.19, July 2008, Obtained from web on April 2, 2010, http://on.dot.wi.gov/dtid_bos/extranet/structures/docs/estandard/w3019.pdf.
75. Wisconsin Department of Transportation, *Vertical Face Parapet 'A'*, Standard 30.07, January 2009, Obtained from web on April 2, 2010, http://on.dot.wi.gov/dtid_bos/extranet/structures/docs/estandard/w307.pdf.
76. Wisconsin Department of Transportation, *WisDOT Bridge Manual, Chapter 30 – Railings*, July 2009.
77. AASHTO LRFD Bridge Design Specifications, Customary U.S. Units (4th Edition) with 2008 U.S. Edition Interims, American Association of State Highway and Transportation Officials (AASHTO), 2008.
78. Reddy, J.N., *An Introduction to Continuum Mechanics: with Applications*, Cambridge University Press, Cambridge, UK, 2008.
79. Boyce, W.E., DiPrima, R.C., *Elementary Differential Equations and Boundary Value Problems*, John Wiley and Sons Inc., New York, NY, 2001.
80. ICC Evaluation Service, *ICC-ES Evaluation Report ESR-2322*, International Code Council, July 1, 2009.
81. Society of Automotive Engineers (SAE), *Instrumentation for Impact Test – Part 1 – Electronic Instrumentation*, SAE J211/1 MAR95, New York City, NY, July, 2007.
82. Bligh, R.P., Briaud, J.L., Kim, K.M., Abu-Odeh, A., *Design of Roadside Barrier Systems Placed on MSE Retaining Walls*, National Cooperative Highway Research Program (NCHRP) Report No. 663, Transportation Research Board, Washington D.C., 2010.
83. ASTM Committee E06, *ASTM E488 - Standard Test Methods for Strength of Anchors in Concrete Elements*, ASTM International, 100 Barr Harbor Drive, PO Box C700, West Conshohocken, PA 19428-2959, United States, February 2011.
84. ACI Committee 318, *Building Code Requirements for Structural Concrete (ACI 318-11) and Commentary*, Farmington Hills, MI, American Concrete Institute, August 2011.
85. Comité Euro-International du Béton, *CEB-FIP Model Code 1990*, Redwood Books, Trowbridge, Wiltshire, UK, 1993.
86. PROFIS Anchor Software version 2.0.7, Hilti Inc., Obtained from web on April 2, 2010.
87. American Institute of Steel Construction Inc., *Steel Construction Manual*, 2005.

88. Power Fasteners, *Wedge Bolt Screw Anchor Product Information*, Obtained from web on June 23, 2010, <http://www.powers.com/pdfs/mechanical/07246BT.pdf>.
89. Concrete Fasteners Inc., *Technical Specifications - Tapcon Concrete Screws*, Obtained from web on July 7, 2010, <http://www.concretefasteners.com/anchors-fasteners/tapcon-screw/technical-specifications.aspx>.

12 APPENDICIES

Appendix A. Comparison of Epoxy Manufacturers' Test Data

Table A-1. Epoxy Manufacturers' Test Data with Threaded Rod

Anchor Diameter (in)	Embedment Depth (in)	Product	Tensile Strength (k)	Shear Strength (k)	f _c (ksi)	Ave Tensile Strength (k)	Ave Shear Strength (k)	Max Tensile Strength (k)	Max Shear Strength (k)	Max Tensile Product	Max Shear Product
3/8	1.75	Hilti HIT-RE 500	4.37	6.405	4	4.12	5.25	4.744	7.072	USP Structural Connectors CIA-GEL 7000	Adhesives Technology HS200
	1.5	Power Fasteners Power Fast +	4.4	4.6	4						
	2	Power Fasteners T308+	4.06	N/A	4						
	1.875	USP Structural Connectors CIA-GEL 7000	4.744	2.905	2						
	1.6875	Adhesives Technology HS200	3.037	7.072	>2						
	3.375	Hilti HIT-RE 500	10.345	13.38	4	9.68	7.78	11.78	13.38	Power Fasteners Power Fast +	Hilti HIT-RE 500
	3.375	Power Fasteners Power Fast +	11.78	6	4						
	3.375	Power Fasteners T308+	9.58	N/A	4						
	3.375	Adhesives Technology HS200	8.214	7.072	>2						
	3.375	Adhesives Technology Ultrabond 1	9.248	7.189	2						
	3.375	Adhesives Technology Ultrabond 3	10.9	7.312	3						
	3.375	USP Structural Connectors CIA-GEL 7000	8.608	5.88	2						
	3.5	Simpson ET	8.777	7.615	2						
	4.5	Hilti HIT-RE 500	10.335	20.58	4	11.72	13.53	15.56	20.58	Power Fasteners Power Fast +	Hilti HIT-RE 500
5.25	Power Fasteners Power Fast +	15.56	6.48	4							
4.5	Adhesives Technology HS200	9.277	7.072	>2							
1/2	2.25	Hilti HIT-RE 500	7.86	10.64	4	7.80	8.14	10.82	12.23	Power Fasteners Power Fast +	Adhesives Technology HS200
	2	Power Fasteners Power Fast +	10.82	6.8	4						
	2.5	Power Fasteners T308+	6.89	N/A	4						
	2.5	USP Structural Connectors CIA-GEL 7000	7.757	2.905	2						
	2.25	Adhesives Technology HS200	5.696	12.23	>2						
	4.5	Hilti HIT-RE 500	21.095	23.8	4	17.35	13.64	22.328	23.8	Adhesives Technology Ultrabond 1	Hilti HIT-RE 500
	4.5	Power Fasteners Power Fast +	18.86	12.8	4						
	4	Power Fasteners T308+	15.42	N/A	4						
	4.5	Adhesives Technology HS200	18.374	12.23	>2						
	4.5	Adhesives Technology Ultrabond 1	22.328	12.863	2						
	4.5	Adhesives Technology Ultrabond 3	13.384	8.316	3						
	4.5	USP Structural Connectors CIA-GEL 7000	13.983	14.22	2						
	4.25	Simpson ET	15.368	11.273	2						
	6	Hilti HIT-RE 500	21.52	36.62	4	23.39	24.71	26.44	36.62	Power Fasteners Power Fast +	Hilti HIT-RE 500
	7	Power Fasteners Power Fast +	26.44	12.8	4						
6	Adhesives Technology HS200	22.224	12.23	>2							

Table A-1. Epoxy Manufacturers' Test Data with Threaded Rod (continued)

Anchor Diameter (in)	Embedment Depth (in)	Product	Tensile Strength (k)	Shear Strength (k)	f _c (ksi)	Ave Tensile Strength (k)	Ave Shear Strength (k)	Max Tensile Strength (k)	Max Shear Strength (k)	Max Tensile Product	Max Shear Product
5/8	2.875	Hilti HIT-RE 500	12.175	22.25	4	10.41	14.49	12.175	23.19	Hilti HIT-RE 500	Adhesives Technology HS200
	2.5	Power Fasteners Power Fast +	9.4	9.6	4						
	3.125	USP Structural Connectors CIA-GEL 7000	10.393	2.905	2						
	2.8125	Adhesives Technology HS200	9.68	23.19	>2						
	5.625	Hilti HIT-RE 500	29.42	37.18	4	25.30	23.00	29.95	37.18	Adhesives Technology Ultrabond 1	Hilti HIT-RE 500
	5.625	Power Fasteners Power Fast +	23.4	22.8	4						
	5.625	Power Fasteners T308+	26.81	N/A	4						
	5.625	Adhesives Technology HS200	26.581	23.19	>2						
	5.625	Adhesives Technology Ultrabond 1	29.95	22.855	2						
	5.625	Adhesives Technology Ultrabond 3	21.692	16.344	3						
	5.625	USP Structural Connectors CIA-GEL 7000	21.631	19.06	2						
	5	Simpson ET	22.877	19.559	2						
	7.5	Hilti HIT-RE 500	30.06	57.24	4	32.44	57.24	34.819	57.24	Adhesives Technology HS200	Hilti HIT-RE 500
	7.5	Adhesives Technology HS200	34.819	23.19	>2						
3/4	3.375	Hilti HIT-RE 500	18.065	31.108	4	15.24	20.81	18.065	31.853	Hilti HIT-RE 500	Adhesives Technology HS200
	3	Power Fasteners Power Fast +	14.84	14.4	4						
	3.75	USP Structural Connectors CIA-GEL 7000	15.663	5.88	2						
	3.375	Adhesives Technology HS200	12.388	31.853	>2						
	6.75	Hilti HIT-RE 500	43.02	53.52	4	35.15	31.85	43.02	53.52	Hilti HIT-RE 500	Hilti HIT-RE 500
	6.75	Power Fasteners Power Fast +	37.52	25.6	4						
	6.75	Power Fasteners T308+	30.79	N/A	4						
	6.75	Adhesives Technology HS200	38.414	31.853	>2						
	6.75	Adhesives Technology Ultrabond 1	39.278	32.304	2						
	6.75	Adhesives Technology Ultrabond 3	30	24.376	3						
	6.75	USP Structural Connectors CIA-GEL 7000	26.74	27.62	2						
6.75	Simpson ET	35.459	27.696	2							
7/8	4	Hilti HIT-RE 500	22.67	33.05	4	17.24	27.33	22.67	34.953	Hilti HIT-RE 500	Adhesives Technology HS200
	3.5	Power Fasteners Power Fast +	15.58	14	4						
	4	Power Fasteners T308+	14.6	N/A	4						
	3.9375	Adhesives Technology HS200	16.107	34.953	>2						
	7.875	Hilti HIT-RE 500	63.495	72.86	4	46.54	42.63	63.495	72.86	Hilti HIT-RE 500	Hilti HIT-RE 500
	7.875	Power Fasteners Power Fast +	42.16	36.8	4						
	7.875	Power Fasteners T308+	30.46	N/A	4						
	7.875	Adhesives Technology HS200	52.393	34.953	>2						
	7.875	Adhesives Technology Ultrabond 1	53.862	36.214	2						
	7.875	Adhesives Technology Ultrabond 3	39.94	32.344	3						
	7.75	Simpson ET	43.459	27.696	2						

Table A-1. Epoxy Manufacturers' Test Data with Threaded Rod (continued)

Anchor Diameter (in)	Embedment Depth (in)	Product	Tensile Strength (k)	Shear Strength (k)	f _c (ksi)	Ave Tensile Strength (k)	Ave Shear Strength (k)	Max Tensile Strength (k)	Max Shear Strength (k)	Max Tensile Product	Max Shear Product
1	4.5	Hilti HIT-RE 500	33.765	42.565	4	24.72	30.48	33.765	42.565	Hilti HIT-RE 500	Hilti HIT-RE 500
	4	Power Fasteners Power Fast +	18.78	18.4	4						
	4.5	Adhesives Technology HS200	21.606	N/A	>2						
1 1/4	5.625	Hilti HIT-RE 500	51.27	62.61	4	37.72	42.31	51.27	62.61	Hilti HIT-RE 500	Hilti HIT-RE 500
	5	Power Fasteners Power Fast +	30.76	22	4						
	5.625	Adhesives Technology HS200	31.142	N/A	>2						

Table A-2. Epoxy Manufacturers' Test Data with Deformed Reinforcing Bars

Reinforcing Bar Size	Embedment Depth (in)	Product	Tensile Strength (k)	Shear Strength (k)	f _c (ksi)	Ave Tensile Strength (k)	Ave Shear Strength (k)	Max Tensile Strength (k)	Max Shear Strength (k)	Max Tensile Product	Max Shear Product
#3	3.375	Hilti HIT-RE 500	10.345	13.38	4	13.49	10.84	16.63	13.38	Power Fasteners Power Fast +	Hilti HIT-RE 500
	3.375	Power Fasteners Power Fast +	16.63	8.3	4						
	4.5	Hilti HIT-RE 500	10.335	20.58	4	13.40	12.41	22.18	20.58	Power Fasteners Power Fast +	Hilti HIT-RE 500
	4	USP Structural Connectors CIA-GEL 7000	7.692	8.36	2						
	4.5	Power Fasteners Power Fast +	22.18	8.3	4						
#4	4.5	Hilti HIT-RE 500	21.095	23.8	4	19.54	15.12	23.20	23.80	Adhesives Technology Ultrabond 1	Hilti HIT-RE 500
	4.5	USP Structural Connectors CIA-GEL 7000	14.8	15.18	2						
	4.5	Power Fasteners Power Fast +	21.56	14.82	4						
	4.5	Adhesives Technology HS200	18.975	12.121	>2						
	4.5	Adhesives Technology Ultrabond 1	23.203	11.242	>2						
	4.25	Simpson ET	17.596	13.56	>2						
	6	Hilti HIT-RE 500	21.52	36.62	4	25.13	25.72	28.75	36.62	Power Fasteners Power Fast +	Hilti HIT-RE 500
6	Power Fasteners Power Fast +	28.745	14.82	4							
#5	5.625	Hilti HIT-RE 500	29.42	37.18	4	28.04	24.92	32.33	37.18	Adhesives Technology Ultrabond 1	Hilti HIT-RE 500
	5.625	USP Structural Connectors CIA-GEL 7000	19.48	23.54	2						
	5.625	Power Fasteners Power Fast +	30.04	26.24	4						
	5.625	Adhesives Technology HS200	31.555	20.597	>2						
	5.625	Adhesives Technology Ultrabond 1	32.326	21.032	>2						
	5	Simpson ET	25.427	20.914	>2						
	7.5	Hilti HIT-RE 500	30.06	57.24	4	35.06	41.74	40.05	57.24	Power Fasteners Power Fast +	Hilti HIT-RE 500
7.5	Power Fasteners Power Fast +	40.05	26.24	4							
#6	6.75	Hilti HIT-RE 500	43.02	53.52	4	39.47	34.59	44.481	53.52	Adhesives Technology Ultrabond 1	Hilti HIT-RE 500
	6.75	USP Structural Connectors CIA-GEL 7000	29.08	33.4	2						
	6.75	Power Fasteners Power Fast +	39.295	28.06	4						
	6.75	Adhesives Technology HS200	39.109	30.114	>2						
	6.75	Adhesives Technology Ultrabond 1	44.481	32.294	>2						
6.75	Simpson ET	41.812	30.148	>2							
#7	7.875	Hilti HIT-RE 500	63.495	72.86	4	49.26	46.20	63.50	72.86	Hilti HIT-RE 500	Hilti HIT-RE 500
	7.875	USP Structural Connectors CIA-GEL 7000	34.88	45.56	2						
	7.875	Power Fasteners Power Fast +	49.745	49.22	4						
	7.875	Adhesives Technology HS200	47.523	34.302	>2						
	7.875	Adhesives Technology Ultrabond 1	49.647	35.438	>2						
	7.75	Simpson ET	50.241	39.838	>2						

Appendix B. Conventional Anchorage Design Calculations

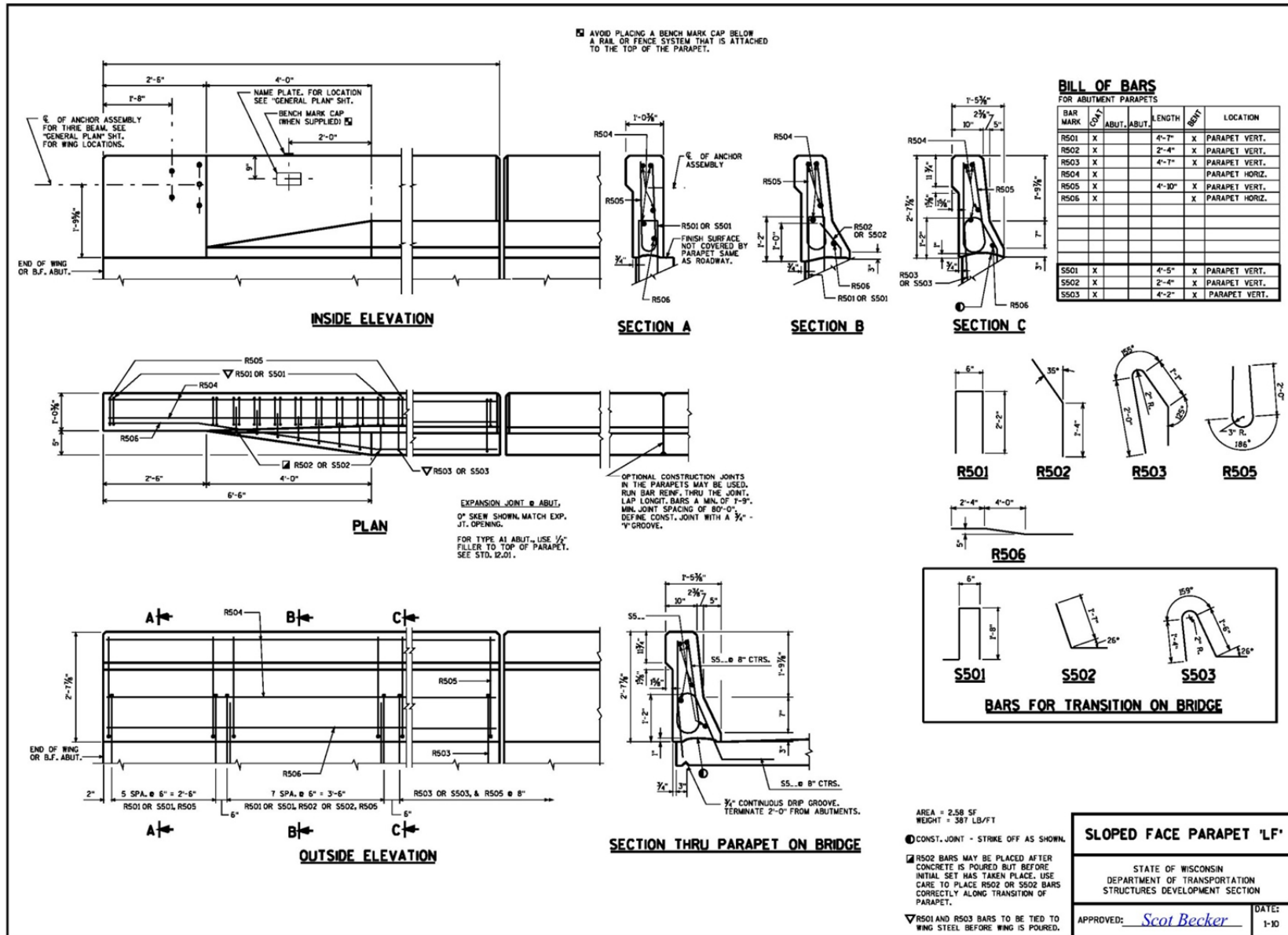
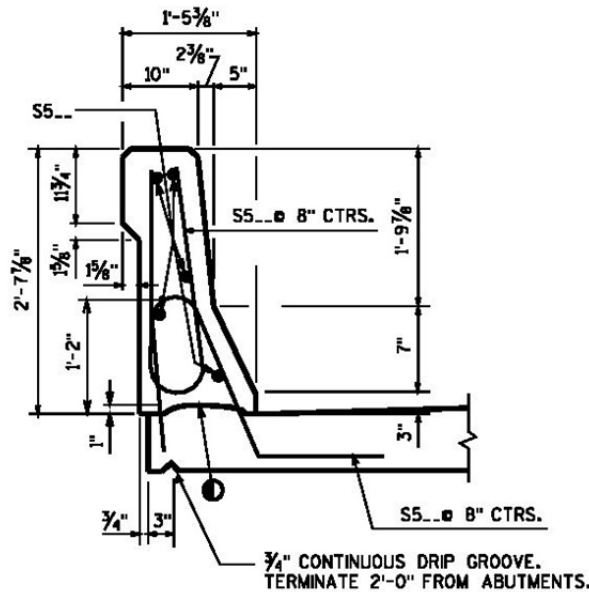


Figure B-1. Wisconsin Sloped Face Parapet 'LF' Detailed Drawing [70]

Conventional Design Calculations for the Sloped Face Parapet ‘LF’

The highest strength attachment to the bridge deck utilizes 2-#5 bars spaced at 8 in. O.C.



WI Standard
30.12 [70]

SECTION THRU PARAPET ON BRIDGE

Determine Moment Strength of Hooked Bar for 2 in. Clear Cover

- Assume the right leg acts as a standard 90 degree hook
- Assume an 8 in. thick bridge deck
- Assume concrete compressive strength to be 4000 psi

$$l_{emb} = (8 \text{ in.}) - (2 \text{ in.}) - 0.5 \left(\frac{5}{8} \text{ in.} \right) = 5.6875 \text{ in.}$$

$$l_{dh} = (8 \text{ in.}) - (2 \text{ in.}) = 6 \text{ in}$$

$$l_{dh} = \frac{0.02\psi_e f_y}{\lambda \sqrt{f'_c}} d_b$$

ACI 318-08
12.5.2

$\psi_e = 1.2$ for epoxy-coated reinforcement

$\lambda = 1.0$ for normalweight concrete

$$6 \text{ in.} = \frac{0.02(1.2)f_s}{1.0\sqrt{4000 \text{ psi}}} (0.625 \text{ in.})$$

$$f_s = 25,298 \text{ psi}$$

$$F = f_s A_s = (25,298 \text{ psi})(0.31 \text{ in.}^2) = 7,842 \text{ lb} = 7.842 \text{ k}$$

The right leg is angled 64° from the concrete slab surface

$$F_{y\text{-component}} = (7.842 \text{ k}) \sin 64^\circ = 7.048 \text{ k}$$

Normalize to a force per foot of barrier by dividing by the anchor spacing

$$F_{per \text{ foot}} = \frac{7.048 \text{ k}}{\left(\frac{8}{12} \text{ ft} \right)} = 10.57 \text{ k/ft}$$

-The distance from the hooked bar to the edge of the concrete slab is approximately 1 ft. The moment strength is calculated by the tensile force times the moment arm. Conservatively assume the moment arm as the distance from the hooked bar to the

edge of the concrete.

$$M_{per\ foot} = \left(10.57 \frac{k}{ft}\right) (1.0\ ft) = 10.57 \frac{k \cdot ft}{ft}$$

Determine Moment Strength of Hooked Bar for 2.5 in. Clear Cover

$$l_{dh} = (8\ in.) - (2.5\ in.) = 5.5\ in.$$

$$l_{dh} = \frac{0.02\psi_e f_y}{\lambda\sqrt{f_c'}} d_b (0.7) \quad \text{ACI 318-08} \quad 12.5.2, 12.5.3(a)$$

$$5.5\ in. = \frac{0.02(1.2)f_s}{1.0\sqrt{4000\ psi}} (0.625\ in.) (0.7)$$

$$f_s = 33,129\ psi$$

$$F = f_s A_s = (33,129\ psi)(0.31\ in.^2) = 10,270\ lb = 10.270\ k$$

$$F_{y\text{-component}} = (10.270\ k) \sin 64^\circ = 9.231\ k$$

Normalize to a force per foot of barrier by dividing by the anchor spacing

$$F_{per\ foot} = \frac{9.231\ k}{\left(\frac{8}{12}\ ft\right)} = 13.85\ k/ft$$

$$M_{per\ foot} = \left(13.85 \frac{k}{ft}\right) (1.0\ ft) = 13.85 \frac{k \cdot ft}{ft}$$

Determine Shear Strength of Right Leg Based on Shear Friction

$$V_n = A_{vf} f_y (\mu \sin \alpha + \cos \alpha) \quad \text{ACI 318-08} \quad (11-26)$$

$$\alpha = 64^\circ$$

-The hooked end of the bar does not have enough length to develop the yield stress of the bar, therefore f_s will be used in lieu of f_y

-Assume the edge effects are negligible for the right leg

$$\mu = 0.6\lambda \quad \text{ACI 318-08} \quad 11.6.4.3$$

$$V_n = (0.31\ in.^2)(33,129\ psi)((0.6)(1.0) \sin 64^\circ + \cos 64^\circ) = 10,040\ lb = 10.04\ k$$

Determine Shear Strength of Left Leg Based on ACI Appendix D and ICC-ES AC308

Steel Strength of Anchor in Shear

$$V_{sa} = n0.6A_{se}v f_{uta} \quad \text{ACI 318-08} \quad (D-20)$$

$$f_{uta} = 90,000\ psi\ \text{for grade 60 steel}$$

$$1.9f_{yta} = 1.9(60,000\ psi) = 114,000\ psi$$

$$f_{uta} \leq 114,000\ psi \leq 125,000\ psi$$

$$V_{sa} = 1(0.6)(0.31\ in.^2)(90,000\ psi) = 16,740\ lb = 16.74\ k$$

Concrete Breakout of Anchor in Shear

-Assume the anchor is located 2 in. clear from the slab edge

-Assume the concrete is uncracked, this will be conservative in determining the equivalent strength of the barrier

$$c_{a1} = (2\ in.) + 0.5\left(\frac{5}{8}\ in.\right) = 2.3125\ in.$$

$$1.5c_{a1} = 1.5(2.3125 \text{ in.}) = 3.4688 \text{ in.}$$

$$A_{Vc} = 2(1.5c_{a1})(1.5c_{a1}) = 2(3.4688 \text{ in.})(3.4688 \text{ in.}) = 24.07 \text{ in.}^2$$

ACI 318-08
Fig RD.6.2.1

$A_{Vc0} = A_{Vc}$ for a single anchor with $h_a \geq 1.5c_{a1}$ and no corner effects

$$\psi_{ed,V} = 1.0$$

ACI 318-08
(D-27)

$$\psi_{c,V} = 1.4$$

ACI 318-08
D.6.2.7

$\psi_{h,V}$ is not applicable for $h_a > 1.5c_{a1}$

$$V_b = \left(7 \left(\frac{l_e}{d_a} \right)^{0.2} \sqrt{d_a} \right) \lambda \sqrt{f'_c} (c_{a1})^{1.5}$$

ACI 318-08
(D-24)

$$l_e = h_{ef} = 6 \text{ in.}$$

$$d_a = 0.625 \text{ in.}$$

$$V_b = \left(7 \left(\frac{6 \text{ in.}}{0.625 \text{ in.}} \right)^{0.2} \sqrt{0.625 \text{ in.}} \right) (1.0) \sqrt{4000 \text{ psi}} (2.3125 \text{ in.})^{1.5}$$

$$= 1935 \text{ lb}$$

$$V_{cb} = \frac{A_{Vc}}{A_{Vc0}} \psi_{ed,V} \psi_{c,V} \psi_{h,V} V_b$$

ACI 318-08
(D-21)

$$V_{cb} = \frac{24.07 \text{ in.}^2}{24.07 \text{ in.}^2} (1.0)(1.4)(1.0)(1,935 \text{ lb}) = 2,709 \text{ lb} = 2.71 \text{ k}$$

Concrete Pryout Strength of Anchor in Shear

-This bar will behave more like an adhesive anchor than a headed or mechanical anchor due to the fact that a full concrete cone will most likely not form because the concentration of stress transfer will not be at the bottom of the anchor. Therefore, the concrete pryout strength for this anchor will be analyzed from the provisions of adhesive anchors (ICC-ES AC308).

$$V_{cp} = \min |k_{cp} N_a; k_{cp} N_{cb}|$$

ICC-ES AC308
(D-30a)

$$k_{cp} = 2.0 \text{ for } h_{ef} > 2.5 \text{ in.}$$

ICC-ES AC308
D.6.3.2

$$N_a = \frac{A_{Na}}{A_{Na0}} \psi_{ed,Na} \psi_{p,Na} N_{a0}$$

ICC-ES AC308
(D-16a)

$$N_{a0} = \tau_k \pi d h_{ef}$$

ICC-ES AC308
(D-16f)

-This is equal to the pullout strength of the bar and will be designed based on the development strength of a straight bar.

$$l_d = (8 \text{ in.}) - (2 \text{ in.})$$

$$l_d = \left(\frac{3}{40} \frac{f_y}{\lambda \sqrt{f'_c}} \frac{\psi_t \psi_e \psi_s}{\left(\frac{c_b + K_{tr}}{d_b} \right)} \right) d_b$$

ACI 318-08
(12-1)

$$K_{tr} = 0$$

ACI 318-08
12.2.3

$$\psi_t = 1.0$$

ACI 318-08
12.2.4(a)

$$3d_b = 3(0.625 \text{ in.}) = 1.875 \text{ in.}$$

$$\text{cover} = 2.0 \text{ in.}$$

$$\psi_e = 1.2$$

ACI 318-08

$$\psi_t \psi_e = 1.2 < 1.7$$

12.2.4(b)

$$\psi_s = 0.8$$

ACI 318-08

12.2.4(c)

$$c_b = (2 \text{ in.}) + 0.5(0.625 \text{ in.}) = 2.3125 \text{ in.}$$

$$\lambda = 1.0 \text{ for normal weight concrete}$$

$$6 \text{ in.} = \left(\frac{3}{40} \frac{f_s}{1.0 \sqrt{4000 \text{ psi}}} \frac{(1.0)(1.2)(0.8)}{\left(\frac{2.3125 \text{ in.} + 0 \text{ in.}}{0.625 \text{ in.}} \right)} \right) 0.625 \text{ in.}$$

$$f_s = 31,201 \text{ psi}$$

$$N_{a0} = f_s A_s = (31,201 \text{ psi})(0.31 \text{ in.}^2) = 9,672 \text{ lb}$$

$$c_{cr,Na} = \frac{s_{cr,Na}}{2}$$

ICC-ES AC308

(D-16e)

$$s_{cr,Na} = 20d \sqrt{\frac{\tau_k}{1450}} \leq 3h_{ef}$$

ICC-ES AC308

(D-16d)

-Estimate the bond strength based on the pullout capacity

$$\tau_k = \frac{N_{a0}}{A_{bond}} = \frac{N_{a0}}{\pi d h_{ef}} = \frac{9,672 \text{ lb}}{\pi (0.625 \text{ in.})(6 \text{ in.})}$$

$$= 821.0 \text{ psi}$$

$$s_{cr,Na} = 20(0.625 \text{ in.}) \sqrt{\frac{821.0 \text{ psi}}{1450}} = 9.41 \text{ in.}$$

$$\leq 3(6 \text{ in.}) = 18 \text{ in.}$$

$$c_{cr,Na} = \frac{9.41 \text{ in.}}{2} = 4.71 \text{ in.}$$

$$A_{Na} = (4.71 \text{ in.} + 2.3125 \text{ in.})(2(4.71 \text{ in.})) = 66.15 \text{ in.}^2$$

$$A_{Na0} = s_{cr,Na}^2 = (9.41 \text{ in.})^2 = 88.55 \text{ in.}^2$$

ICC-ES AC308

(D-16c)

$$c_{a,min} > 1.5h_{ef}$$

$$\psi_{ed,Na} = 0.7 + 0.3 \frac{c_{a,min}}{c_{cr,Na}} \leq 1.0$$

ICC-ES AC308

(D-16m)

$$\psi_{ed,Na} = 0.7 + 0.3 \frac{2.3125 \text{ in.}}{4.71 \text{ in.}} = 0.85$$

$$\frac{h}{h_{ef}} = \frac{8 \text{ in.}}{6 \text{ in.}} = 1.33$$

$$c_{ac} = 2.5h_{ef} = 2.5(6 \text{ in.}) = 15 \text{ in.}$$

ICC-ES ESR 2322

4.1.10

$$c_{a,min} < c_{ac}$$

$$\psi_{p,Na} = \frac{\max\{c_{a,min}; c_{cr,Na}\}}{c_{ac}}$$

ICC-ES AC308

(D-16p)

$$\psi_{p,Na} = \frac{4.71 \text{ in}}{15 \text{ in}} = 0.31$$

$$N_a = \frac{66.15 \text{ in.}^2}{88.55 \text{ in.}^2} (0.85)(0.31)(9,672 \text{ lb}) = 1,904 \text{ lb} = 1.90 \text{ k}$$

$$N_{cb} = \frac{A_{Nc}}{A_{Nc0}} \psi_{ed,N} \psi_{c,N} \psi_{cp,N} N_b \quad \text{ACI 318-08 (D-4)}$$

$$N_b = k_c \lambda \sqrt{f'_c} h_{ef}^{1.5} \quad \text{ACI 318-08 (D-7)}$$

-Let $k_c = 17$ as this anchor will behave more like a post-installed anchor than a cast-in-place anchor

$$N_b = 17(1.0)\sqrt{4000 \text{ psi}}(6 \text{ in.})^{1.5} = 15,802 \text{ lb}$$

$$c_{a,min} < 1.5h_{ef}$$

$$\psi_{ed,N} = 0.7 + 0.3 \frac{c_{a,min}}{1.5h_{ef}} \quad \text{ACI 318-08 (D-11)}$$

$$\psi_{ed,N} = 0.7 + 0.3 \frac{2.3125 \text{ in.}}{1.5(6 \text{ in.})} = 0.78$$

$$\psi_{c,N} = 1.4 \quad \text{ACI 318-08 D.5.2.6}$$

$$\psi_{cp,N} = \frac{c_{a,min}}{c_{ac}} = \frac{2.3125 \text{ in.}}{15 \text{ in.}} = 0.15 \quad \text{ACI 318-08 (D-13)}$$

$$A_{Nc} = (2.3125 \text{ in.} + 1.5(6 \text{ in.})) \times (2(1.5)(6 \text{ in.})) = 203.63 \text{ in.}^2 \quad \text{ACI 318-08 Fig RD.5.2.1}$$

$$A_{Nc0} = 9h_{ef}^2 = 9(6 \text{ in.})^2 = 324 \text{ in.}^2 \quad \text{ACI 318-08 (D-6)}$$

$$N_{cb} = \frac{203.63 \text{ in.}^2}{324 \text{ in.}^2} (0.78)(1.4)(0.15)(15,802 \text{ lb}) = 1,627 \text{ lb} = 1.63 \text{ k}$$

$$V_{cp} = 2(1.63 \text{ k}) = 3.26 \text{ k}$$

Total Shear Strength of Barrier

$$V_n = V_{n,right \text{ leg}} + V_{n,left \text{ leg}} = 10.04 \text{ k} + 2.71 \text{ k} = 12.75 \text{ k}$$

Normalize to a force per foot of barrier by dividing by the anchor spacing

$$V_n = \frac{12.75 \text{ k}}{\left(\frac{8}{12} \text{ ft}\right)} = 19.13 \text{ k/ft}$$

Load Summary

$$M_n = 13.85 \frac{\text{k} \cdot \text{ft}}{\text{ft}}$$

$$V_n = 19.13 \frac{\text{k}}{\text{ft}}$$

Notation

A_{bond}	= Area of bond
A_{Na}	= The projected area of the failure surface for the anchor or group of anchors
A_{Na0}	= The projected area of the failure surface of a single anchor without the influence of proximate edges
A_s	= Area of steel
$A_{se,V}$	= Effective cross-sectional area of the anchor in shear
A_{Vc}	= Projected concrete area of a single anchor or group of anchors
A_{Vc0}	= Projected concrete failure area of a single anchor
A_{vf}	= Area of shear-friction reinforcement
c_{a1}	= Distance from the center of an anchor shaft to the edge of concrete
c_{ac}	= Critical edge distance require to develop the basic concrete breakout strength
c_b	= The smaller of the distance from the center of a bar to nearest concrete and one-half the center-to-center spacing of bars being developed
$c_{cr,Na}$	= Critical adhesive anchor edge distance for tension loading
d	= Nominal diameter of the anchor element
d_a	= Outside diameter of anchor
d_b	= Nominal diameter of bar
h	= Thickness of member in which an anchor is installed
h_a	= Thickness of member in which an anchor is located
h_{ef}	= Effective embedment depth, measured from the concrete surface to the deepest point on the anchor element at which a bond to the concrete is established
f'_c	= Specified compressive strength of concrete
f_s	= Stress in steel
f_y	= Specified yield strength of the reinforcement
k_c	= Coefficient for basic concrete breakout strength in tension
k_{cp}	= Coefficient for pryout strength
K_{tr}	= Transverse reinforcement index
l_d	= Development length in tension of a deformed bar
l_{dh}	= Development length in tension of a deformed bar with a standard hook
l_e	= Load bearing length of anchor for shear
l_{emb}	= Embedment length of the anchor
n	= Number of anchors
N_a	= Nominal strength of an adhesive anchor in tension as limited by bond/concrete failure
N_{a0}	= Characteristic tension capacity of a single adhesive anchor between the adhesive and the concrete
N_{cb}	= Nominal concrete strength of a single anchor in tension as limited by concrete cone breakout
$s_{cr,Na}$	= Critical adhesive anchor spacing for tension loading
V_b	= Basic concrete breakout strength in shear of a single anchor in cracked concrete
V_{cp}	= Nominal concrete pryout strength of a single anchor
V_n	= Nominal shear strength
α	= Angle defining the orientation of reinforcement
λ	= Modification factor reflecting the reduced mechanical properties of lightweight concrete relative to normalweight concrete of the same compressive strength
μ	= Coefficient of friction

- τ_k = Characteristic bond strength
- $\psi_{c,V}$ = Factor used to modify shear strength of anchors based on presence or absence of cracks in concrete and presence or absence of supplementary reinforcement
- $\psi_{h,V}$ = Factor used to modify shear strength of anchors located in concrete members with $h_a < 1.5c_{a1}$
- $\psi_{ed,Na}$ = Factor used to modify the tensile strength of a single or group of anchors based on edge effects
- $\psi_{ed,V}$ = Factor used to modify shear strength of anchors based on proximity to edges of a concrete member
- $\psi_{p,Na}$ = Factor used to modify the tensile strength of a single or group of anchors based on the critical edge distance
- ψ_s = Factor used to modify development length based on reinforcement size
- ψ_t = Factor used to modify development length based on reinforcement location

Appendix C. Conversion of Cook's Equations from Metric to English Units

Conversion of Cook's Equations from Metric to English Units

In metric units Equation (3) is shown below where h_{cone} is in mm, d_0 is in mm, τ_0 is in MPa, and f'_c is in MPa.

$$h_{cone} = \frac{\tau_0 \pi d_0}{1.84 \sqrt{f'_c}}$$

$$mm = \frac{(MPa) \pi (mm)}{1.84 \sqrt{MPa}}$$

SI units for the coefficient of 1.84 are:

$$1.84 \sqrt{MPa}$$

Conversion to English units of psi:

$$(1.84 \sqrt{MPa}) \left(\frac{\sqrt{145.0377 \text{ psi}}}{\sqrt{MPa}} \right) = 22.16 \sqrt{\text{psi}}$$

Therefore, the equation in English units is:

$$h_{cone} = \frac{\tau_0 \pi d_0}{22.16 \sqrt{f'_c}}$$

In metric units Equation (4) is shown below where N_τ is in N, h_{ef} is in mm, f'_c is in MPa.

$$N_\tau = 0.92 h_{ef}^2 \sqrt{f'_c}$$

SI units for the coefficient of 0.92 are:

$$0.92 \frac{N}{mm^2 \sqrt{MPa}}$$

Conversion to English units of lbf, in., and psi:

$$\left(0.92 \frac{N}{mm^2 \sqrt{MPa}} \right) \left(\frac{\sqrt{MPa}}{\sqrt{145.0377 \text{ psi}}} \right) \left(\frac{\text{lbf}}{4.448222 \text{ N}} \right) \left(\frac{25.4^2 \text{ mm}^2}{\text{in}^2} \right)$$

$$= 11.08 \frac{\text{lbf}}{\text{in}^2 \sqrt{\text{psi}}}$$

Therefore, the equation in English units is:

$$N_\tau = 11.08 h_{ef}^2 \sqrt{f'_c}$$

In metric the expression $40 \sqrt{d_0}$ in Equation (5) has d_0 in units of mm.

$$40 \sqrt{d_0}$$

SI units for the coefficient of 0.92 are:

$$40 \sqrt{mm}$$

Conversion to English units of in.:

$$(40 \sqrt{mm}) \left(\frac{\sqrt{\text{in.}}}{\sqrt{25.4 \text{ mm}}} \right) = 7.94 \sqrt{\text{in.}}$$

Therefore, the equation in English units is:

$$7.94 \sqrt{d_0}$$

Appendix D. Static Model Comparison to Hilti HIT-RE 500 Test Data

Table D-1. Model Comparison Using the Bond Stress Specified in the Hilti Documentation

Hilti					Full Uniform Bond Model	Concrete Cone Model	Cone or Full Uniform Bond Model			Cone or Cone Plus Partial Uniform Bond Model with Calculated Cone Height						
d	d ₀	h _{ef}	τ ₀	Actual Test Capacity	Capacity	Test-to-Predicted Ratio	Capacity	Test-to-Predicted Ratio	h _{cone}	Capacity	Test-to-Predicted Ratio	h _{cone}	Capacity	Test-to-Predicted Ratio		
(in)	(in)	(in)	(psi)	(k)	(k)		(k)		(in)	(k)		(in)	(k)			
0.375	0.4375	1.75	1800	2.58	4.33	0.60	2.15	1.20	1.77	2.15	1.20	1.77	2.15	1.20		
0.375	0.4375	3.375	1800	8.76	8.35	1.05	7.98	1.10	1.77	8.35	1.05	1.77	5.50	1.59		
0.375	0.4375	4.5	1800	9.685	11.13	0.87	14.19	0.68	1.77	11.13	0.87	1.77	7.81	1.24		
0.5	0.5625	2.25	1800	4.53	7.16	0.63	3.55	1.28	2.27	3.55	1.28	2.27	3.55	1.28		
0.5	0.5625	4.5	1800	16.185	14.31	1.13	14.19	1.14	2.27	14.31	1.13	2.27	9.35	1.73		
0.5	0.5625	6	1800	19.095	19.09	1.00	25.23	0.76	2.27	19.09	1.00	2.27	13.21	1.45		
0.625	0.75	2.875	1800	6.77	12.19	0.56	5.79	1.17	3.03	5.79	1.17	3.03	5.79	1.17		
0.625	0.75	5.625	1800	26.24	23.86	1.10	22.17	1.18	3.03	23.86	1.10	3.03	15.01	1.75		
0.625	0.75	7.5	1800	29.29	31.81	0.92	39.42	0.74	3.03	31.81	0.92	3.03	21.20	1.38		
0.75	0.875	3.375	1800	9.25	16.70	0.55	7.98	1.16	3.54	7.98	1.16	3.54	7.98	1.16		
0.75	0.875	6.75	1800	34.685	33.40	1.04	31.93	1.09	3.54	33.40	1.04	3.54	20.87	1.66		
0.75	0.875	9	1800	41.535	44.53	0.93	56.76	0.73	3.54	44.53	0.93	3.54	29.35	1.42		
0.875	1	4	1800	12.03	22.62	0.53	11.21	1.07	4.04	11.21	1.07	4.04	11.21	1.07		
0.875	1	7.875	1800	49.975	44.53	1.12	43.46	1.15	4.04	44.53	1.12	4.04	27.59	1.81		
0.875	1	10.5	1800	58.82	59.38	0.99	77.26	0.76	4.04	59.38	0.99	4.04	38.65	1.52		
1	1.125	4.5	1800	15.79	28.63	0.55	14.19	1.11	4.55	14.19	1.11	4.55	14.19	1.11		
1	1.125	9	1800	55.38	57.26	0.97	56.76	0.98	4.55	57.26	0.97	4.55	35.15	1.58		
1	1.125	12	1800	71.74	76.34	0.94	100.91	0.71	4.55	76.34	0.94	4.55	49.07	1.46		
1.25	1.375	5.625	1800	23.045	43.74	0.53	22.17	1.04	5.56	43.74	0.53	5.56	22.01	1.05		
1.25	1.375	11.25	1800	98.43	87.47	1.13	88.69	1.11	5.56	87.47	1.13	5.56	52.66	1.87		
1.25	1.375	15	1800	136.525	116.63	1.17	157.67	0.87	5.56	116.63	1.17	5.56	73.10	1.87		
					Mean=	0.87	Mean=	1.00	Mean=			1.04	Mean=			1.45
					St Dev=	0.24	St Dev=	0.19	St Dev=			0.16	St Dev=			0.27
					COV=	0.27	COV=	0.19	COV=			0.15	COV=			0.19

Table D-1. Model Comparison Using the Bond Stress Specified in the Hilti Documentation (continued)

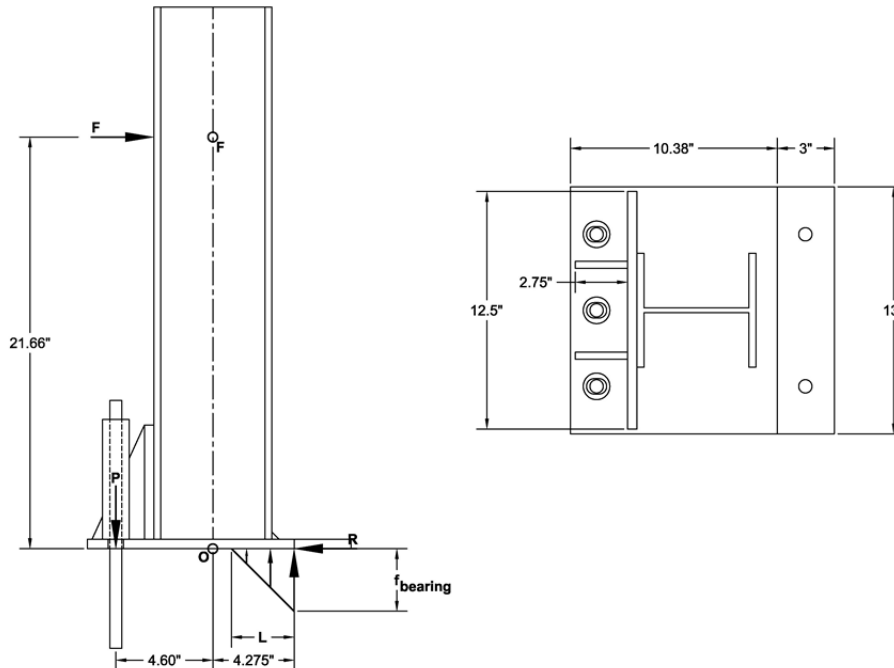
Hilti					Cone or Cone Plus Partial Uniform Bond Model with Assumed Cone Height			Modified Cone or Cone Plus Partial Uniform Bond Model with Assumed Cone Height			Cone or Partial Uniform Bond with Calculated Cone Height			Cone or Partial Uniform Bond with Assumed Cone Height			
d	d ₀	h _{ef}	τ ₀	Actual Test Capacity	h _{cone}	Capacity	Test-to-Predicted Ratio	h _{cone}	Capacity	Test-to-Predicted Ratio	h _{cone}	Capacity	Test-to-Predicted Ratio	h _{cone}	Capacity	Test-to-Predicted Ratio	
(in)	(in)	(in)	(psi)	(k)	(in)	(k)		(in)	(k)		(in)	(k)		(in)	(k)		
0.375	0.4375	1.75	1800	2.58	2.00	2.15	1.20	2.00	2.15	1.20	1.77	2.15	1.20	2.00	2.15	1.20	
0.375	0.4375	3.375	1800	8.76	2.00	5.47	1.60	2.00	6.20	1.41	1.77	3.98	2.20	2.00	3.40	2.58	
0.375	0.4375	4.5	1800	9.685	2.00	7.65	1.27	2.00	8.99	1.08	1.77	6.76	1.43	2.00	6.19	1.57	
0.5	0.5625	2.25	1800	4.53	2.00	3.48	1.30	2.00	3.60	1.26	2.27	3.55	1.28	2.00	0.80	5.70	
0.5	0.5625	4.5	1800	16.185	2.00	9.58	1.69	2.00	10.76	1.50	2.27	7.08	2.28	2.00	7.95	2.04	
0.5	0.5625	6	1800	19.095	2.00	13.64	1.40	2.00	15.53	1.23	2.27	11.86	1.61	2.00	12.72	1.50	
0.625	0.75	2.875	1800	6.77	2.00	6.16	1.10	2.00	6.51	1.04	3.03	5.79	1.17	2.00	3.71	1.82	
0.625	0.75	5.625	1800	26.24	2.00	16.70	1.57	2.00	18.18	1.44	3.03	11.00	2.38	2.00	15.37	1.71	
0.625	0.75	7.5	1800	29.29	2.00	23.88	1.23	2.00	26.13	1.12	3.03	18.96	1.55	2.00	23.33	1.26	
0.75	0.875	3.375	1800	9.25	2.00	9.09	1.02	2.00	9.61	0.96	3.54	7.98	1.16	2.00	6.80	1.36	
0.75	0.875	6.75	1800	34.685	2.00	24.51	1.42	2.00	26.31	1.32	3.54	15.91	2.18	2.00	23.50	1.48	
0.75	0.875	9	1800	41.535	2.00	34.79	1.19	2.00	37.44	1.11	3.54	27.04	1.54	2.00	34.64	1.20	
0.875	1	4	1800	12.03	2.00	13.41	0.90	2.00	14.11	0.85	4.04	11.21	1.07	2.00	11.31	1.06	
0.875	1	7.875	1800	49.975	2.00	33.95	1.47	2.00	36.03	1.39	4.04	21.68	2.30	2.00	33.22	1.50	
0.875	1	10.5	1800	58.82	2.00	47.86	1.23	2.00	50.87	1.16	4.04	36.53	1.61	2.00	48.07	1.22	
1	1.125	4.5	1800	15.79	2.00	17.87	0.88	2.00	18.71	0.84	4.55	14.19	1.11	2.00	15.90	0.99	
1	1.125	9	1800	55.38	2.00	45.00	1.23	2.00	47.34	1.17	4.55	28.34	1.95	2.00	44.53	1.24	
1	1.125	12	1800	71.74	2.00	63.09	1.14	2.00	66.42	1.08	4.55	47.42	1.51	2.00	63.62	1.13	
1.25	1.375	5.625	1800	23.045	2.00	29.90	0.77	2.00	30.99	0.74	5.56	0.54	42.57	2.00	28.19	0.82	
1.25	1.375	11.25	1800	98.43	2.00	71.94	1.37	2.00	74.73	1.32	5.56	44.28	2.22	2.00	71.92	1.37	
1.25	1.375	15	1800	136.525	2.00	99.97	1.37	2.00	103.88	1.31	5.56	73.44	1.86	2.00	101.08	1.35	
						Mean=	1.25				Mean=	1.17				Mean=	3.63
						St Dev=	0.24				St Dev=	0.21				St Dev=	8.93
						COV=	0.19				COV=	0.18				COV=	2.46

Table D-2. Model Comparison Using the Bond Stress Specified in ICC-ES ESR-2322

ESR-2322					Full Uniform Bond Model		Concrete Cone Model		Cone or Full Uniform Bond Model			Cone or Cone Plus Partial Uniform Bond Model with Calculated Cone Height				
d	d ₀	h _{ef}	τ ₀	Actual Test Capacity	Capacity	Test-to-Predicted Ratio	Capacity	Test-to-Predicted Ratio	h _{cone}	Capacity	Test-to-Predicted Ratio	h _{cone}	Capacity	Test-to-Predicted Ratio		
(in)	(in)	(in)	(psi)	(k)	(k)		(k)		(in)	(k)		(in)	(k)			
0.375	0.4375	1.75	2265	2.58	5.45	0.47	2.15	1.20	2.22	2.15	1.20	2.22	2.15	1.20		
0.375	0.4375	3.375	2265	8.76	10.51	0.83	7.98	1.10	2.22	10.51	0.83	2.22	6.29	1.39		
0.375	0.4375	4.5	2265	9.685	14.01	0.69	14.19	0.68	2.22	14.01	0.69	2.22	9.05	1.07		
0.5	0.5625	2.25	2235	4.53	8.89	0.51	3.55	1.28	2.82	3.55	1.28	2.82	3.55	1.28		
0.5	0.5625	4.5	2235	16.185	17.77	0.91	14.19	1.14	2.82	17.77	0.91	2.82	10.63	1.52		
0.5	0.5625	6	2235	19.095	23.70	0.81	25.23	0.76	2.82	23.70	0.81	2.82	15.15	1.26		
0.625	0.75	2.875	2145	6.77	14.53	0.47	5.79	1.17	3.61	5.79	1.17	3.61	5.79	1.17		
0.625	0.75	5.625	2145	26.24	28.43	0.92	22.17	1.18	3.61	28.43	0.92	3.61	16.64	1.58		
0.625	0.75	7.5	2145	29.29	37.91	0.77	39.42	0.74	3.61	37.91	0.77	3.61	23.62	1.24		
0.75	0.875	3.375	2065	9.25	19.16	0.48	7.98	1.16	4.06	7.98	1.16	4.06	7.98	1.16		
0.75	0.875	6.75	2065	34.685	38.32	0.91	31.93	1.09	4.06	38.32	0.91	4.06	22.63	1.53		
0.75	0.875	9	2065	41.535	51.09	0.81	56.76	0.73	4.06	51.09	0.81	4.06	31.91	1.30		
0.875	1	4	2000	12.03	25.13	0.48	11.21	1.07	4.49	11.21	1.07	4.49	11.21	1.07		
0.875	1	7.875	2000	49.975	49.48	1.01	43.46	1.15	4.49	49.48	1.01	4.49	29.37	1.70		
0.875	1	10.5	2000	58.82	65.97	0.89	77.26	0.76	4.49	65.97	0.89	4.49	41.18	1.43		
1	1.125	4.5	1945	15.79	30.93	0.51	14.19	1.11	4.91	14.19	1.11	4.91	14.19	1.11		
1	1.125	9	1945	55.38	61.87	0.90	56.76	0.98	4.91	61.87	0.90	4.91	36.79	1.51		
1	1.125	12	1945	71.74	82.49	0.87	100.91	0.71	4.91	82.49	0.87	4.91	51.39	1.40		
1.25	1.375	5.625	1860	23.045	45.19	0.51	22.17	1.04	5.74	22.17	1.04	5.74	22.17	1.04		
1.25	1.375	11.25	1860	98.43	90.39	1.09	88.69	1.11	5.74	90.39	1.09	5.74	53.68	1.83		
1.25	1.375	15	1860	136.525	120.52	1.13	157.67	0.87	5.74	120.52	1.13	5.74	74.49	1.83		
Mean=						0.76	Mean=		1.00	Mean=			0.98	Mean=		1.36
St Dev=						0.22	St Dev=		0.19	St Dev=			0.16	St Dev=		0.24
COV=						0.29	COV=		0.19	COV=			0.16	COV=		0.18

Appendix E. Test Jig Design Calculations and Drawings

Tensile Test Jig Calculations



Estimate Loads

The estimated pullout capacity for two 5.25 in. embedded anchors is 53 k.

The test jig will be designed to a safety factor of 2. Therefore the downward force at the anchor will be $P = 106 k$

$$+\uparrow \sum F_y = 0 = (-106 k) + \frac{1}{2} L w f_{bearing}$$

$$w = 13 \text{ in.}$$

$$f_{bearing} = 0.85 f'_c$$

ACI 318-08
10.14.1

$$(106 k) = \frac{1}{2} L (13 \text{ in.}) (0.85) (4 \text{ ksi})$$

$$\therefore L = 4.8 \text{ in.}$$

$$+\curvearrowright \sum M_0 = 0$$

$$= (106 k)(4.6 \text{ in.}) - F(21.66 \text{ in.})$$

$$+ (106 k) \left(4.275 \text{ in.} - \frac{4.80 \text{ in.}}{3} \right)$$

$$F = 35.60 k$$

$$M_{max} = (35.60 k)(21.66 \text{ in.}) = 771.10 k \cdot \text{in.} = 64.26 k \cdot \text{ft}$$

$$V_{max} = 35.60 k$$

Design using a W6x25 for the I-beam ($f_y = 50 \text{ ksi}$)

Check limiting width-thickness ratios

AISC 360-05 [87]
Table B4.1

$$\frac{b}{t} = 6.68$$

$$\lambda_p = 0.38 \sqrt{\frac{E}{F_y}} = 0.38 \sqrt{\frac{29000 \text{ ksi}}{50 \text{ ksi}}} = 9.15 > 6.68$$

AISC 360-05
Table B4.1

∴ The flanges are compact for flexure

$$\frac{h}{t_w} = 15.5$$

$$\lambda_p = 3.76 \sqrt{\frac{E}{F_y}} = 3.76 \sqrt{\frac{29000 \text{ ksi}}{50 \text{ ksi}}} = 90.55 > 15.5$$

AISC 360-05
Table B4.1

∴ The web is compact for flexure

Yielding

$$Z_x = 18.9 \text{ in.}^3$$

$$M_n = M_p = F_y Z_x = (50 \text{ ksi})(18.9 \text{ in.}^3) = 945 \text{ k} \cdot \text{in.}$$

$$= 78.8 \text{ k} \cdot \text{ft}$$

AISC 360-05
(F2-1)

Lateral-Torsional Buckling

$$L_b = 21.66 \text{ in.}$$

$$r_y = 1.52 \text{ in.}$$

AISC 360-05
(F2-5)

$$L_p = 1.76 r_y \sqrt{\frac{E}{F_y}} = 1.76(1.52 \text{ in.}) \sqrt{\frac{29,000 \text{ ksi}}{50 \text{ ksi}}} = 64.43 \text{ in.}$$

$$> 21.66 \text{ in.}$$

∴ Lateral-torsional buckling does not apply

The section is compact so local buckling does not apply

$$M_u = 64.26 \text{ k} \cdot \text{ft} < M_n = 78.8 \text{ k} \cdot \text{ft}$$

∴ The beam is adequate for the anticipated loading

Punching Capacity of Base Plate

The estimated maximum strength of any anchor is governed by the tensile capacity of the steel anchor = 35 k.

By multiplying the maximum strength by a safety factor of 2, the ultimate capacity is $F_u = 70 \text{ k}$.

Diameter of coupler = 1.38 in.

Thickness of baseplate = $t = 1.0 \text{ in.}$

Yield stress of baseplate = $f_y = 36 \text{ ksi}$

$$A_b = \pi dt = \pi(1.38 \text{ in.})(1.0 \text{ in.}) = 4.34 \text{ in.}^2$$

Allowable shear stress = $f_{v,allow} = 0.6f_y = 0.6(36 \text{ ksi}) = 21.6 \text{ ksi}$

$$V_{allow} = A_b f_{v,allow} = (4.34 \text{ in.}^2)(21.6 \text{ ksi}) = 93.74 \text{ k} > 70 \text{ k}$$

Bending Capacity of Base Plate

The estimated maximum load applied to the outside holes is 26.5 k.

Assume that the load will be carried by one-way bending of the baseplate and half the load will go to each gusset.

$$I_{x1} = \frac{bh^3}{12} = \frac{(3.0 \text{ in.})(1.0 \text{ in.})^3}{12} = 0.25 \text{ in.}^4$$

$c = 0.5 \text{ in.}$

$$M = \left(\frac{26.5 \text{ k}}{2}\right)(1.62 \text{ in.}) = 21.47 \text{ k} \cdot \text{in.}$$

$$\sigma = \frac{Mc}{I} = \frac{(21.47 \text{ k} \cdot \text{in.})(0.5 \text{ in.})}{0.25 \text{ in.}^4} = 42.94 \text{ ksi}$$

$$I_{x2} = \frac{bh^3}{12} = \frac{(3.93 \text{ in.})(1.0 \text{ in.})^3}{12} = 0.32 \text{ in.}^4$$

$$M = \left(\frac{26.5 \text{ k}}{2}\right)(2.0 \text{ in.}) = 26.5 \text{ k} \cdot \text{in.}$$

$$\sigma = \frac{Mc}{I} = \frac{(26.5 \text{ k} \cdot \text{in.})(0.5 \text{ in.})}{0.32 \text{ in.}^4} = 41.41 \text{ ksi}$$

These stress values are both slightly above the yield stress of the steel, however they are unconservative values since they are based on one-way cantilever bending and are still well below the ultimate strength of the steel.

Tensile Weld Strength

A 0.375 in. weld is used around the I-beam and the gusset plates.

$$(\text{throat depth}) = 0.707(\text{weld size}) = 0.707(0.375 \text{ in.}) = 0.265 \text{ in.}$$

$$F_{EXX} = 70 \text{ ksi}$$

$$F_v = 0.3(F_{EXX}) = 21 \text{ ksi}$$

$$f_{weld} = F_v(\text{throat depth}) = (21 \text{ ksi})(0.265 \text{ in.}) = 5.57 \text{ k/in.}$$

$$\text{Total length of weld above neutral axis} = 4(2.75 \text{ in.}) + 2(12.5 \text{ in.}) + 0.5(6.38 \text{ in.}) - 0.46 \text{ in.} = 38.73 \text{ in.}$$

$$F_{weld} = f_{weld}L_{weld} = (5.57 \text{ k/in.})(38.73 \text{ in.}) = 216 \text{ k} > 106 \text{ k}$$

Shear Strength of Anchors on Kick Plate

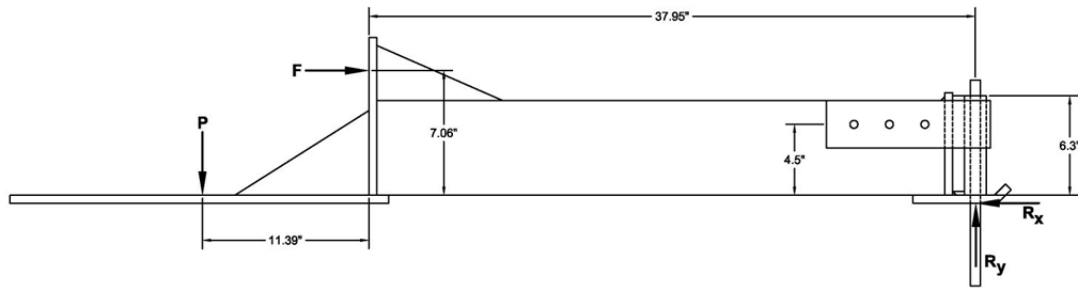
Use two 3/4 in. Power Fasteners wedge bolts

$$\text{Shear capacity/bolt} = 21.96 \text{ k}$$

Power Fasteners
Product Documentation [88]

$$V_n = 2(21.96 \text{ k}) = 43.92 \text{ k} > 35.6 \text{ k}$$

Shear Test Jig Calculations



Estimate Loads

The estimated shear capacity is 20.09 k

The test jig will be designed to a safety factor of 2. Therefore the reaction in the x-direction will be $R_x = 40.18 k$

$$+\uparrow \sum F_x = 0 = F - 40.18 k$$

$$\therefore F = 40.18 k$$

$$+\circlearrowleft \sum M_P = 0 = (-40.18 k)(7.06 \text{ in.}) + (-40.18 k)(0.5 \text{ in.}) + R_y(49.34 \text{ in.})$$

$$\therefore R_y = 6.16 k$$

$$+\circlearrowleft \sum M_F = 0 = (-40.18 k)(7.56 \text{ in.}) + (6.16 k)(37.95 \text{ in.}) + P(11.39 \text{ in.})$$

$$\therefore P = 6.14 k$$

Design Tapcon Screws for Uplift at Load P

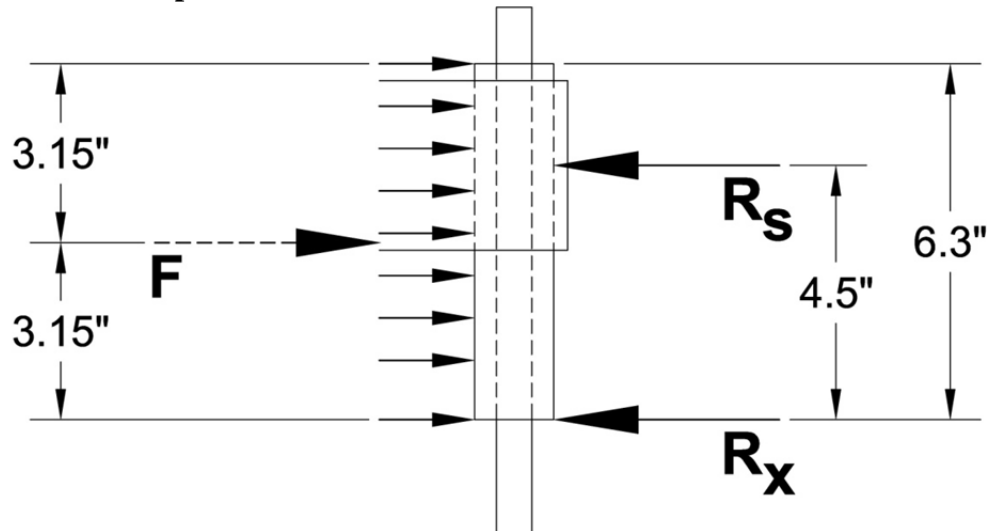
Tensile strength of one 3/8"x2" screw in 4,000 psi concrete =
2.55 k

Concrete
Fasteners
Specification [89]

Strength of 4 tapcons = $4(2.55 k) = 10.2 k > 6.14 k$

Use a 3/8"x3" tapcon screw since the screw will not be bonded for the top 1.25"

Estimate Loads on Strap



$$+\circlearrowleft \sum M_{R_s} = 0 = (-40.18 k)(4.5 \text{ in.}) + F(1.35 \text{ in.})$$

$$\therefore F = 133.9 k$$

$$+\circlearrowleft \sum M_F = 0 = R_s(1.35 \text{ in.}) - (40.18 k)(3.15 \text{ in.})$$

$$\therefore R_s = 93.75 k$$

The strap is angled 48° from the end of the channels.

Each side of the strap will take half the load.

$$R_{s1} = \frac{R_s}{2} = \frac{93.75 k}{2} = 46.88 k$$

Calculate the tension in the angled portions of the strap.

$$T = \frac{46.88 k}{\sin 48^\circ} = 63.08 k$$

Fracture of Strap at Angled Section

The strap will be made of a 3 in. x 0.5 in. A36 plate.

$$P_n = A_{strap} f_u = (3 \text{ in.})(0.5 \text{ in.})(60 \text{ ksi}) = 90 k > 63.08 k$$

Facture of Strap at Bolts

Use 0.75 in. bolts. The diameter of the bolt hole will be 0.875 in.

$$P_n = (A_{strap} - A_{bolt \text{ hole}}) f_u = ((3 \text{ in.} - 0.875 \text{ in.})(0.5 \text{ in.}))(60 \text{ ksi}) = 63.75 k > 46.88 k$$

Shear at Bolts

Use three 0.75 in. grade 5 bolts.

$$V_n = 0.6 A_{bolt} f_u$$

$$A_{bolt} = 0.334 \text{ in.}^2$$

$$f_u = 120 \text{ ksi}$$

$$V_n = 0.6(0.334 \text{ in.}^2)(120 \text{ ksi}) = 24.05 k > \frac{46.88 k}{3} = 15.63 k$$

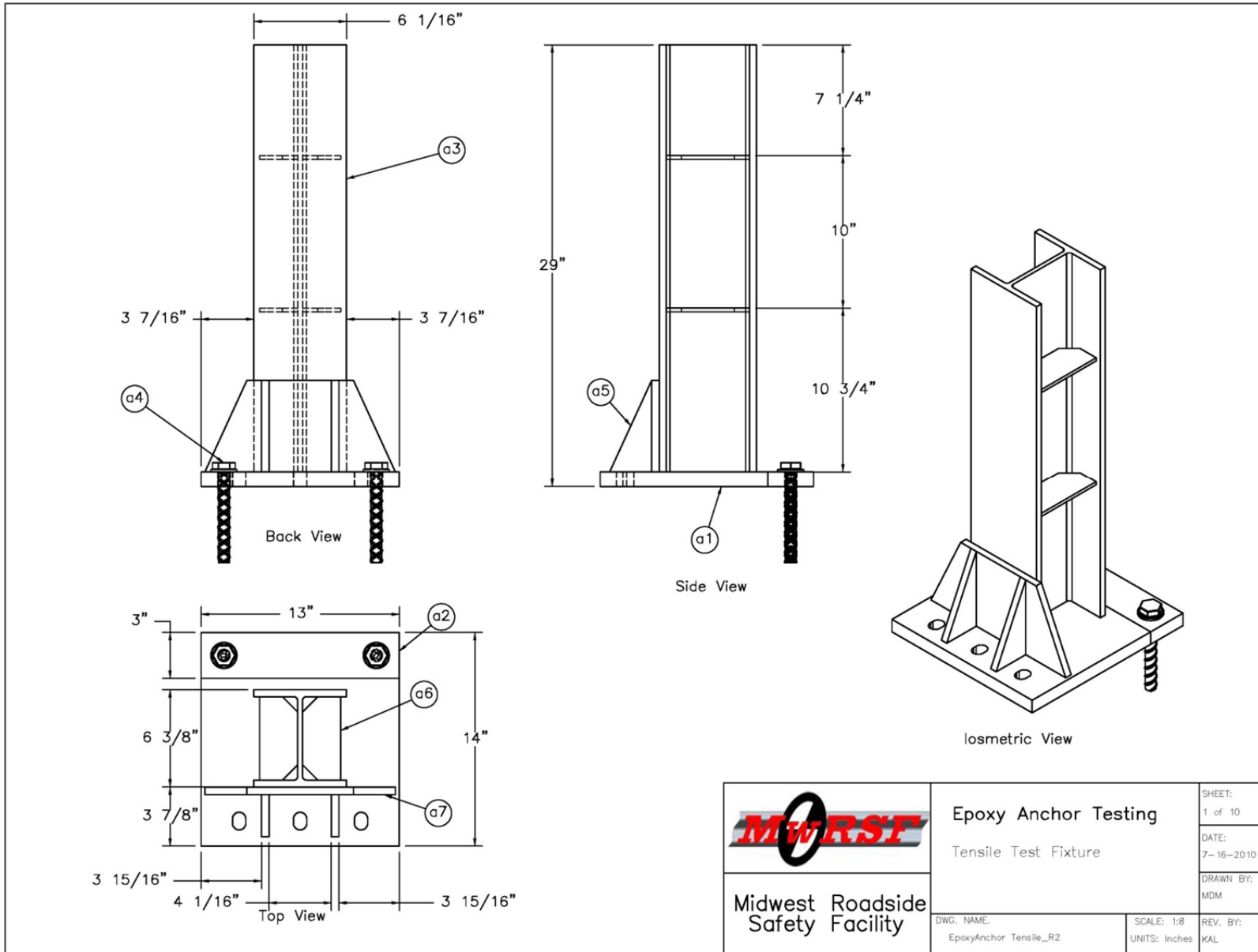


Figure E-1. Tensile Test Jig

	Epoxy Anchor Testing Tensile Test Fixture		SHEET: 1 of 10
	Midwest Roadside Safety Facility		DATE: 7-16-2010
DWG. NAME: EpoxyAnchor Tensile_R2		SCALE: 1:8 UNITS: Inches	DRAWN BY: MDM
		REV. BY: KAL	

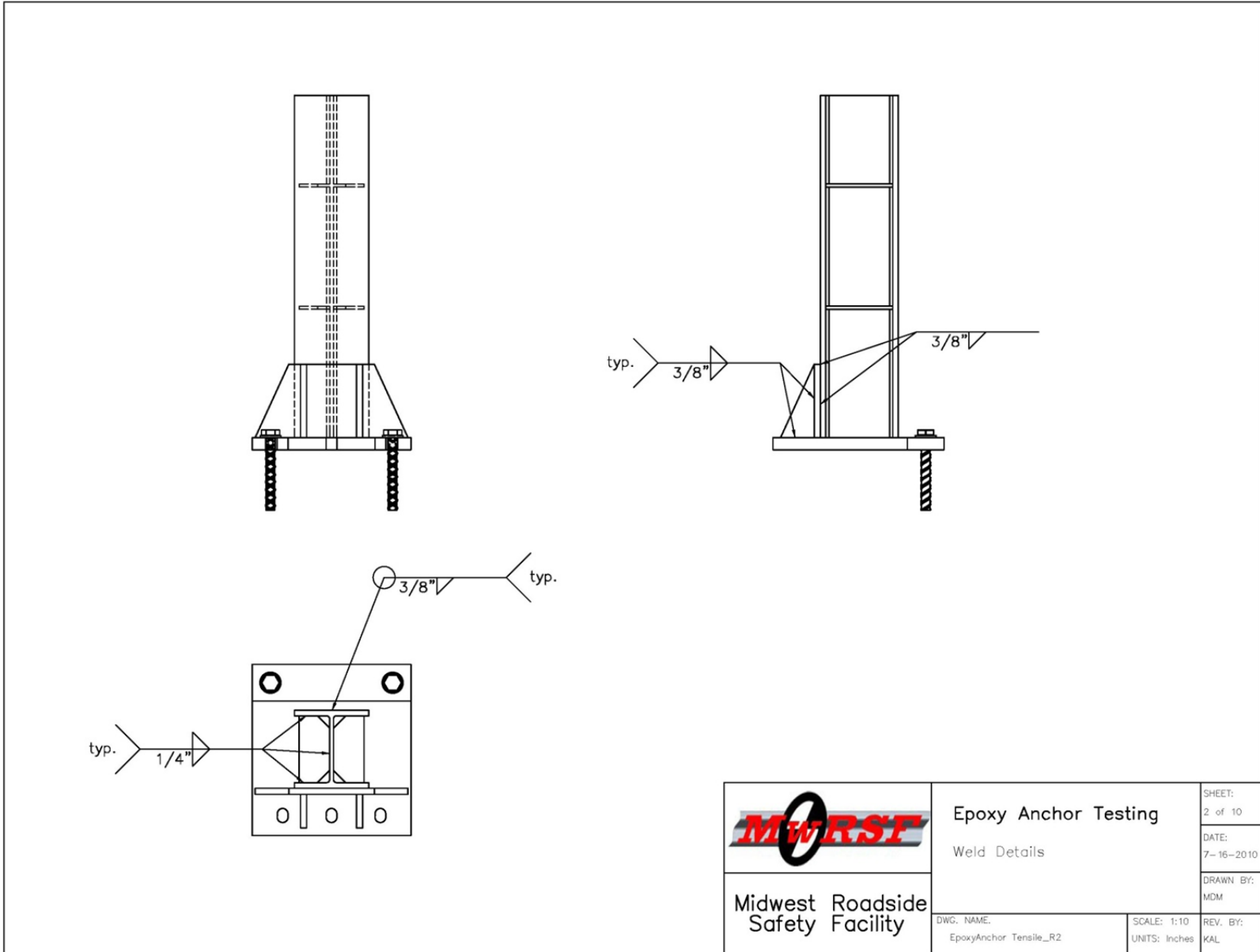


Figure E-2. Tensile Test Jig Weld Details

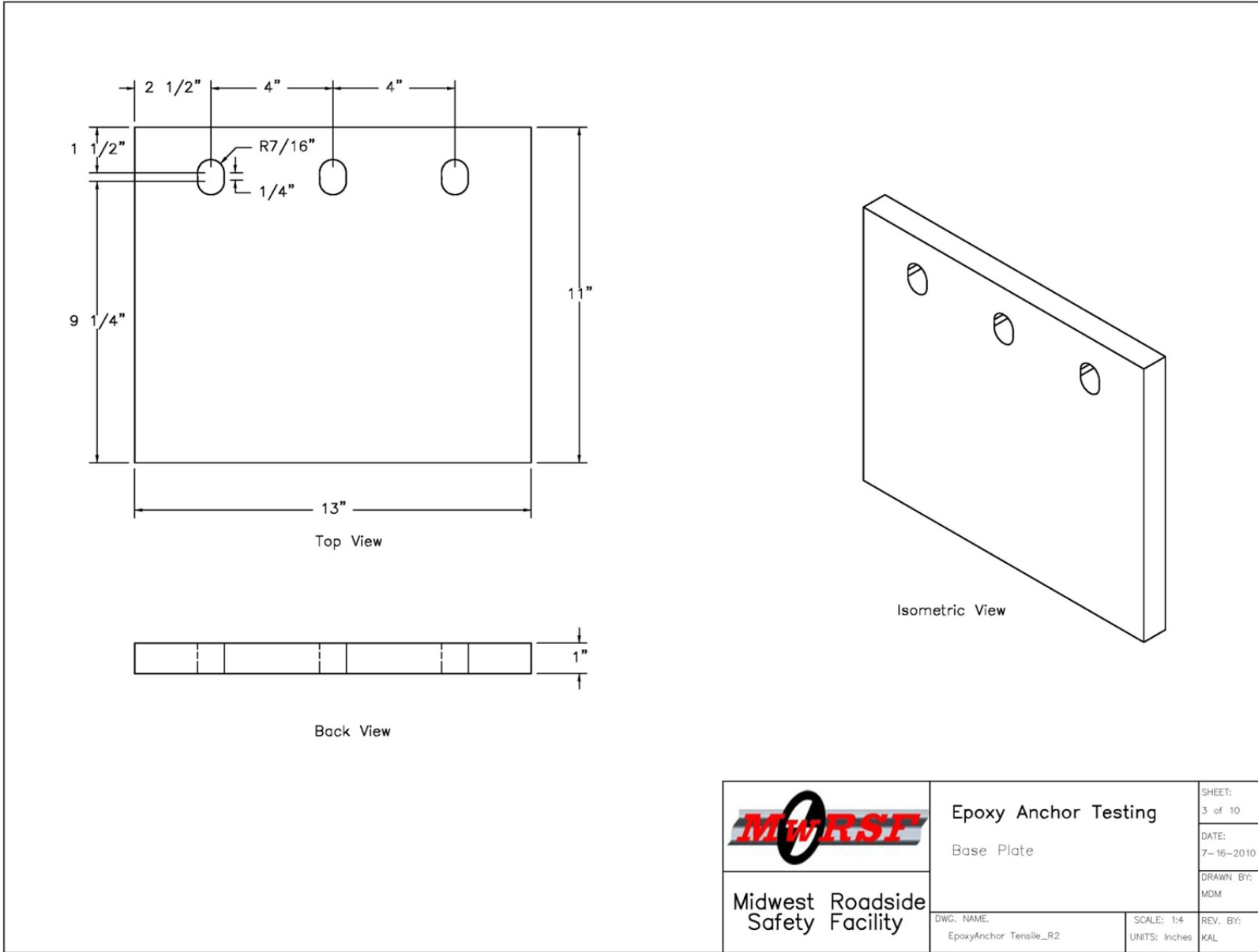


Figure E-3. Tensile Test Jig Base Plate Detail

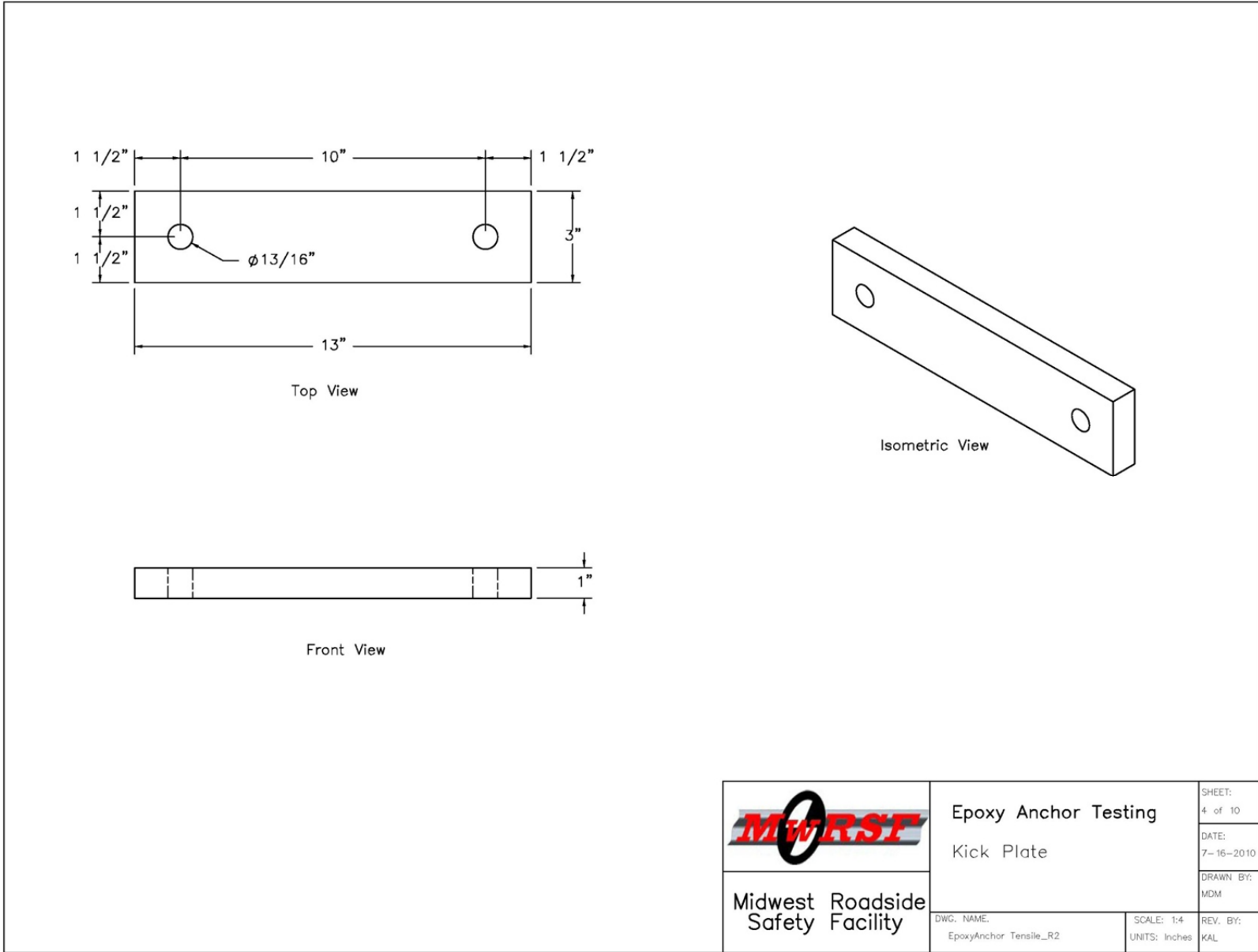


Figure E-4. Tensile Test Jig Kick Plate Detail

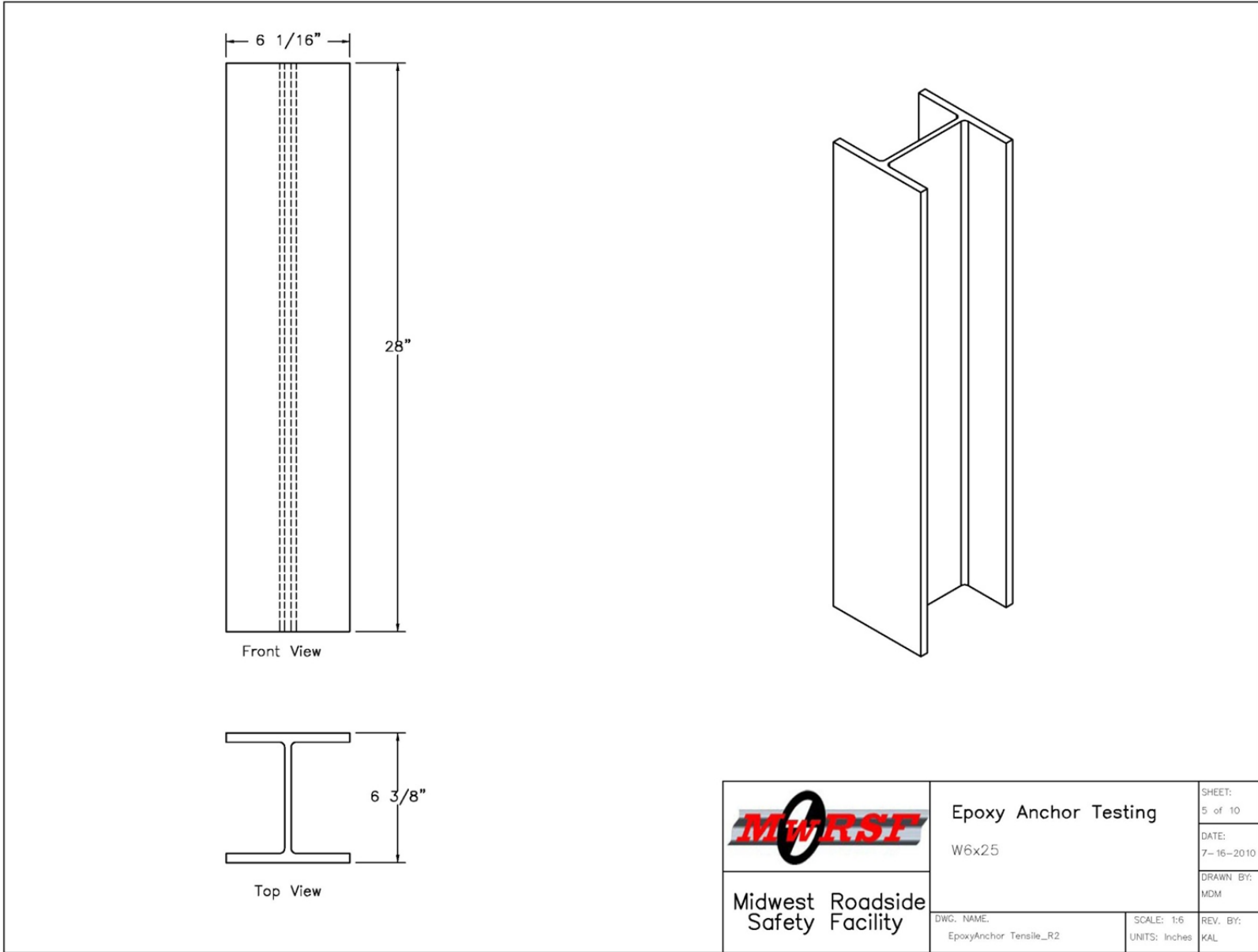


Figure E-5. Tensile Test Jig W6x25 Beam Detail

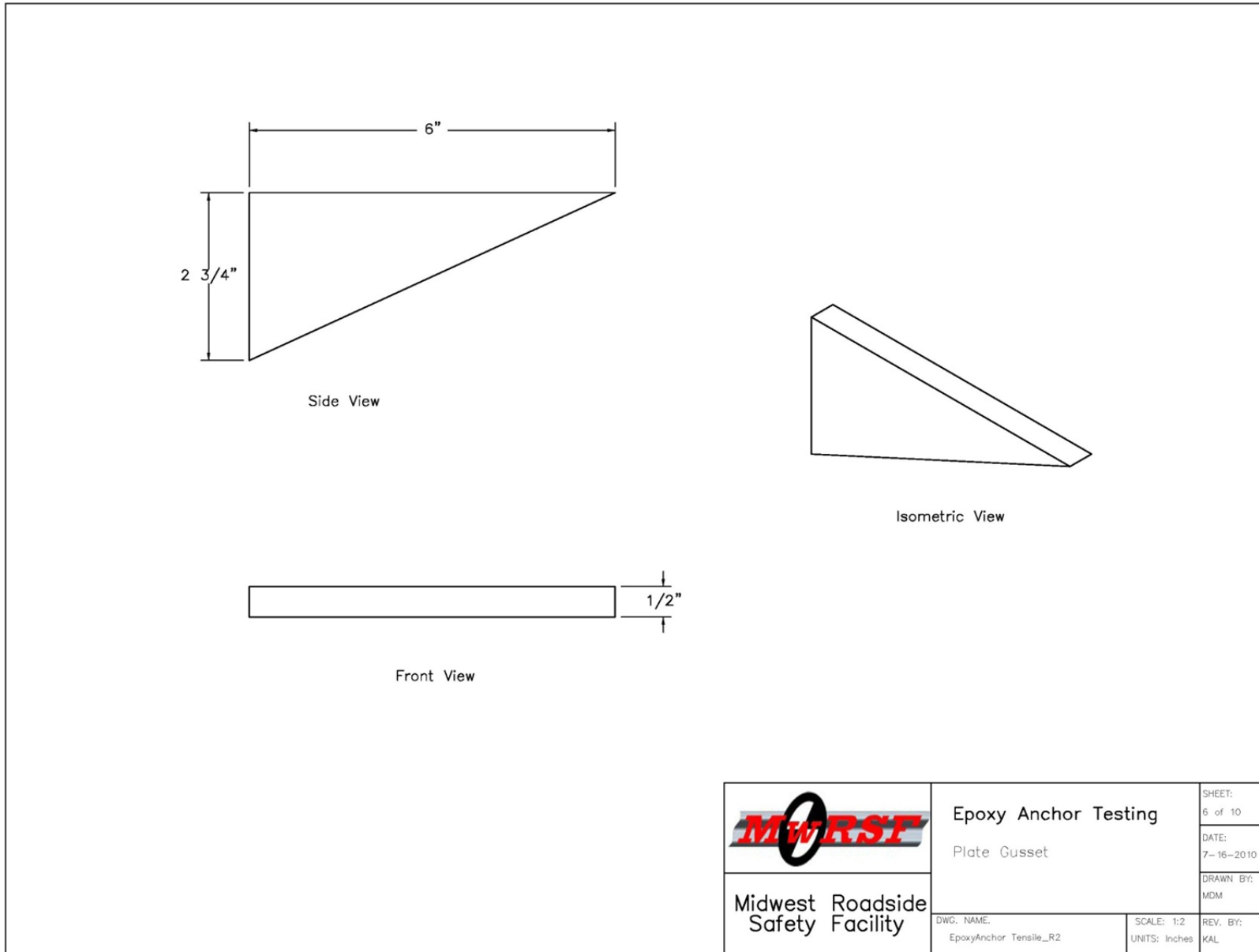


Figure E-6. Tensile Test Jig Plate Gusset Detail

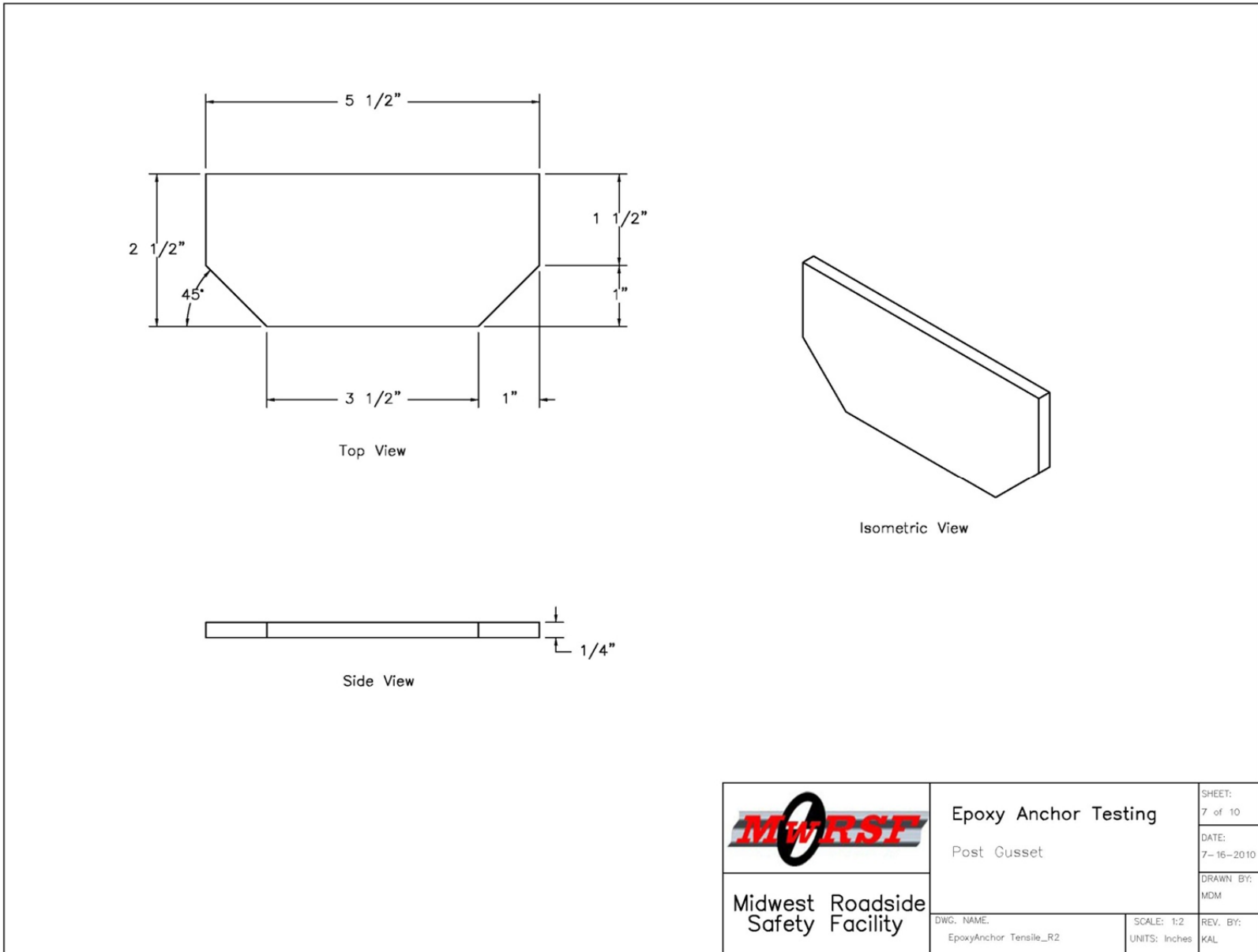


Figure E-7. Tensile Test Jig Post Gusset Detail

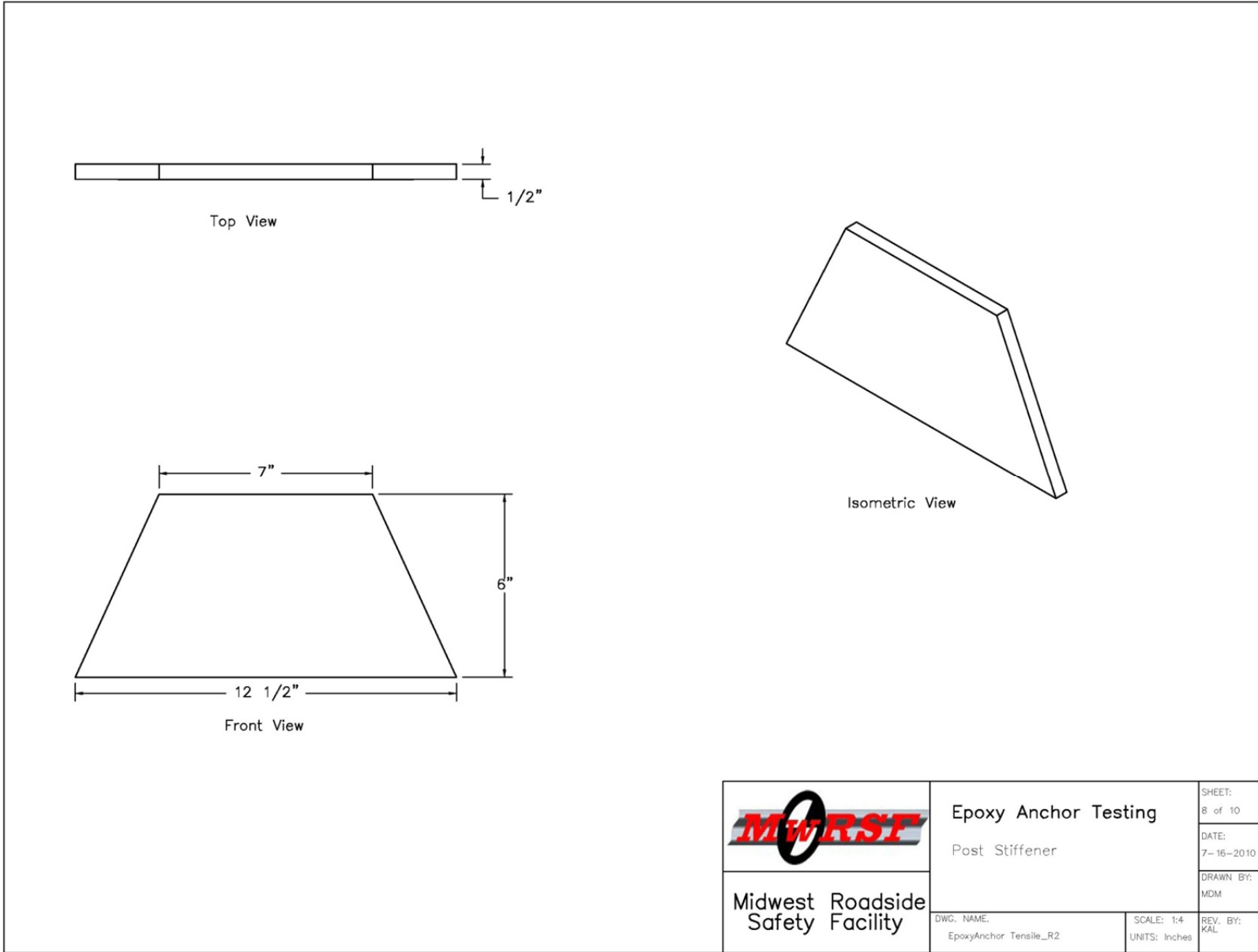
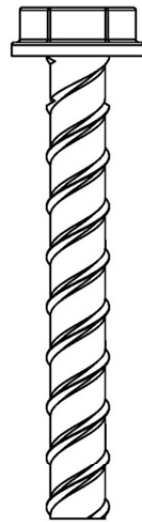
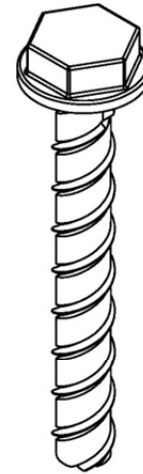


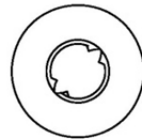
Figure E-8. Tensile Test Jig Post Stiffener Detail



Side View



Isometric View



Bottom View

Notes: (1) Powers Fasteners ϕ 3/4" x 6" long Wedge Bolt Screw Anchor

 Midwest Roadside Safety Facility	Epoxy Anchor Testing Powers Fasteners Wedge Bolt	SHEET: 9 of 10
	DWG. NAME: EpoxyAnchor Tensile_R2	SCALE: 1:2 UNITS: Inches

Figure E-9. Tensile Test Jig Wedge Bolt Detail

Epoxy Anchor Tension Test Fixture			
Item No.	QTY.	Description	Material Spec
a1	1	Base Plate 13x11x1	ASTM A36
a2	1	Kick Plate 13x3x1	ASTM A36
a3	1	Post W6x25x28	ASTM A992 or ASTM A572 (50 ksi strength)
a4	2	Wedge Bolt ϕ 3/4 x 6 in. long	Powers Fasteners
a5	2	Plate Gusset 6x2.75x0.5	ASTM A36
a6	4	Post Gusset 5.5x2.5x0.25	ASTM A36
a7	1	Post Stiffener 12.5x6x0.5	ASTM A36


 Midwest Roadside Safety Facility	Epoxy Anchor Testing Bill of Materials	SHEET: 10 of 10
	DWG. NAME: EpoxyAnchor Tensile_R2	SCALE: None UNITS: Inches

Figure E-10. Tensile Test Jig Bill of Materials

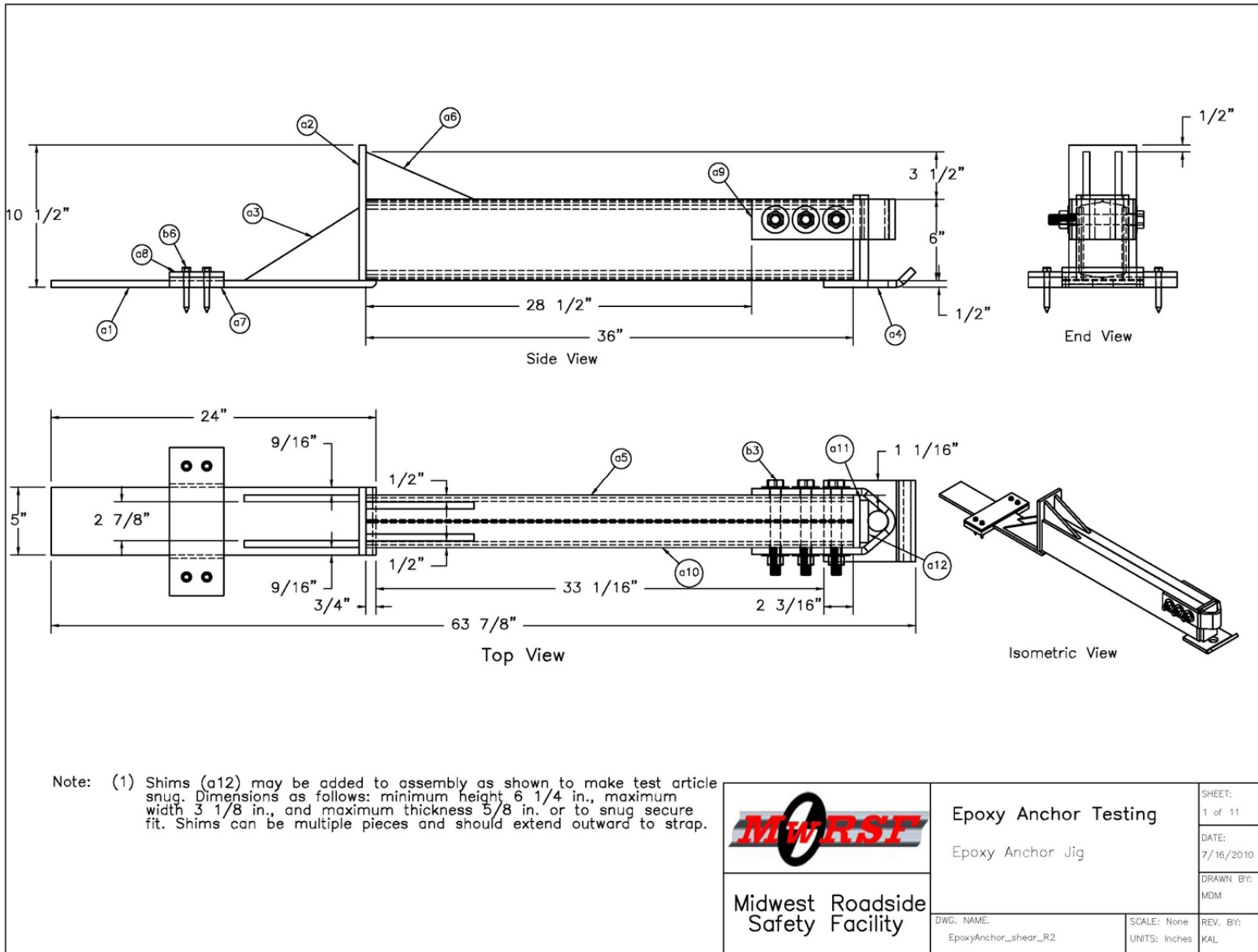


Figure E-11. Shear Test Jig

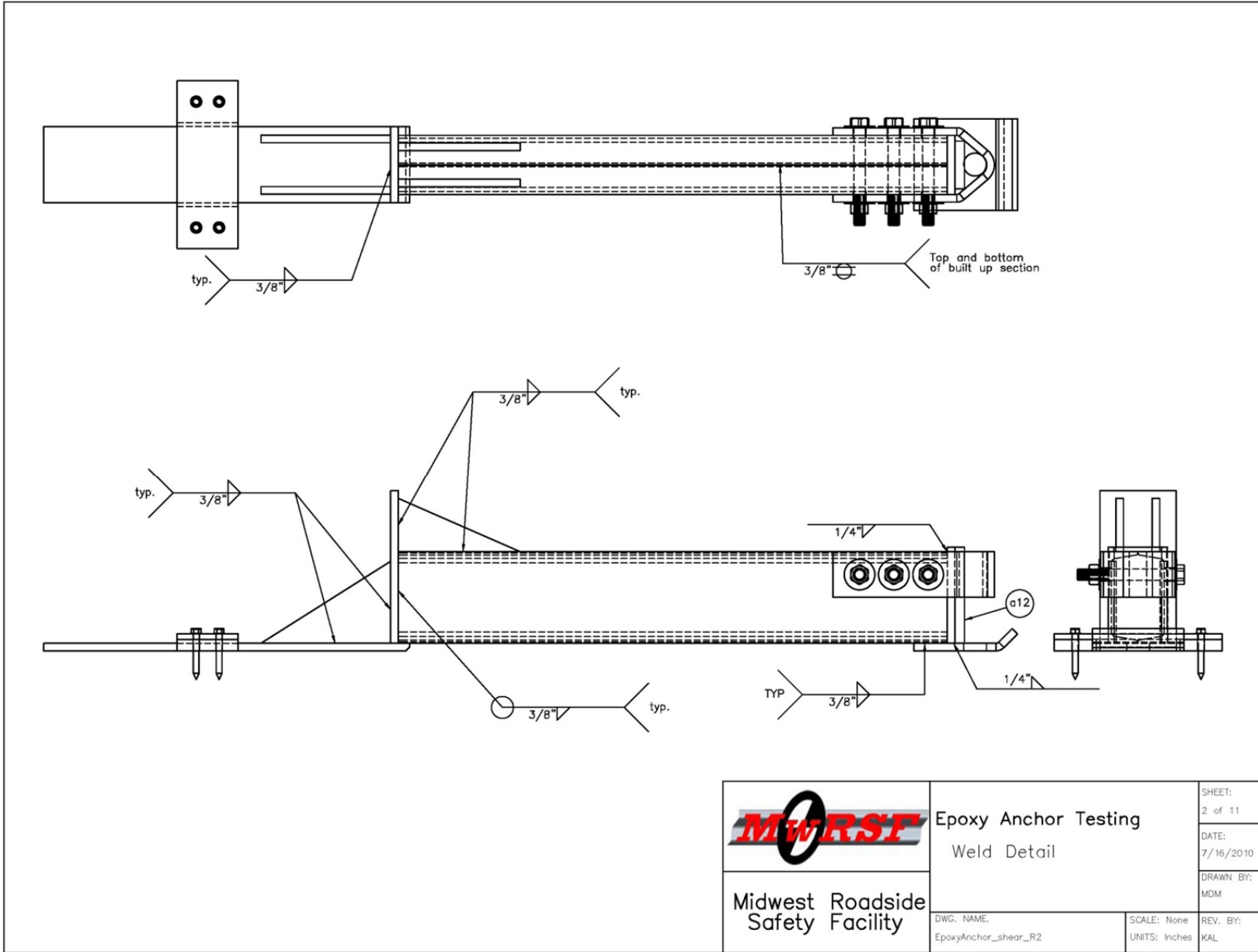


Figure E-12. Shear Test Jig Weld Details

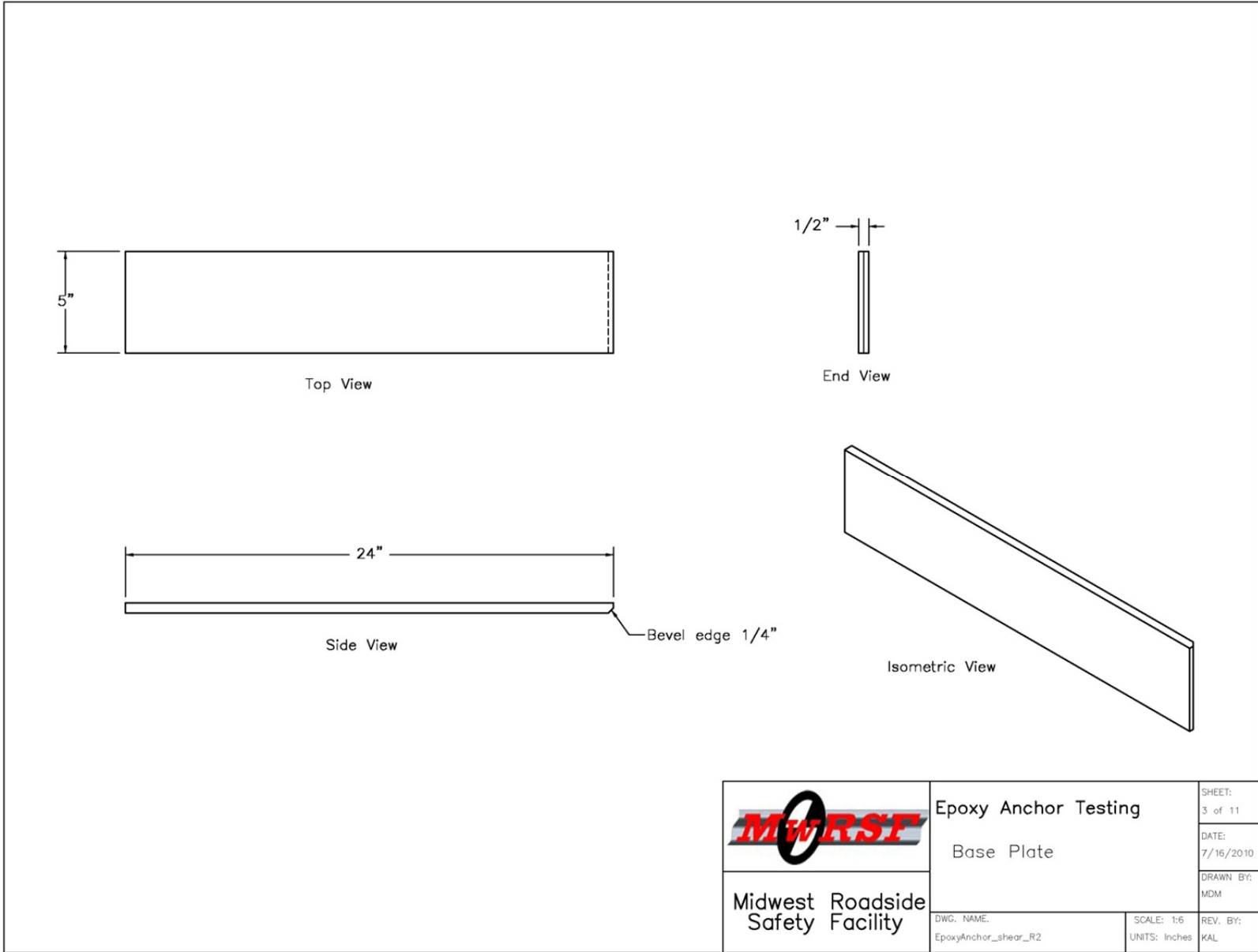


Figure E-13. Shear Test Jig Base Plate Detail

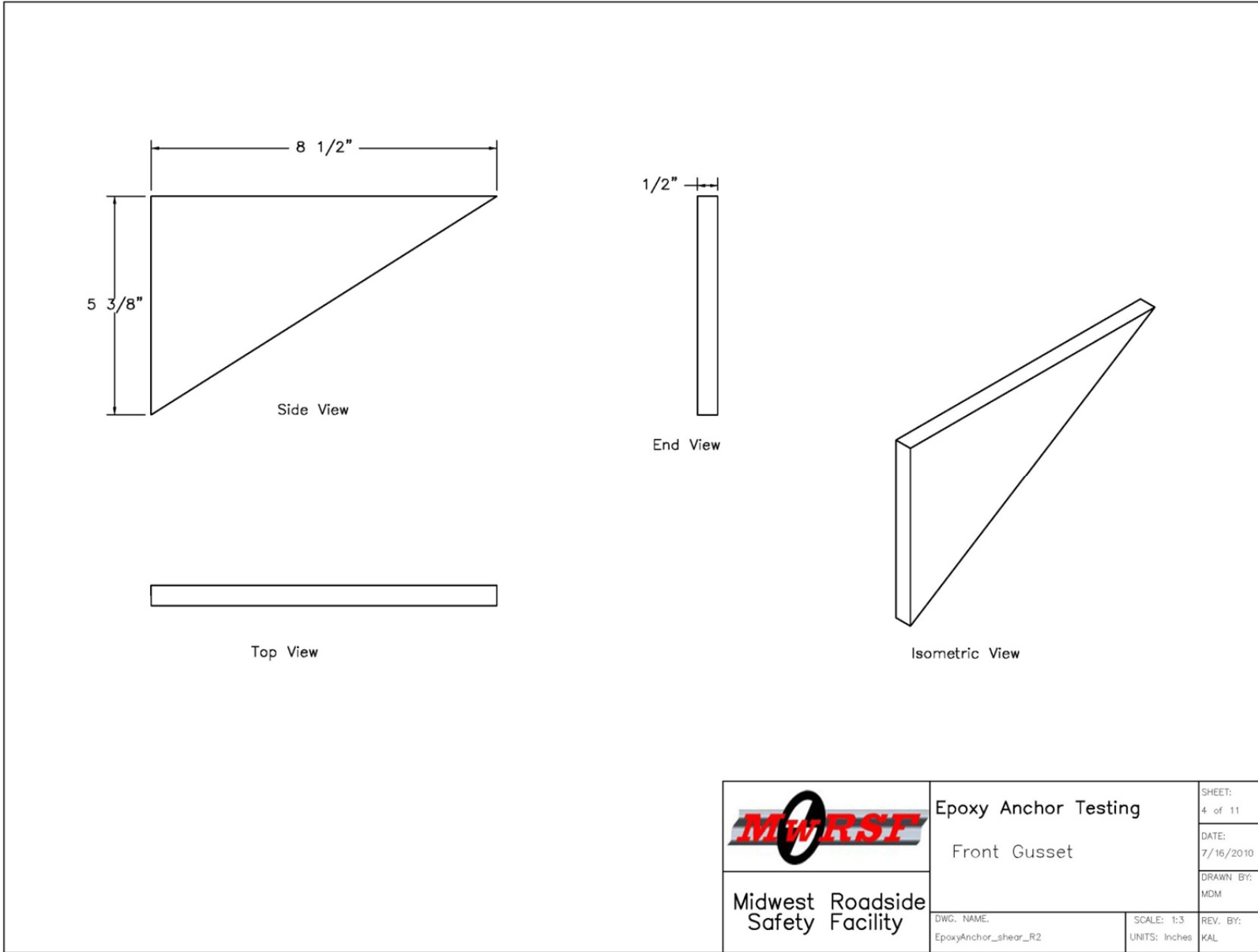


Figure E-14. Shear Test Jig Front Gusset Detail

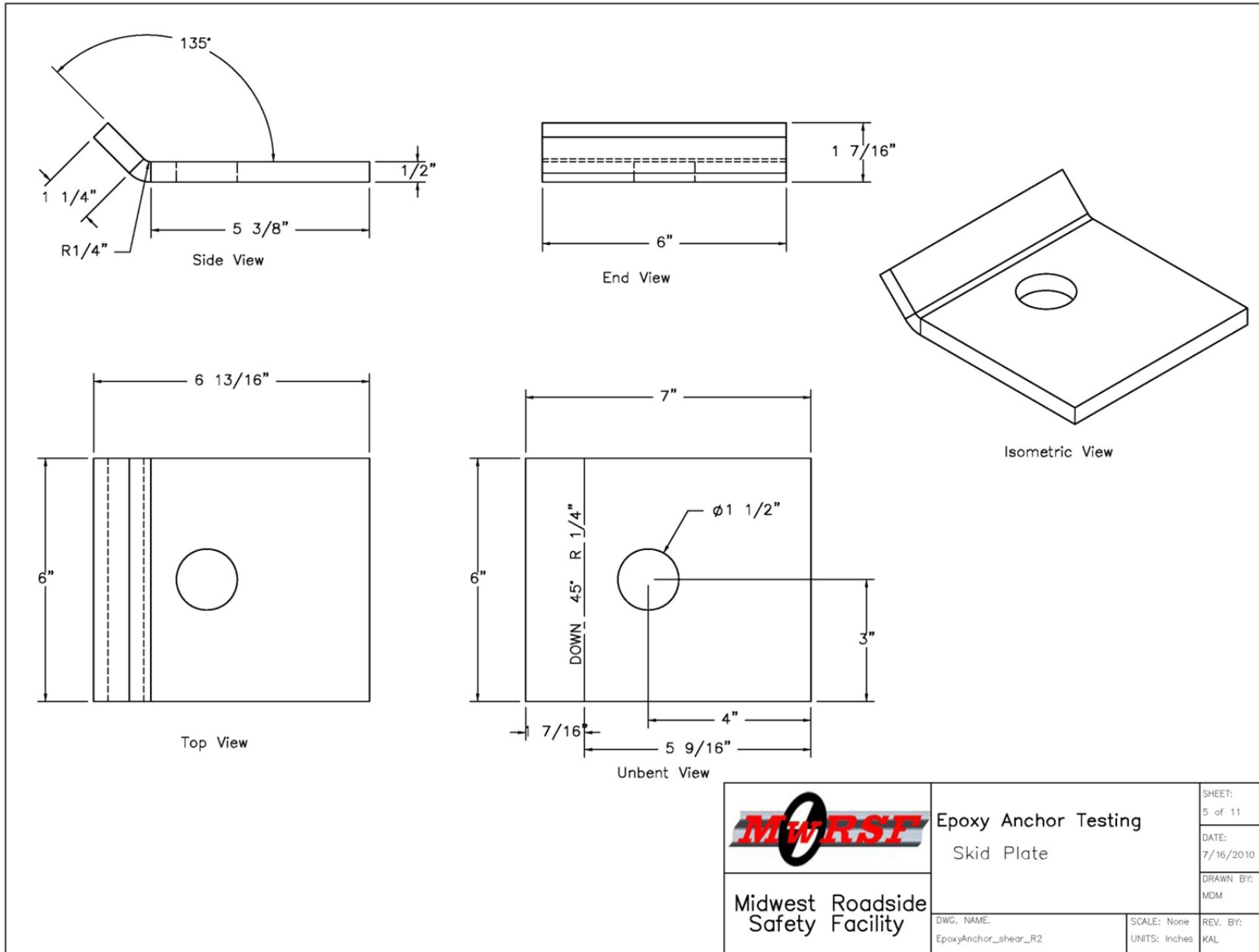


Figure E-15. Shear Test Jig Skid Plate Detail

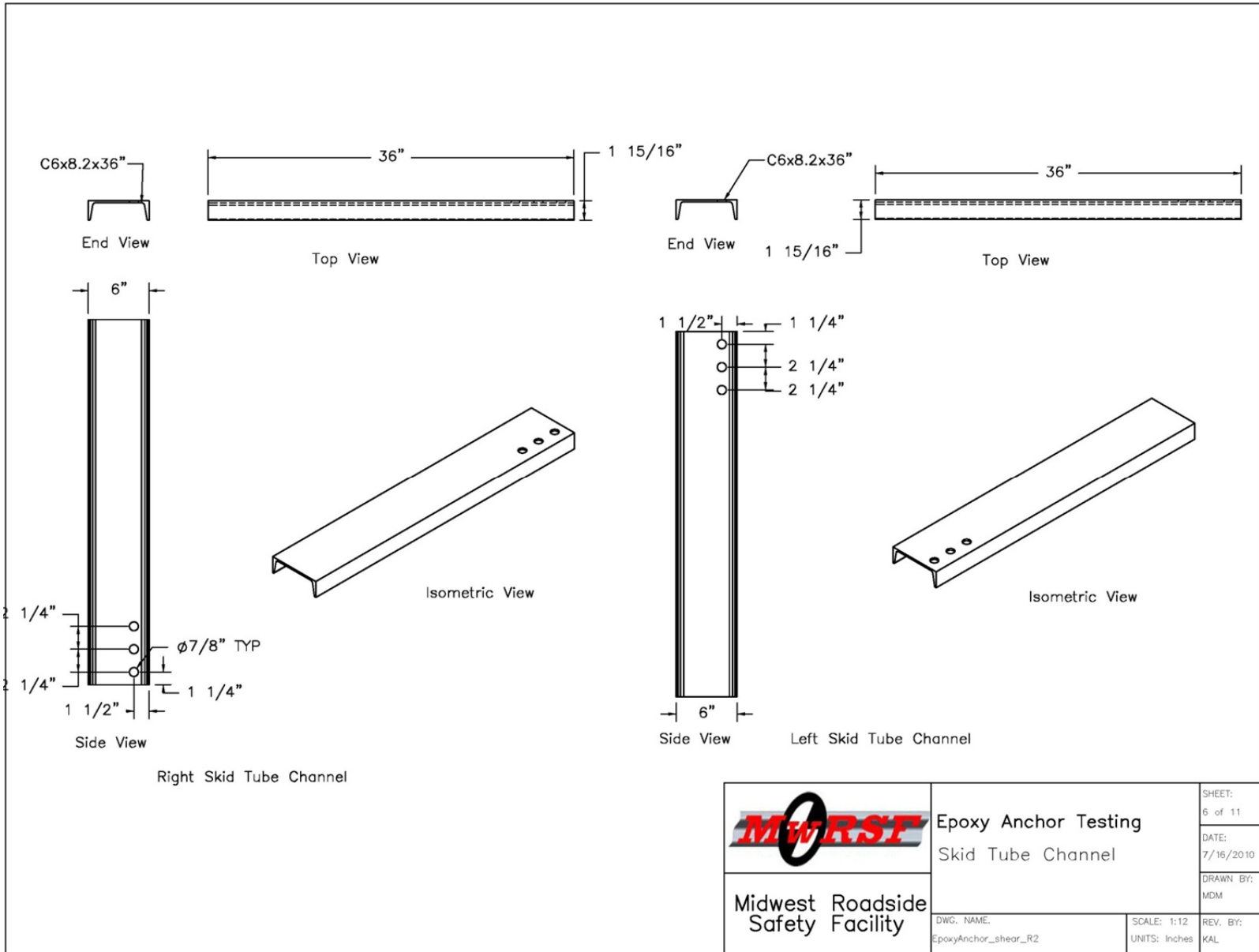


Figure E-16. Shear Test Jig Skid Tube Channel Detail

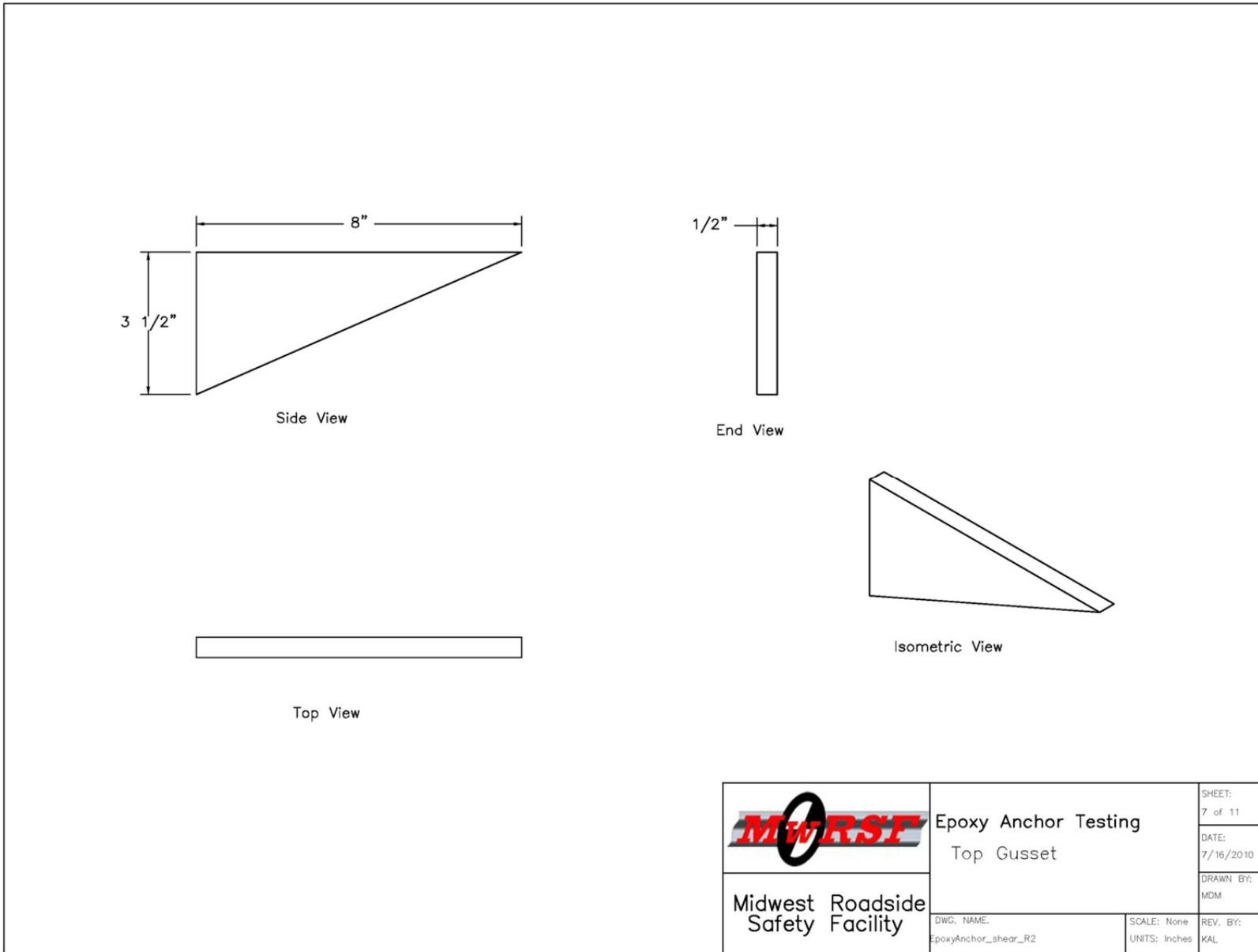


Figure E-17. Shear Test Jig Top Gusset Detail

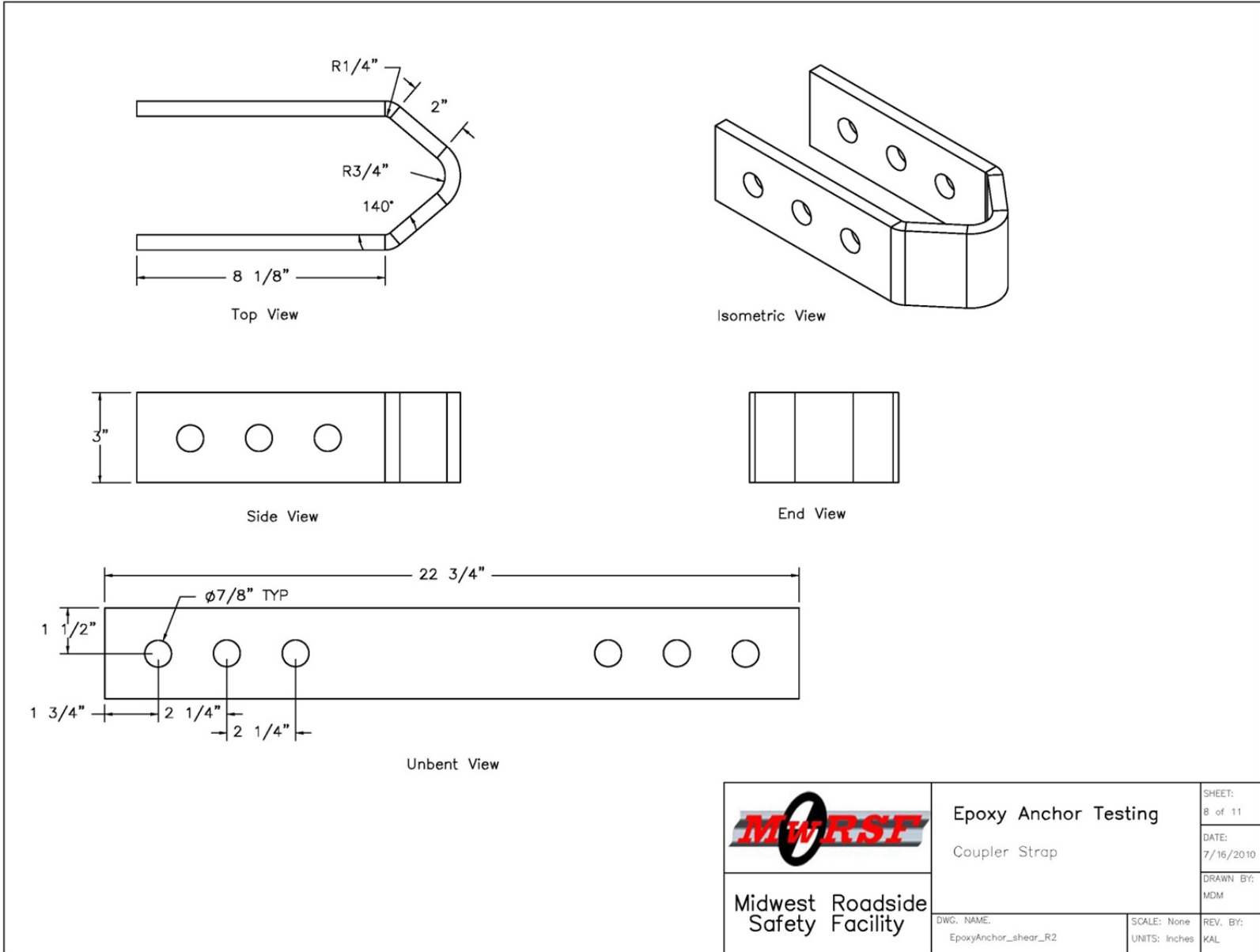


Figure E-18. Shear Test Jig Coupler Strap Detail

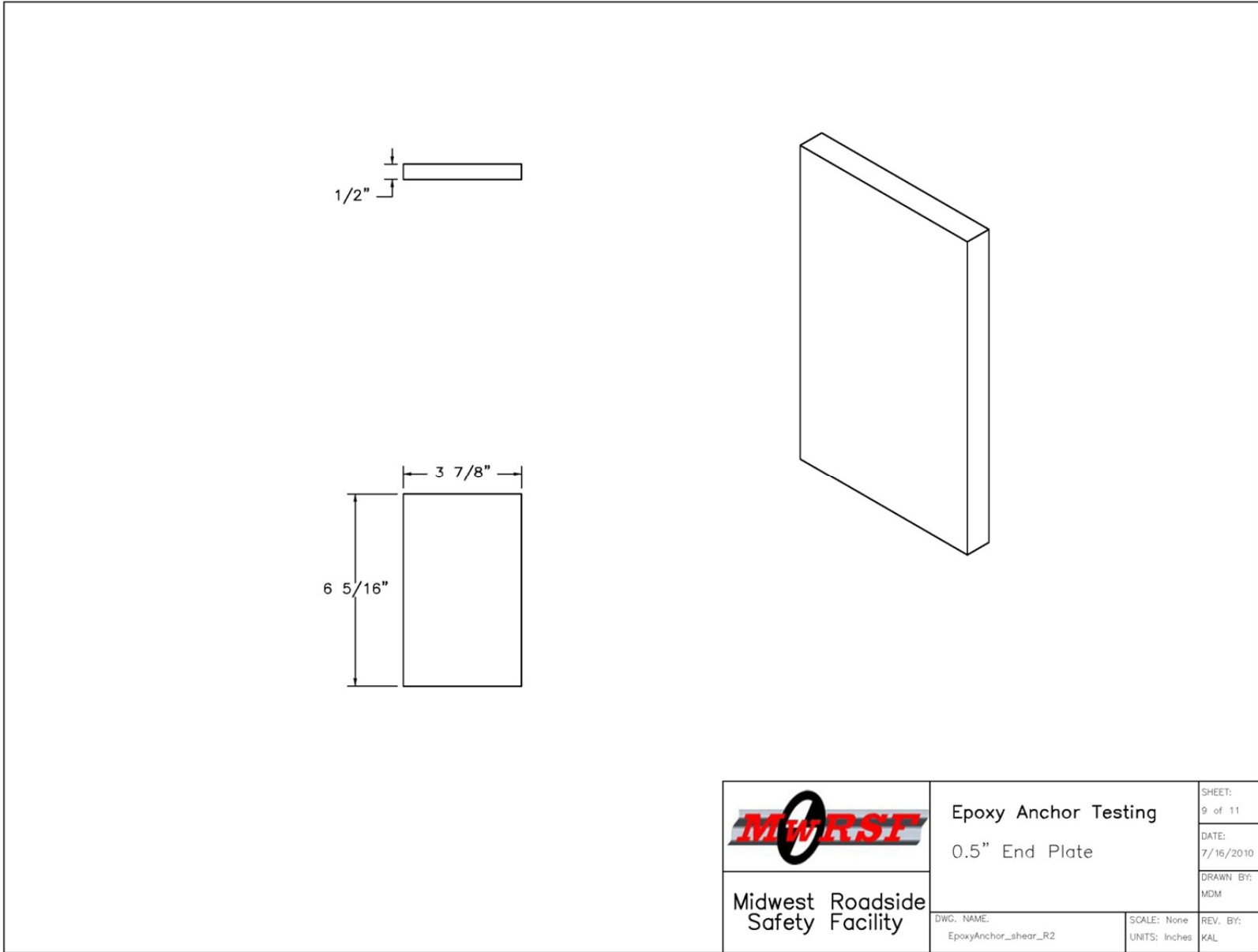


Figure E-19. Shear Test Jig End Plate Detail

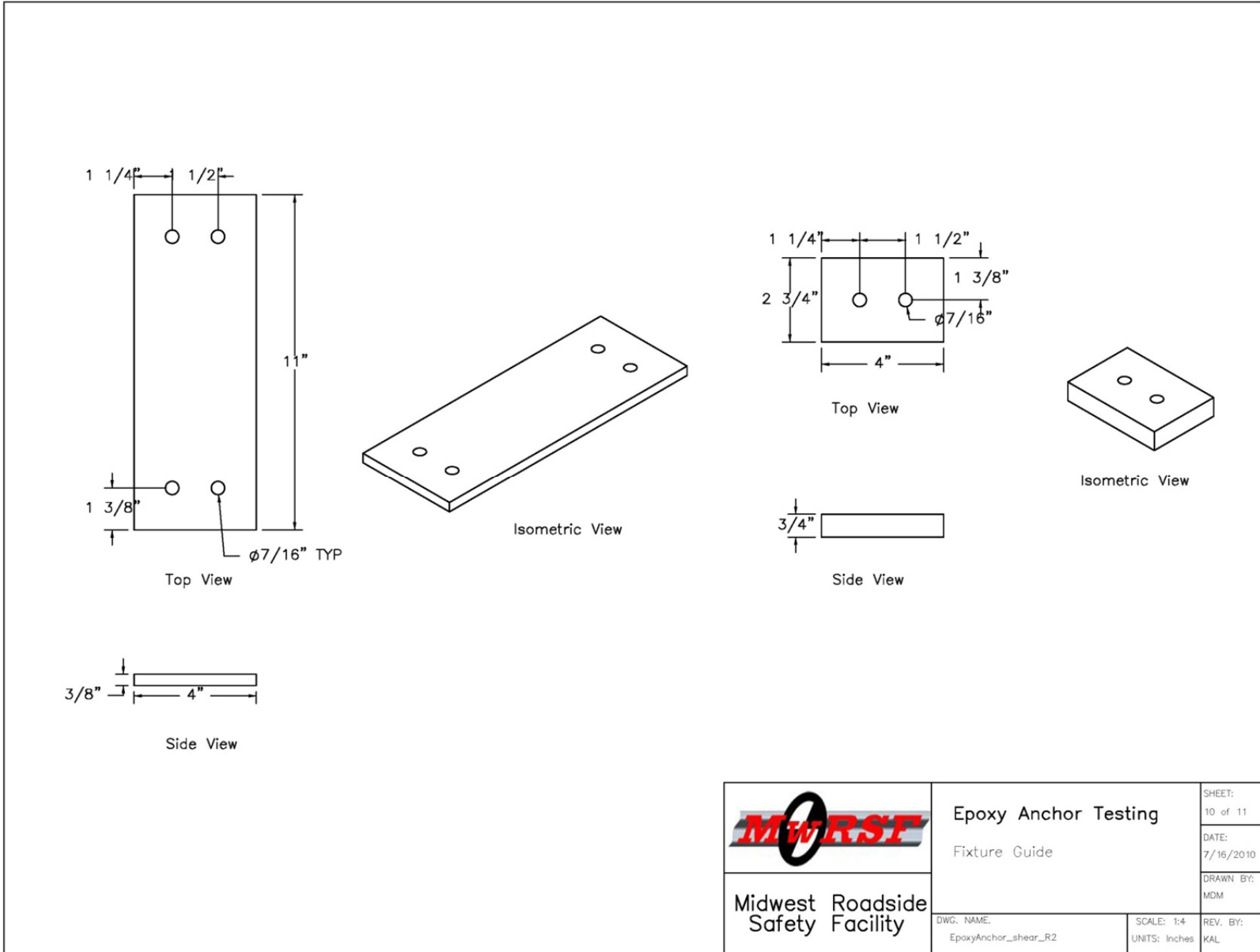


Figure E-20. Shear Test Jig Fixture Guide Detail

Epoxy Anchor Shear test Fixture			
Item No.	QTY.	Description	Material Spec
a1	1	Base Plate 24x5x0.5	ASTM A36
a2	1	Vertical Plate 10x4x0.5	ASTM A36
a3	2	Front Gusset 5.375x8.5x0.5	ASTM A36
a4	1	Skid Plate 6x7x0.5	ASTM A36
a5	1	Right Skid Tube Channel C6x8.2x36	ASTM A36
a6	2	Top Gusset 3.5x8x0.5	ASTM A36
a7	2	Fixture Guide Lower Plate 2.75x4x0.75	ASTM A36
a8	1	Fixture Guide Upper Plate 11x4x0.375	ASTM A36
a9	1	Coupler Strap 22.75x3x0.5	ASTM A36
a10	1	Left Skid Tube Channel C6x8.2x36	ASTM A36
a11	1	End Plate 3.875x6.3125x0.5	ASTM A36
a12	1	Shims	Steel
b3	3	Hex Head Bolt 0.7500-10x6.5x2-N	Grade 5
b4	6	Flat Washer 0.75	Grade 5
b5	3	Hex Nut 0.75	Grade 5
b6	4	Concrete Screw 3/8"x3"	Tapcon Concrete Screw

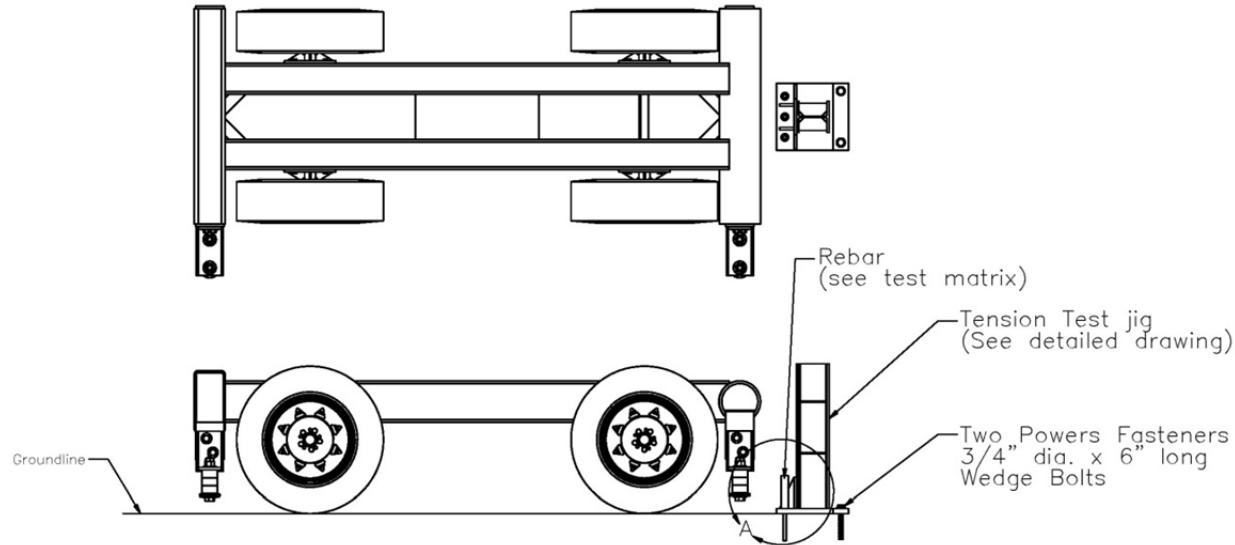
	Epoxy Anchor Testing		SHEET: 11 of 11
	Bill of Materials		DATE: 7/16/2010
Midwest Roadside Safety Facility	DWC. NAME: EpoxyAnchor_shear_R2		DRAWN BY: MDM
	SCALE: None UNITS: Inches	REV. BY: KAL	

Figure E-21. Shear Test Jig Bill of Materials

Appendix F. Test Setup Drawings

Epoxy Anchor Rebar Bogie Testing—Tensile Test Setup

1. Bogie No. 3 – Small Bogie with standard round impact head
2. Speed = 15 mph
3. One high-speed digital camera perpendicular
4. One high-speed digital camera perpendicular zoomed in on the tensile test jig and rebar.
5. JVC digital video
6. DTS and EDR-3
7. Note any installation issues or problems in fieldbook.
8. Note failure mode in fieldbook.
9. Each test must be at least 2' from any previous test anchor holes to prevent anchor spacing and edge spacing issues from affecting results.
10. Kick plate anchors must be replaced each test.
11. Epoxy and epoxy-coated rebar will be donated.
12. Before installation of anchors, measure the bar deformation rib height as well as the epoxy-coating thickness.
13. Epoxy used for first round of testing will be Hilti HIT-RE 500.




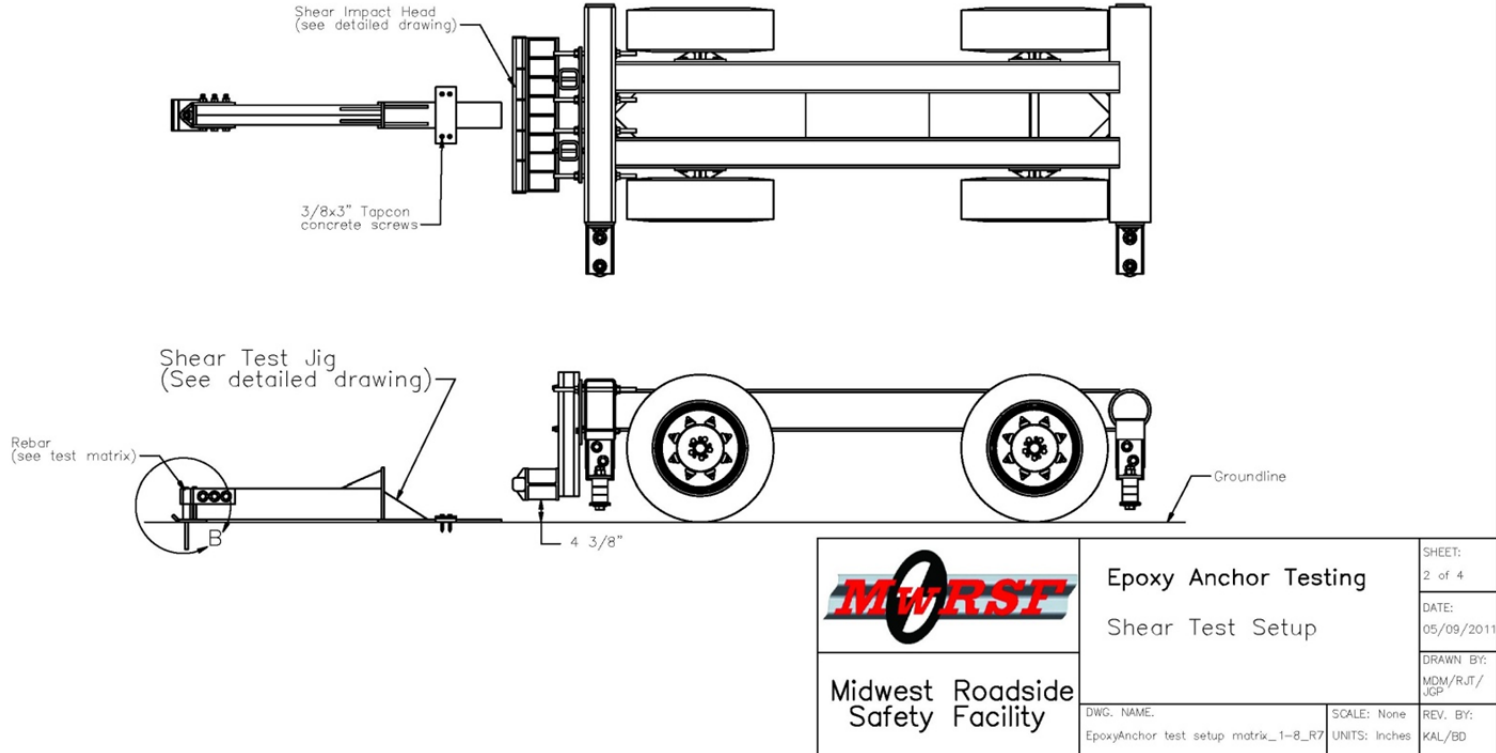
 Midwest Roadside Safety Facility	Epoxy Anchor Testing Tension Test Setup	SHEET: 1 of 4
	DWG. NAME: EpoxyAnchor test setup matrix_1-8_R7	SCALE: None UNITS: Inches
		DRAWN BY: MDM/RJT/ JGP
		REV. BY: KAL/BD

Figure F-1. Tension Test Setup, Test Nos. WEAB-1 Through WEAB-4 and WEAB-7 Through WEAB-8

Epoxy Anchor Rebar Bogie Testing—Shear Test Setup

1. Bogie No. 3 – Small Bogie with Shear Impact Head
2. Speed = 10 mph
3. One high-speed digital camera perpendicular
4. One high-speed digital camera perpendicular zoomed in on the shear test jig and rebar.
5. JVC digital video
6. DTS and EDR-3
7. Note any installation issues or problems in fieldbook.
8. Note failure mode in fieldbook.
9. Each test must be at least 2' from any previous test anchor holes to prevent anchor spacing and edge spacing issues from affecting results.
10. Epoxy and epoxy-coated rebar will be donated.
11. Before installation of anchors, measure the bar deformation rib height as well as the epoxy coating thickness.
12. Tapcon concrete screws need to be replaced after each test.
13. Epoxy used for first round of testing will be Hilti HIT-RE 500.




 Midwest Roadside Safety Facility	Epoxy Anchor Testing Shear Test Setup	SHEET: 2 of 4
	DWG. NAME: EpoxyAnchor test setup matrix_1-8_R7	SCALE: None UNITS: Inches
		DRAWN BY: MDM/RJT/ JGP
		REV. BY: KAL/BD

Figure F-2. Shear Test Setup, Test Nos. WEAB-5 Through WEAB-6

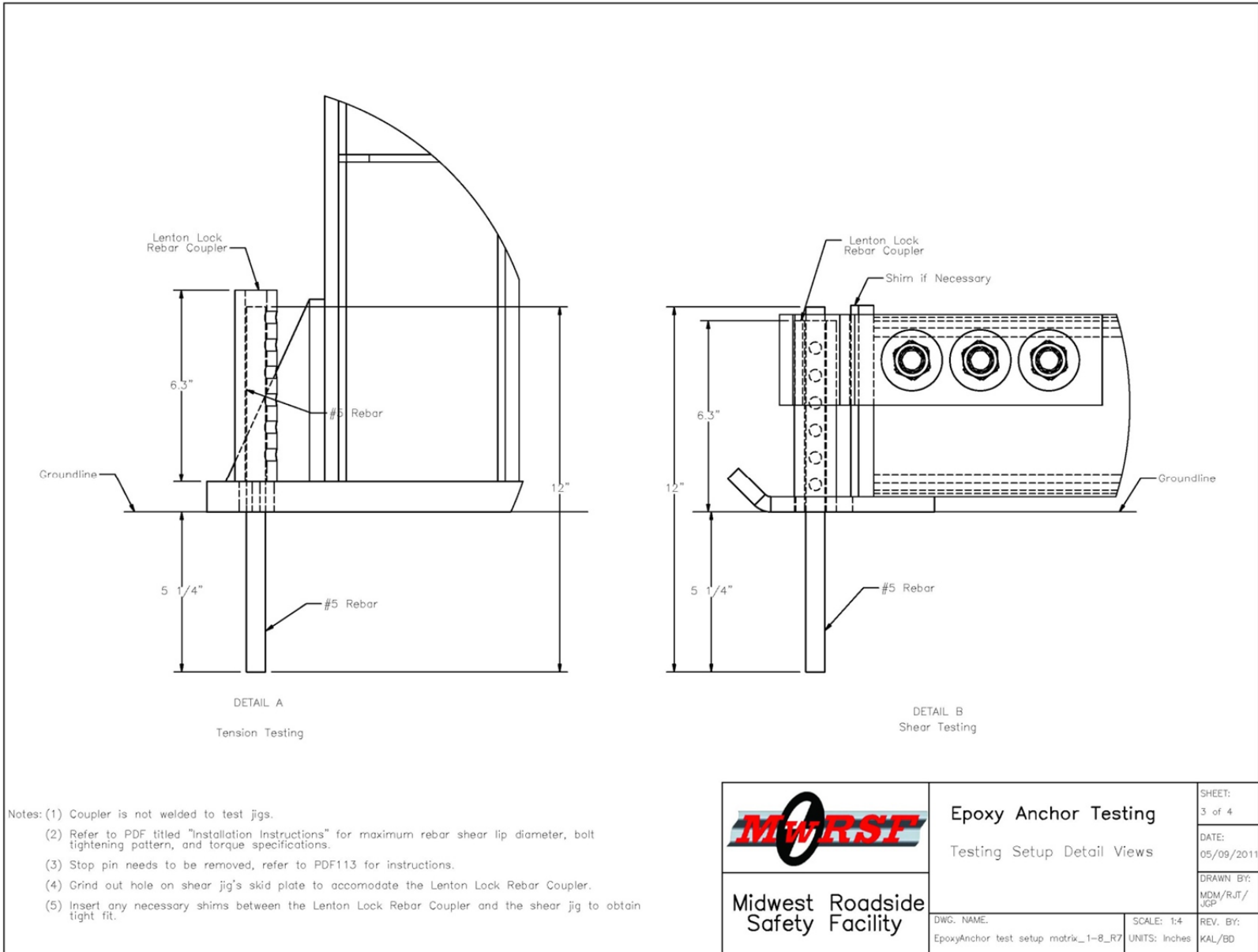


Figure F-3. Anchor Attachment Details, Test Nos. WEAB-1 Through WEAB-8

Test No.	Test Type	Bar Size	Bar Coating	Embedment Depth	Spacing	Speed
WEAB-1	Tensile	#5	None	5 1/4"	Single	10 mph
WEAB-2	Tensile	#5	None	5 1/4"	Single	10 mph
WEAB-3	Tensile	#5	Epoxy	5 1/4"	Single	10 mph
WEAB-4	Tensile	#5	Epoxy	5 1/4"	Single	10 mph
WEAB-5	Shear	#5	Epoxy	5 1/4"	Single	10 mph
WEAB-6	Shear	#5	Epoxy	5 1/4"	Single	10 mph
WEAB-7	Tensile	#5	Epoxy	5 1/4"	2 @ 8"	10 mph
WEAB-8	Tensile	#5	Epoxy	5 1/4"	2 @ 8"	10 mph


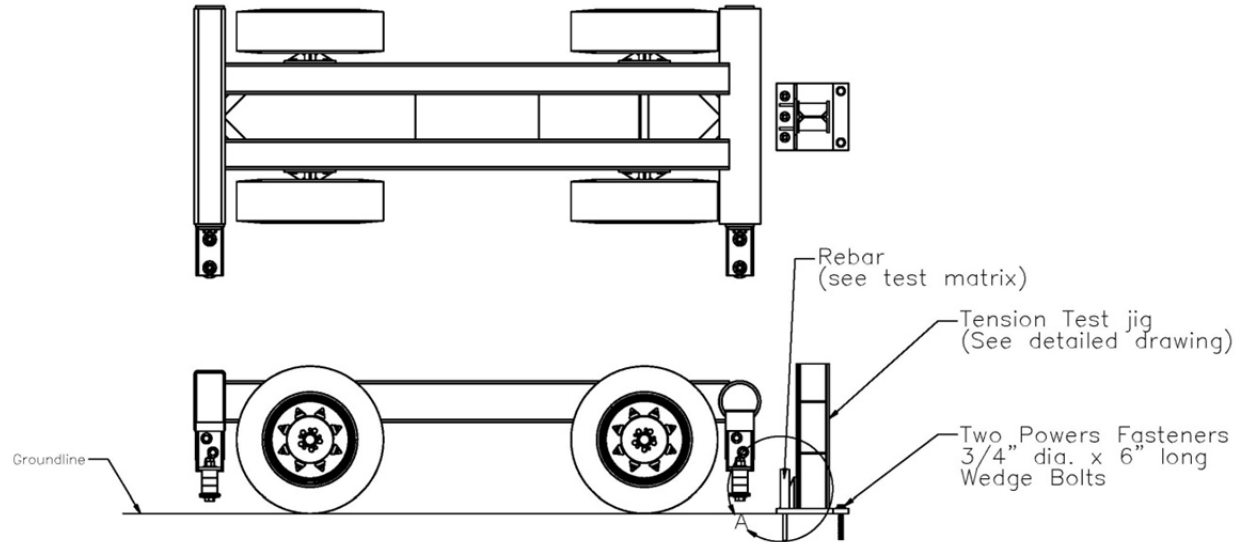
	Epoxy Anchor Testing	SHEET: 4 of 4
	Bogie Testing Matrix	DATE: 05/09/2011
Midwest Roadside Safety Facility	DWG. NAME: EpoxyAnchor test setup matrix_1-8_R7	SCALE: None UNITS: Inches
		REV. BY: KAL/BD
		DRAWN BY: MDM/RJT/ JGP

Figure F-4. Test Matrix, Test Nos. WEAB-1 Through WEAB-8

Epoxy Anchor Rebar Bogie Testing—Tensile Test Setup

1. Bogie No. 3 – Small Bogie with standard round impact head
2. Speed = 15 mph
3. One high-speed digital camera perpendicular
4. One high-speed digital camera perpendicular zoomed in on the tensile test jig and rebar.
5. JVC digital video
6. DTS and EDR-3
7. Note any installation issues or problems in fieldbook.
8. Note failure mode in fieldbook.
9. Each test must be at least 2' from any previous test anchor holes to prevent anchor spacing and edge spacing issues from affecting results.
10. Kick plate anchors must be replaced each test.
11. Epoxy and epoxy-coated rebar will be donated.
12. Before installation of anchors, measure the bar deformation rib height as well as the epoxy-coating thickness.
13. Bore out existing test jig anchor holes 1/8" to accommodate #6 reinforcing bars.
14. Anchors must be installed while the concrete temperature remains above 45° during curing time for the epoxy. If required, heat the concrete to the desired temperature.
15. Anchors are to be installed in same concrete slabs as used in test nos. WEAB 1–8.
16. Epoxy used for first round of testing will be Hilti HIT-RE 500-SD.



 Midwest Roadside Safety Facility	Epoxy Anchor Testing Tension Test Setup	SHEET: 1 of 4
		DATE: 04/15/2011
	DWG. NAME: EpoxyAnchor test setup matrix_9-13_R7	DRAWN BY: MDM/RJT/ JGP
	SCALE: None UNITS: Inches	REV. BY: KAL/BD

Figure F-5. Tension Test Setup, Test Nos. WEAB-9 Through WEAB-12

Epoxy Anchor Rebar Bogie Testing—Shear Test Setup

1. Bogie No. 3 – Small Bogie with Shear Impact Head
2. Speed = 10 mph
3. One high-speed digital camera perpendicular
4. One high-speed digital camera perpendicular zoomed in on the shear test jig and rebar.
5. JVC digital video
6. DTS and EDR-3
7. Note any installation issues or problems in fieldbook.
8. Note failure mode in fieldbook.
9. Each test must be at least 2' from any previous test anchor holes to prevent anchor spacing and edge spacing issues from affecting results.
10. Epoxy and epoxy-coated rebar will be donated.
11. Before installation of anchors, measure the bar deformation rib height as well as the epoxy coating thickness.
12. Tapcon concrete screws need to be replaced after each test.
13. Bore out existing test jig anchor holes to a total diameter of 2" to accommodate increased rebar coupler size due to #6 rebar.
14. Anchors must be installed while the concrete temperature remains above 45° during curing time for the epoxy. If required, heat the concrete to the desired temperature.
15. Anchors are to be installed in same concrete slabs as used in test nos. WEAB 1–8.
16. Epoxy used for first round of testing will be Hilti HIT-RE 500-SD.

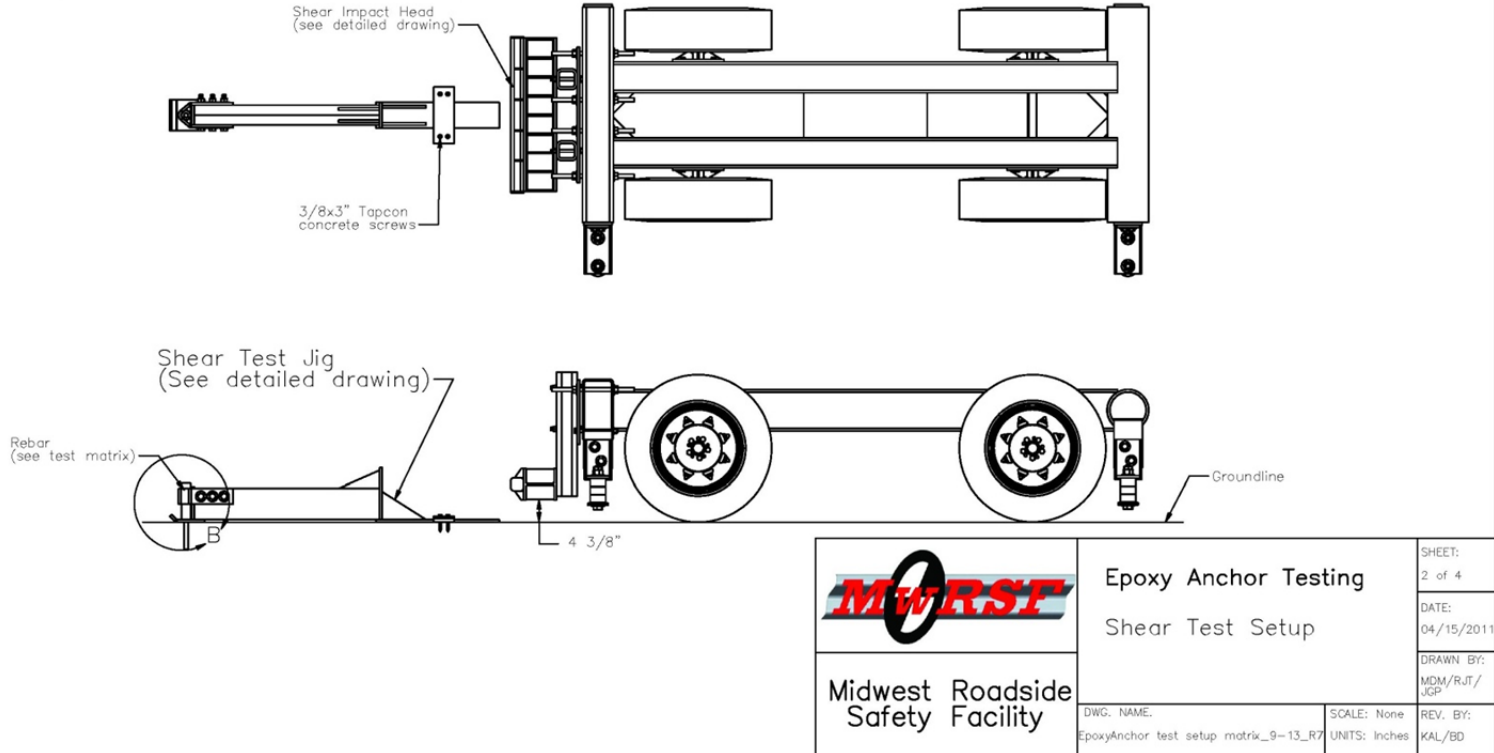


Figure F-6. Shear Test Setup, Test No. WEAB-13

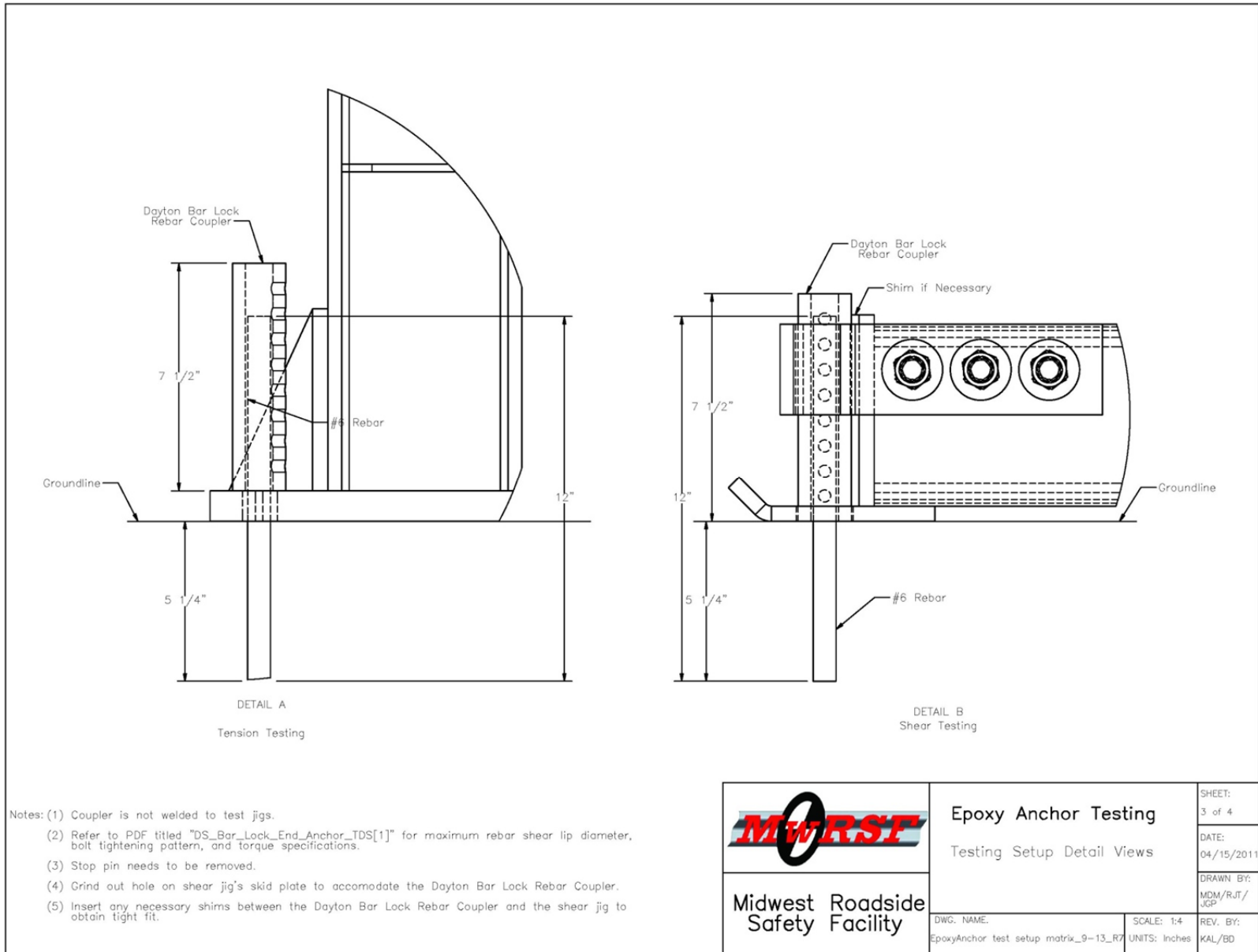


Figure F-7. Anchor Attachment Details, Test Nos. WEAB-9 Through WEAB-13

Test No.	Test Type	Bar Size	Bar Coating	Embedment Depth	Spacing	Speed
WEAB-9	Tensile	#6	Epoxy	5 1/4"	Single	15 mph
WEAB-10	Tensile	#6	Epoxy	5 1/4"	Single	15 mph
WEAB-11	Tensile	#6	Epoxy	5 1/4"	2 @ 8"	15 mph
WEAB-12	Tensile	#6	Epoxy	5 1/4"	2 @ 8"	15 mph
WEAB-13	Shear	#6	Epoxy	5 1/4"	Single	10 mph


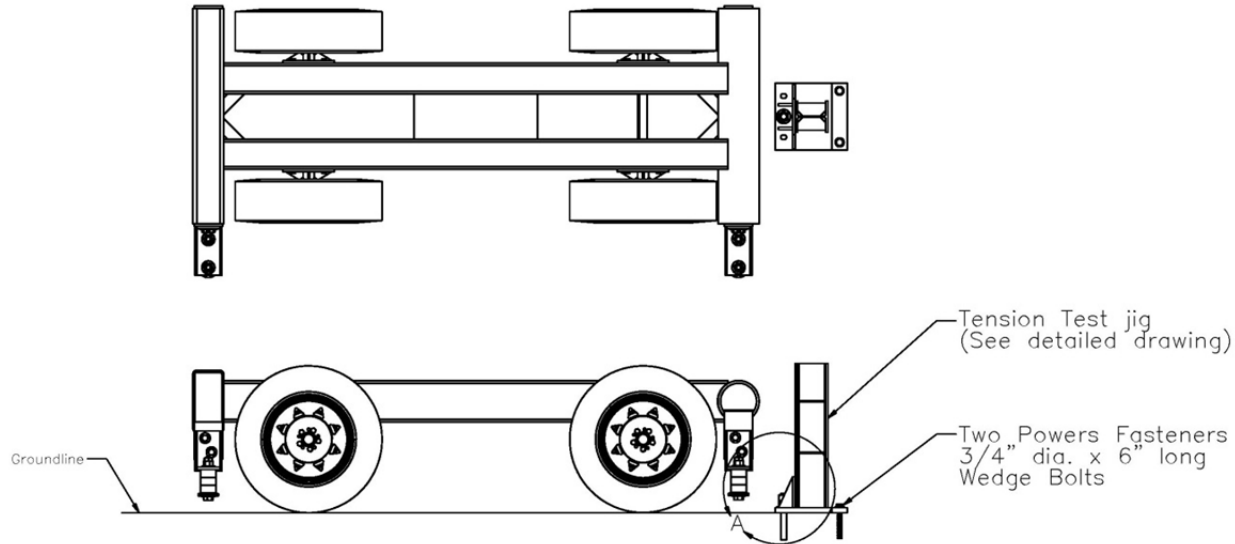
	Epoxy Anchor Testing	SHEET: 4 of 4
	Bogie Testing Matrix	DATE: 04/15/2011
Midwest Roadside Safety Facility	DWG. NAME: EpoxyAnchor test setup matrk_9-13_R7	DRAWN BY: MDM/RJT/ JGP
	SCALE: None UNITS: Inches	REV. BY: KAL/BD

Figure F-8. Test Matrix, Test Nos. WEAB-9 Through WEAB-13

Epoxy Anchor Rebar Bogie Testing—Tensile Test Setup

1. Bogie No. 3 – Small Bogie with standard round impact head
2. Speed = 15 mph
3. One high-speed digital camera perpendicular
4. One high-speed digital camera perpendicular zoomed in on the tensile test jig and anchor.
5. JVC digital video
6. DTS and EDR-3
7. Note any installation issues or problems in fieldbook.
8. Note failure mode in fieldbook.
9. Each test must be at least 2' from any previous test anchor holes to prevent anchor spacing and edge spacing issues from affecting results.
10. Kick plate anchors must be replaced each test.
11. Anchors must be installed while the concrete temperature remains above 45° during curing time for the epoxy. If required, heat the concrete to the desired temperature.
12. Anchors are to be installed in same concrete slabs as used in test nos. WEAB 1–13.
13. Epoxy used for third round of testing will be Hilti HIT-RE 500-SD.
14. 1 1/8" A307 rods with 5 1/4" embedment.
15. Tension jig must be modified to have larger slot. See sheet 3 of "EpoxyAnchor Tensile_R3".




 Midwest Roadside Safety Facility	Epoxy Anchor Testing Tension Test Setup	SHEET: 1 of 4
		DATE: 06/02/2011
	DWG. NAME: EpoxyAnchor_testsetupmatrk_14-15_R3	DRAWN BY: JGP/MDM
	SCALE: None UNITS: Inches	REV. BY: RWB/BJD

Figure F-9. Tension Test Setup, Test No. WEAB-14

Epoxy Anchor Rebar Bogie Testing—Shear Test Setup

1. Bogie No. 3 – Small Bogie with Shear Impact Head
2. Speed = 10 mph
3. One high-speed digital camera perpendicular
4. One high-speed digital camera perpendicular zoomed in on the shear test jig and anchor.
5. JVC digital video
6. DTS and EDR-3
7. Note any installation issues or problems in fieldbook.
8. Note failure mode in fieldbook.
9. Each test must be at least 2' from any previous test anchor holes to prevent anchor spacing and edge spacing issues from affecting results.
10. Tapcon concrete screws need to be replaced after each test.
11. Anchors must be installed while the concrete temperature remains above 45° during curing time for the epoxy. If required, heat the concrete to the desired temperature.
12. Anchors are to be installed in same concrete slabs as used in test nos. WEAB 1–13.
13. Epoxy used for third round of testing will be Hilti HIT-RE 500-SD.
14. 1 1/8" A307 rods with 5 1/4" embedment.
15. Shear jig must be modified with fabricated plug. See sheet 2 and 5 of "EpoxyAnchor_shear_R3".

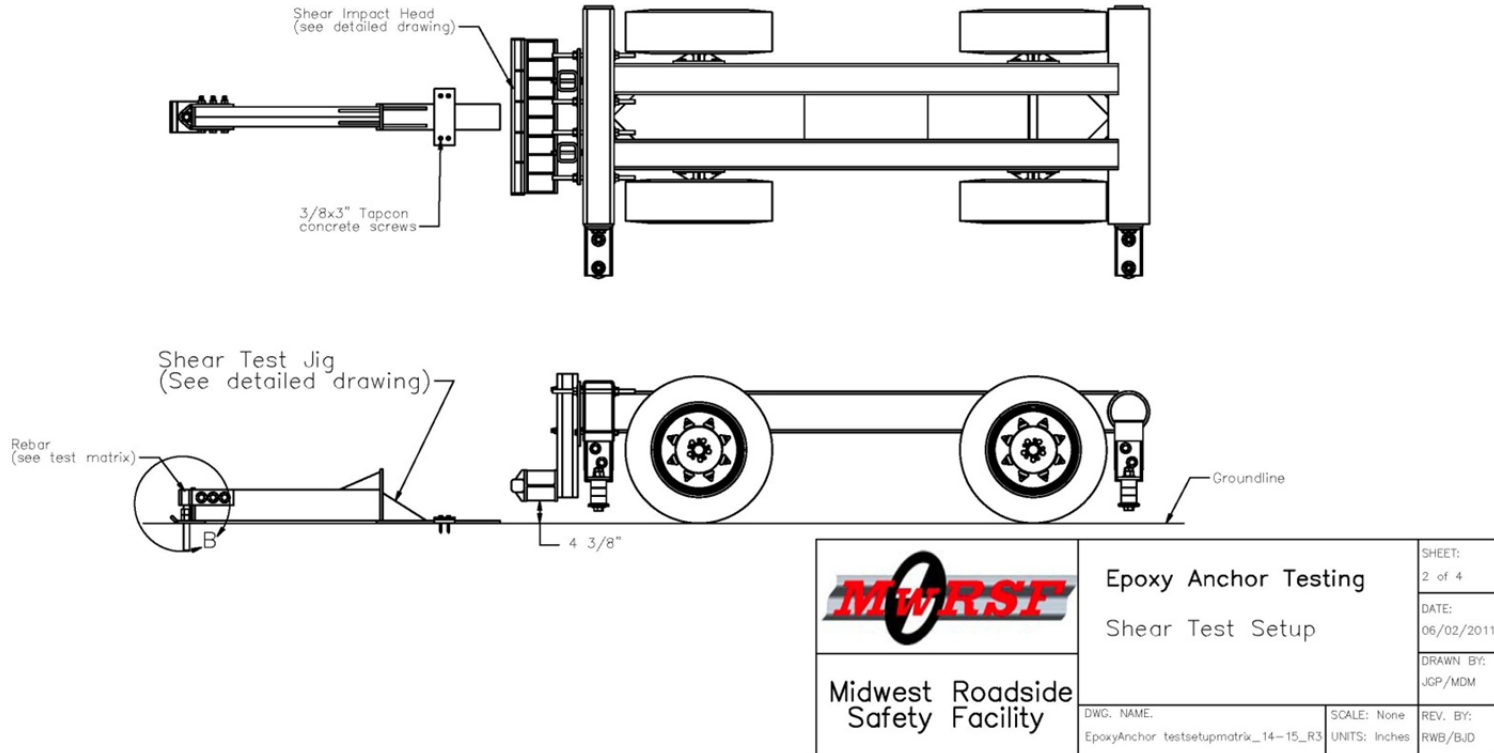


Figure F-10. Shear Test Setup, Test No. WEAB-15

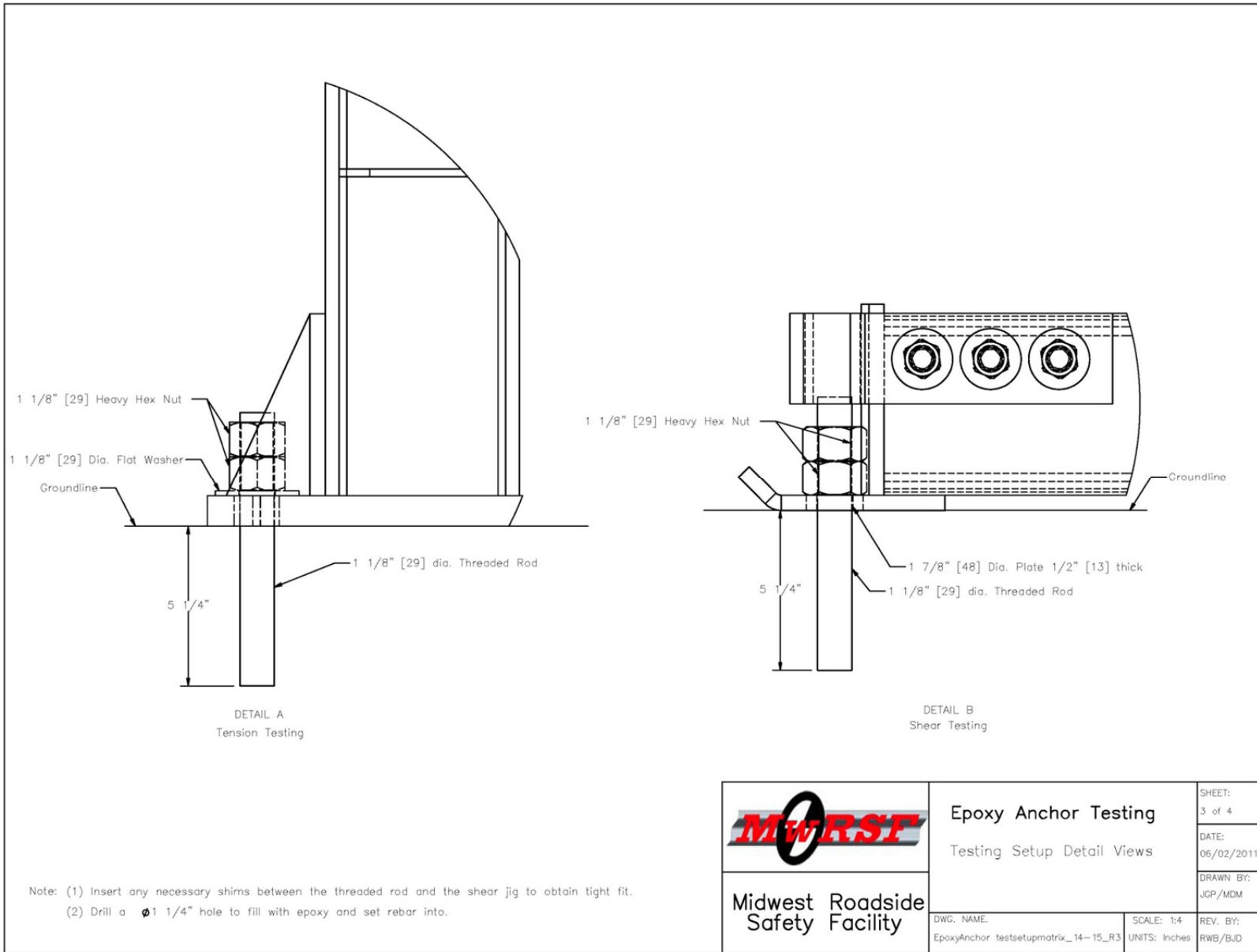
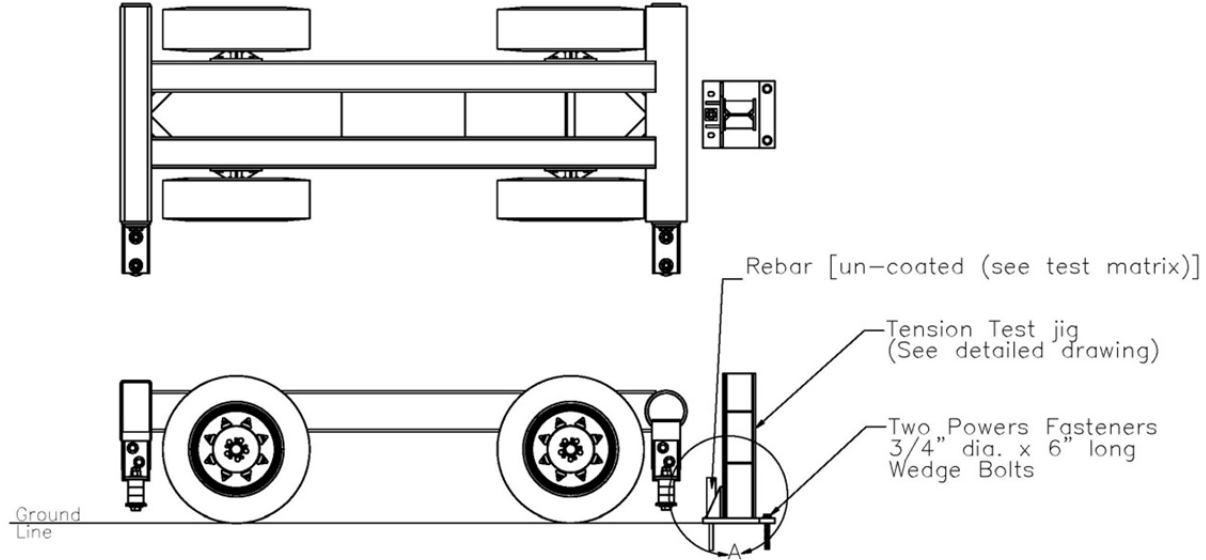


Figure F-11. Anchor Attachment Details, Test Nos. WEAB-14 and WEAB-15

Epoxy Anchor Rebar Bogie Testing—Tensile Test Setup

1. Bogie No. 3 – Small Bogie with standard round impact head
2. Speed = 15 mph
3. One high-speed digital camera perpendicular
4. One high-speed digital camera perpendicular zoomed in on the tensile test jig and rebar.
5. JVC digital video
6. DTS and EDR-3
7. Note any installation issues or problems in fieldbook.
8. Note failure mode in fieldbook.
9. Each test must be at least 2' from any previous test anchor holes to prevent anchor spacing and edge spacing issues from affecting results.
10. Kick plate anchors must be be replaced each test.
11. Before installation of anchors, measure the bar deformation rib height.
12. Anchors must be installed while the concrete temperature remains above 45° during curing time for the epoxy. If required, heat the concrete to the desired temperature.
13. Anchors are to be installed in same concrete slabs as used in test nos. WEAB 1–15.
14. Epoxy used for fourth round of testing will be Hilti HIT-RE 500-SD.




 Midwest Roadside Safety Facility	Epoxy Anchor Testing Tension Test Setup	SHEET: 1 of 3
	DWG. NAME: EpoxyAnchor test setup_matrix_16_R1	SCALE: None UNITS: Inches

Figure F-13. Tension Test Setup, Test No. WEAB-16

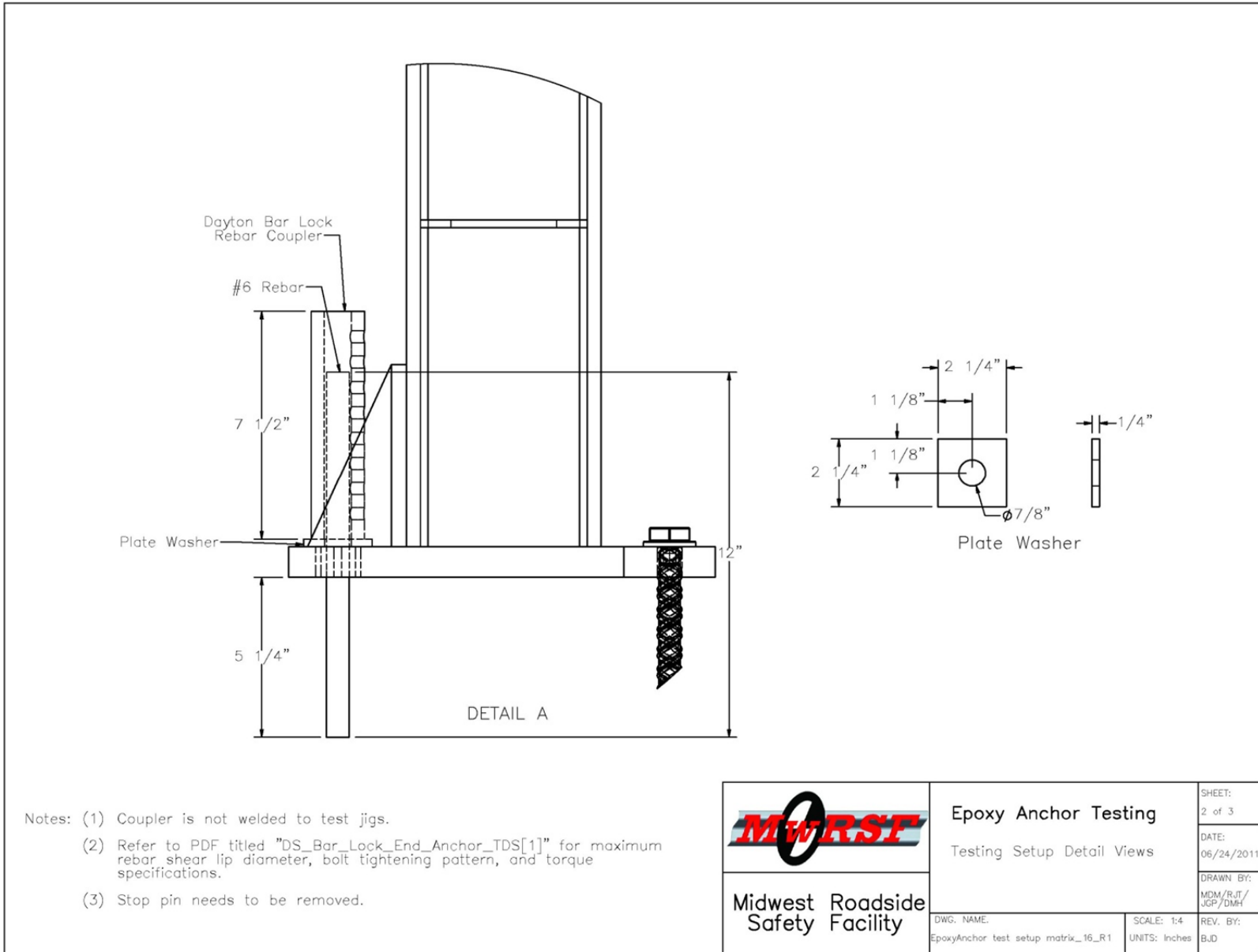
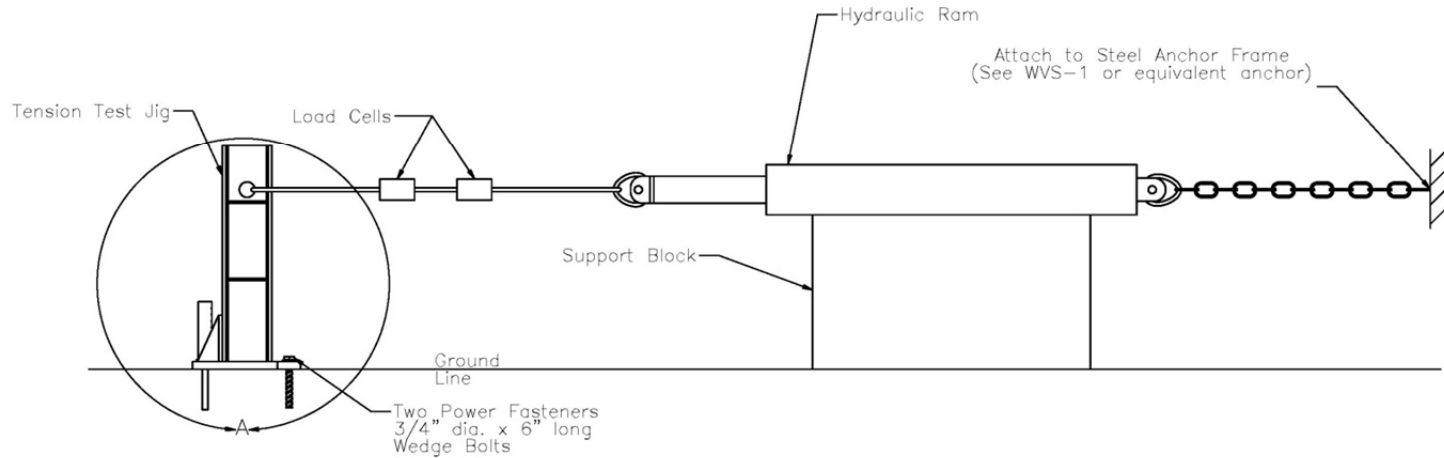


Figure F-14. Anchor Attachment Details, Test No. WEAB-16

Epoxy Anchor Rebar Static Testing—Tensile Test Setup

1. Hydraulic Ram
2. One high-speed digital camera perpendicular
3. One high-speed digital camera perpendicular zoomed in on the tensile test jig and rebar.
4. JVC digital video
5. Two Load Cells
6. Note any installation issues or problems in fieldbook.
7. Note failure mode in fieldbook.
8. Each test must be at least 2' from any previous test anchor holes to prevent anchor spacing and edge spacing issues from affecting results.
9. Kick plate anchors must be replaced each test.
10. Before installation of anchors, measure the bar deformation rib height.
11. Anchors must be installed while the concrete temperature remains above 45° during curing time for the epoxy. If required, heat the concrete to the desired temperature.
12. Anchors are to be installed in same concrete slabs as used in test nos. WEAB 1–15.
13. Epoxy used for fourth round of testing will be Hilti HIT-RE 500-SD.




 Midwest Roadside Safety Facility	Epoxy Anchor Testing Static Test Setup	SHEET: 1 of 3
	DWG. NAME: EpoxyAnchor test setup matrix_17_R1	SCALE: None UNITS: Inches

Figure F-16. Tension Test Setup, Test No. WEAB-17

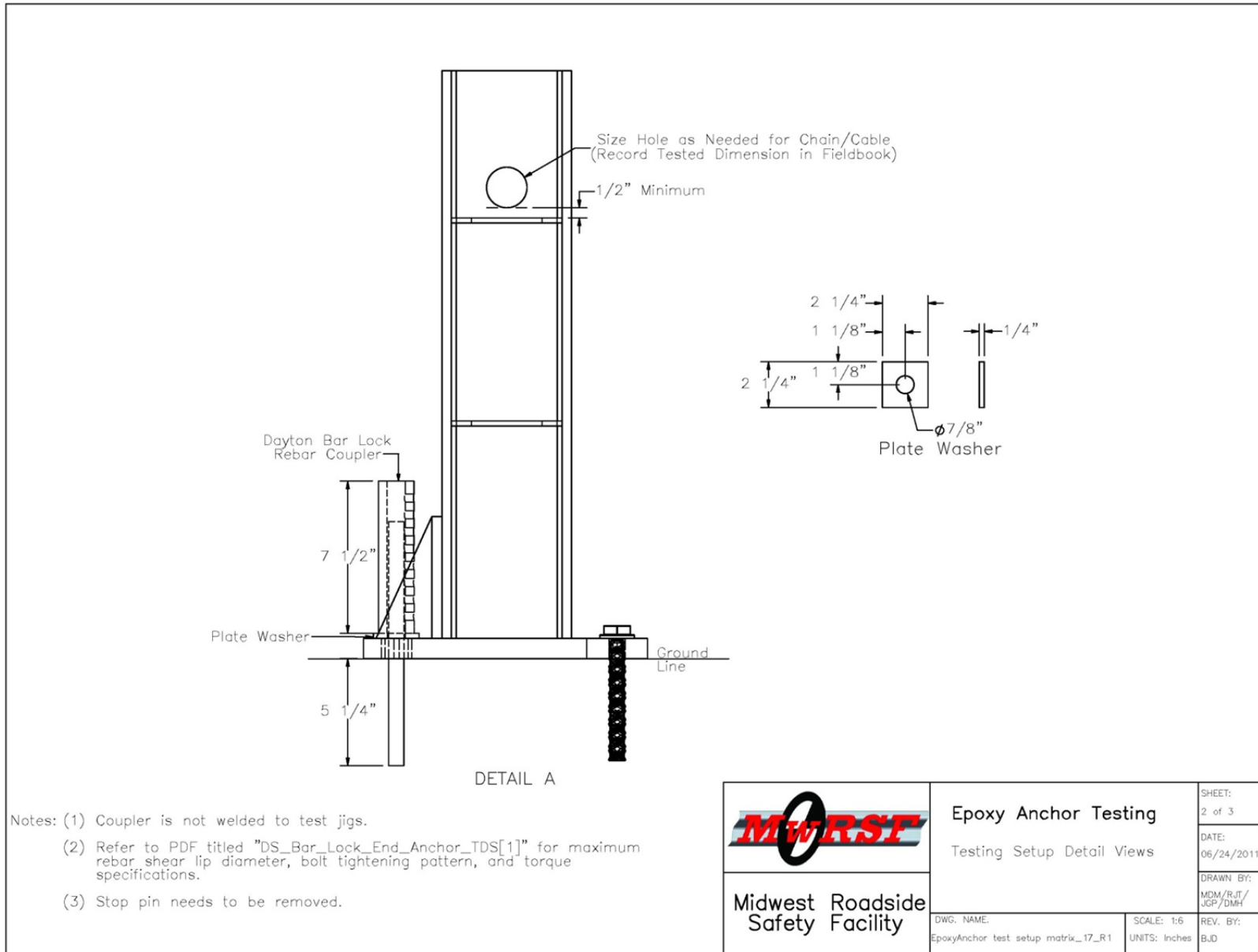


Figure F-17. Anchor Attachment Details, Test No. WEAB-17

Test No.	Test Type	Bar Size	Bar Coating	Embedment Depth	Spacing	Speed
WEAB-17	Tensile	#6	None	5 1/4"	Single	Static

	Epoxy Anchor Testing		SHEET: 3 of 3
	Bogie Testing Matrix		DATE: 06/24/2011
Midwest Roadside Safety Facility			DRAWN BY: MDM/RJT/ JGP/DMH
	DWG. NAME: EpoxyAnchor test setup matrix_17_R1	SCALE: None UNITS: Inches	REV. BY: BUD

Figure F-18. Test Matrix, Test No. WEAB-17

Appendix G. Material Specifications


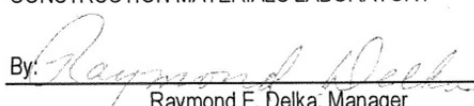
		LINCOLN OFFICE 825 J Street Lincoln, NE 68508 402/479-2200	
		COMPRESSION TEST OF Cylindrical CONCRETE SPECIMENS ASTM Designation: C39-03	
Client:	UNL	Date:	December 10, 2010
Project:	MwRSF		
Placement Location:	WI - East 1, 2, 3		
Mix Type:	Class:	Mix No.:	
Type of Forms		Cement Factor, Sks/Yd	na
		Water-Cement Ratio	na
Admixture Quantity	na	Slump Inches	na
Admixture Type	na	Unit Wt, lbs/cu. Ft.	na
Admixture Quantity	na	Air Content, %	na
Average Field Temperature	na	Batch Volume, Cu. Yds.	na
Temperature of Concrete F	na	Ticket No.	na
Identification Laboratory	East 1	East 2	East 3
Date Cast			
Date Received in Laboratory	11/30/2010	11/30/2010	11/30/2010
Date Tested			
Days Cured in Field			
Days Cured in Laboratory			
Age of Test, Days			
Length, in.	7.78	7.81	7.75
Average Width (1), in.	3.72	3.72	3.72
Cross-Sectional Area, sq. in.	10.874	10.869	10.874
Maximum Load, lbf	71,030	76,470	73,310
Compressive Strength, psi	6,530	7,040	6,740
Length/Diameter Ratio	2.091	2.099	2.083
Correction			
Corrected Compressive Strength, psi	0	0	0
Type of Fracture	4	4	4
Required Strength, psi			
Remarks: All concrete break data in this report was produced by Benesch personnel using ASTM Standard Methods and Practices unless otherwise noted. This report shall not be reproduced except in full, without the written approval of Alfred Benesch & Company <div style="text-align: right;"> ALFRED BENESCH & COMPANY CONSTRUCTION MATERIALS LABORATORY By:  Raymond E. Delka, Manager </div>			

Figure G-1. Concrete Cylinder Test Results



LINCOLN OFFICE
825 J Street
Lincoln, NE 68508
402/479-2200

COMPRESSION TEST OF Cylindrical CONCRETE SPECIMENS
ASTM Designation: C39-03

Client:	UNL		Date:	December 13, 2010	
Project:	MwRSF				
Placement Location:	WI - Epoxy West 4 & 5				
Mix Type:	Class:		Mix No.:		
Type of Forms			Cement Factor, Sks/Yd	na	
			Water-Cement Ratio	na	
Admixture Quantity	na		Slump inches	na	
Admixture Type	na		Unit Wt, lbs/cu. Ft.	na	
Admixture Quantity	na		Air Content, %	na	
Average Field Temperature	na		Batch Volume, Cu. Yds.	na	
Temperature of Concrete F	na		Ticket No.	na	
Identification Laboratory	4	5			
Date Cast					
Date Received in Laboratory	12/13/2010	12/13/2010			
Date Tested					
Days Cured in Field					
Days Cured in Laboratory					
Age of Test, Days	na	na			
Length, in.	8.05	8.06			
Average Width (1), in.	3.91	3.90			
Cross-Sectional Area, sq. in.	11.977	11.952			
Maximum Load, lbf	71,500	71,630			
Compressive Strength, psi	5,970	5,990			
Length/Diameter Ratio	2.061	2.065			
Correction					
Corrected Compressive Strength, psi	0	0			
Type of Fracture	3	3			
Required Strength, psi					

Remarks:

All concrete break data in this report was produced by Benesch personnel using ASTM Standard Methods and Practices unless otherwise noted.

This report shall not be reproduced except in full, without the written approval of Alfred Benesch & Company

ALFRED BENESCH & COMPANY
CONSTRUCTION MATERIALS LABORATORY

By:

Raymond E. Delka
Raymond E. Delka, Manager

Figure G-2. Concrete Cylinder Test Results

SOLD AMBASSADOR STEEL CORP.
 PO BOX 2340
 TO: KOKOMO, IN 46904-2340

NUCOR
 BAR MILL GROUP
 NUCOR STEEL KANKAKEE, INC.

CERTIFIED MILL TEST REPORT

Ship from:
 Nucor Steel Kankakee, Inc.
 One Nucor Way
 Bourbonnais, IL 60914
 815-937-3131

Page: 1

SHIP AMBASSADOR STEEL CORP-EPOXY
 FOR EPOXY COATING ONLY
 TO: KOKOMO, IN 00000-

Date: 1-May-2009
 B.L. Number: 389597
 Load Number: 5576035

Material Safety Data Sheets are available at www.nucorbar.com or by contacting your inside sales representative.

NEM-03 March 24, 2009

HEAT NUM. *	DESCRIPTION	PHYSICAL TESTS					CHEMICAL TESTS												
		YIELD P.S.I.	TENSILE P.S.I.	ELONG % IN 8"	BEND	WT% DEF	C	Ni	Mn	Cr	P	Mo	S	V	Si	Co	Cu	Sn	C.E.
	FOR EPOXY COATING																		
PO# => KN0910079201	0000076035 Nucor Steel - Kankakee Inc 16/#5 Rebar 60' A615M Gr 420 (Gr60) ASTM A615/A615M-08b GR 60[420] Melted 02/10/09 Rolled 02/16/09	68,608 473MPa	103,937 717MPa	13.8%	OK	-3.6%	.38	.88	.013	.051	.20	.34	.56	.035	.24	.14	.080	.007	.001
PO# => KN0910079301	0000078035 Nucor Steel - Kankakee Inc 16/#5 Rebar 60' A615M Gr 420 (Gr60) ASTM A615/A615M-08b GR 60[420] Melted 02/10/09 Rolled 02/16/09	74,128 511MPa	108,672 749MPa	10.0%	OK	-3.2%	.40	.94	.015	.047	.19	.41	.59	.034	.24	.18	.078	.008	.001

I HEREBY CERTIFY THAT THE ABOVE FIGURES ARE CORRECT AS CONTAINED IN THE RECORDS OF THE CORPORATION.

ALL MANUFACTURING PROCESSES OF THE STEEL MATERIALS IN THIS PRODUCT, INCLUDING MELTING, HAVE OCCURRED WITHIN THE UNITED STATES. ALL PRODUCTS PRODUCED ARE WELD FREE. MERCURY, IN ANY FORM, HAS NOT BEEN USED IN THE PRODUCTION OR TESTING OF THIS MATERIAL.

QUALITY ASSURANCE: Curtis Glenn



268

Figure G-3. Reinforcing Steel Specifications, Test Nos. WEAB-1 Through WEAB-8

November 26, 2012
 MwRSF Report No. TRP-03-264-12



CMC STEEL TEXAS
1 STEEL MILL DRIVE
SEGUIN TX 78155-7510

CERTIFIED MILL TEST REPORT
For additional copies call
830-372-8771

We hereby certify that the test results are accurate and conform to the reported grade and specification

Daniel J. Schacht
Daniel J. Schacht
Quality Assurance Manager

HEAT NO.:3011610 SECTION: REBAR 19MM (#6) 40'0" 420/60 GRADE: ASTM A615-08b Gr 420/60 ROLL DATE: 08/29/2009 MELT DATE: 08/29/2009	S O L D T O	ABC Coating Co - Tulsa 2236 S Yukon Ave Tulsa OK US 74107-2765 9185852587	S H I P T O	ABC Coating Co - Tulsa 2236 S Yukon Ave Tulsa OK US 74107-2765 9185852587	Delivery#: 80183653 BOL#: 70057675 CUST PO#: 09-0811A CUST P/N: DLVRY LBS / HEAT: 30280.000 LB DLVRY PCS / HEAT: 504 EA
--	----------------------------	---	----------------------------	---	--

Characteristic	Value	Characteristic	Value	Characteristic	Value
Yield Strength test 1	62.9ksi				
Tensile Strength test 1	100.4ksi				
Elongation test 1	15%				
Elongation Gage Lgth test 1	8IN				
Bend Test Diameter	3.750IN				
Bend Test	Passed				

THIS MATERIAL IS FULLY KILLED, 100% MELTED AND MANUFACTURED IN THE USA, WITH NO WELD REPAIR OR MERCURY CONTAMINATION IN THE PROCESS.
REMARKS :

09/01/2009 13:33:34
Page 1 OF 1

Figure G-4. Reinforcing Steel Specifications, Test Nos. WEAB-9 Through WEAB-13

269

November 26, 2012
MWRSF Report No. TRP-03-264-12

Revised April 2011

ABC Coating Company, Inc. (An Acuña Co.)

Line 2: Drum Date: (Start):

Line 1: Drum Date: (Start):

Epoxy Coated Reinforcing Steel Test Record

Line 2: Drum Date: (Empty):

Line 1: Drum Date: (Empty):

Oklahoma

Preheat Temperature: 438

Line 1: 1/4 1/2 3/4 Full

Line 2: 1/4 1/2 3/4 Full

Date: 1-17-11

Gel Time: 9 Seconds

Valspar 720A009:

Shift: 004

Boxes Used: 111

3M - Scotchkote - 413:

Coating Lines: 1 & 2

Holidays Line 1: 19-210

DuPont 7-2719:

41010057848

Holidays Line 2: 19-448

Mill	Heat Number	Size / Grade	Length	Qty	30 Readings	Bend Test
CML	3011610	191420 40-0 25	99	11010 88999	11010 88999	11010 88999
CML	3011610	191420 40-0 25	110	999110 999	11010 88999	11010 88999
CML	3011610	191420 40-0 25	1010	88999110 109110	11010 88999	11010 88999
CML	3011610	191420 40-0 25	99	11010 88999	11010 88999	11010 88999
CML	3011610	191420 40-0 25	110	999110 999	11010 88999	11010 88999
CML	3011610	191420 40-0 25	1010	88999110 109110	11010 88999	11010 88999
CML	3011610	191420 40-0 25	99	11010 88999	11010 88999	11010 88999

Mill	Heat Number	Size / Grade	Length	Qty	30 Readings	Bend Test
CML	3011610	191420 40-0 25	99	11010 88999	11010 88999	11010 88999
CML	3011610	191420 40-0 25	110	999110 999	11010 88999	11010 88999
CML	3011610	191420 40-0 25	1010	88999110 109110	11010 88999	11010 88999
CML	3011610	191420 40-0 25	99	11010 88999	11010 88999	11010 88999
CML	3011610	191420 40-0 25	110	999110 999	11010 88999	11010 88999
CML	3011610	191420 40-0 25	1010	88999110 109110	11010 88999	11010 88999
CML	3011610	191420 40-0 25	99	11010 88999	11010 88999	11010 88999
CML	3011610	191420 40-0 25	110	999110 999	11010 88999	11010 88999
CML	3011610	191420 40-0 25	1010	88999110 109110	11010 88999	11010 88999
CML	3011610	191420 40-0 25	99	11010 88999	11010 88999	11010 88999
CML	3011610	191420 40-0 25	110	999110 999	11010 88999	11010 88999
CML	3011610	191420 40-0 25	1010	88999110 109110	11010 88999	11010 88999

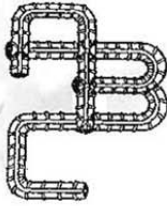
Certified by:

Lbs.: 51,555

Plant Operator: ERDIN IBERA

Quality Control: [Signature]

Figure G-5. Reinforcing Steel Specifications, Test Nos. WEAB-9 Through WEAB-13



ABC COATING COMPANY, INC.

P. O. BOX 9693
TULSA, OKLAHOMA 74157-0693
(918) 585-2587
FAX (918) 585-8131

AN ACUÑA CO.

DATE SHIPPED:	<u>1/24/2011</u>	CONTRACTOR:	<u>CONCRETE INDUSTRIES</u>
INVOICE NO:	<u>37859</u>	COUNTY:	<u>LINCOLN, NE</u>
OUR JOB NO:	<u>NE 447 #1</u>	PROJECT:	<u>CUSTOMER STOCK 201</u>
CUSTOMER:	<u>CONCRETE INDUSTRIES</u>	CUSTOMER PO:	<u>8000</u>

Gentlemen:

This is to certify that the materials used, the preparation of the bars, coating and curing were done in accordance with the Nebraska State Highway Department Specifications for Epoxy Coated Reinforcing Steel (6-14-0379) for the above referenced project. No rebar contains more than two (2) holidays per lineal foot.

MILL	SIZE	HEAT	WEIGHT	LOT NO.	POWDER
CMC-TX	#5(16MM)	3019186	24,406	H1010057437	DUPONT
CMC-TX	#6(19MM)	3011610	12,016	H1010057848	DUPONT
TOTAL			36,422 #		

STATE OF OKLAHOMA)
)
 COUNTY OF ROGERS)

SUBSCRIBED AND SWORN TO BEFORE ME, a Notary Public in and for said County and State, on this the 18th Day of January, 2011.

[Signature]
 Notary Public in and for ROGERS County
 State of Oklahoma



My commission No. 02012302 expires 8-24-2014.

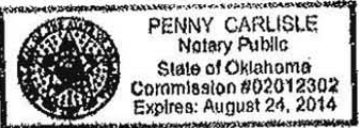


Figure G-6. Reinforcing Steel Specifications, Test Nos. WEAB-9 Through WEAB-13
271



DuPont Industrial Coating Solutions
9800 Genard Rd,
Houston, Texas 77041
Tel. (713) 939-4000
Fax (713) 939-4025
www.dupontpowder.com

ISO 9001



TO WHOM IT MAY CONCERN:

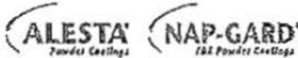
This is to certify that the batch number of Nap-Gard 7-2719 Rebar listed below is chemically the same material that was tested by Valley Forge Laboratories Inc. of Devon, Pennsylvania to A775. I certify that it meets the requirements of Annex A1 of A775-00. Nap-Gard 7-2750 Rebar also meets the requirements of ASTM D3963-93a and AASHTO M284-95.

The following batch was manufactured in the United States.

<u>Lot Number</u>	<u>Batch Number</u>	<u>Batch Size (Lbs)</u>
H1010057848	071001101021B	5000

Sincerely,

Mike Wittenhagen
Quality Control Manager



Alesta® and Nap-Gard® are registered trademarks of E. I. du Pont de Nemours and Company for its brand of Powder Coatings. Only DuPont makes Alesta® and Nap-Gard®.

WARRANTY POLICY: Seller certifies that all coatings delivered to Customer in unopened factory filled containers meet all pertinent quality standards presented in its current published literature. Since matters of surface preparation, application procedures, curing procedures and other local factors that affect coating performance are beyond Seller's control, Seller assumes no liability for coating failure other than to supply replacement material for a coating material proven to be defective. Customer will determine suitability of this product for its use and thereby assumes all risks and liabilities in connection therewith. Seller will not be liable for any injuries, damages or other losses derived, directly or indirectly, from or as a consequence of Customer's use of the product. SELLER DISCLAIMS ALL OTHER WARRANTIES, EXPRESS OR IMPLIED, RELATING TO ITS PRODUCTS AND THEIR APPLICATION, INCLUDING BUT NOT LIMITED TO WARRANTIES OF MERCHANTABILITY AND FITNESS FOR PARTICULAR PURPOSES.

Figure G-7. Reinforcing Steel Specifications, Test Nos. WEAB-9 Through WEAB-13

Appendix H. Bogie Test Results

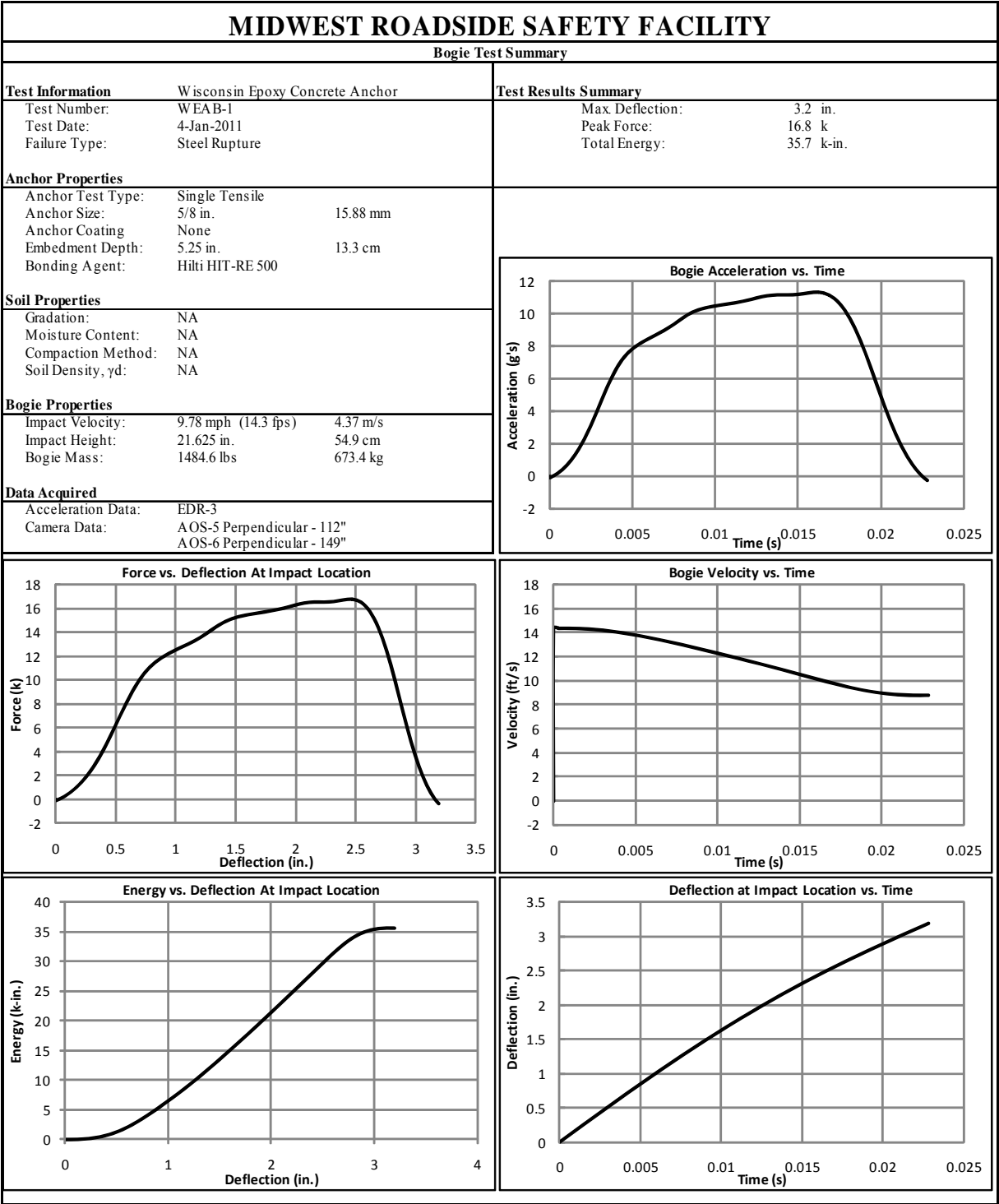


Figure H-1. Results of Test No. WEAB-1 (EDR-3)

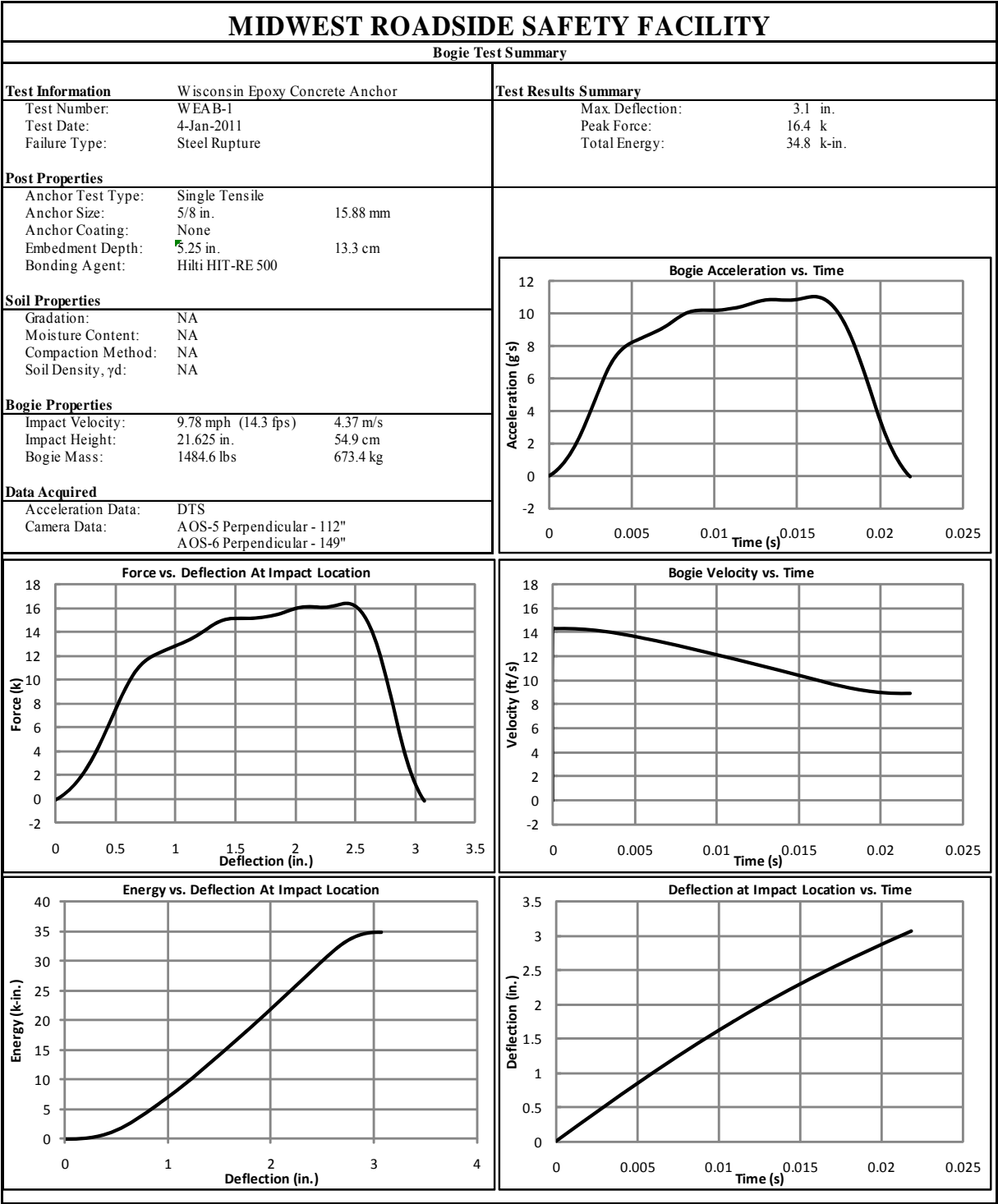


Figure H-2. Results of Test No. WEAB-1 (DTS)

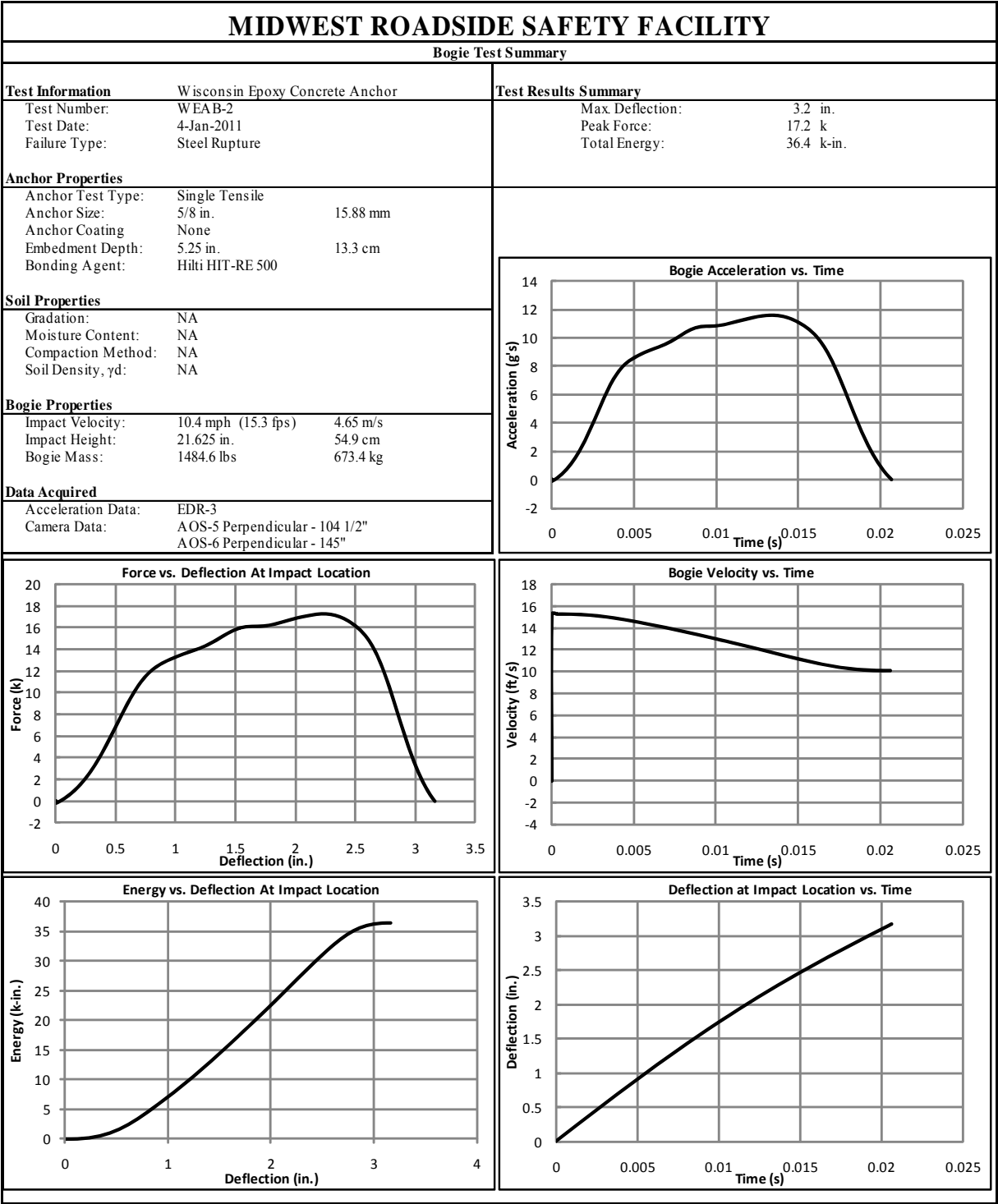


Figure H-3. Results of Test No. WEAB-2 (EDR-3)

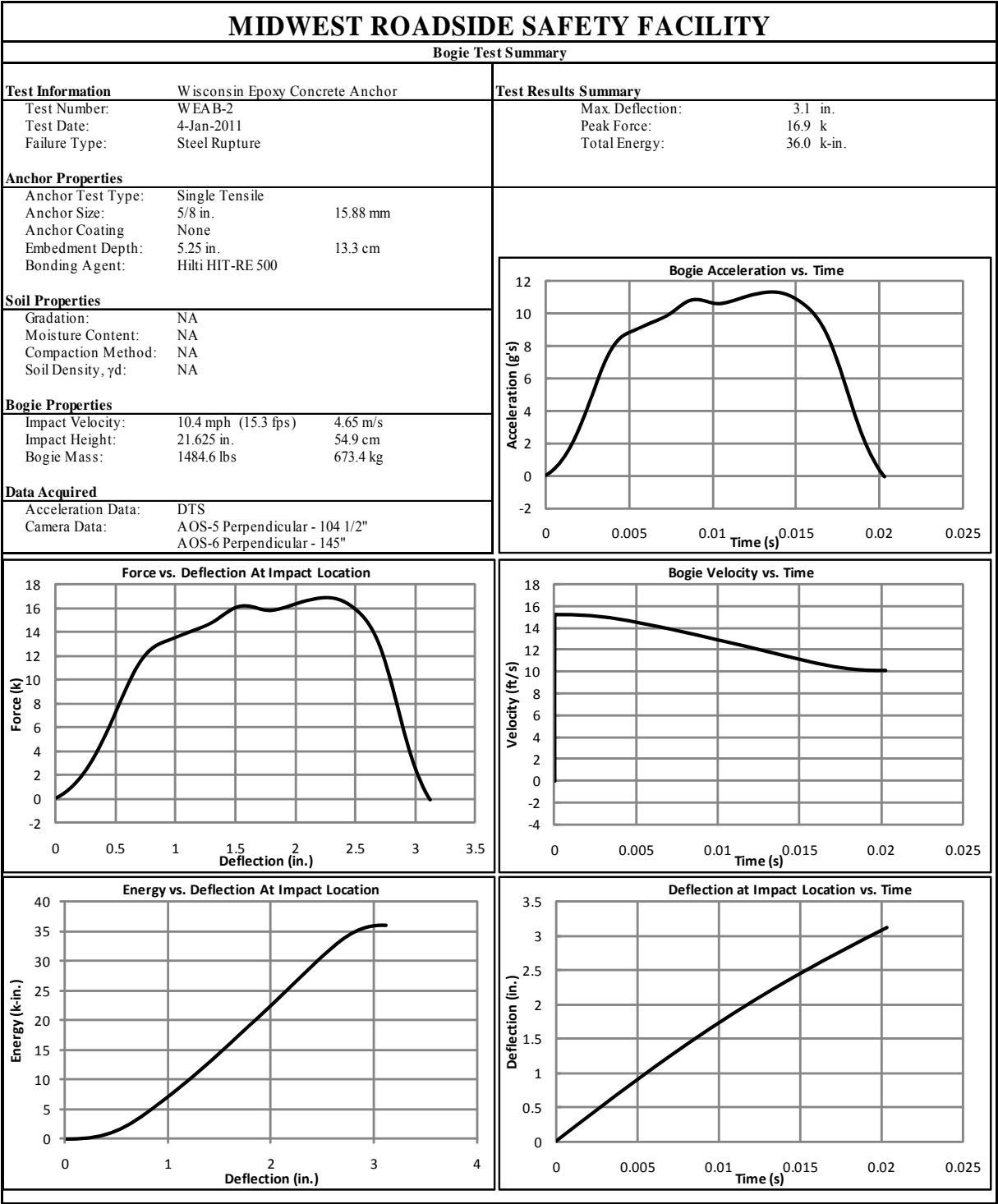


Figure H-4. Results of Test No. WEAB-2 (DTS)

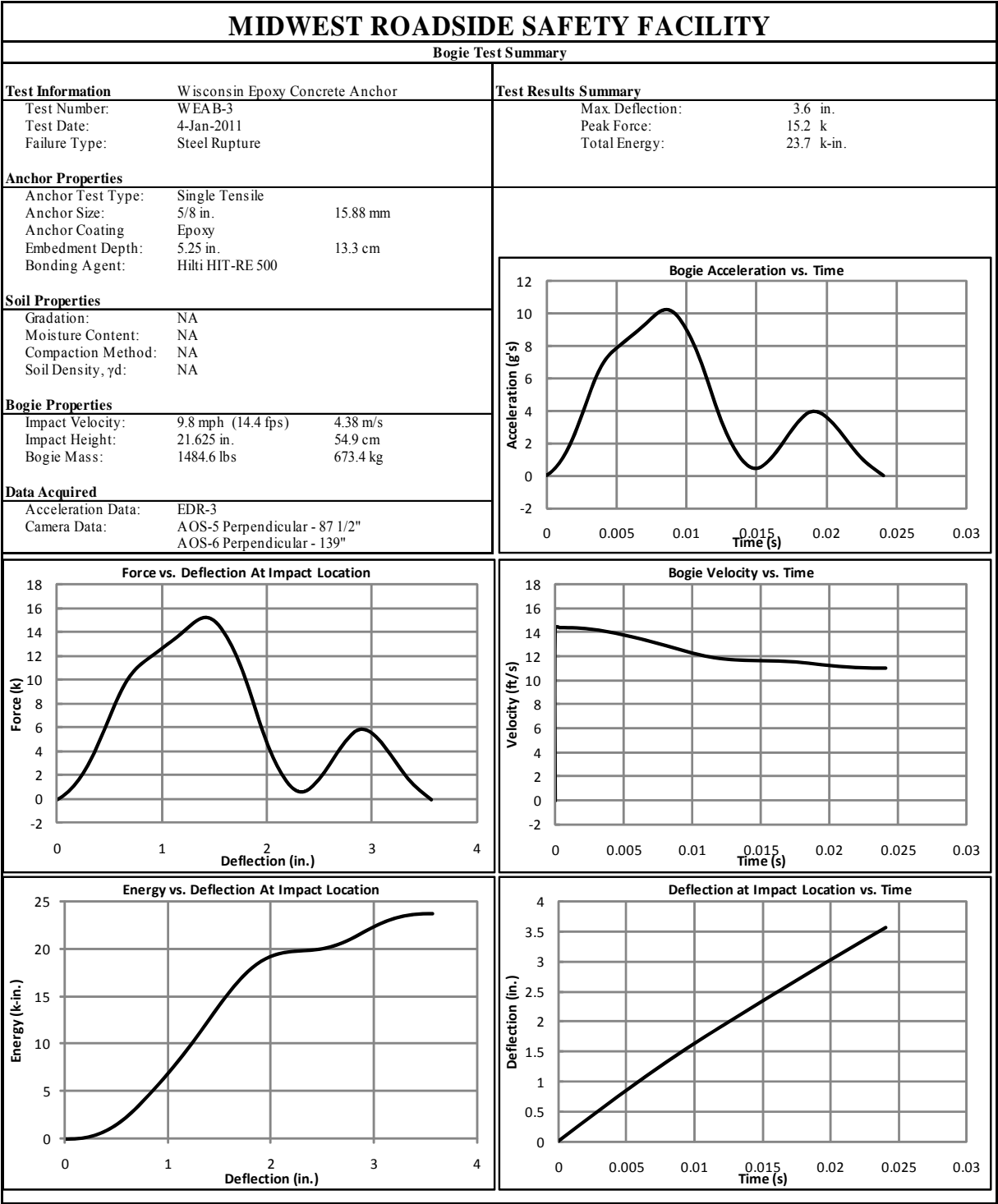


Figure H-5. Results of Test No. WEAB-3 (EDR-3)

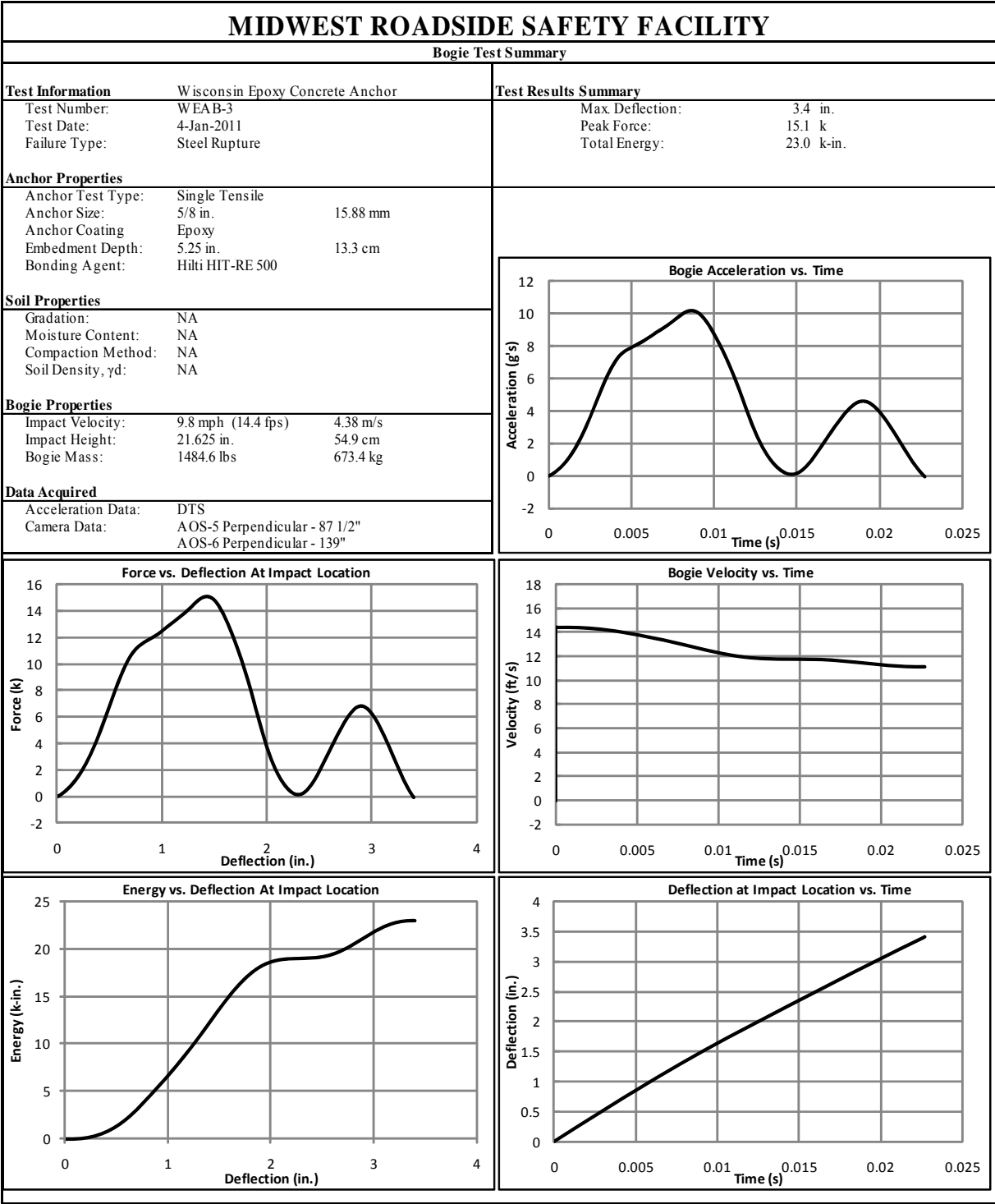


Figure H-6. Results of Test No. WEAB-3 (DTS)

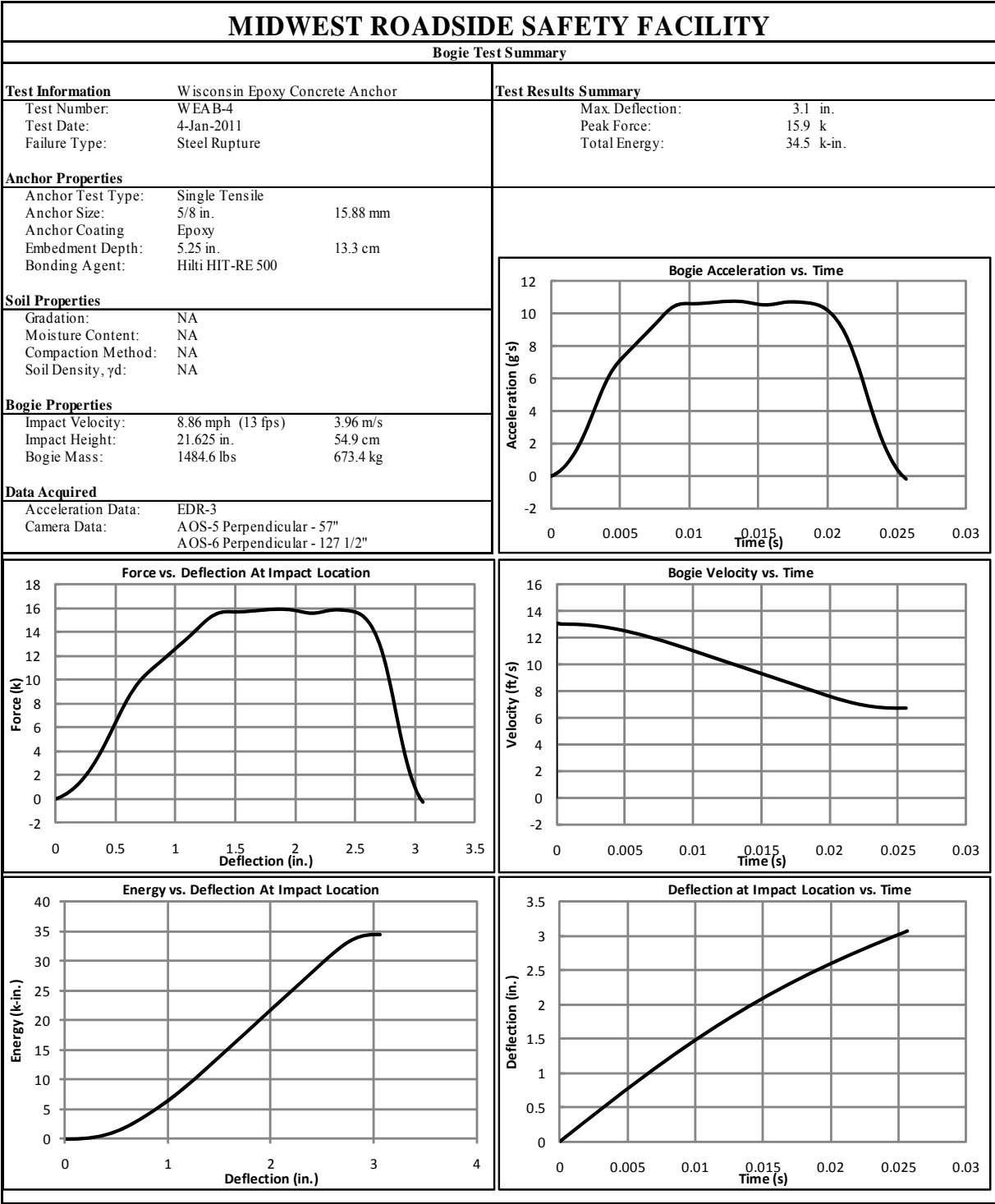


Figure H-7. Results of Test No. WEAB-4 (EDR-3)

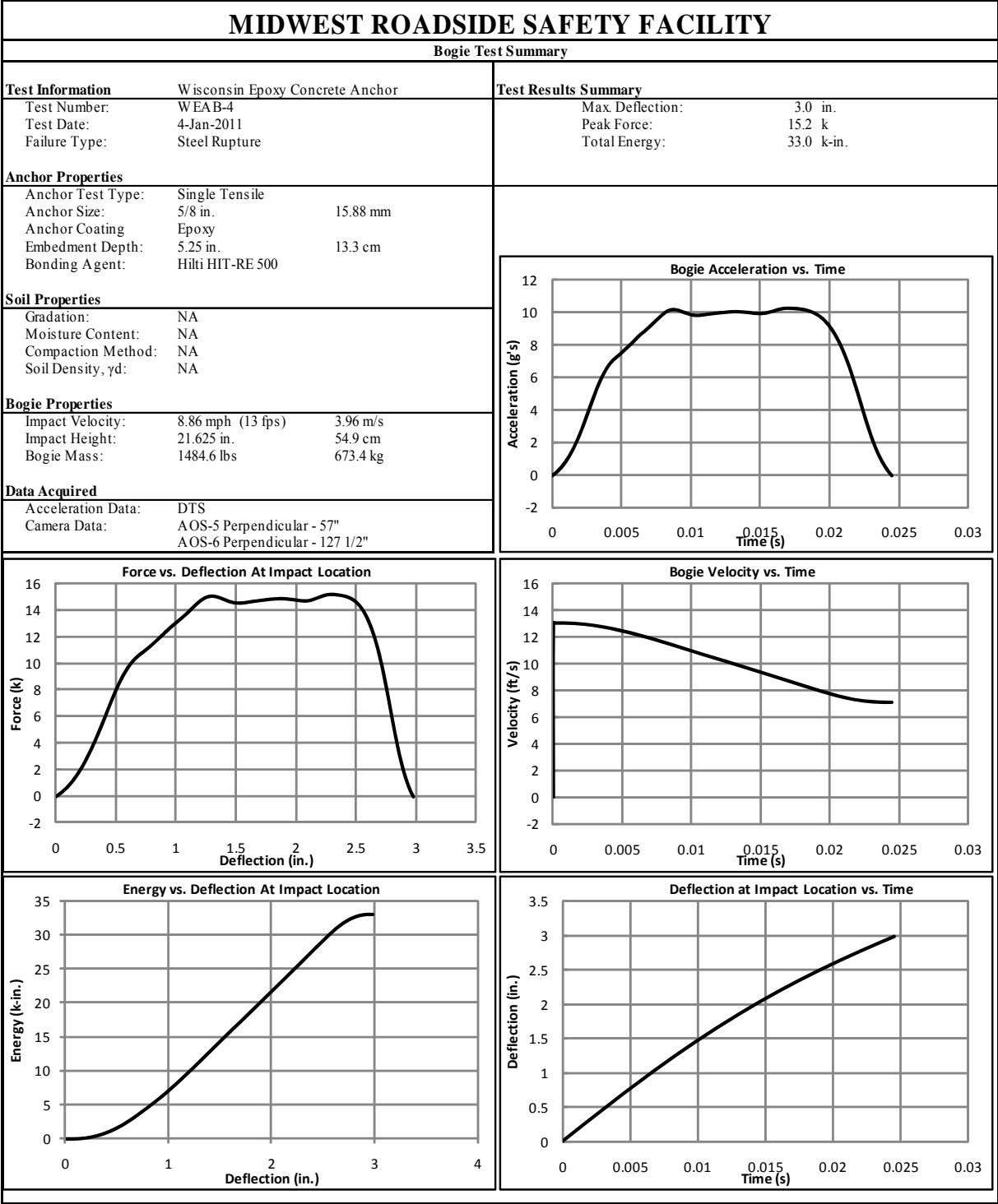


Figure H-8. Results of Test No. WEAB-4 (DTS)

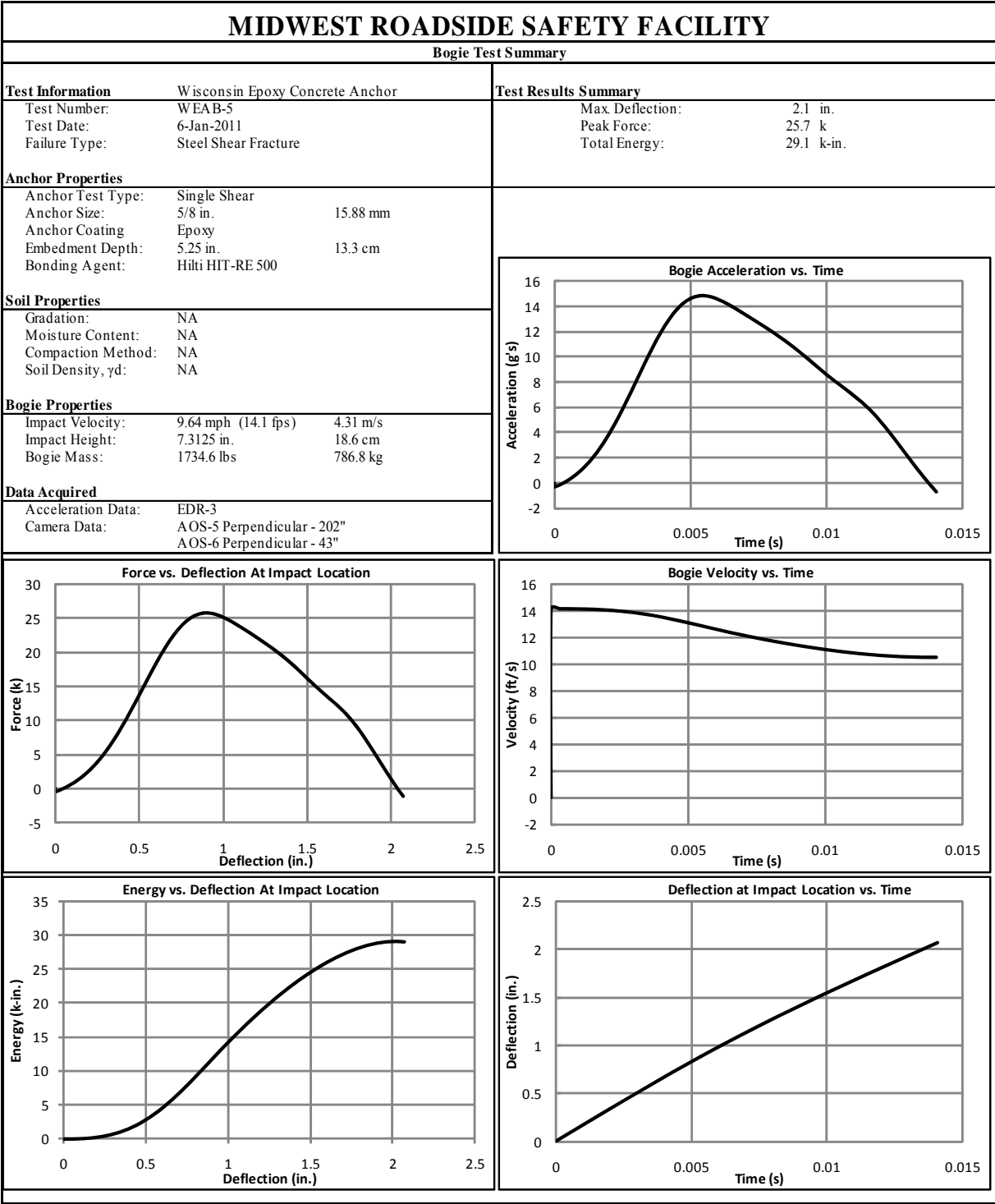


Figure H-9. Results of Test No. WEAB-5 (EDR-3)

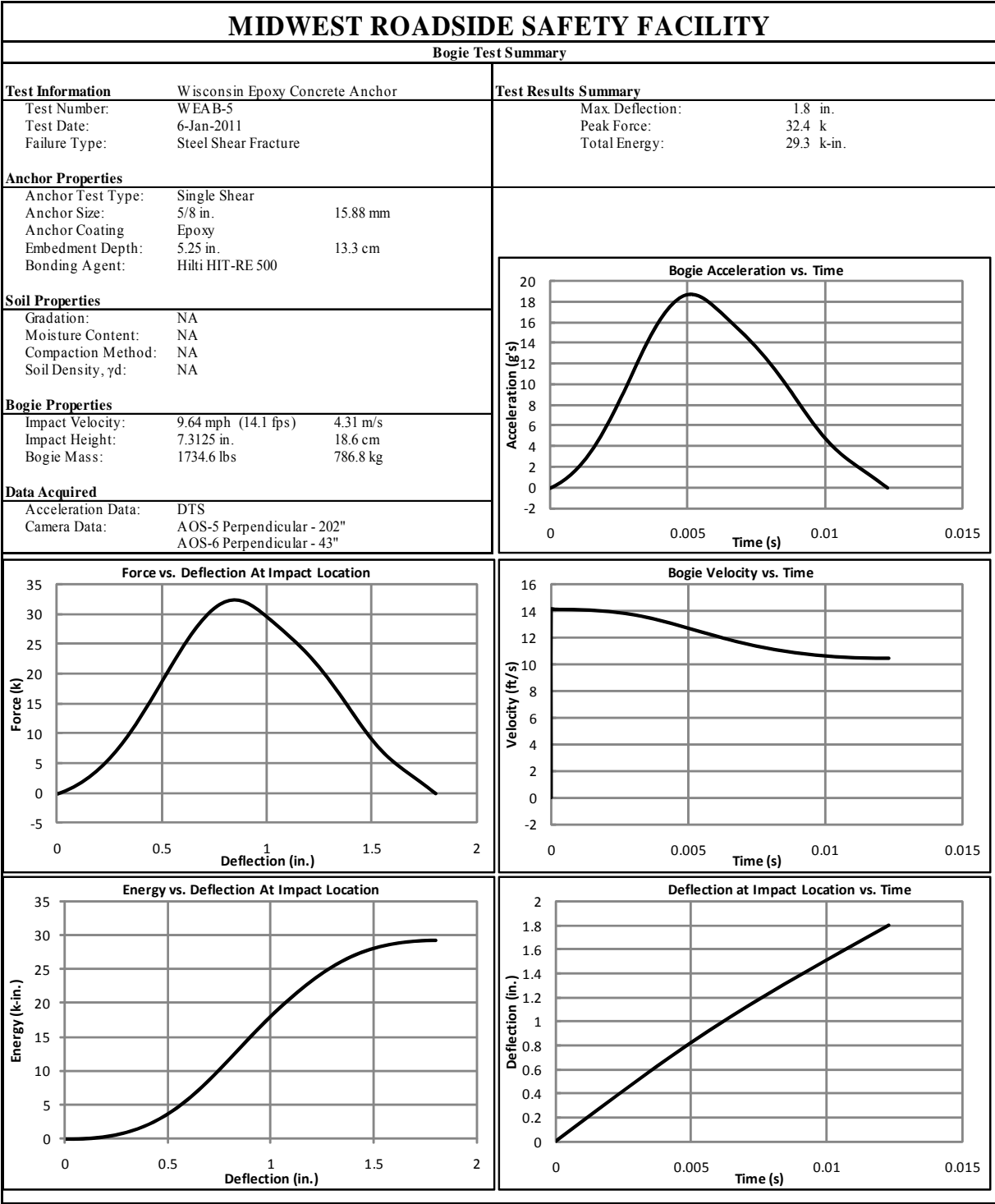


Figure H-10. Results of Test No. WEAB-5 (DTS)

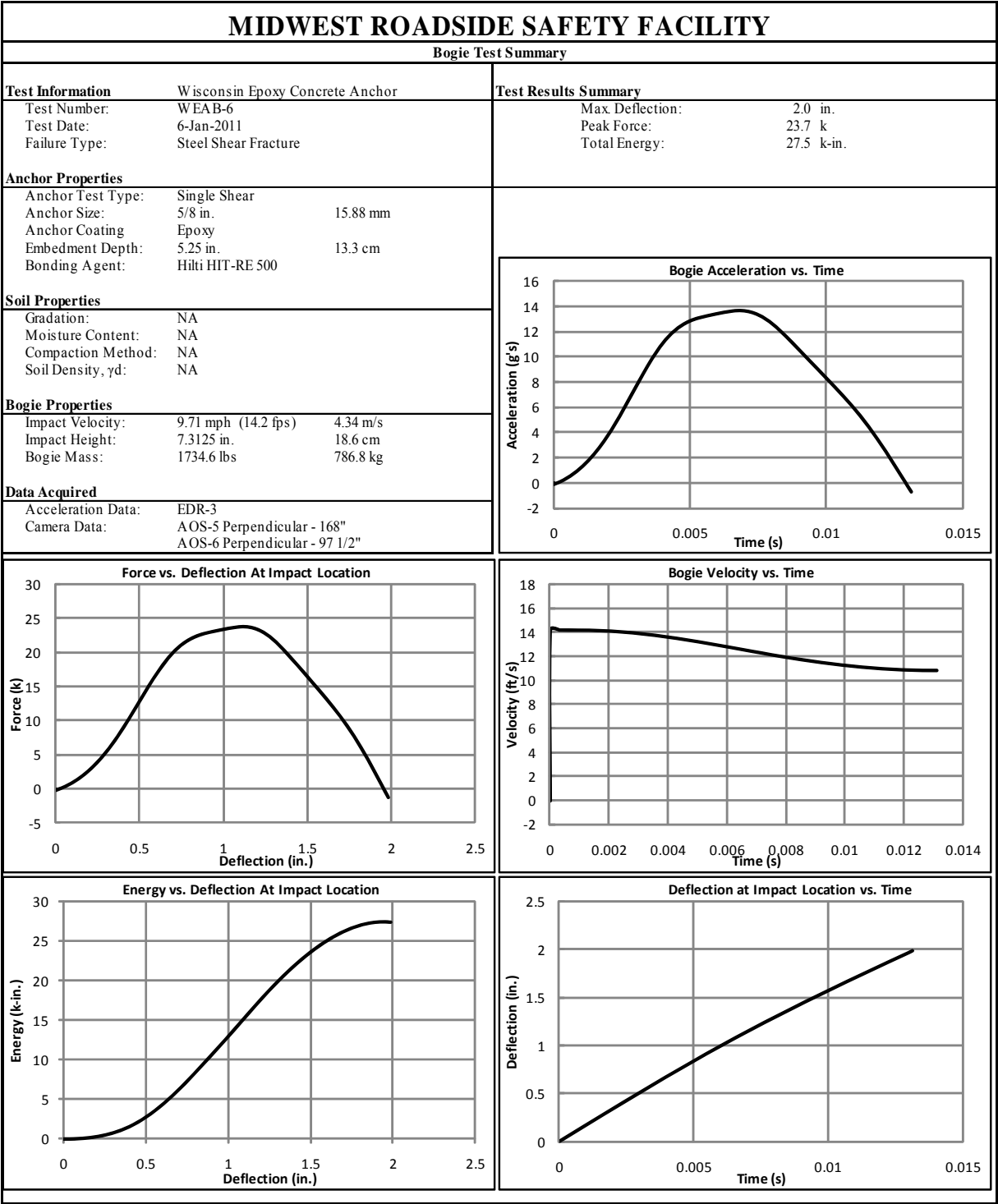


Figure H-11. Results of Test No. WEAB-6 (EDR-3)

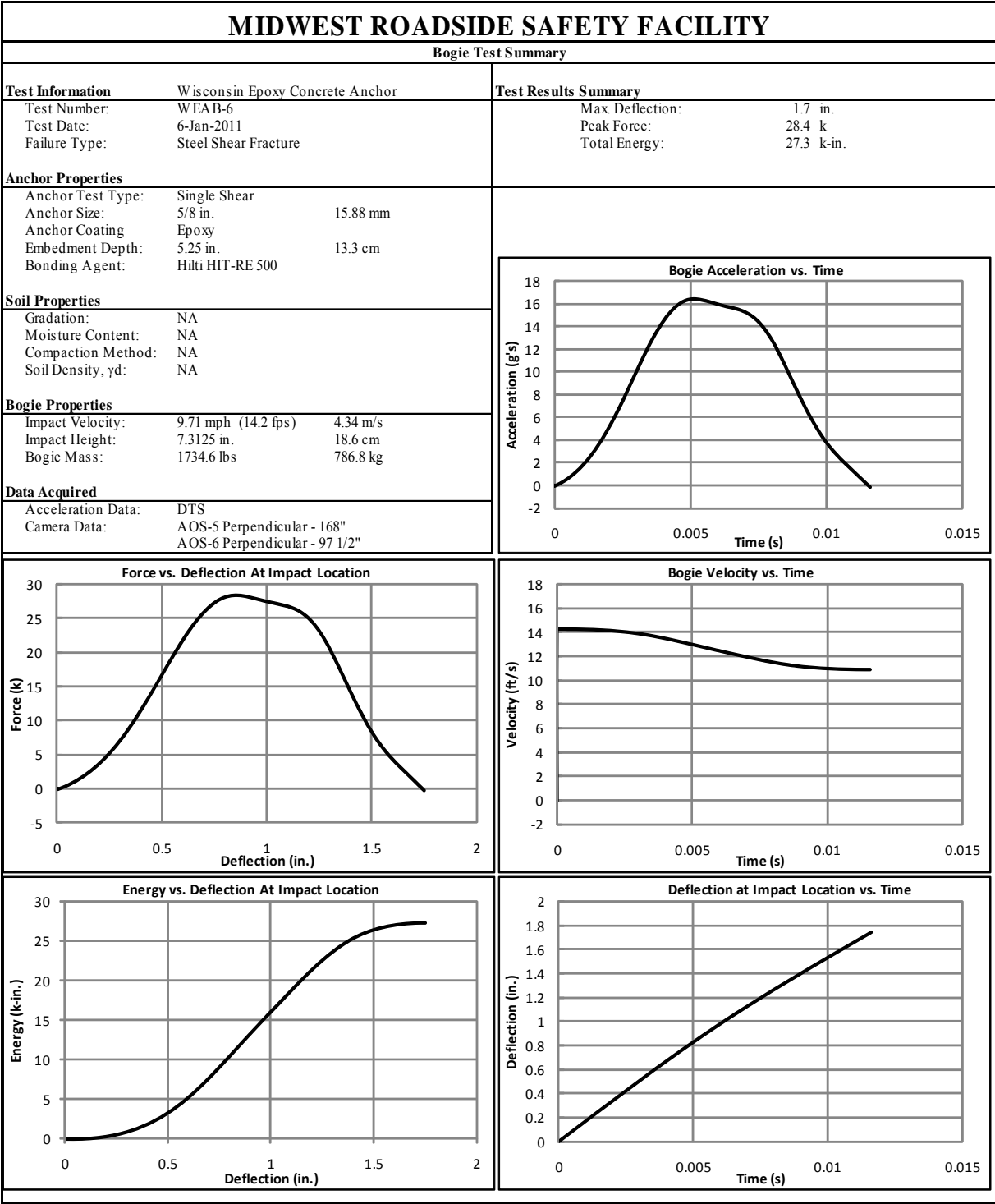


Figure H-12. Results of Test No. WEAB-6 (DTS)

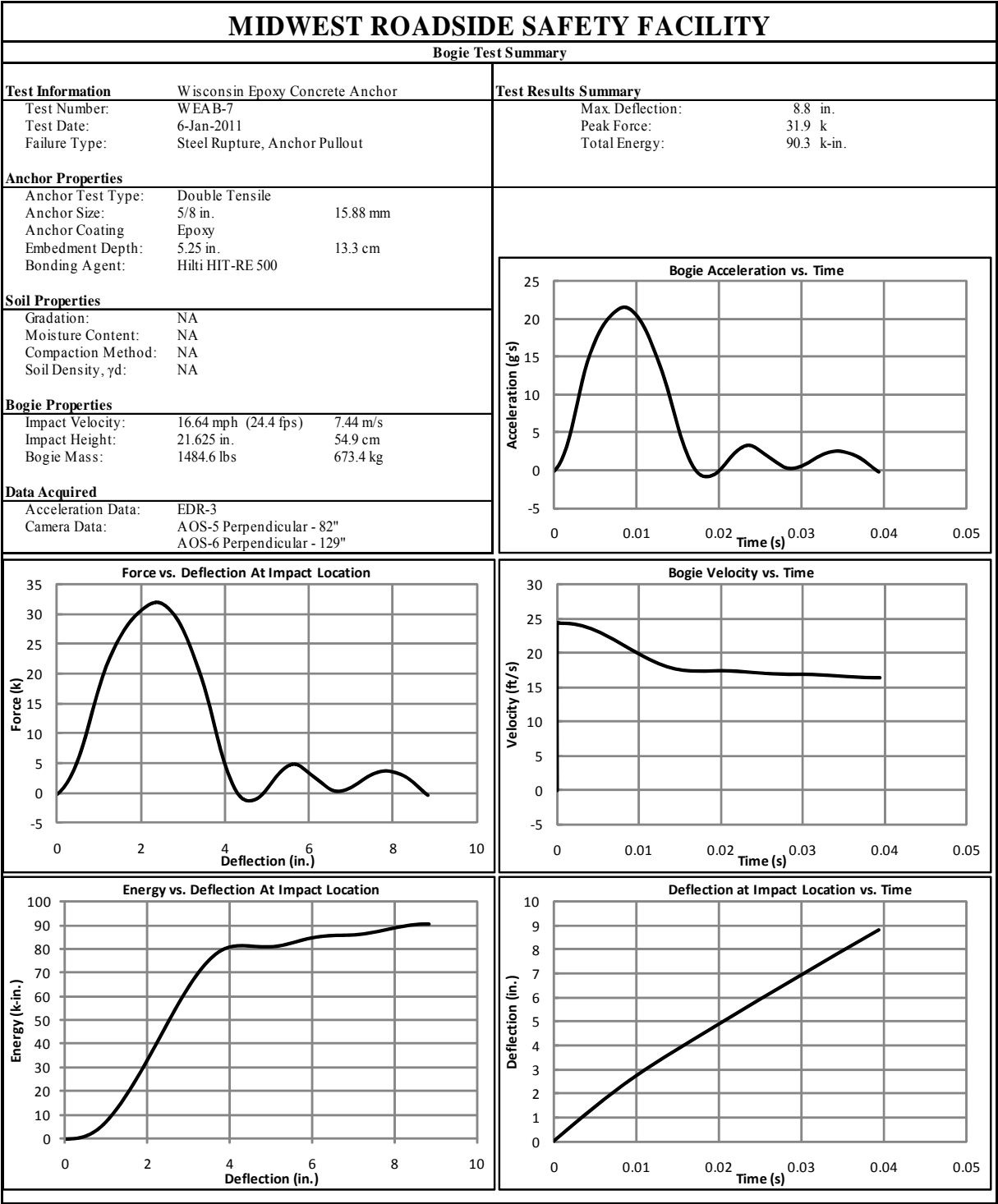


Figure H-13. Results of Test No. WEAB-7 (EDR-3)

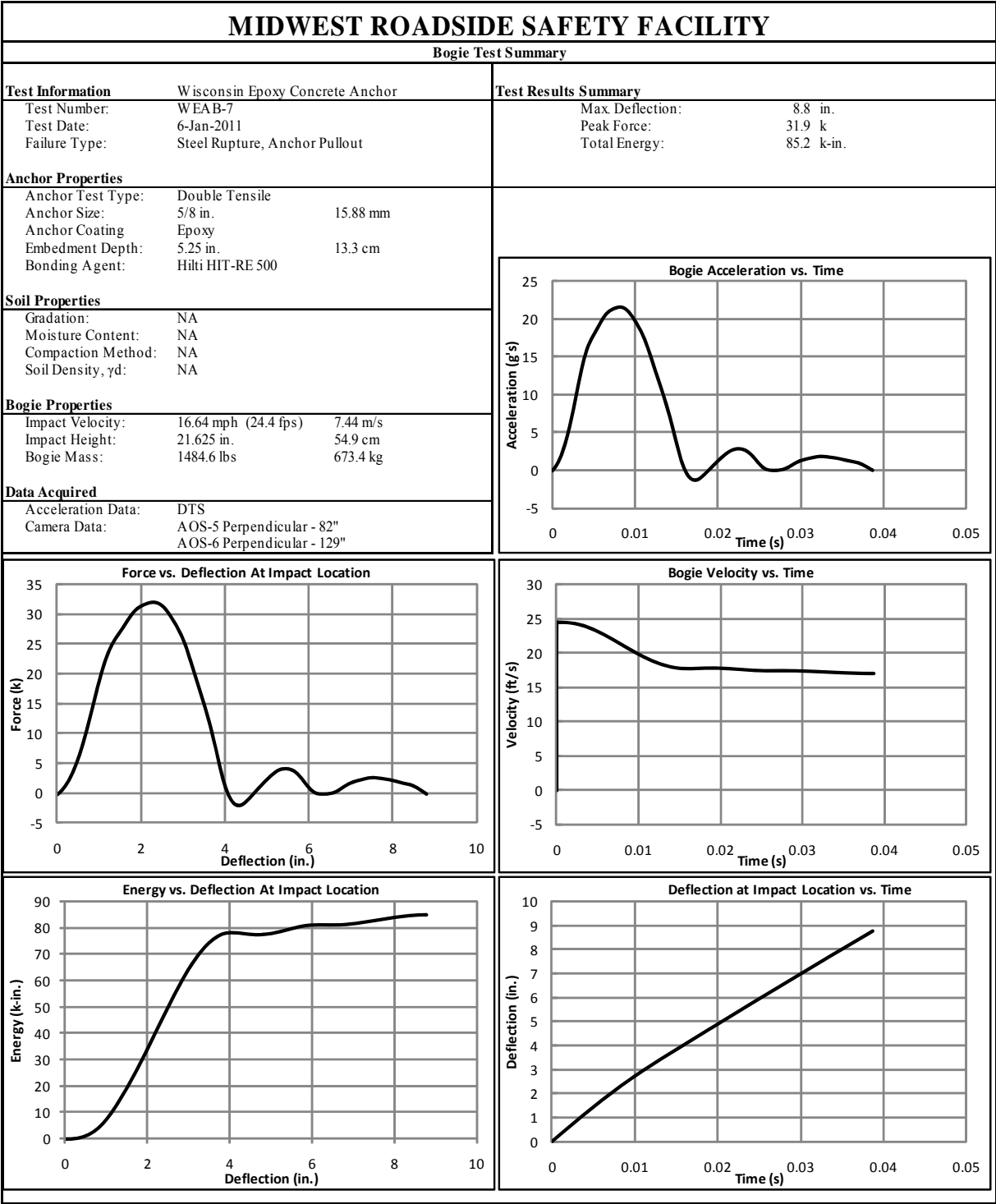


Figure H-14. Results of Test No. WEAB-7 (DTS)

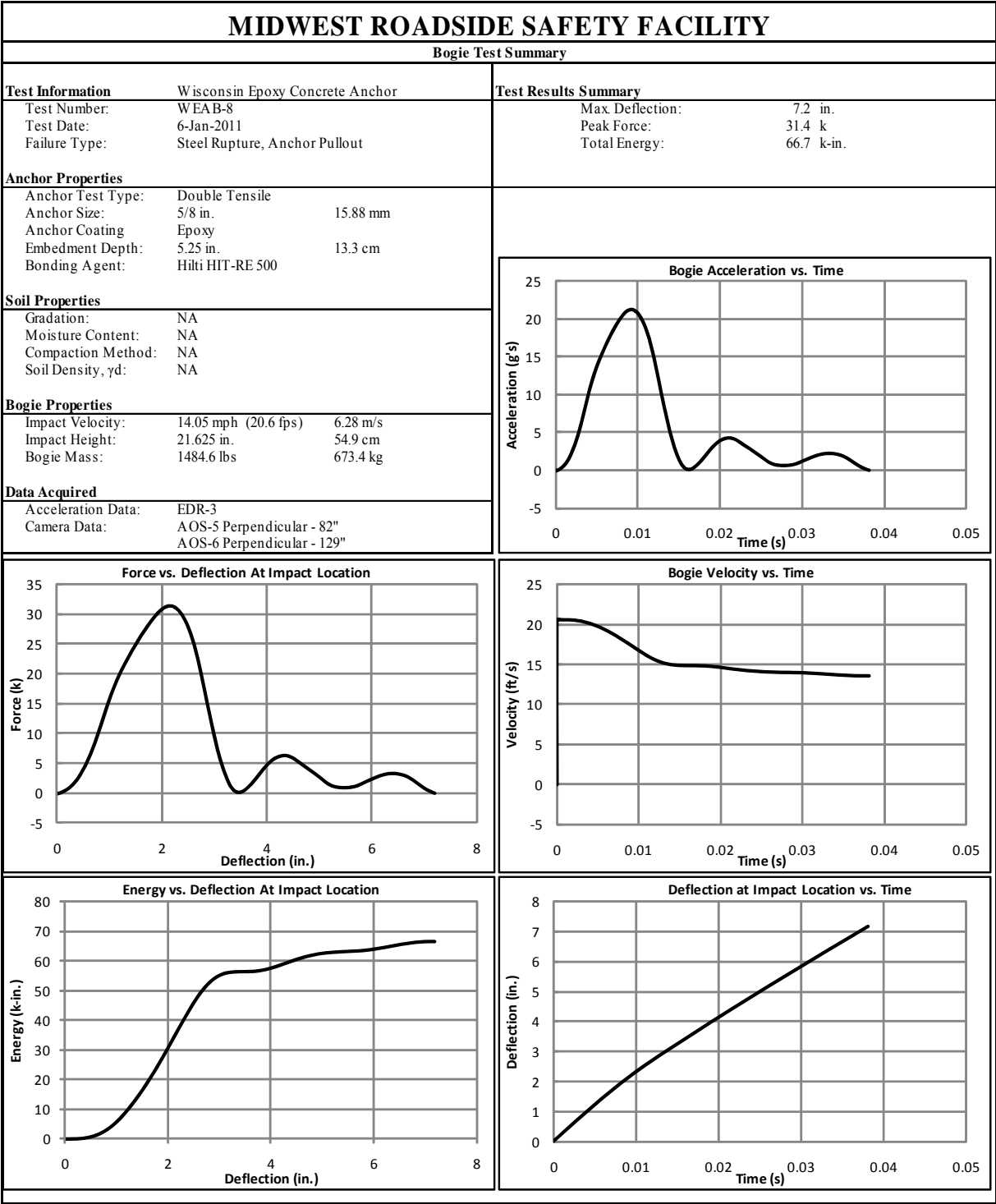


Figure H-15. Results of Test No. WEAB-8 (EDR-3)

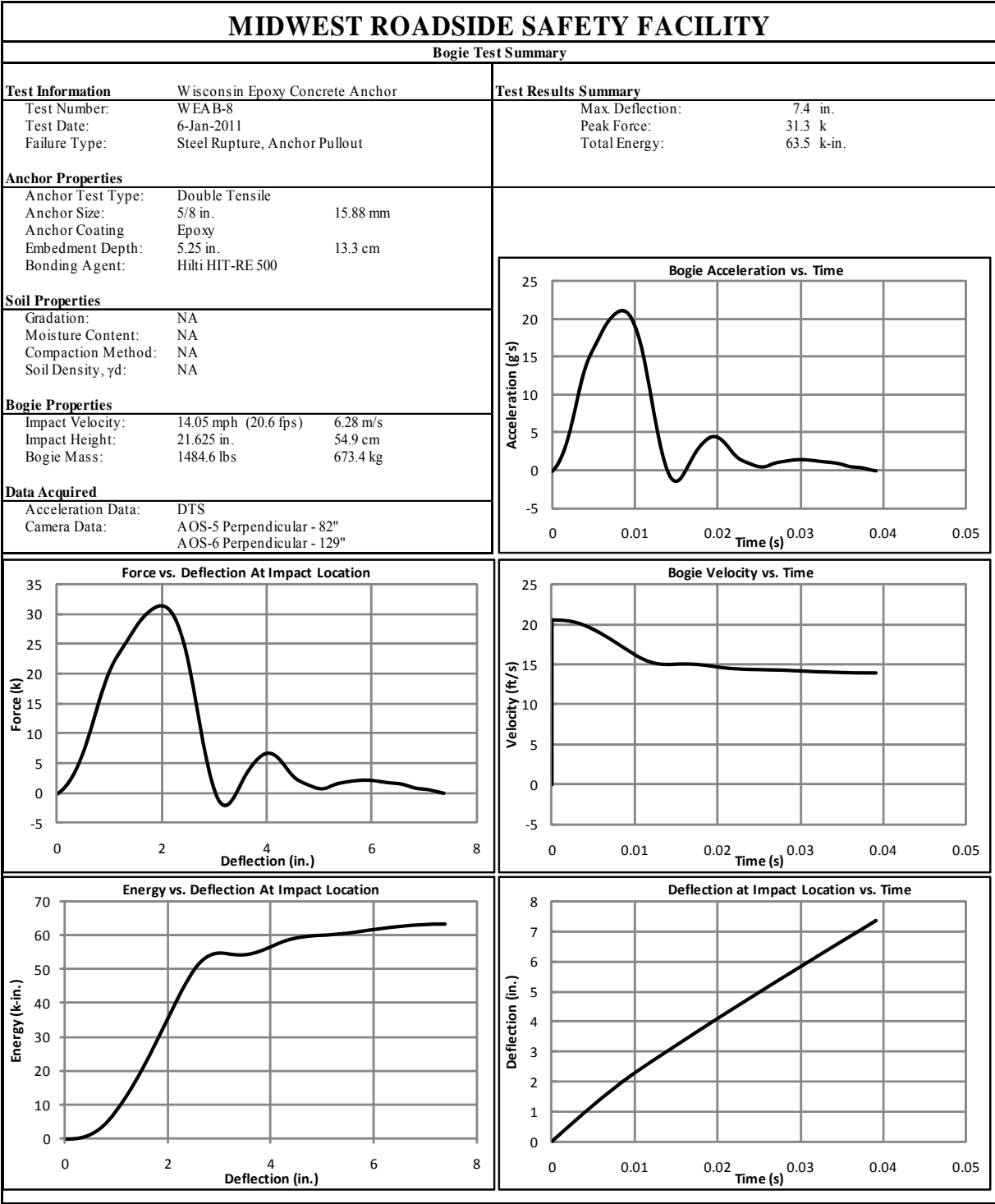


Figure H-16. Results of Test No. WEAB-8 (DTS)

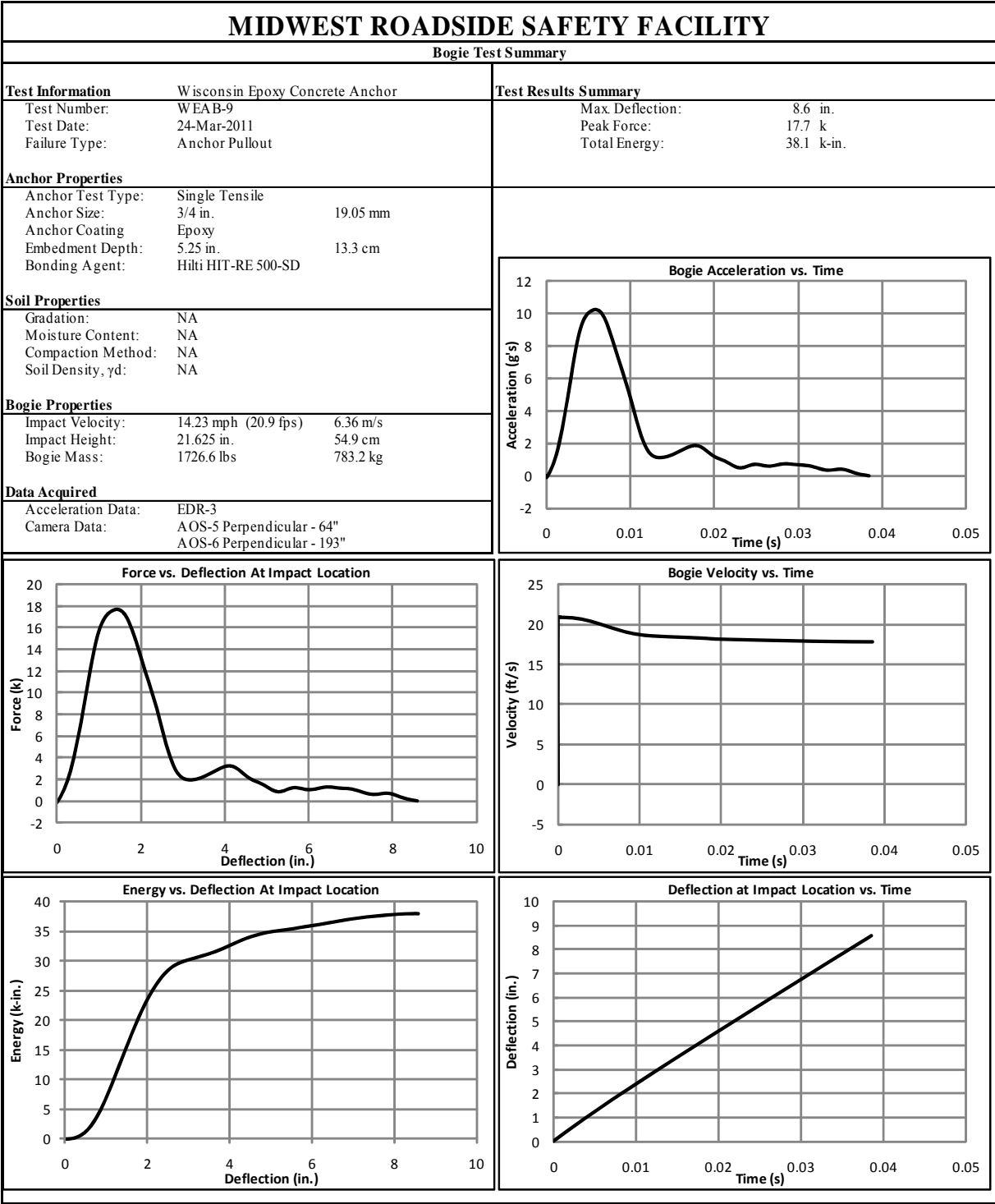


Figure H-17. Results of Test No. WEAB-9 (EDR-3)

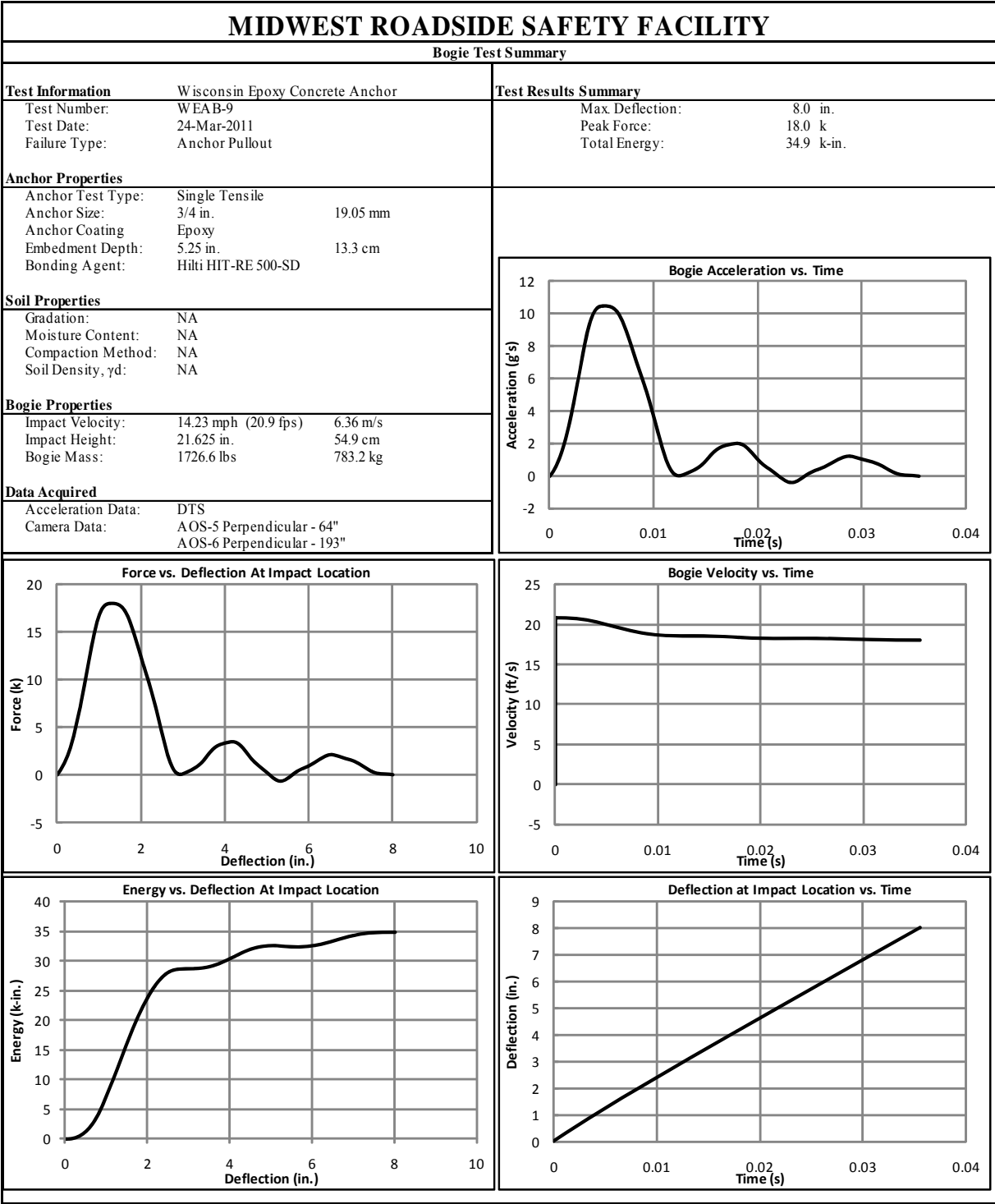


Figure H-18. Results of Test No. WEAB-9 (DTS)

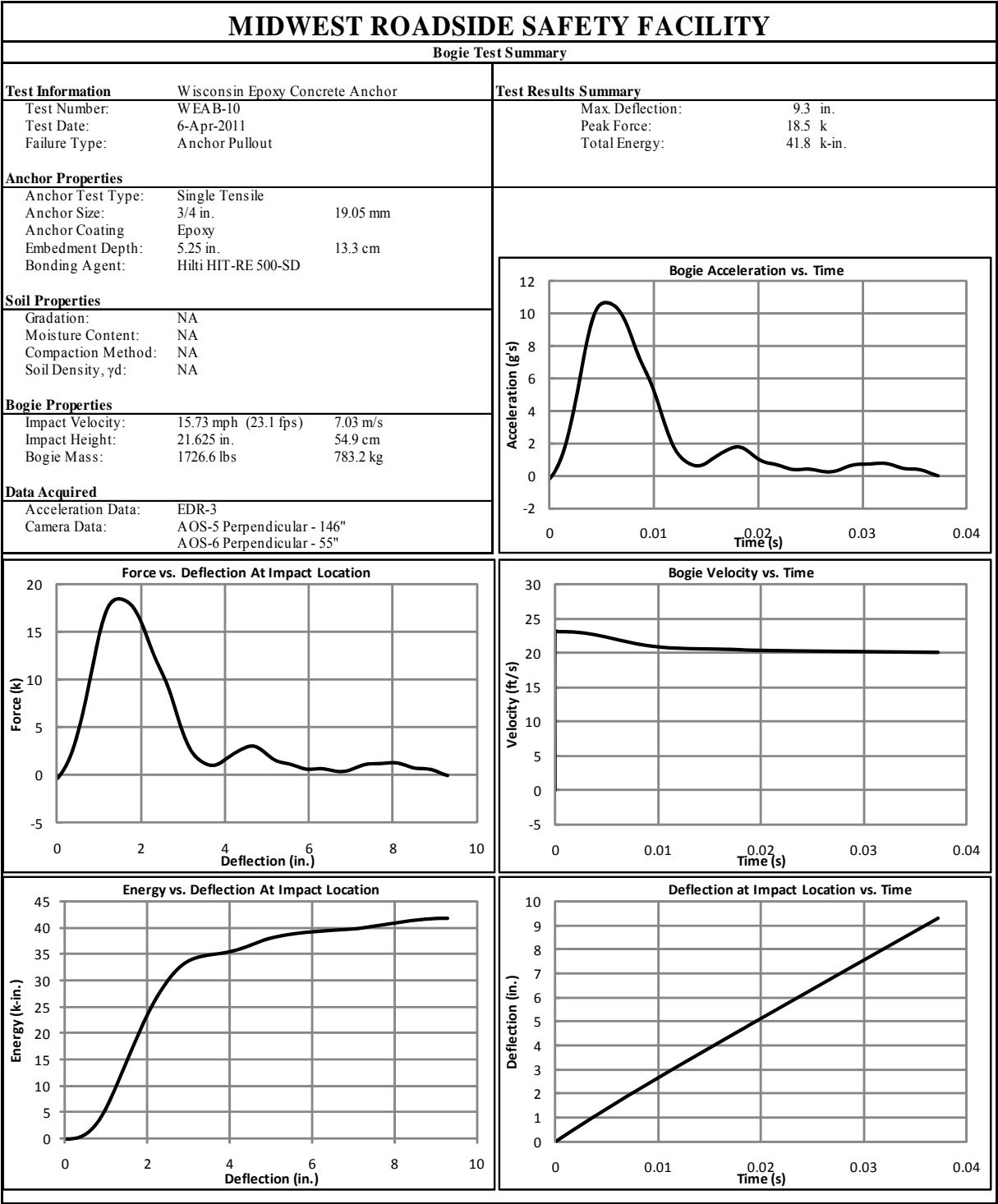


Figure H-19. Results of Test No. WEAB-10 (EDR-3)

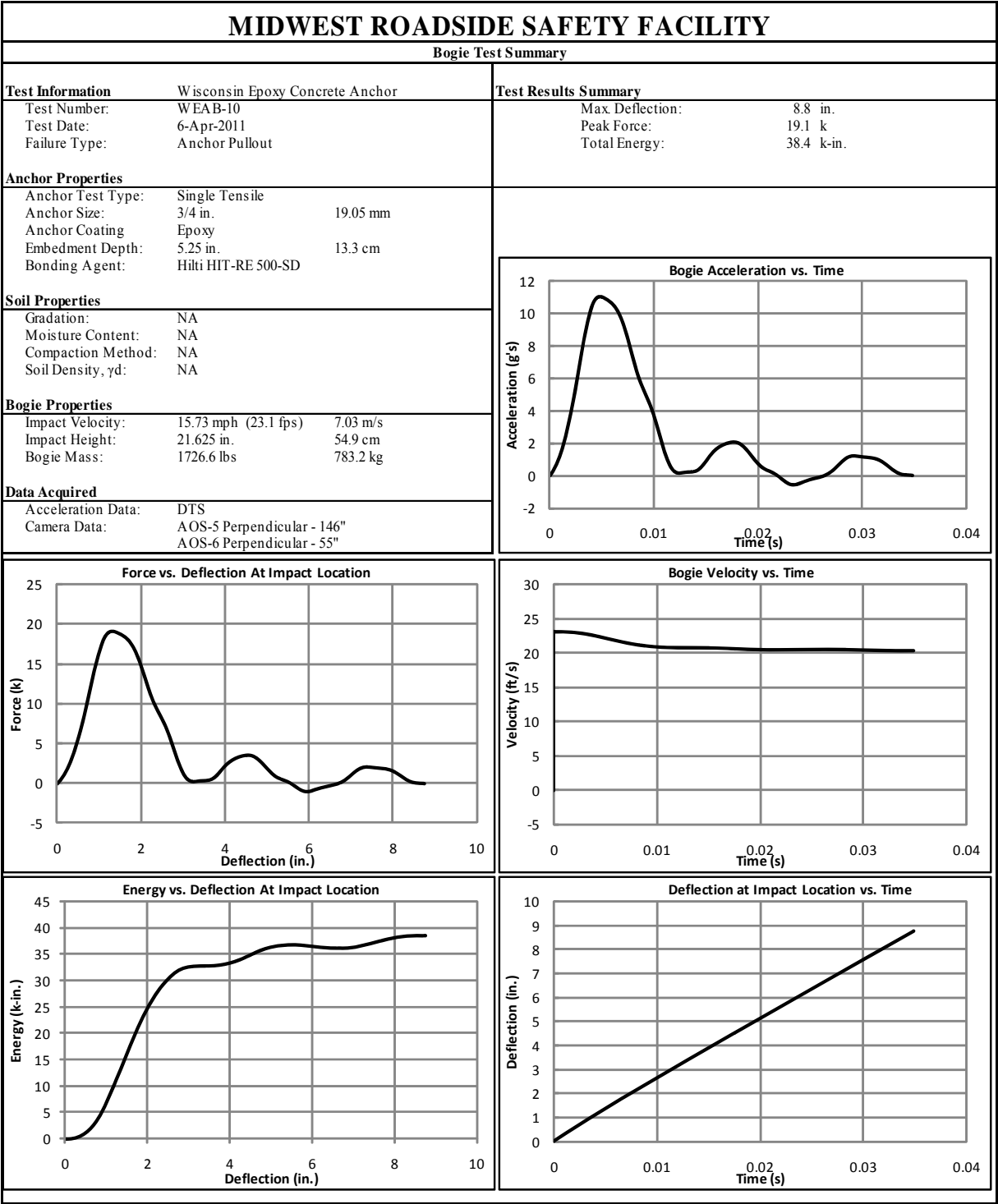


Figure H-20. Results of Test No. WEAB-10 (DTS Set 1)

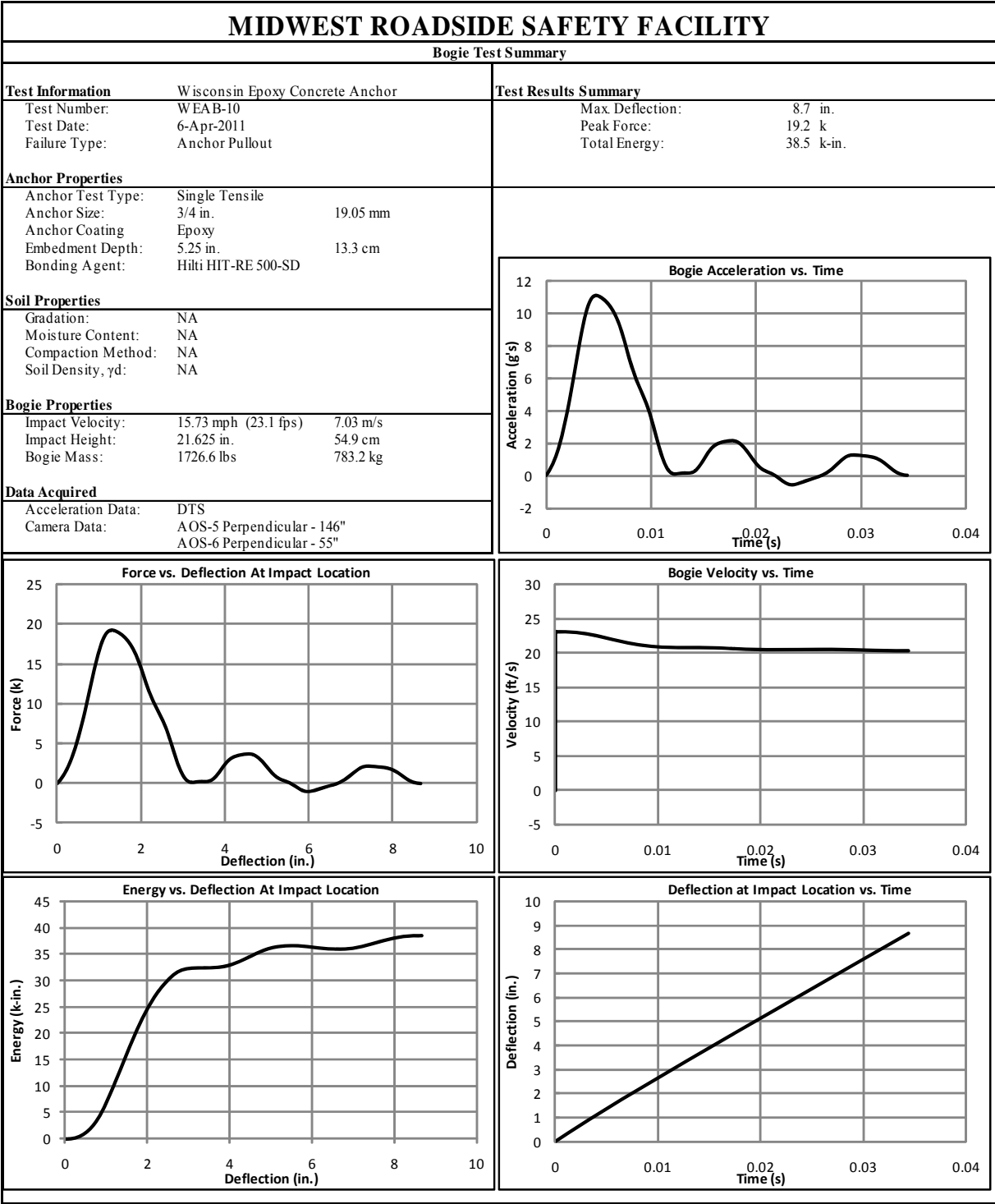


Figure H-21. Results of Test No. WEAB-10 (DTS Set 2)

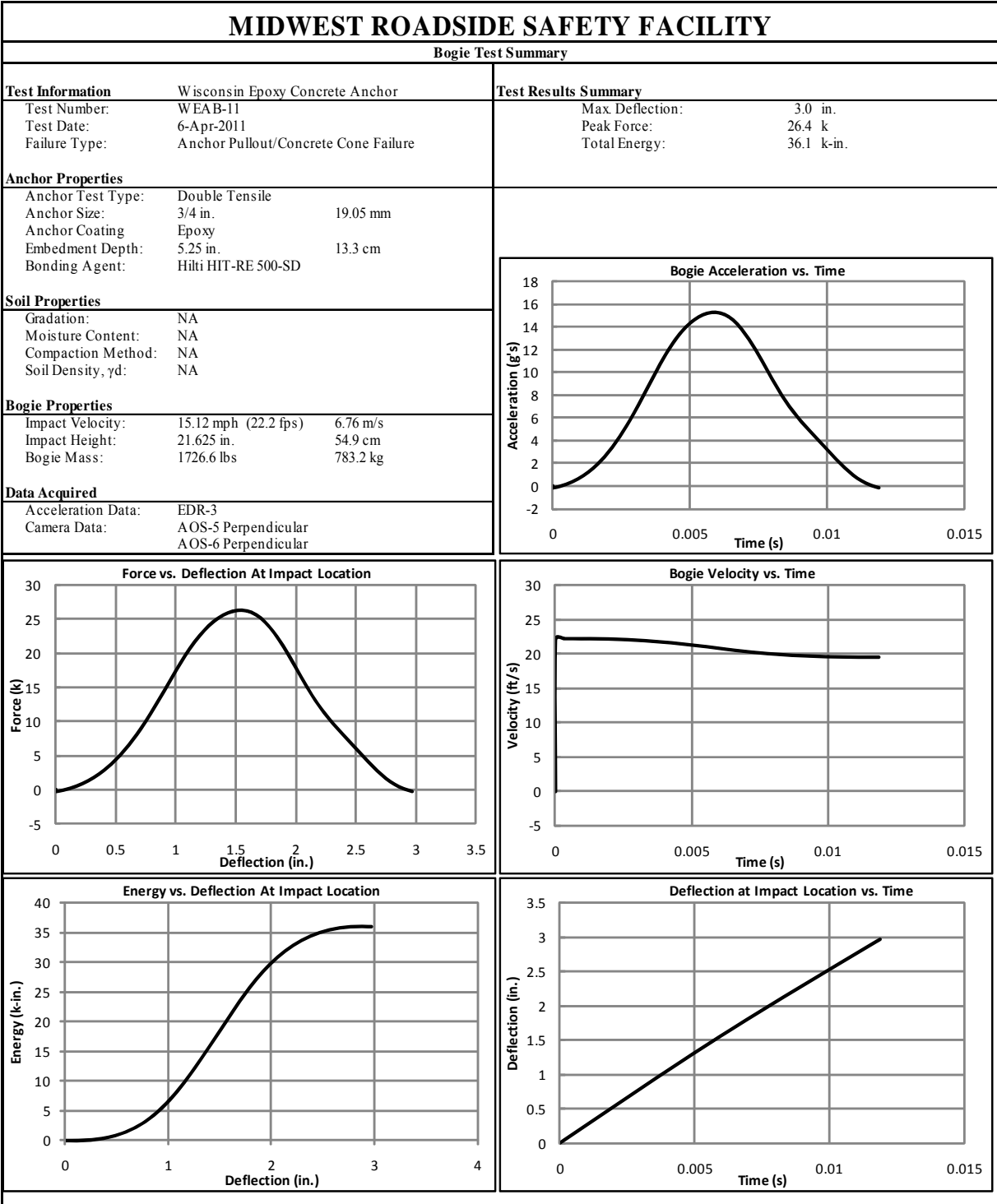


Figure H-22. Results of Test No. WEAB-11 (EDR-3)

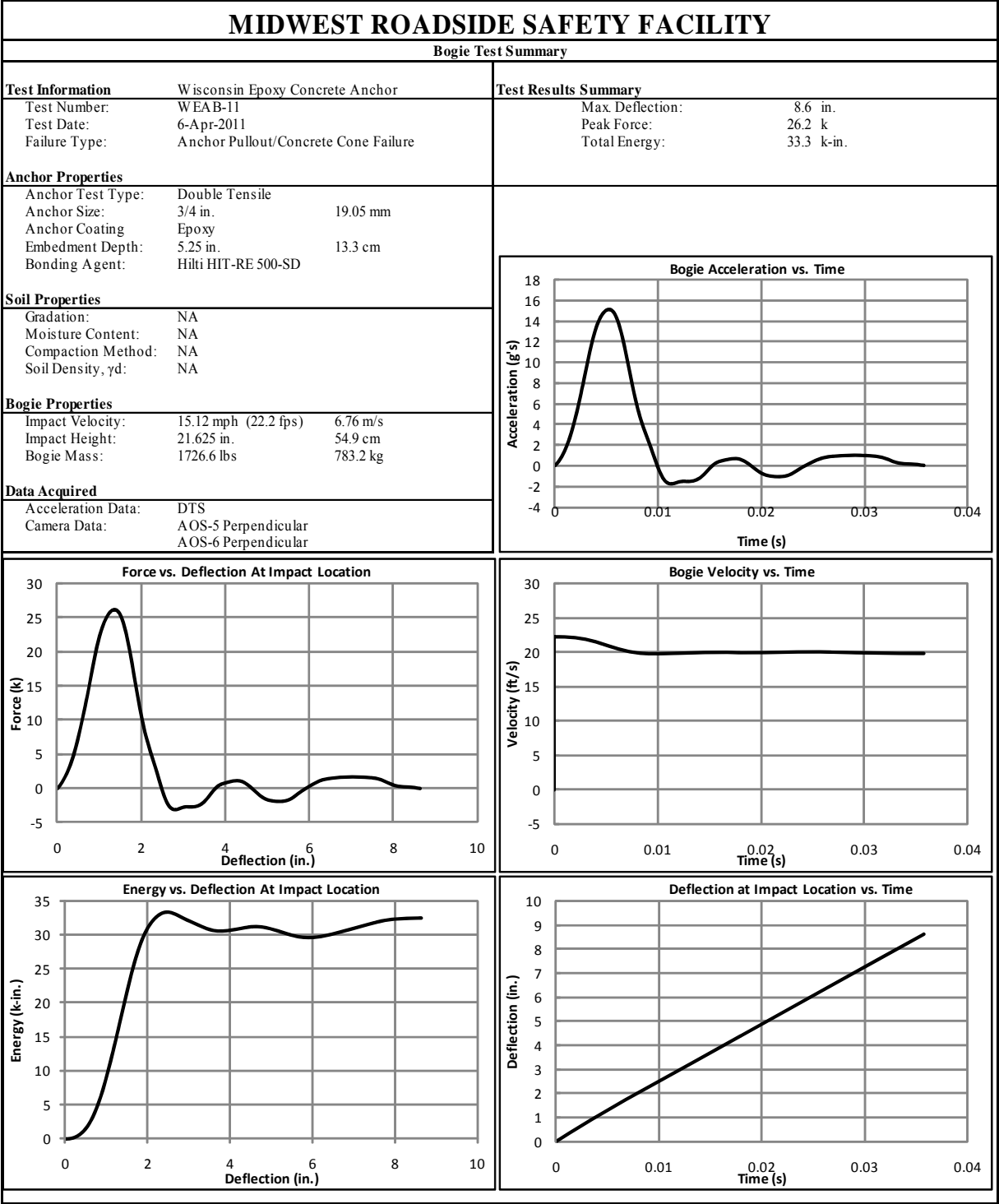


Figure H-23. Results of Test No. WEAB-11 (DTS Set 1)

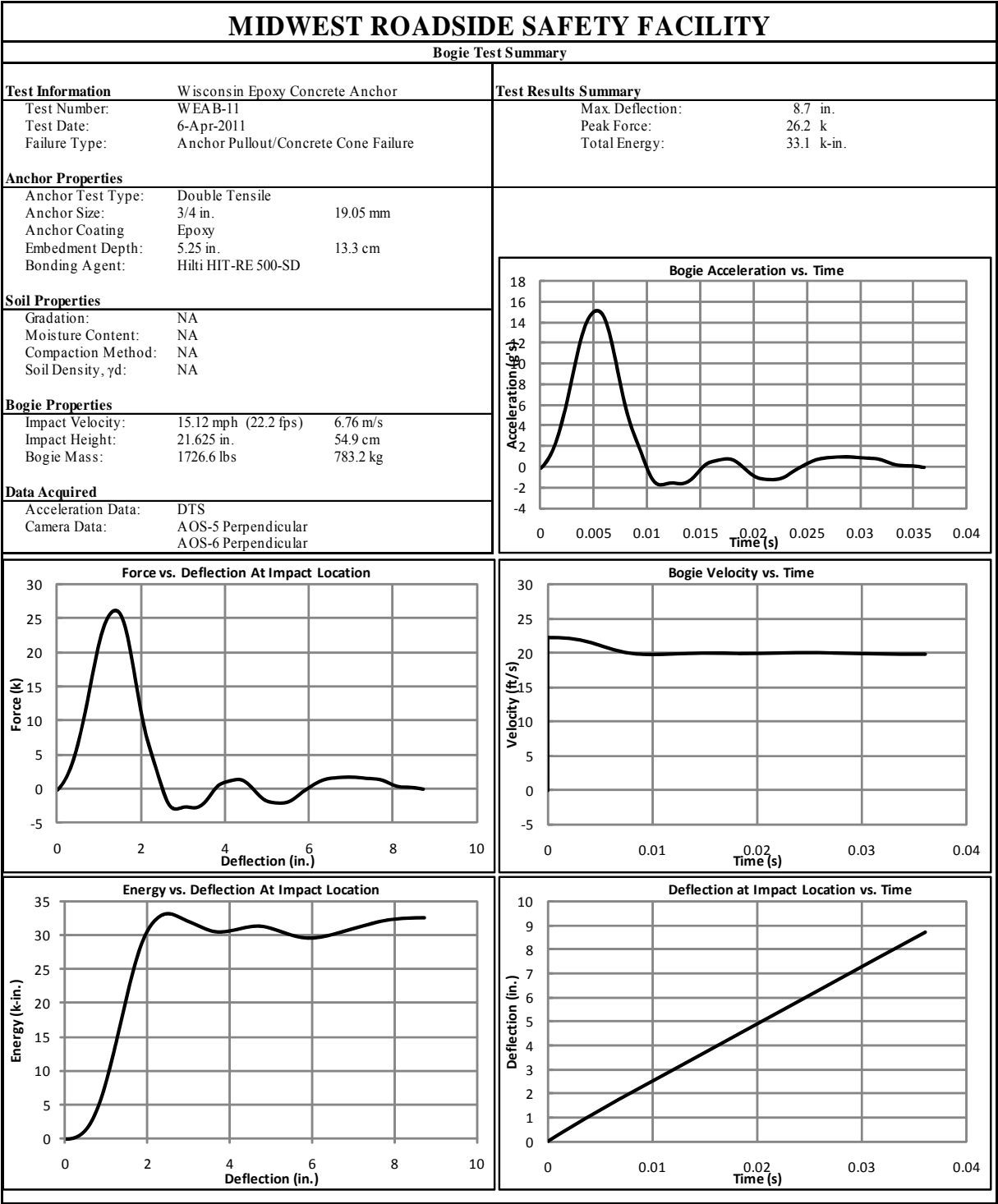


Figure H-24. Results of Test No. WEAB-11 (DTS Set 2)

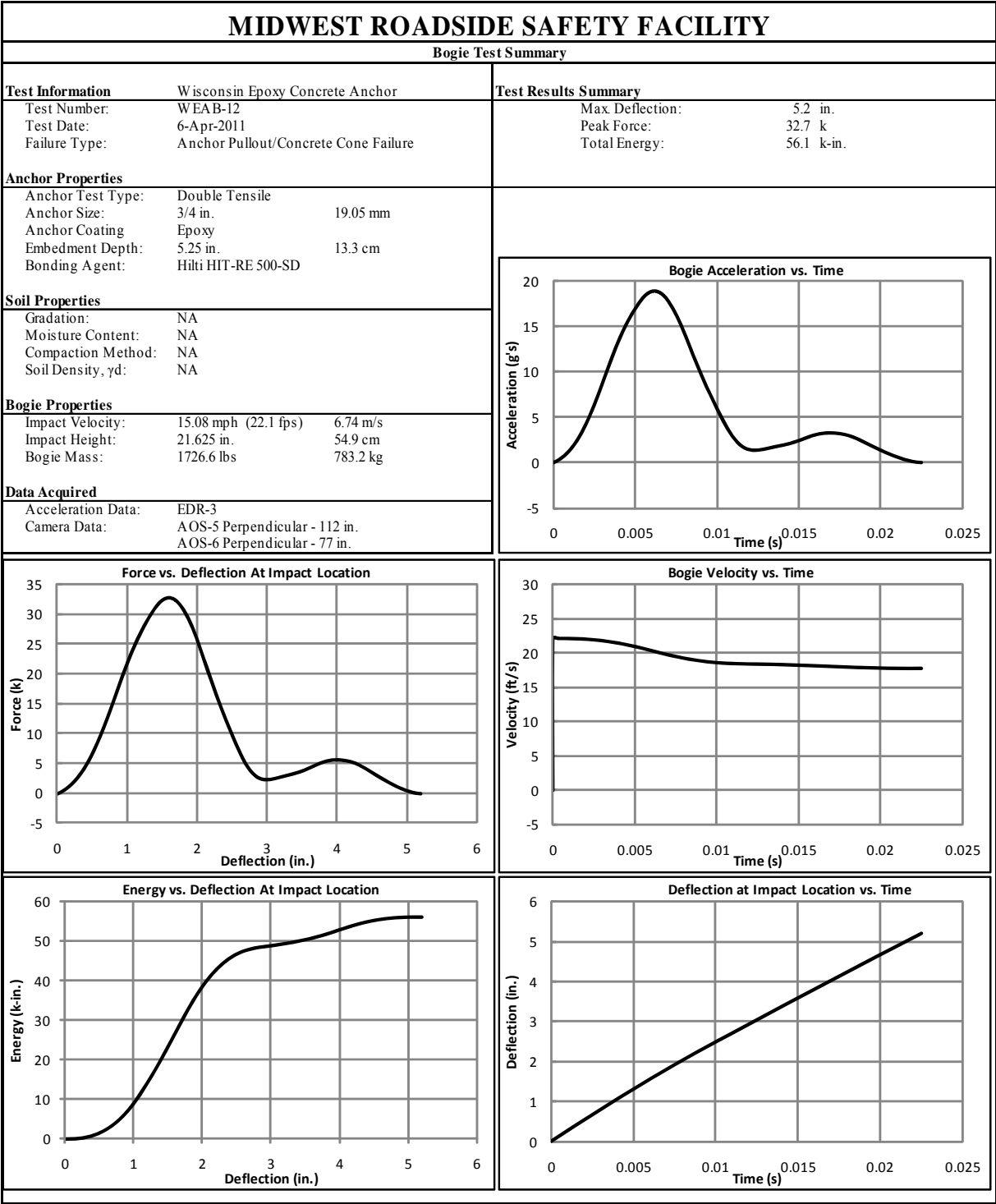


Figure H-25. Results of Test No. WEAB-12 (EDR-3)

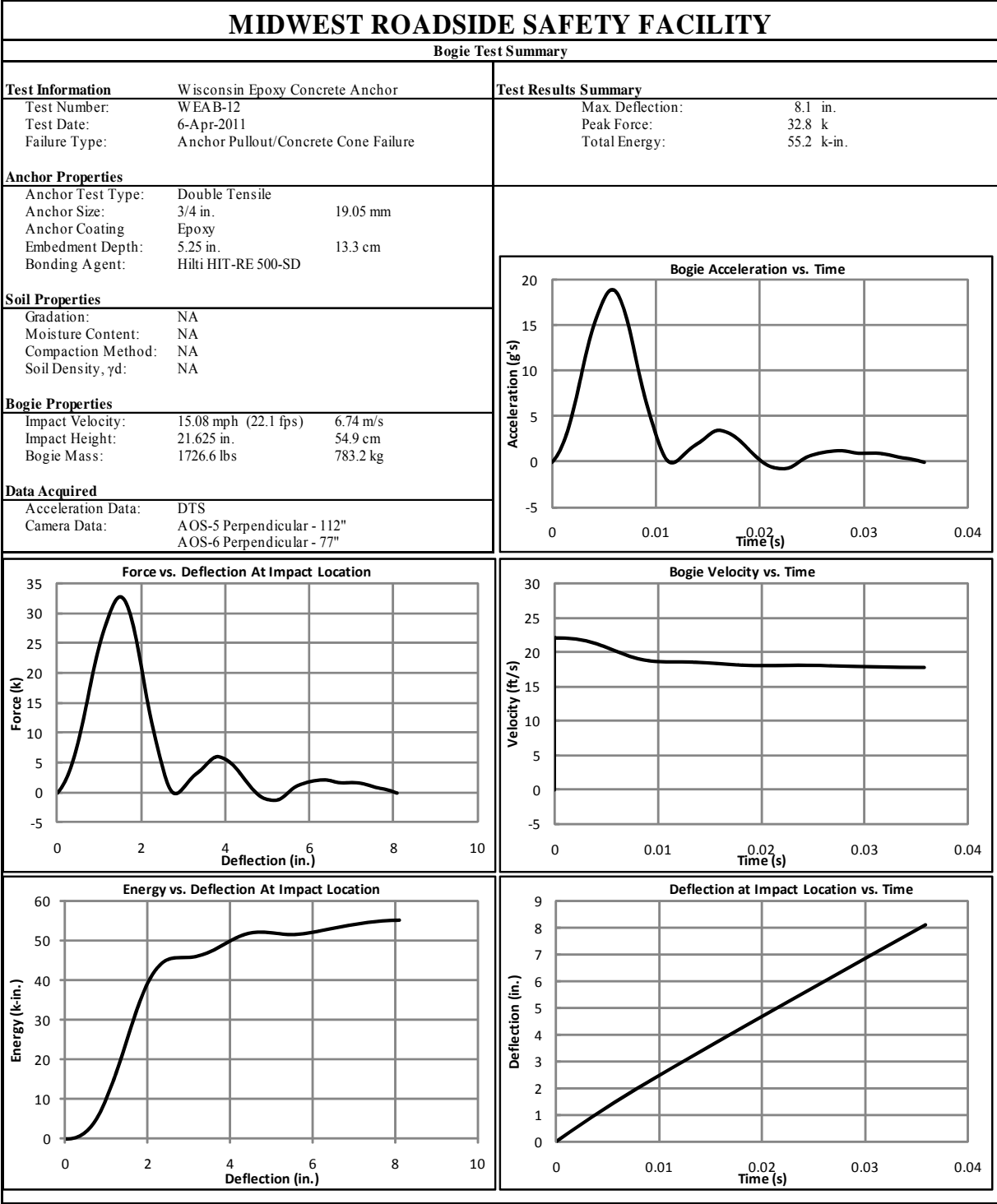


Figure H-26. Results of Test No. WEAB-12 (DTS Set 1)

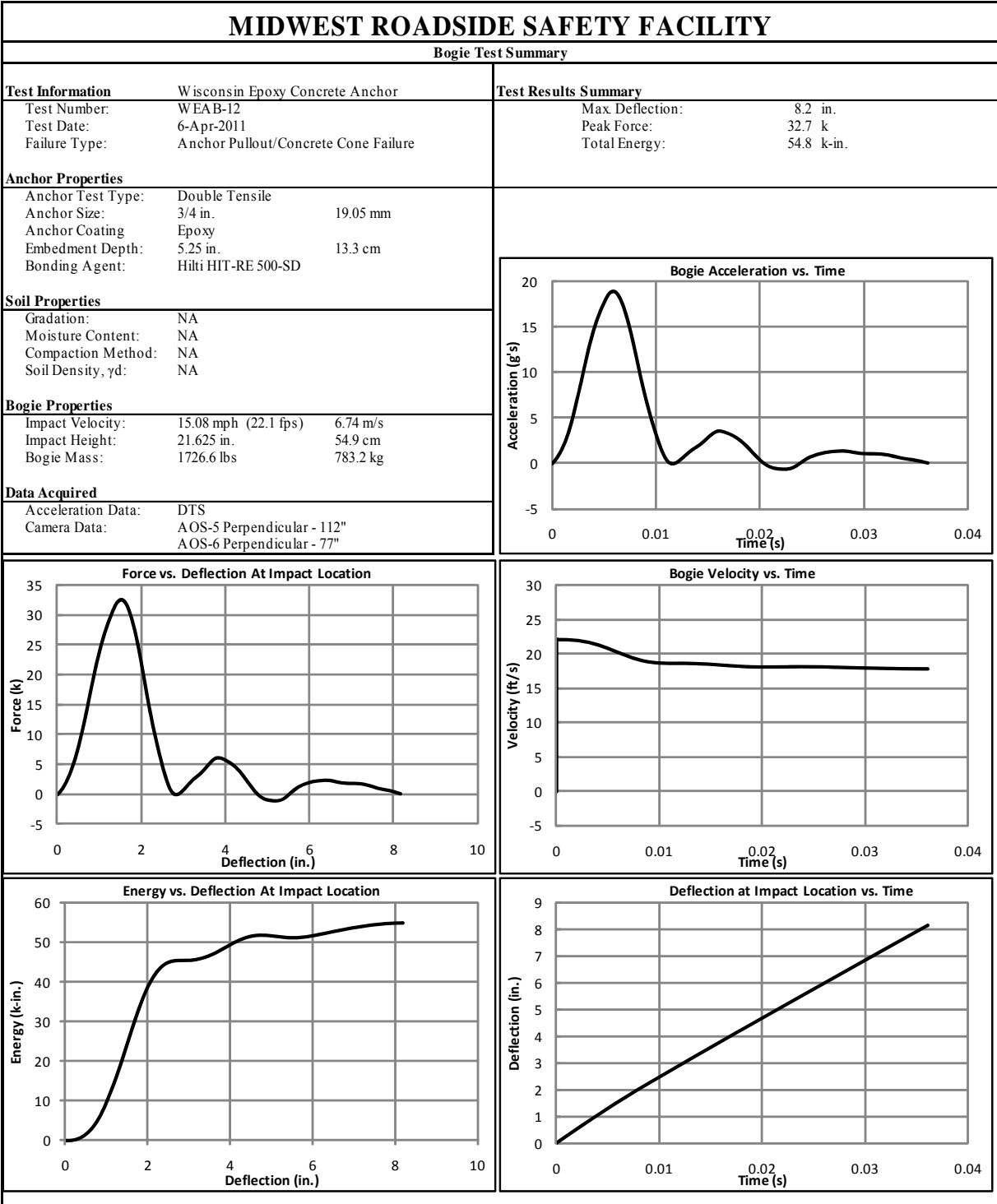


Figure H-27. Results of Test No. WEAB-12 (DTS Set 2)

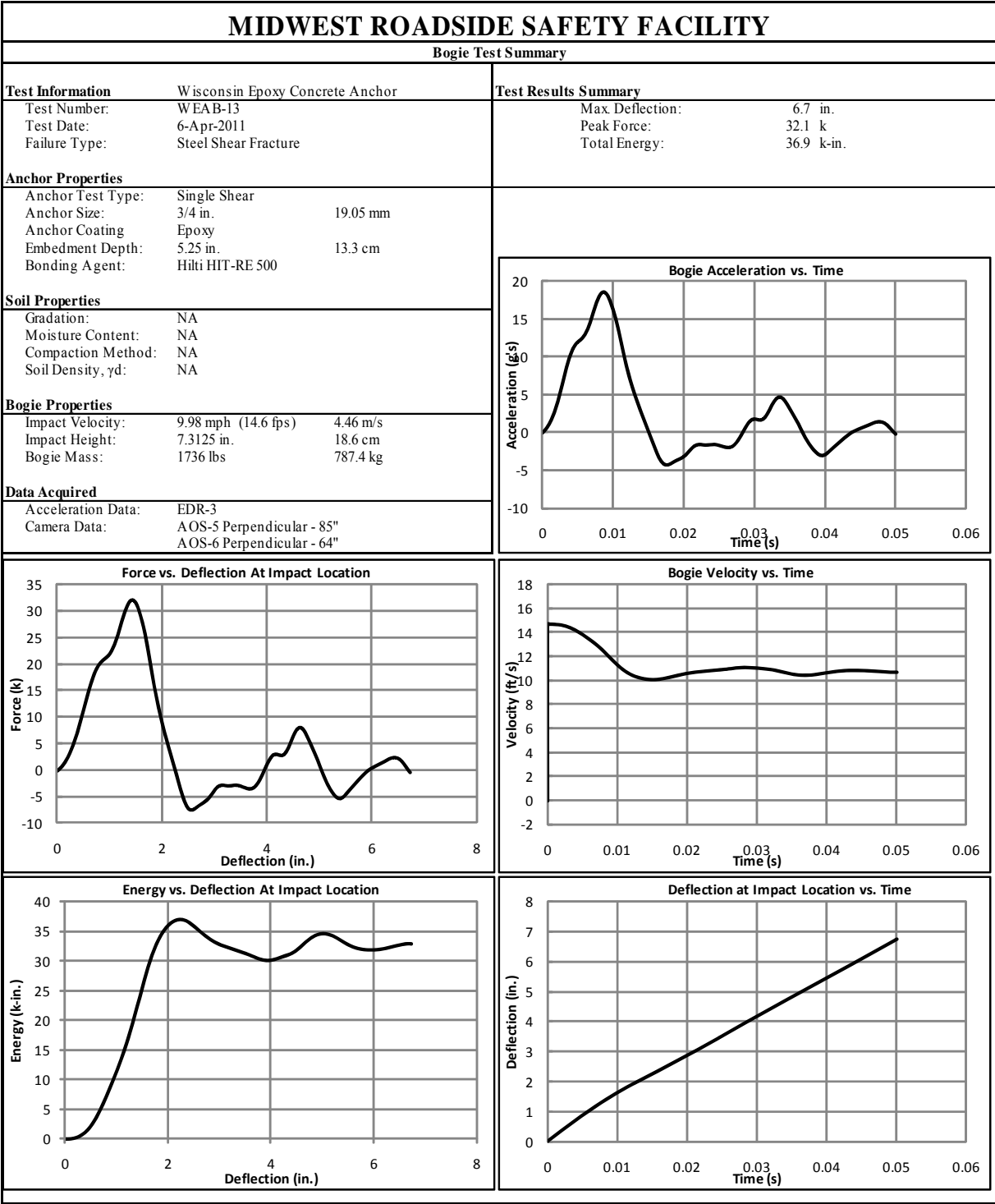


Figure H-28. Results of Test No. WEAB-13 (EDR-3)

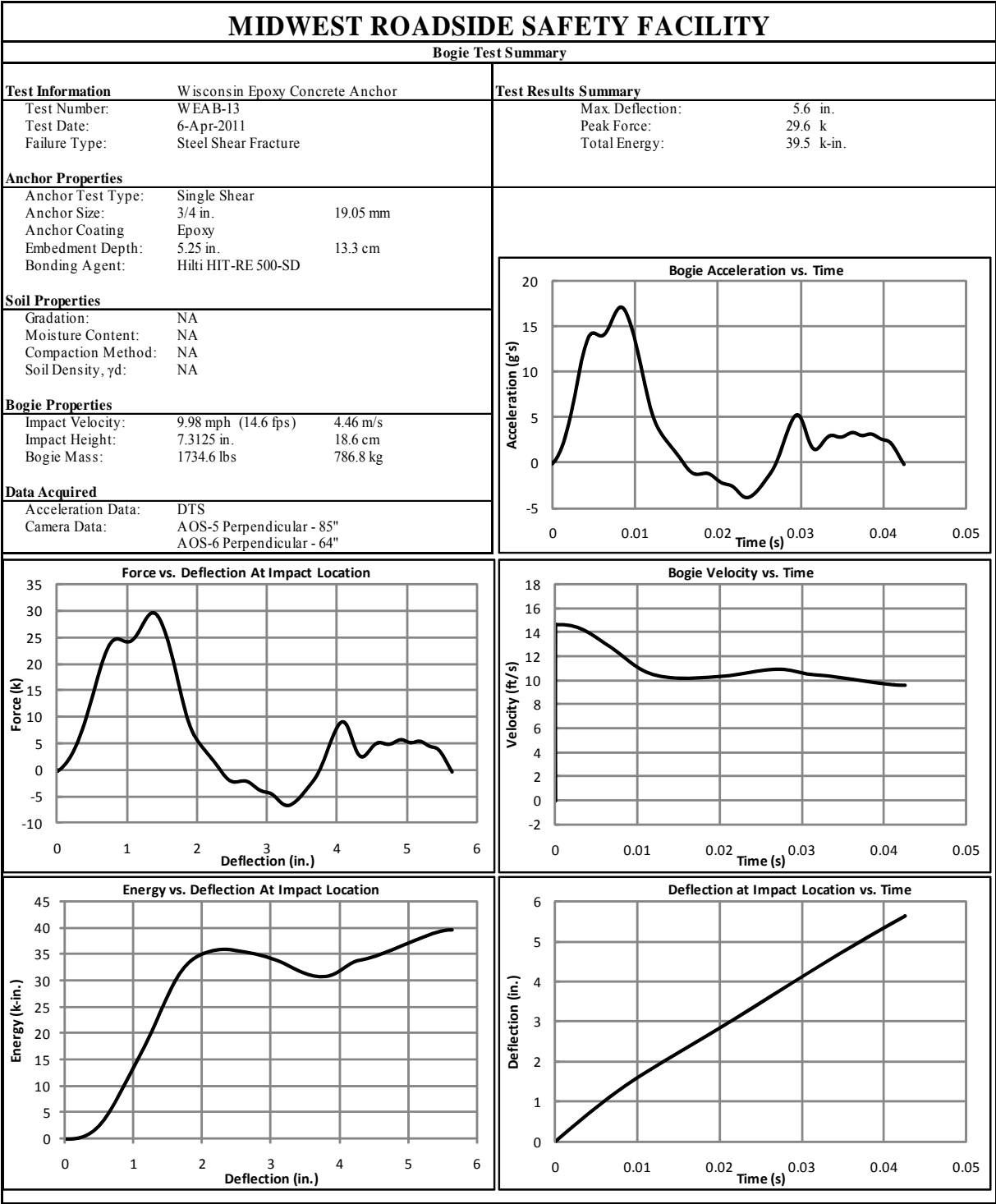


Figure H-29. Results of Test No. WEAB-13 (DTS Set 1)

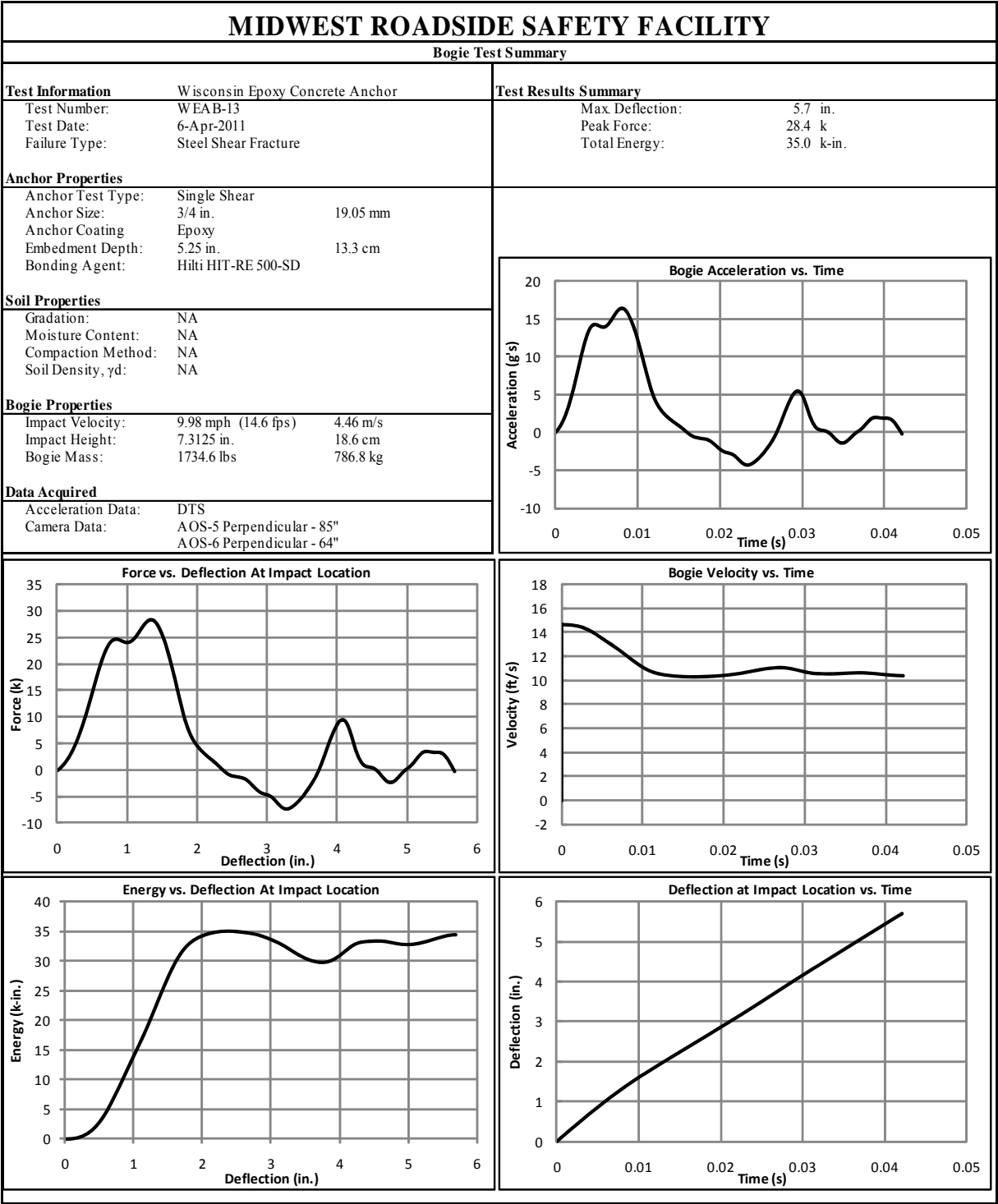


Figure H-30. Results of Test No. WEAB-13 (DTS Set 2)

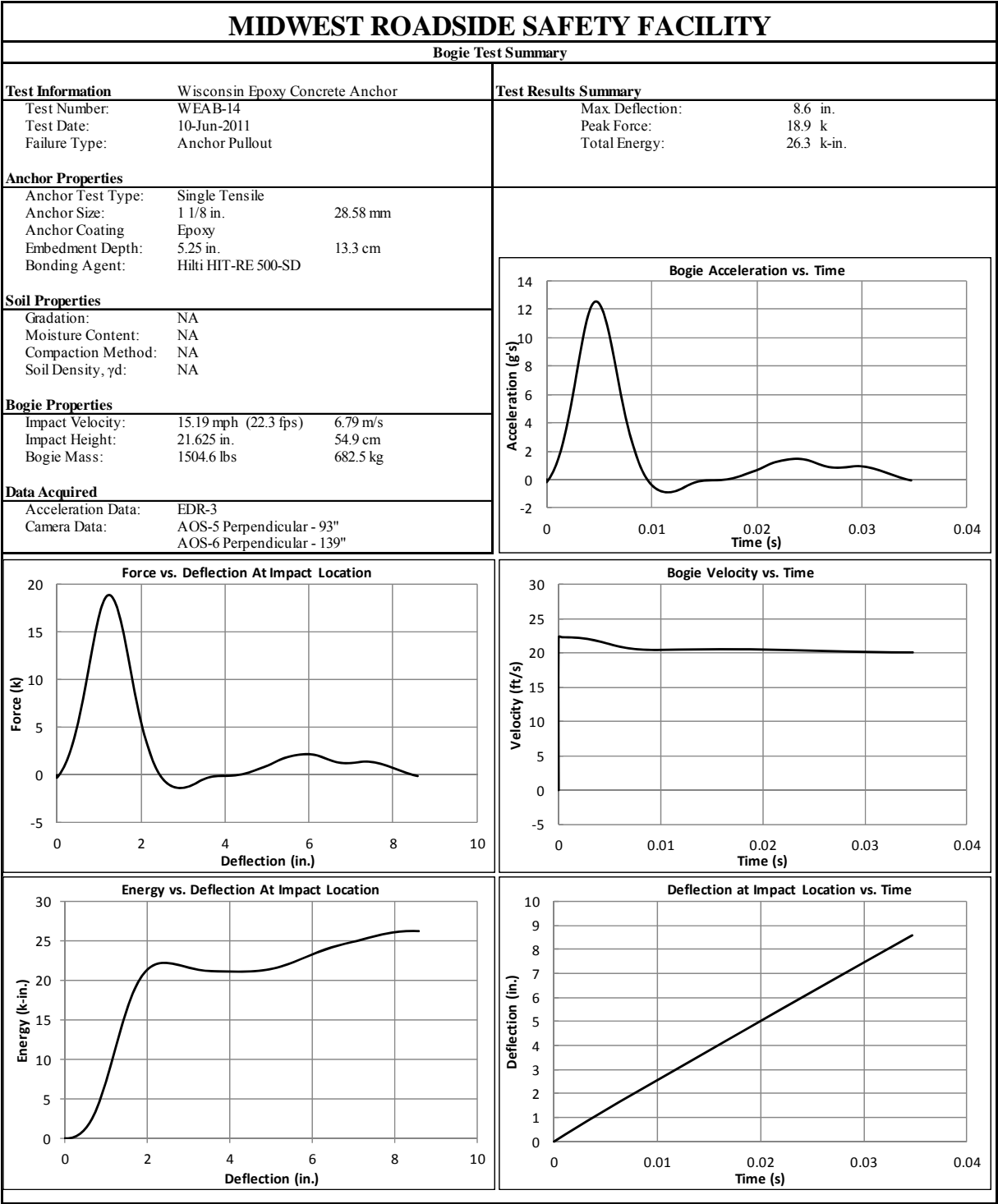


Figure H-31. Results of Test No. WEAB-14 (EDR-3)

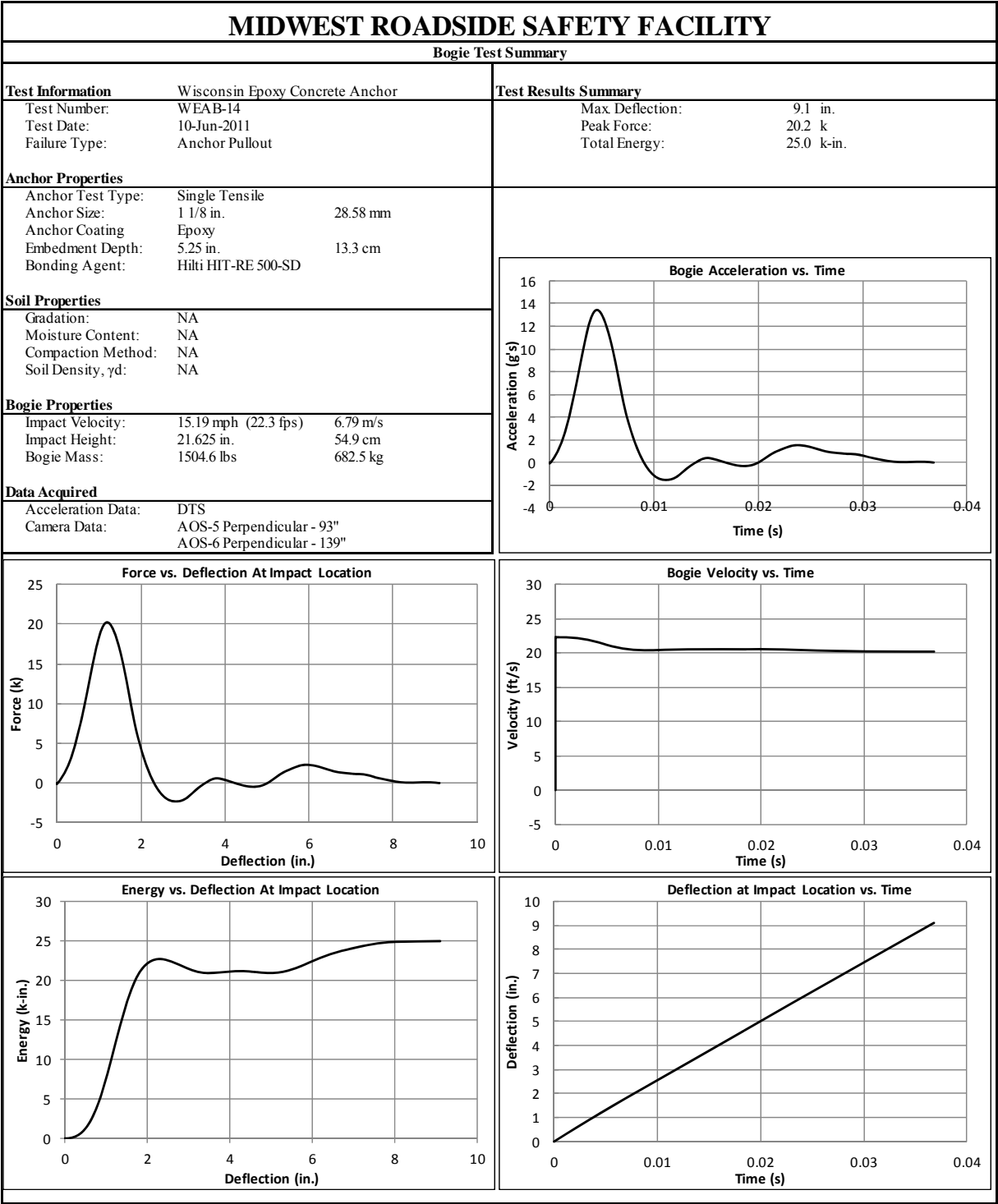


Figure H-32. Results of Test No. WEAB-14 (DTS Set 1)

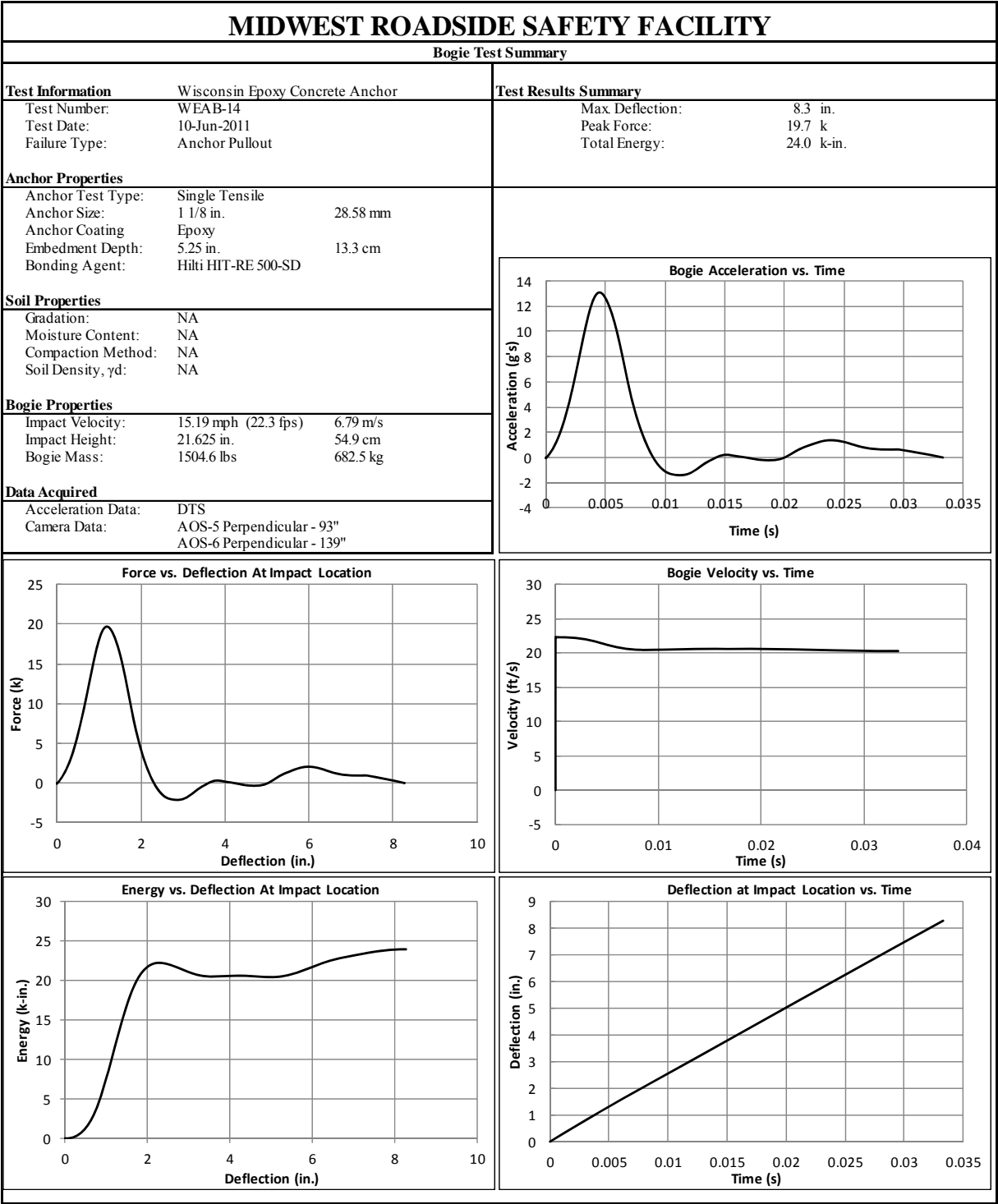


Figure H-33. Results of Test No. WEAB-14 (DTS Set 2)

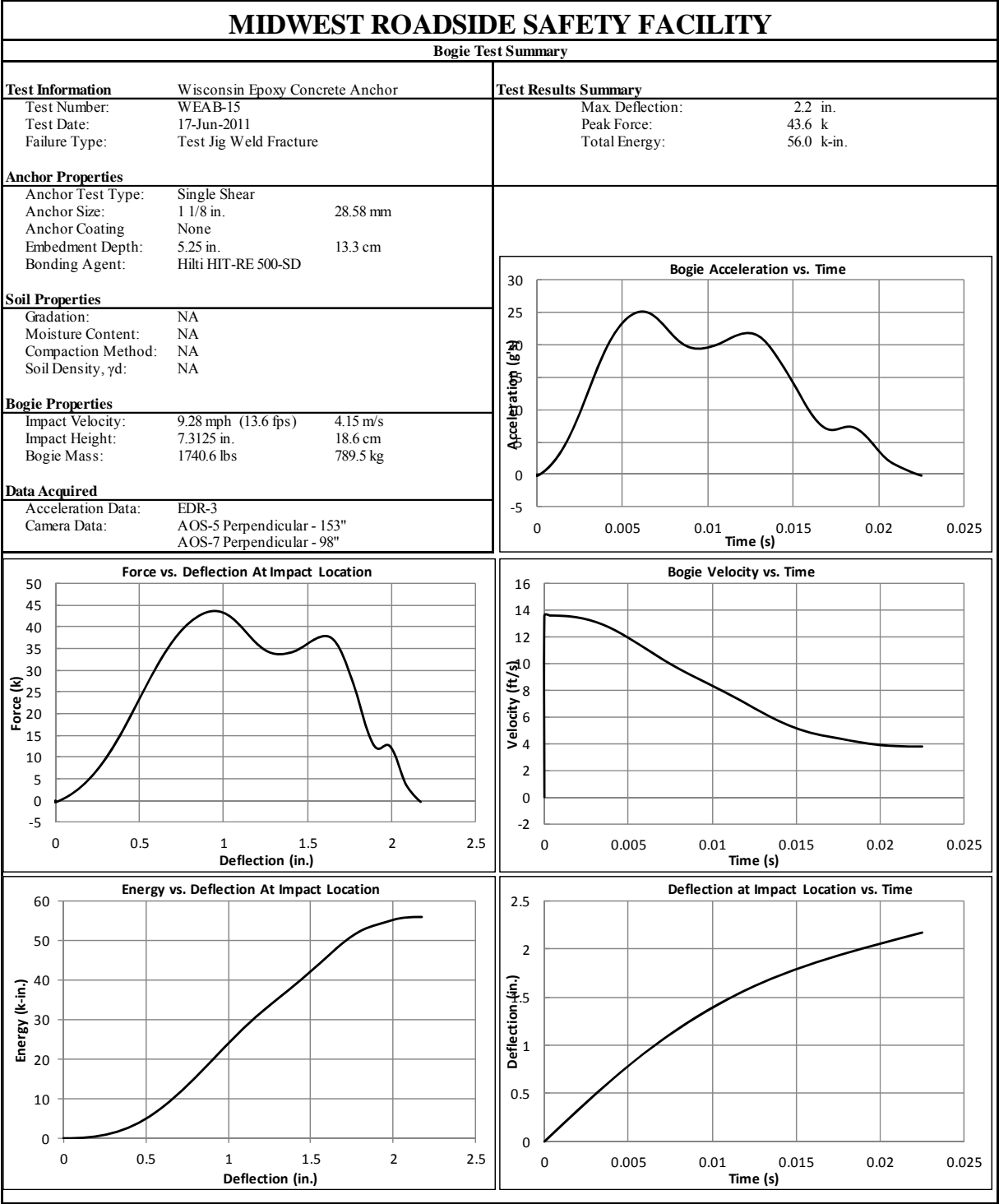


Figure H-34. Results of Test No. WEAB-15 (EDR-3)

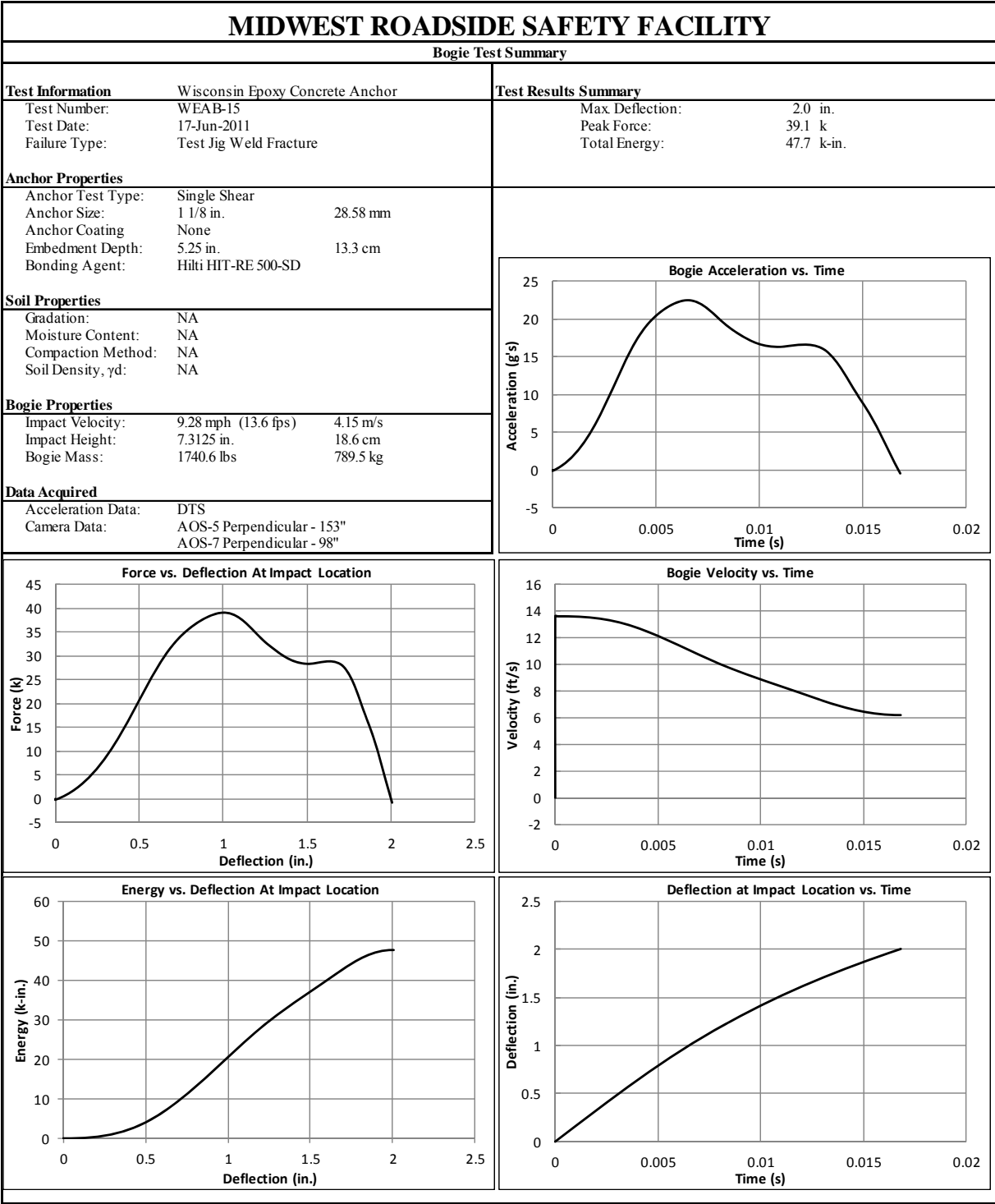


Figure H-35. Results of Test No. WEAB-15 (DTS Set 1)

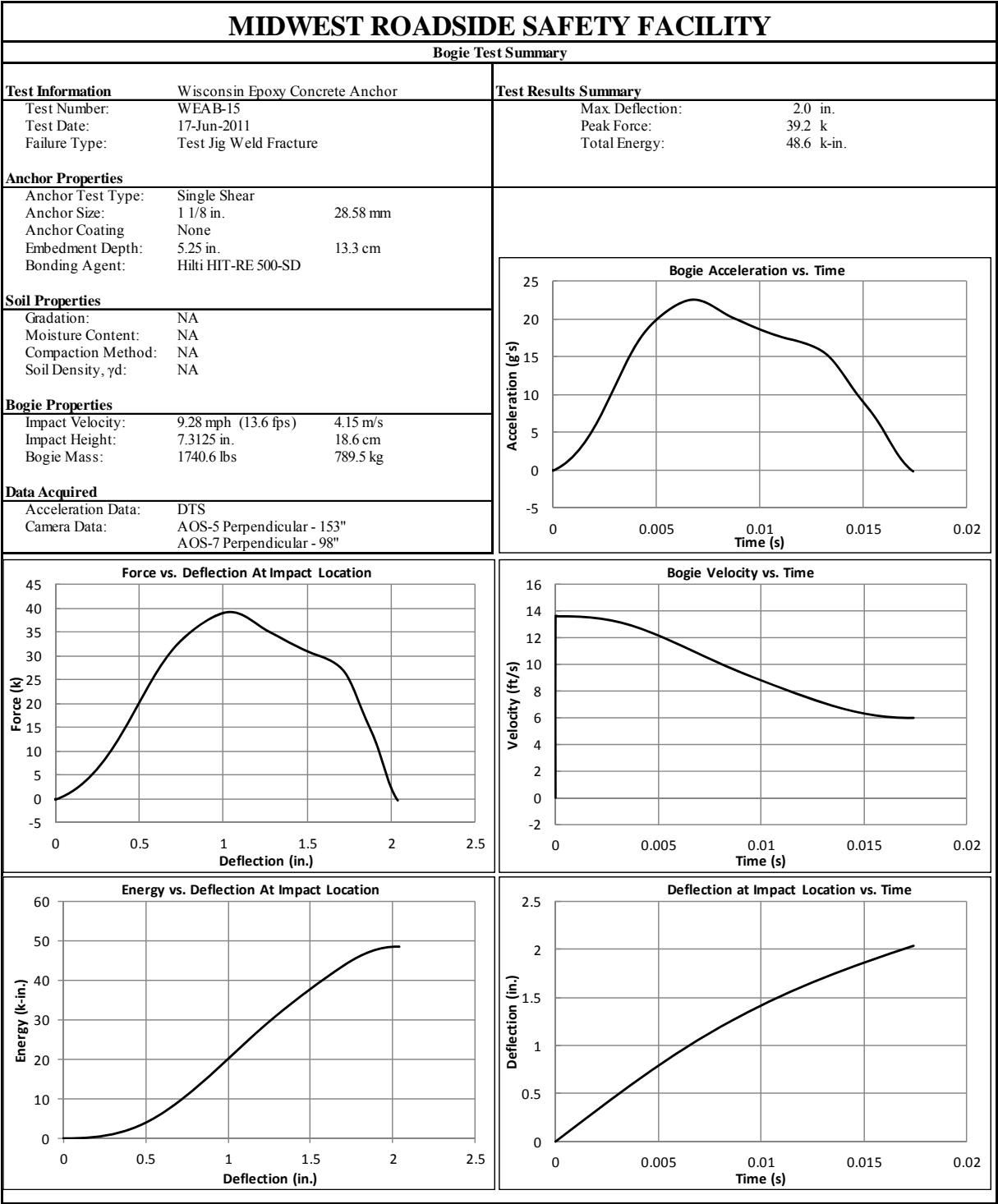


Figure H-36. Results of Test No. WEAB-15 (DTS Set 2)

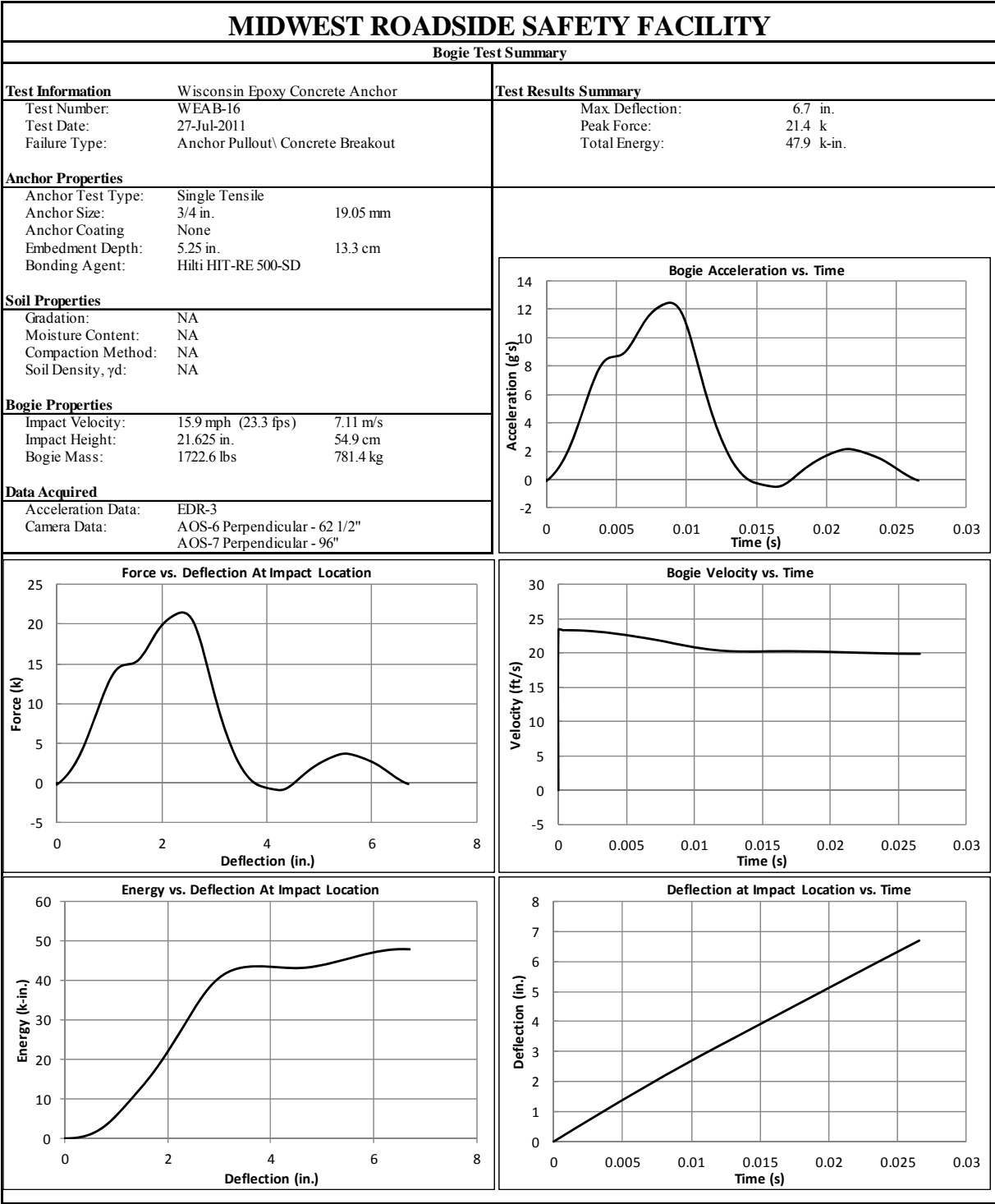


Figure H-37. Results of Test No. WEAB-16 (EDR-3)

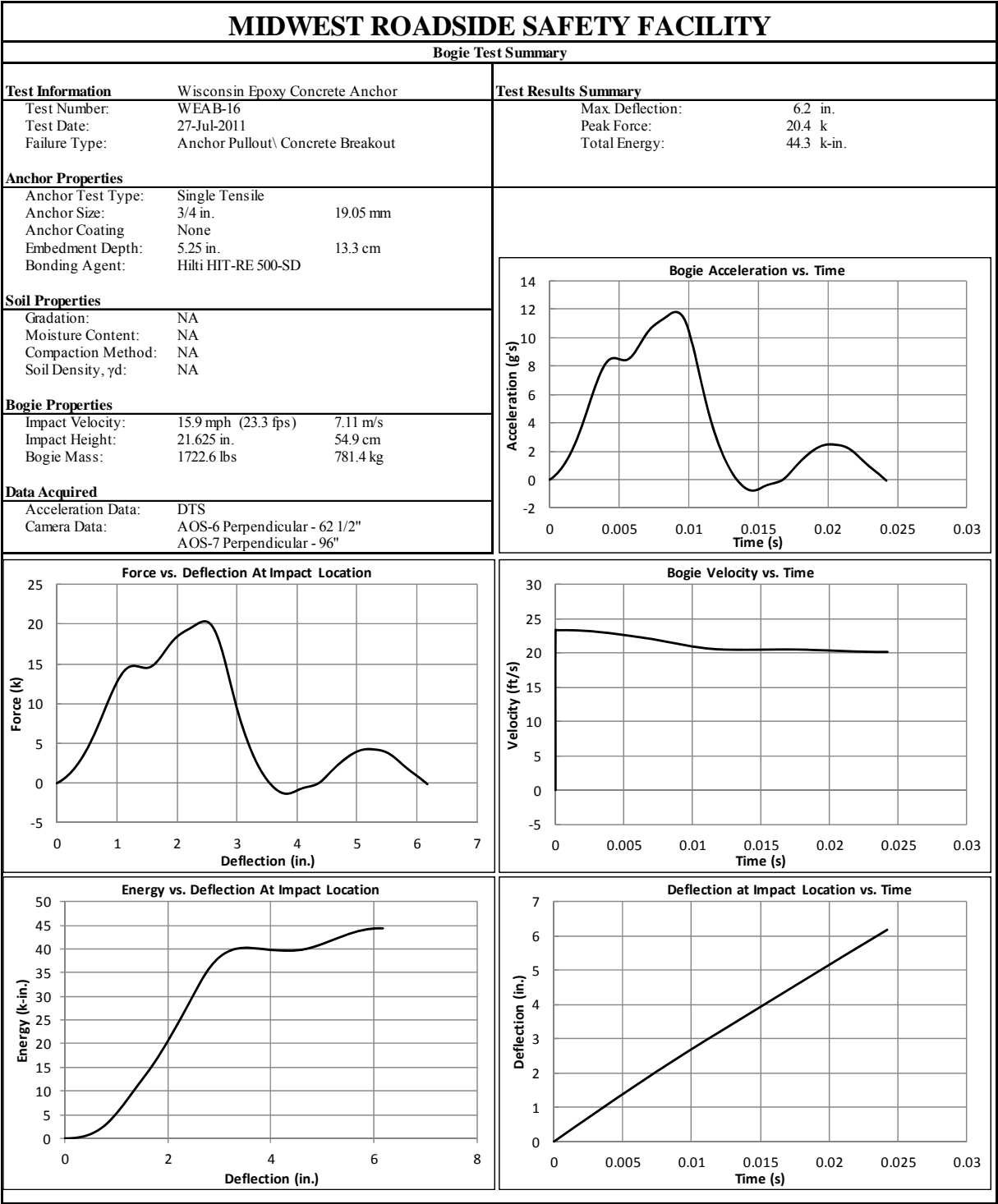


Figure H-38. Results of Test No. WEAB-16 (DTS Set 1)

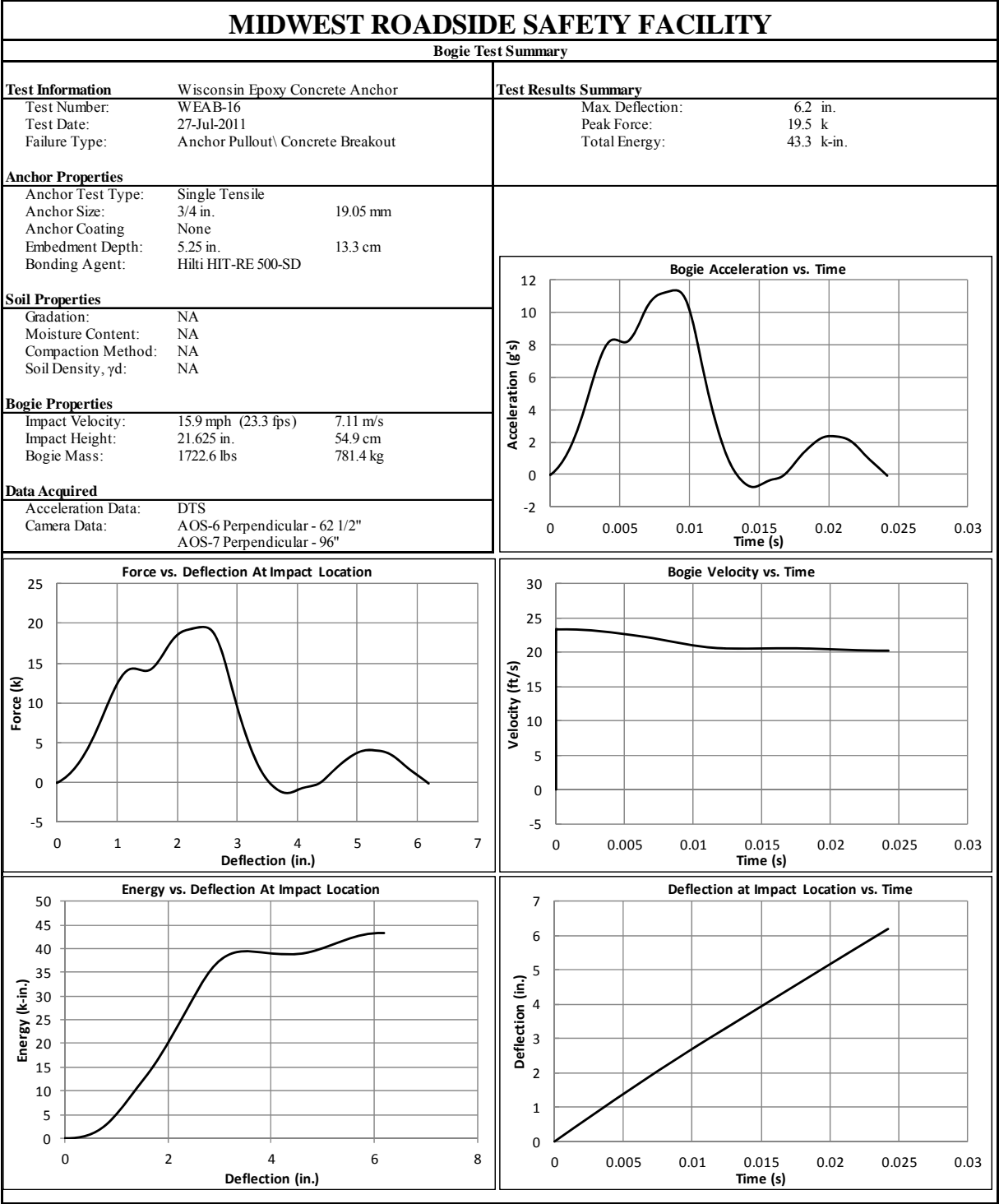


Figure H-39. Results of Test No. WEAB-16 (DTS Set 2)

END OF DOCUMENT